

*Tmx 71321*

# STUDIES OF TRANSIENT X-RAY SOURCES WITH THE ARIEL 5 ALL-SKY MONITOR

(NASA-TM-X-71321) STUDIES OF TRANSIENT  
X-RAY SOURCES WITH THE ARIEL 5 ALL-SKY  
MONITOR Ph.D. Thesis - Maryland Univ.  
(NASA) 251 p HC A12/MF A01

N77-25051

CSSL 03B

G3/93

Unclas  
30680

**LOUIS JOSEPH KALUZIENSKI**

**MAY 1977**



**GODDARD SPACE FLIGHT CENTER**  
**GREENBELT, MARYLAND**

STUDIES OF TRANSIENT X-RAY SOURCES  
WITH THE ARIEL 5 ALL-SKY MONITOR\*

by  
Louis Joseph Kaluziński

Dissertation submitted to the Faculty of the Graduate School  
of the University of Maryland in partial fulfillment  
of the requirements for the degree of  
Doctor of Philosophy  
1977

\*Work supported by NASA Grant NGR 21-002-316

## ABSTRACT

Title of Thesis: Studies of Transient X-ray Sources with the  
Ariel 5 All-Sky Monitor

Louis Joseph Kaluzienski, Doctor of Philosophy, 1977

Thesis directed by: Professor Frank B. McDonald

Since the discovery of the nova-like X-ray source Cen X-2 in 1967, the nature and origin of this extremely variable class of objects, the so-called transient X-ray sources, has remained largely unresolved. The Goddard Space Flight Center All-Sky Monitor, an imaging X-ray detector launched aboard the Ariel 5 satellite in late 1974, has proven to be a useful instrument in the detection and continued monitoring of the transient sources and of transient phenomena in previously catalogued sources. The ability to observe more than 80% of the 3-6 keV X-ray sky on a virtually continuous basis over long periods has revealed a broad spectrum of long-term temporal variability of the "permanent" galactic X-ray sources and led to the detection of regular variability on time scales of days - weeks in several of the latter sources (e.g. Cygnus X-1, Circinus X-1).

With respect to the problem of the transient X-ray sources, the All-Sky Monitor has obtained detailed light curves of three new sources and provided additional data essential to the determination of the characteristic luminosities, rates of occurrence (and possible recurrence), and spatial distribution of these objects. The present observations (and those from other experiments) are consistent with a roughly uniform galactic disk population consisting of at least two source sub-classes, with one group ('Type I') radiating at approximately the Eddington-limit ( $L_E \approx 1.3 \times 10^{38} M_X/M_\odot \text{ erg}^{-1}$ ,  $M_X = 1 - 10 M_\odot$ ) and characterized by a mean occurrence rate

of  $1 \lesssim \tau_I^{-1} (\text{yr}^{-1}) \lesssim 10$ , and the second group ('Type II') at least an order of magnitude less luminous and correspondingly more frequent,  $5 \lesssim \tau_{II}^{-1} (\text{yr}^{-1}) \lesssim 100$ . While it is shown that both sub-types are probably unrelated to the classical optical novae (or supernovae), they are most readily interpreted within the standard mass-exchange X-ray binary model, with outbursts triggered by Roche-lobe overflow (Type I) or enhancements in the stellar wind density of the companion (Type II), respectively.



## CURRICULUM VITAE

Name: Louis Joseph Kaluziensi.

Permanent address: 3427-14 Tulane Drive, Hyattsville, Maryland 20783.

Degree and date to be conferred: Ph.D., 1977.

Date of birth: [REDACTED].

Place of birth: [REDACTED].

Secondary education: Keyport High School, Keyport, New Jersey, 1966.

Collegiate institutions attended	Dates	Degree	Date of Degree
Rutgers (New Brunswick)	1966-1970	B.A.	May 1970
University of Maryland	1970-1977	M.S.	May 1974
University of Maryland	1970-1977	Ph.D.	May 1977

Majors: Physics, Astronomy.

Professional publications:

"Observations of a New Transition in the Emission from Cyg X-1", S. S. Holt, E. A. Boldt, L. J. Kaluziensi and P. J. Serlemitsos, Nature 256, 108, 1975.

"Decay of X-ray Source A0535+26", L. J. Kaluziensi, S. S. Holt, E. A. Boldt, and P. J. Serlemitsos, Nature 256, 633, 1975.

"The Early Light Curve of A0620-00", L. J. Kaluziensi, S. S. Holt, E. A. Boldt, and P. J. Serlemitsos, X-ray Binaries, NASA SP-389, 311, 1975.

"The Light Curve of a Transient X-ray Source", L. J. Kaluziensi, S. S. Holt, E. A. Boldt, P. J. Serlemitsos, G. Eadie, K. A. Pounds, M. J. Ricketts, and M. Watson, Ap. J. (Letters) 201, L121, 1975.

"New Results from Long-term Observations of Cyg X-1", S. S. Holt, E. A. Boldt, P. J. Serlemitsos, and L. J. Kaluziensi, Ap. J. (Letters) 203, L63, 1976.

"Long-term X-ray Studies of Scorpius X-1. I. Search for Binary Periodicity", S. S. Holt, E. A. Boldt, P. J. Serlemitsos, and L. J. Kaluziensi, Ap. J. (Letters) 205, L27, 1976.

"Long-term X-ray Studies of Scorpius X-1. II. Evidence for Flare-dominated Intensity Variations", S. S. Holt, E. A. Boldt, P. J. Serlemitsos, and L. J. Kaluziensi, Ap. J. (Letters) 205, L79, 1976.

- "Evidence for a 17-d Periodicity from Cyg X-3", S. S. Holt, E. A. Boldt, P. J. Serlemitsos, L. J. Kaluziński, S. H. Pravdo, A. Peacock, M. Elvis, M. G. Watson, and K. A. Pounds, Nature 260, 592, 1976.
- "Evidence for an 11.2 day Periodicity from Cygnus X-2", S. S. Holt, E. A. Boldt, P. J. Serlemitsos, and L. J. Kaluziński, Ap. J. (Letters) 205, L143, 1976.
- "A Return to the Pre-1971 Intensity Level and a 5.6-d Modulation for Cyg X-1", S. S. Holt, L. J. Kaluziński, E. A. Boldt, and P. J. Serlemitsos, Nature 261, 213, 1976.
- "Evidence for a 16.6 day Period from Circinus X-1", L. J. Kaluziński, S. S. Holt, E. A. Boldt, and P. J. Serlemitsos, Ap. J. (Letters) 208, L71, 1976.
- "The 35-d X-ray Profile of Her X-1", S. S. Holt, E. A. Boldt, L. J. Kaluziński, P. J. Serlemitsos, and J. H. Swank, Nature 263, 484, 1976.
- "All-Sky Monitor Observations of the Decay of A0620-00 (Nova Monocerotis 1975)", L. J. Kaluziński, S. S. Holt, E. A. Boldt, and P. J. Serlemitsos, Ap. J., in press.
- "Recurrent X-ray Outbursts from Aquila X-1", L. J. Kaluziński, S. S. Holt, E. A. Boldt, and P. J. Serlemitsos, Nature, in press.

Positions held: Post-doctoral Research Associate  
Laboratory for High Energy Astrophysics  
NASA/Goddard Space Flight Center  
Greenbelt, Maryland 20771

TO

Geneann, Michael, and Mark

## ACKNOWLEDGMENTS

I would like to take this opportunity to thank the many people who aided in this research, which was conducted in its entirety with the X-Ray Astronomy Group of the Laboratory for High Energy Astrophysics (LHEA) at NASA/Goddard Space Flight Center. First, I gratefully acknowledge my thesis advisor, Dr. Frank B. McDonald, for his continued encouragement during my association with the LHEA and for his careful reading and critical appraisal of this work. I also wish to thank Dr. Howard Laster and Dr. Alexander Dragt, the former and present Chairman of the Department of Physics and Astronomy for their approval of this research position. I am further obliged to Dr. Joseph O'Gallagher who advised me during my earlier graduate studies and introduced me to the LHEA.

In the X-Ray Astronomy Group, I wish to express my special appreciation to Dr. Stephen Holt who has patiently and unselfishly directed the course of my research and the development of this thesis. I am most indebted to Dr. Holt for his role in the initial conception and development of the Ariel 5 All-Sky Monitor experiment, for guidance in the data analysis, and for interesting and helpful discussions on the subject of the transient X-ray sources. I would also like to thank Dr. Elihu Boldt, Dr. Peter Serlemitsos, and Dr. Richard Rothschild for their valuable assistance, and Dr. Upendra Desai for his part in the development of the All-Sky Monitor.

It is a pleasure to recognize those people who have contributed to the success of the All-Sky Monitor experiment. For their role in the construction, calibration, and testing of the instrument, I am particularly indebted to Mr. Emanuel Karageorge and Mr. Charles Glasser. With regard to the development of the computer software employed in the data analysis, I am greatly obliged to Ms. Mae Silbergeld, Mr. Louis Perazzoli, and

Mr. Philip Yu. For their help in the data handling, I wish to thank Ms. Mary Des Jardins, Mary Ann Esfandiari, Mr. Cornelius Murphy, Mr. Jonathan Taylor, Ms. Kim Tolbert, and Mr. Fernando Lopez. I likewise acknowledge support from the Information Processing Division (IPD) at Goddard Space Flight Center and from the U.K. Operations Control Center in Slough, England.

I wish to further express my appreciation to Mssrs. Frank Shaffer, Larry White, Adam Thompson, and Harry Trexel of the Drafting Section of the LHEA for their willing assistance and skilled work in drawing the majority of the figures appearing in this thesis. It is also a pleasure to acknowledge Ms. Barbara Dallas and Ms. Barbara Shavatt for their valuable assistance during my tenure at Goddard. I am especially indebted to Ms. Sandra Shrader for her perseverance in the demanding task of typing this thesis.

Finally, I thank my wife, Geneann, and our parents whose constant encouragement and assistance helped make this work possible.

## TABLE OF CONTENTS

Chapter	Page
DEDICATION . . . . .	ii
ACKNOWLEDGMENTS. . . . .	iii
LIST OF TABLES . . . . .	vii
LIST OF FIGURES. . . . .	ix
I. INTRODUCTION. . . . .	1
A. Variability in Astronomy. . . . .	1
B. X-ray Astronomy . . . . .	2
C. Galactic X-ray Sources. . . . .	4
D. Transient X-ray Sources . . . . .	8
E. Purpose . . . . .	10
II. EXPERIMENT DESCRIPTION. . . . .	13
A. Position Measurement. . . . .	14
B. X-ray Pinhole Camera. . . . .	16
C. Energy Characteristics. . . . .	19
D. Background. . . . .	21
E. Octant Mode . . . . .	23
F. Satellite Operation . . . . .	24
III. DATA ANALYSIS . . . . .	26
A. Source Library. . . . .	26
B. Computation Factors . . . . .	27
C. Source Measurement and Detection. . . . .	32
D. Experiment Performance. . . . .	35
IV. OBSERVATIONS. . . . .	39
A. Transient X-ray Sources . . . . .	40
B. Variable Sources. . . . .	56

Chapter	Page
V. DISCUSSION AND CONCLUSIONS. . . . .	66
A. Spatial Distribution. . . . .	67
B. Occurrence Rates and Luminosities . . . . .	70
C. Observational Constraints on Source Models. . . . .	80
D. Summary . . . . .	104
APPENDIX A. UHURU-ASM FLUX CONVERSION . . . . .	106
APPENDIX B. EARTH OCCULTATION . . . . .	107
APPENDIX C. COMPUTATION OF SOURCE LATITUDINAL CORRECTION FACTOR .	111
APPENDIX D. COMPUTATION OF 'GEOMETRICAL FACTORS'. . . . .	113
APPENDIX E. CONSTRAINTS ON THE LUMINOSITIES, FREQUENCY, AND SPATIAL DISTRIBUTION OF THE TRANSIENT X-RAY SOURCES .	116
REFERENCES . . . . .	122
TABLES . . . . .	135
FIGURES. . . . .	146



## LIST OF TABLES

Table		Page
1.1	Classification of Variable Stars (from Strohmeier 1972) . . . . .	135
1.2	Summary of the Observations of the Pre-Ariel 5 Transient X-ray Sources. . . . .	136
1.3	Summary of the Observations of the Post-UHURU Transient X-ray Sources. . . . .	137
3.1	All-Sky Monitor Source Library (first 80 sources). Listed are the source designation, common name (if any), coordinates (R.A. and Dec.; $l$ and $b$ ), minimum intensity (converted to ASM units of incident 3-6 keV photons $\text{cm}^{-2}\text{s}^{-1}$ ), and source variability (from the Third UHURU (3U) Catalog).....	138
3.2	Geometrical Factors ( $G_i$ ) for the Sixteen Latitudinal Regions (anode segments) of the ASM Pinhole Cameras. . .	139
3.3	Source Latitudinal Extent vs. Spacecraft Latitude. . . .	140
4.1	Summary of Transient X-ray Source Candidates and Transient-Like Variables . . . . .	141
5.1	Distance and Z-displacement of the Transient X-ray Sources as a Function of (Peak) Luminosity. The Variable $r_e$ Represents the Computed Distance from the Sun to the Edge of the Galaxy as a Function of Source Galactic Longitude, with Assumed Values for the Sun-Galactic Center Displacement and Galactic Radius of $r_s = 10$ Kpc and $R = 15$ Kpc, respectively. All Distances are in Kpc . . . . .	142

Table	Page
5.2 Summary of Type I & II Transient X-ray Source Characteristics. . . . .	143
5.3 Long-Term Variability of Galactic X-ray Sources. . . . .	144
A.1 Values of UHURU-ASM Flux Conversion factor ( $\kappa$ ) for Representative Power-law (photon-spectral index $n$ ) and Exponential Spectra (temperature parameter $kT$ ) . . .	145

FIGURE CAPTIONS

Figure	Page
1.1 (a)	Evolution of a star with $M = 5 M_{\odot}$ in the HR (Hertzsprung-Russell) Diagram (from Kraft 1975); and
(b)	Schematic HR Diagram (lines of constant slope correspond to stars of identical radii; from Harwit 1973). . . . . 146
1.2 (a)	The light curve of a typical Cepheid variable (from Wyatt 1964); and
(b)	Empirical period-luminosity relations (schematic) for classical Cepheids, W Virginis variables, and RR Lyrae variables (from Strohmeier 1972) . . . . . 147
1.3	Light curves of
(a)	the flare star AD Leonis (from Glasby 1969); and
(b)	the Mira variable R Cassiopeiae ( $P = 430.5$ days; from Strohmeier 1972) . . . . . 148
1.4	Light curves of
(a)	the U Gem variable SS Cygni in 1966; and
(b)	the recurrent nova T Coronae Borealis (from Glasby 1969). . . . . 149
1.5	Schematic light curve of a classical nova, showing typical stages in its evolution (from Payne-Gaposchkin 1964). Characteristic time scales of the rise and decline phases are $\sim$ hrs-days and months- $\sim$ 1 yr, respectively. . . . . 150

Figure		Page
1.6	Map of the X-ray sky in galactic coordinates derived from the Third UHURU (3U) catalog (the size of each dot is proportional to the logarithm of the X-ray intensity; from Giacconi 1976) . . . . .	151
1.7	Schematic representation of an X-ray binary system (subscripts 1 and 2 denote the optical companion and the collapsed X-ray emitting object, respectively; courtesy of S. Holt). . . . .	152
1.8	Schematic diagram illustrating the Roche-lobe overflow (left) and stellar wind (right) modes of mass transfer in binary systems (from Kraft 1975). . . . .	153
1.9	Millisecond bursts from Cygnus X-1 observed in a rocket flight on 1973 October 4 at 340 UT. Count rates are binned every 0.64 ms; shaded bins denote bursts with $\geq 12$ counts per 1.28 ms (from Rothschild <u>et al.</u> 1974) . . . . .	154
1.10	Counting rate data ( $\sim 1.5 - 10$ keV) for the rapid X-ray burster MXB 1730-335 from SAS-3 (from Lewin <u>et al.</u> 1976). . . . .	155
1.11	The characteristic short term variability (2-60 keV counting rates) of three galactic binary X-ray sources as observed in brief rocket exposures. While the 1.24 sec pulsations of Her X-1 and bursting nature of the emission from Cyg X-1 are clearly apparent, the intensity of Cyg X-3 is consistent with statistical	

Figure		Page
	fluctuations about the mean flux level (constant over the time scale of the observation ( $\approx 1$ minute); courtesy of R. Rothschild).....	156
1.12	Three 'ON' states (occultation-modulated at the $1.7^d$ binary period) in the $35^d$ cycle of Hercules X-1 as observed by UHURU (from Gursky and Schreier 1975) . .	157
1.13	X-ray ( $\sim 3$ -12 keV) light curves of the transient sources Cen X-2 and Cen X-4. The data for the former source are from various rocket observations (see Table 1.2 for references), while the latter were obtained via the Vela 5A and 5B satellites. The hardness ratio (Cen X-4) is defined as the ratio of the 6-12 keV to 3-6 keV counting rates, the corresponding scale of which is shown at the right (from Evans, Belian, and Conner 1970) . . . . .	158
1.14	Combined X-ray light curve of 3U1543-47 from the Vela, UHURU, and OSO-7 satellites, with intensities normalized to the UHURU count-rates (from Li, Sprott, and Clark 1976) . . . . .	159
2.1	Artist's conception of the Ariel 5 satellite in Earth orbit . . . . .	160

Figure		Page
2.2	The Ariel 5 spacecraft showing the four pole-aligned pointing experiments (A (Rotation Modulation Collimator) C(proportional counter spectrometer), D (polarimeter/spectrometer), and F (scintillation telescope)) and two scanning experiments (B (Sky Survey Instrument) and G (All-Sky Monitor); (from Smith and Courtier 1976).....	161
2.3	The instantaneous fields of view of the six Ariel 5 experiments seen in the satellite reference frame. Angular limits correspond to the aperture full widths at half maximum response (FWHM; from Smith and Courtier 1976). . . . .	162
2.4	Schematic diagram of position-sensitive proportional counter, demonstrating the principle of charge division along a highly resistive anode . . . . .	163
2.5	Typical pulse amplitudes and rise-times from the resistive anode/charge sensitive preamplifier circuit employed in the ASM . . . . .	164
2.6	Block diagram of the voltage measurement circuit: the voltage of events whose sum pulse heights lie within the nominal thresholds (window disc) are measured with the crossover detectors, digitized via the gated oscillator, and stored in the register. . . . .	165
2.7	Block diagram illustrating the analog-to-digital converter . . . . .	166

Figure		Page
2.8	Isometric schematic of the experiment geometry. X-rays may enter only through one of the two pinholes, and are recorded on one of the two position-sensitive detectors (the planes of which are represented by the pairs of diagonal dashed lines) mounted at $45^{\circ}$ with respect to the spacecraft spin axis. The instantaneous field of view (static "fan-beam" response) of each detector is $\sim 4^{\circ} \times 90^{\circ}$ . . . . .	167
2.9	Static fan-beam spatial response; a,b, and h denote the pinhole (aperture), detector element, and aperture-anode separation dimensions, respectively. . . . .	168
2.10	Nominal All-Sky mode latitudinal borders (DTLAT (1-16)) in spacecraft coordinates . . . . .	169
2.11	The disposition of the 512 All-Sky mode resolution elements in spacecraft coordinates. The blacked-in regions represent instantaneous "dead" bands which are inaccessible to the instrument, while the lightly shaded region is subject to occasional contamination from solar X-rays (the sun may appear in either the upper or lower hemisphere, or neither, if within $\approx \pm 10^{\circ}$ of the spacecraft equator). The solar image shown of $\sim 4^{\circ} \times 4^{\circ}$ is a typical source image size. . . . .	170



Figure		Page
2.12	Detector energy response (efficiency) as a function of incident X-ray energy. A detector cross-section is also displayed, and the computed efficiency is only for the $\sim 1/6$ of the counter volume which is used for X-ray analysis. The Beryllium window has no supports which shadow any portion of this X-ray volume . . . . .	171
2.13	Mean 3-6 keV "efficiency" ( $\epsilon$ ) as a function of counter gain, for three representative spectra. The electronic thresholds are permanently set at $E_v = 2.5$ keV and 7.5 keV for nominal gain $A_g = 1$ . . . . .	172
2.14	Portion of the energy response curve sampled at the four high-voltage settings (nominal gas pressure) . . .	173
2.15	Octant mode detector elements in the spacecraft coordinate system. The 512 "fine" ASM core-store locations are now allocated to $\sim 1/16$ of the sky (i.e., $1/8$ of one hemisphere), with the "octant" divided into a 16 (longitude) x 32 (latitude) dimensional array of resolution elements ( $\approx 3^0 \times 3^0$ ) . . . . .	174
2.16	Diagram illustrating the interlinking of the major components of the Ariel 5 spacecraft systems (from Smith and Courtier 1976). . . . .	175
3.1	Mean unocculted fraction ( $\eta$ ) vs. source right ascension (R.A.) for sources of differing declination (Dec.; solar declination = $0^0$ ). . . . .	176

Figure	Page
3.2	Source latitudinal correction factor (LCOR) vs. spacecraft latitude (D). The shaded regions correspond to the equatorial and polar dead bands . . . 177
3.3	Detector spatial response vs. (a) spacecraft latitude ( $\Delta\theta$ = source latitudinal extent); and (b) spacecraft longitude ( $\Delta\phi$ = source longitudinal extent) . . . . . 178
3.4	Longitudinal response as a function of source spacecraft latitude; the increased longitudinal extent with increasing latitude illustrates the origin of the latitudinal correction factor . . . . . 179
3.5	Single-orbit raw data (all-sky mode) from five strong sources, which were each confined (in this orbit) almost entirely to single resolution elements. Sco X-1 typically gives $\sim 100$ -400 counts, and the other sources $\sim 10$ -40. The background varies with spacecraft latitude, but ranges typically from $\sim 2$ (near-equatorial elements) to $\sim 7$ (polar elements) counts per element. . . . . 180
3.6	Computer output for one all-sky mode orbit. At the top of the page are shown the orbit identification number (core dump number), orbit mid- and end-times, array of computed source exposure times, aspect information (sun and spin angles), and housekeeping parameters (temperature, power and sunlight/eclipse

- status, high voltage and anti-coincidence analog parameters, and event-time array). The 512 element sky grid is displayed, with rows and columns corresponding to spacecraft longitudinal sectors and latitudinal segments, respectively. At the bottom of the page are shown the average net counts per element (as a function of latitude) and those elements with net counts (detected-expected)  $\geq 3\sigma$  above background. . . . . 181
- 3.7 Computer output for one all-sky mode "accumulation" ( $\sim \frac{1}{2}$  day integration). Shown at the top are the net detector on-times, accumulated core dumps and mid-time, and aspect data. The computed internal background per element (for a given latitudinal segment) is listed at the bottom of the page. . . . . 182
- 3.8 Octant mode observation (3 orbit accumulation) of the Taurus region in 1975. The 512 resolution elements cover a region of  $\sim 1/16$  of the sky ( $\Delta D \approx 70^\circ$ ,  $\Delta A = 45^\circ$ ), with spacecraft latitude increasing from bottom (equator) to top (pole) and longitude from left to right. The rows marked 'sum' represent the sum of eight latitudinal elements for each of the 16 longitudinal regions. The bottom half of the page represents a map (in spacecraft coordinates) of the count array, with the computed standard deviations above background denoted by numbers and the locations of known

Figure

Page

X-ray sources indicated by letters. Note the relatively good spatial resolution of the nearby sources A0535+26 and the Crab Nebula ( $\Delta\theta_s \approx 5^\circ$ ) . . . . . 183

3.9 ASM measurements (daily averages; fluxes are effective incident 3-6 keV photons  $\text{cm}^{-2}\text{s}^{-1}$ ) of four bright sources from 1974 October - 1976 September. The dashed lines indicate the range of source variability as observed by UHURU. . . . . 184

3.10 ASM measurements of the Crab Nebula (daily averages) over an approximately two year interval. Dashed lines represent long-term averages of the data over the indicated intervals and 'N' and 'S' denote measurements of the source via the 'North' and 'South' counters, respectively. Points with relatively large systematic errors resulting from spatial offsets in the detector have not been removed from this data. . . . . 185

3.11 High voltage calibration of the South counter performed in 1976 July - August. Half-day accumulations of Sco X-1 and the Crab Nebula (normalized to their values at the "nominal" gain setting) are plotted vs. gain for each of the four high-voltage settings . . . 186

3.12 Approximately 100 d of single-orbit Cyg X-3 and Cyg X-1 ASM data obtained between 1974 December and

- 1975 March folded at the Cyg X-3 period (with indicated phase) of Leach et al. (1975). The indicated  $\chi^2$  values are for 10-bin folds (9 degrees of freedom) against the hypothesis of a constant source intensity . . . . . 187
- 3.13 Data taken before the 1975 April increase (upper trace: 1974 November - 1975 April) and after the start of the 1975 November increase (lower trace: 1975 November - 1976 January) folded in 5 bins using the HDE226868 ephemeris of Bolton (1975) . . . . . 188
- 3.14 ASM 34.9-d light curve of Her X-1 in 15 bins. The ordinate is normalized to approximate UHURU counts for comparison with other measurements. The epoch of the start of bin 1 is JD2,442,442.0. . . 189
- 4.1 The 3-6 keV X-ray light curve of A1524-62. The points are data from the ASM accumulated over 3-7 orbits ( $\sim 4.5$ -10.5 hours). The solid trace is a representation of the SSI data displayed in Fig. 4.2, normalized to the natural ASM ordinate using the response of both experiments to the Crab Nebula ( $1.2 \text{ cm}^{-2} \text{ s}^{-1}$  in the 3-6 keV band). The shaded regions indicate where the source is out of the field of view of the ASM. SSI data in addition to those taken over days 314-337 consist of a single measurement on day 433 (displayed in the figure), and

- an upper limit of  $0.07 \text{ cm}^{-2} \text{ s}^{-1}$  on day 294 (not displayed). Cir X-1 has the same upper limit for both of these times. The  $1\sigma$  SSI position accuracy is  $0.02$  . . . . . 190
- 4.2 The detailed history of the precursor peak from the SSI. The lower trace is the sum of the 1.5-5.8 keV (LE) and 2.4-19.8 keV (HE) count rates, and the upper trace is their ratio. The Crab Nebula has a total SSI count rate of  $510 \text{ s}^{-1}$ . The representative error bars in the upper trace are  $\pm 1\sigma$ , while those in the lower trace are  $\pm 2\sigma$ . . . . . 191
- 4.3 Intensity measured from A0535+26 over approximately half-day accumulation times. The source is not in the usable field of view of the ASM where the abscissa is shaded. The  $2\sigma$  upper limits before and after the measured points are determined primarily by the statistical accuracy in the measurement of the Crab Nebula, with which A0535+26 may be confused in the ASM data . . . . . 192
- 4.4 A0620-00 light curve (3-6 keV) through 1975 November. Points prior to day  $\sim 320$  are single-orbit measurements, while those afterward represent  $\sim 1/2$  day averages. Error bars reflect the  $\pm 1\sigma$  statistical uncertainties. The dashed lines are best exponential fits to the pre- and post-October increase data, and the solid line is the best  $1/t$  fit referenced to the

approximate time of maximum light. The Crab Nebula has an intensity of  $\sim 1.2$  in these units. The arrows represent the times of source discovery and maximum X-ray flux . . . . . 193

4.5 Later decline of A0620-00. All points are  $\sim \frac{1}{2}$  day averages, and the dashed line is an extrapolation of the post-October exponential decay of Fig. 4.4. Upper limits represent measurements of a source flux  $\lesssim 0.1 \text{ cm}^{-2} \text{ s}^{-1}$  . . . . . 194

4.6 ASM measurements of the Norma "transient" (lower trace) and the nearby source 3U1636-53 (upper trace). The data represent  $\sim \frac{1}{2}$ -day (octant-mode) accumulations with  $\pm 1\sigma$  statistical error bars; confusion of the sources may result in systematic errors of comparable magnitude. Also shown are the UHURU ranges for the probable "permanent" counterpart of the Norma Transient (4U1608-52) and the constant level reported from UHURU for 3U1636-53. The table lists the midtimes (T) and fluxes (S) for both sources obtained in additional octant mode accumulations over the period 1974 December - 1976 March. . . . . 195

4.7 The X-ray (3-9 keV) light curve of A1118-61 from the Ariel 5 RMC. The source counting rate (background-subtracted) is plotted as a function of time, and the symbol circle with a vertical bar indicates typical  $\pm 1\sigma$  values near the maximum



	intensity. The variation in the magnitude of the upper limits results primarily from changes in the distance of the source from the spin axis. The intensity in equivalent UHURU counts $s^{-1}$ may be obtained by multiplying the displayed counting rates by a factor of $\sim 13$ (from Eyles <u>et al.</u> 1975a). . . . .	196
4.8	The X-ray (3-9 keV) light curve of the transient A1742-28 as measured by the Ariel 5 RMC experiment (from Eyles <u>et al.</u> 1975b) . . . . .	197
4.9	The 3-6 keV X-ray light curve of the 1975 June flare of Aquila X-1. The points are $\sim \frac{1}{2}$ day averages, and the error bars are $\pm 1\sigma$ (statistical error only). The shaded areas labelled 'equator' are times when Aq1 X-1 was close to the equatorial plane of the Ariel 5 satellite; during these times the source was inaccessible to the ASM, but observable by the SSI. . .	198
4.10	The 1976 June flare of Aquila X-1 as measured by the ASM . . . . .	199
4.11	Summary of Aq1 X-1 observations over the period 1971-76. The OSO-7 data is taken from Markert (1974) and has been approximately converted to ASM units via normalization with respect to the Crab Nebula. Error bars in all data have been conservatively estimated to include possible systematic and normalization errors. Intermittent Copernicus measurements (Davidsen <u>et al.</u> 1975) during 1973-75 (not displayed) are at the level	

Figure		Page
	~0.01-0.02, and do not preclude a 1974 outburst as hypothesized. . . . .	200
4.12	The light curve (2-6 keV) of 3U1630-47 from 1971 - 1976 showing four outbursts separated by ~600 days. The upper limits shown are $3\sigma$ , with the large upper limits resulting when the source was not well centered in the collimator fields of view (UHURU and Ariel 5 SSI observations; from Jones <u>et al.</u> 1976) . . . . .	201
4.13	ASM observations of the "recurrent transient" 3U1630-47 (lower plot) and the nearby source 3U1642-45 (upper plot). Points are $\sim\frac{1}{2}$ day (octant-mode) accumulations with $\pm 1\sigma$ statistical error bars, with possible systematic errors resulting from source confusion at least as large. The UHURU range for 3U1642-45 and the expected time of turn-on for 3U1630-47 (cf. Jones <u>et al.</u> 1976) have also been indicated . . . . .	202
4.14	The 1975 April increase of Cygnus X-1 as observed by the ASM. Points are $\sim\frac{1}{2}$ -day accumulations with $\pm 1\sigma$ statistical error bars. The source is no longer in the field of view of the experiment after day 123 (May 3) . . . . .	203
4.15	The 1975 November - 1976 February "high" state of Cygnus X-1 from the ASM. The data consists of $\sim\frac{1}{2}$ -day accumulations with $\pm 1\sigma$ statistical error bars. The maximum intensity is approximately 1.5 times that of the Crab Nebula . . . . .	204

Figure		Page
4.16	<p>ASM observations of Cir X-1 over <math>\sim 200</math> days between 1975 September and 1976 April. The points represent <math>\sim \frac{1}{2}</math> day averages, and error bars reflect only the <math>\pm 1\sigma</math> statistical uncertainty of each measurement. Blackened dots indicate observations made in the fine resolution mode in which possible systematic errors due to spatial offsets and source confusion are minimized. Periods when the source was out of the effective field of view are marked by the shaded areas along the abscissa, and the arrows indicate the transitions predicted from the period and ephemeris given in Kaluziński <i>et al.</i> (1976c). The apparent peak occurring near 1974 day 670 (upper shaded interval) is probably due to confusion with the Norma transient (cf. IAU Circ., No. 2859).</p>	205
4.17	<p>ASM observations (<math>\sim \frac{1}{2}</math> day accumulations) of Circinus X-1 over the interval 1976 April - 1977 January (upper trace) and OSO-8 observations (2-60 keV) of a transition in the <math>16^d.6</math> cycle (lower trace).</p>	206
4.18	<p>Single-orbit data near the expected times of transition on 1975 November 11 and 1976 February 2. The dashed lines are relative to the best period and transition epoch in Kaluziński <i>et al.</i> (1976c).</p>	207

Figure		Page
4.19	Data of Fig. 4.16 folded at the $16.585^d$ period, with phase 0.0 defined by the transition from high to low intensity. The scatter in the data at phases $\approx 0.75$ is due primarily to folding of cycles with differing peak intensities, and not to finer time scale variations within each cycle. The open circle points are those in Fig. 4.16 which are suspected of arising from the Norma transient . . . . .	208
4.20	Continuous record of Cyg X-3. The data points are daily averages of ASM data, with $\pm 1\sigma$ error bars. The solid bars are $\pm 1\sigma$ thick, 1.6-d averages of SSI data. The latter are 2-18 keV measurements which are normalized to the natural ASM ordinate with the response of both instruments to the Crab Nebula. The grid above the data indicates the positions of expected maxima with the best fold values of period (16.75 d) and epoch ( $\phi_{\text{maximum}} = \text{JD2,442,522}$ ) . . . . .	209
5.1	Galactic map of transient sources, proposed candidates, transient/variables, and long-term variable ( $\approx 10x$ ) UHURU sources (based upon positions given in Tables 1.2, 1.3, 4.1 and the 3U catalog) . . . . .	210

Figure	Page
5.2	Plot of $\log N(>S)$ vs. $\log S$ ( $N(>S) \equiv$ Number of sources observed above flux level $S$ ) for the post-UHURU transient X-ray sources. Fluxes are plotted relative to that of the Crab Nebula, and the curves shown are based upon the assumptions of a (sensitivity-limited) uniform distribution of sources symmetrical about the observer (and in which no sources are missed as a result of source confusion or incompleteness of sky coverage). . . . . 211
5.3	Galactic plane projection of the deduced spatial distribution of the transient X-ray sources. Sources have been divided into the Type I/II subclasses as outlined in the text and, where no classification was obtainable, assigned Type I luminosities. The distance ranges shown are based upon the observed fluxes at maximum light and estimated <u>mean</u> values of the (peak) luminosity distributions of $10^{38} \lesssim \bar{L}_I$ ( $\text{erg s}^{-1}$ ) $\lesssim 10^{39}$ and $5 \times 10^{36} \lesssim \bar{L}_{II}$ ( $\text{erg s}^{-1}$ ) $\lesssim 5 \times 10^{37}$ , which are consistent with the arguments presented in the text. The galactic model shown is based upon 21 cm observations (cf. Simonson 1975). . . . . 212
5.4	Histogram of absolute luminosities (2-10 keV band) of 36 X-ray sources, including Milky Way (GC = Galactic Center; ST = "stellar" source), Small Magellanic Cloud (SMC), and Large Magellanic Cloud (LMC) sources (from Margon and Ostriker 1973) . . . . . 213

Figure		Page
5.5	Schematic model of the dwarf nova variable U Geminorum. The optical companion (2) has overflowed its Roche-lobe (through the inner Lagrange point $L_1$ ), resulting in the formation of an accretion disk (shaded region) about the white dwarf component (1; after Krzeminski 1975; from Strohmeier 1972). . . . .	214
B.1	Sketch showing the relevant Earth/orbital parameters for the computation of Earth occultation .	215
B.2	Diagram illustrating the computation of the occultation angle $\theta_{occ}$ (angle over the orbit during which a source is occulted) as a function of source declination ( $\delta$ ) and Earth/orbital parameters. . . . .	216
B.3	Schematic diagram showing the calculation of source occultation time ( $T_{occ}(\text{end}) - T_{occ}(\text{start})$ ) from the occultation angle $\theta_{occ}(\delta)$ and the relative source-sun separation in Right Ascension ( $\alpha_{rel}$ ). . . . .	217
C.1	Diagram illustrating:	
	(a) the computation of the latitudinal correction factor LCOR as a function of source spacecraft latitude $D$ . The pinhole is represented by the shaded region; $\hat{N}$ and $\hat{S}$ are unit vectors specifying the pinhole normal and source directions, respectively; and	
	(b) Latitude-dependence of static fan-beam detector response, $\phi_f(D)$ . . . . .	218

- D.1 Sketch showing
- (a) the definition of the relevant parameters for the calculation of the geometrical factor for a two-element (rectangular) detector (following Sullivan 1971); and
  - (b) application of (a) to the case of the All-Sky Monitor, with "detecting" elements consisting of the pinhole (dimension  $a \times a$ ) and anode detecting strip (dimension  $b \times \ell$ ) divided into the eight nominal latitudinal segments as shown. . . . . 219
- E.1 Log N - Log S plot for the nine Post-UHURU transient X-ray sources. The solid lines reflect the effect of off-centering of the Sun in the Galaxy ( $R_s \equiv$  Sun-Galactic Center distance,  $R \equiv$  Galactic Radius) for differing values of peak luminosity ( $L_{38} \equiv L/10^{38} \text{ erg s}^{-1}$ ) and an assumed uniform spatial distribution in the galactic disk (compare with Figure 5.2). The dashed lines are a schematic representation of the relatively complex variation of  $N(>S)$  for distances (fluxes) in the range  $R-R_s \leq r \leq R+R_s$ . The fluxes of the Pre-Ariel 5 transients have been indicated at the top of the plot. . . . . 220



## CHAPTER I

### INTRODUCTION

#### A. Variability In Astronomy

The relative steadiness of the emission of the majority of optical stars over time scales short with respect to that of nuclear evolution is a consequence of the stability of the nuclear burning processes underlying the stellar energy production. In the course of its lifetime, a typical isolated star will vary in effective surface temperature (and hence absolute magnitude), gradually tracing out a characteristic path (depending on the initial mass) on the H-R diagram (see Figure 1.1). In addition to the secular variability exhibited by all stars, a small class exists which is characterized primarily by variations on relatively short time scales, with two broad sub-divisions according to the nature of the modulation. The so-called "extrinsic" variables include those systems in which the light is modulated by eclipses due to a binary companion or intervening nebulosity, and have added to our knowledge of fundamental astrophysical parameters (e.g., stellar radii and masses). Of possible significance to the understanding of the nature of certain X-ray emitting systems are the intrinsic variables, i.e., stars in which the fluctuations have been associated with flares (flare stars), pulsations (RR Lyrae Variables; Cepheids; W Virginis stars), quasi-regular expansion/contraction of stellar envelopes (Mira Variables; semiregular variables), chaotic mass accretion (dwarf novae; recurrent novae; cataclysmic variables), variable mass ejection (P Cygni stars; Wolf-Rayet stars; planetary nebulae; OB giants; B emission stars), explosive thermonuclear burning (novae), and gravitational collapse (supernovae). These objects have yielded valuable information on stellar structure, dynamics, and evolution, and

provided a scale for the determination of cosmic distances (via the period-luminosity relation of the Cepheids, Figure 1.2). The characteristic amplitude and frequency of the variations are summarized in Table 1.1, and light curves of typical members of several groups of intrinsic variables are shown in Figures 1.3-1.5.

The study of temporal variations has also played a significant role in radio astronomy. The discovery of the pulsars and their interpretation in terms of the rapid rotation of a highly condensed object in a strong magnetic field provided the first observational evidence for the existence of neutron stars. Specific applications of pulsar observations include measurement of the frequency-dependent delay in pulse arrival times (dispersion measure) and of the pulsar "spindown" rate ( $-\dot{P}/P$ ), which allow determination of the source distance (or, alternatively, the mean line-of-sight electron number density) and age, respectively. Of greater significance to the development of theoretical high energy astronomy was the experimental proof that such collapsed objects represent a natural endpoint to some tracks of stellar evolution. This conclusion provided the framework for the binary accretion hypothesis for most of the galactic X-ray sources, in which the X-ray emission is attributed to the accretion of matter onto a collapsed object (i.e., neutron star or black hole) from a "normal" stellar companion.

### B. X-ray Astronomy

The study of cosmic X-ray sources (i.e., extra-solar objects radiating primarily in the 1-100 keV energy range ( $\lambda \sim .1-10 \text{ \AA}$ )) began in 1962 with the accidental discovery via rocket-borne detectors of the bright source Sco X-1 (flux  $\sim 2 \times 10^{-7}$  ergs  $\text{cm}^{-2}\text{s}^{-1}$ , 2-6 keV). By the end of the decade, numerous rocket and high-altitude balloon flights expanded

the catalog of discrete sources to roughly thirty and established the existence of a virtually isotropic diffuse X-ray background. In addition, these experiments resulted in the detection of X-ray emission from the well-known supernova remnant Tau X-1 (Crab Nebula) and the discovery of the first extragalactic X-ray source in the Virgo cluster of galaxies. In contrast to the stars in the solar neighborhood the majority of X-ray sources were variable in nature and concentrated toward the galactic plane, indicative of a non-local galactic origin.

The first satellite devoted entirely to the study of cosmic X-ray sources, UHURU, was launched in 1970 December. With a significantly longer time base for observations (years vs. minutes) and finer temporal and spatial resolution than those available in the earlier rocket surveys, UHURU increased the number of catalogued sources to 161 and led to the identification of several radio and optical counterparts (e.g., Cyg X-3 and Her X-1). The sources observed by UHURU are shown in galactic coordinates in Figure 1.6. These objects span a flux ( $S_x$ ) range of  $S_x(2-6 \text{ keV}) \simeq 3 \times 10^{-11} - 3 \times 10^{-7} \text{ erg cm}^{-2} \text{ s}^{-1}$ , corresponding to luminosities  $L_x$  in the range  $L_x(2-6 \text{ keV}) \simeq 4 \times 10^{33} - 4 \times 10^{37} d_1^2 \text{ erg s}^{-1}$  ( $d_1 \equiv d/1 \text{ Kpc} \sim 0.5 - 20$  for galactic sources), with the bulk of the emission appearing between  $\sim 1-20 \text{ keV}$ . As seen in Figure 1.6, there exists a clear concentration of sources within approximately  $10^\circ$  of the plane and a relatively sparse, roughly isotropic (excluding the Large and Small Magellanic clouds) source population at higher galactic latitudes. The majority of low-latitude sources (as well as several of the bright, higher latitude sources, e.g., Her X-1 and Sco X-1) have been identified with stellar systems (close mass-exchange binaries; supernova remnants; globular clusters) within the Milky Way. The nature

of the majority of the weak high-latitude sources, however, remains unresolved, with some having been identified with unusual galaxies or clusters of galaxies and others more recently associated with a significantly weaker class of galactic objects including the binary systems Algol and Sirius (Epstein 1976). Although a variety of astrophysical systems are capable of substantial X-ray production, the occurrence of relatively stable, intense ( $L_x \gtrsim 10^{35}$  ergs  $s^{-1}$ ) X-ray sources is rare in the galaxy, the total observed number of such objects amounting to only a small fraction ( $\sim 10^{-9}$ ) of the optical stars.

### C. Galactic X-ray Sources

#### 1. X-ray Binary Hypothesis

As estimated fifty percent (or more) of the stars in the Milky Way occur in binary or multi-component (bound) systems. One of the most significant contributions of UHURU was the association of several X-ray sources with short-period ( $P \lesssim 10$  d) binaries in which mass exchange between a "normal" star and compact secondary is occurring (see Figure 1.7). Early in the development of theoretical X-ray astronomy it had been demonstrated that the infall of material onto a compact object could produce gas temperatures of  $T \sim 10^8$  °K ( $kT \sim 10$  keV) and thus result in substantial thermal X-ray emission (Shklovski; Zel'dovich and Guseinov; Salpeter; Hayakawa and Matsuoka). Since the kinetic energy per particle gained in falling onto the X-ray secondary (denoted by the subscript 'x') is proportional to the ratio  $M_x/R_x$ , accretion onto neutron stars (K.E.  $\sim 100$  MeV/nucleon) and black holes (K.E.  $\sim 60$ -400 MeV/nucleon) is clearly more efficient than accretion onto white dwarfs (K.E.  $\sim 0.1$  MeV/nucleon) or nuclear burning of hydrogen on the stellar surface ( $E_{nuc} \sim 7$  MeV/nucleon). The mass-exchange rates ( $\dot{M}$ ) required

to produce a given luminosity are correspondingly lower for neutron star (ns)/black hole (bh) vs. white dwarf (wd) accretion:  $\dot{M}_{\text{ns/bh}} \simeq 10^{-9} L_{37} M_{\odot} \text{ yr}^{-1}$  vs.  $\dot{M}_{\text{wd}} \simeq 10^{-6} L_{37} M_{\odot} \text{ yr}^{-1}$ , where  $L_{37} \equiv L/10^{37} \text{ erg s}^{-1}$ . Though not attainable via isolated accretion from the interstellar medium ('ism',  $\dot{M}_{\text{ism}} \simeq 10^{-14} - 10^{-16} (M_X/M_{\odot}) M_{\odot} \text{ yr}^{-1}$ , Zel'dovich and Novikov 1967), sufficiently large mass transfer rates have been observed to occur during some stages of stellar evolution ( $\dot{M}_{\text{max}} \simeq 10^{-3} M_{\odot} \text{ yr}^{-1}$ ).

The process of mass-exchange can occur in two basic modes: (1) Roche-lobe overflow of the optical primary; and/or (2) enhanced stellar wind of this companion (see Figure 1.8). Observational evidence for both types of mass transfer exists, with the Her X-1/Hz Her and Cen X-3/Krzeminski's Star systems representing the archetypal examples of Roche-lobe overflow and stellar wind accretion, respectively. In the former case, the angular momentum of the infalling material will preferentially lead to the formation of a differentially rotating, thin accretion disk (cf. Prendergast and Burbidge 1968), while in the latter a much smaller (if any) disk will result. If the accreting object is a magnetized neutron star (e.g., Her X-1), the highly ionized gas will flow in along field lines to the magnetic poles, which, if misaligned with the rotation axis, will result in X-ray emission that appears (to an external observer) to be pulsed at the rotation period. Alternatively, if the accreting object is a black hole (Cyg X-1?), the gas will disappear at the Schwarzschild radius with the X-rays originating in the heated gas at the inner edges of the accretion disk.

## 2. Temporal Variability

The chaotic nature of the accretion mechanism has produced a large and diverse degree of variability in galactic X-ray sources (excluding

supernova remnants) on time scales ranging from milliseconds to years. On the shortest time scales, the detection of aperiodic millisecond "bursts" from Cyg X-1 has been interpreted in terms of shot-like emission resulting from accretion onto a black hole (Rothschild et al. 1974; see Figure 1.9). A similar situation with a neutron star as the accreting object may be implied by the recent discovery of the X-ray "bursters", a fraction of whose emission is sometimes confined to quasi-regularly spaced bursts approximately 1-10 seconds in duration (Figure 1.10).

Regular variations on short time scales ( $\sim .03$  sec - 16 min) have also been observed, with periodically pulsing sources such as Cen X-3, Her X-1, and Vela X-1 being associated with neutron star rotation in mass-transfer binaries. The pulsed nature of the emission from Her X-1 is well illustrated in the short rocket exposure displayed in Figure 1.11, which also shows the contrasting short-term variability of Cyg X-3 (statistical fluctuations) and Cyg X-1 (bursting). On somewhat longer time scales, occulting binaries with periods ranging from 1.7d (Her X-1; Figure 1.12) to 16.6d (Cir X-1) have been observed, facilitating the identification of optical and radio counterparts of several sources and aiding in the determination of the system parameters (e.g., mass function, semi-major axis, and orbital inclination and eccentricity). In addition, the detection of binary-phase-dependent variations such as the 4.8h sinusoidal modulation of Cyg X-3 (Leach et al. 1975), the 5.6d attenuation of Cyg X-1 centered on superior conjunction of the optical companion HDE226868 (Holt et al. 1976a), and the variation in low energy spectral cutoff at the 2.1d orbital period of Cen X-3 (Schreier et al. 1976) has contributed to a better understanding of these systems.

Several periodic and quasi-regular variations occurring on longer timescales (months-years) have also been observed. The nature of the most well-known of these, the "anomalous" 35<sup>d</sup> cycle of Her X-1 (shown in Figure 1.12) in which the source turns "ON" for 11 days and "OFF" for the remaining 24 days<sup>1</sup>, is still not completely resolved, with several mechanisms (e.g., free precession of the X-ray secondary, Brecher 1972; precession of the primary, Roberts 1974; Petterson 1975) apparently consistent with the observations. A longer-term, apparently aperiodic source modulation is exemplified by the extended "highs" and "lows" of sources such as Cen X-3 and Cir X-1 which have been attributed in the former case to large variations in the stellar wind density causing the X-ray source to be alternately "smothered" (i.e., totally self-absorbed by the wind) or "starved" by an accretion rate too low to produce an observable flux (Schreier et al. 1976). Another type of variation, operating on a timescale of  $\sim 10$  yr, has been inferred for Her X-1 based on the observed variability of its optical companion Hz Her (Jones, Forman, and Liller 1973), the brightness of which is linked to the level of X-ray emission through heating effects.

The variability of X-ray sources is not confined to the total energy output; the observed X-ray spectra are variable, as well. Spectral characteristics in general are necessary in determining such source parameters as temperature, particle densities, elemental abundances, and the nature of the energy mechanism itself. A number of distinct source spectra have been observed, which have been interpreted in terms of a variety of thermal (collisional) and non-thermal models. The

<sup>1</sup>There is now evidence for an additional, low-level turn-on near mid-phase of the cycle, cf. Holt et al. 1976f.

measurement of low energy cutoffs, i.e., the preferential absorption of X-rays with decreasing energy,  $S(E) \sim S_0(E) \exp[-N_H \sigma(E)]$ , have been useful in determining the distances to sources (when consistent with absorption by interstellar neutral hydrogen alone) or the presence of cold circumstellar material. In many cases spectral changes have accompanied temporal variations, as exemplified by the observed spectral transition of Cyg X-1 concurrent with an approximately five-fold decrease in the 2-6 keV flux (cf. Thorne and Price 1975). Cyg X-3 has also been observed to exhibit a spectrum which varies from a featureless blackbody distribution to a flat spectrum with iron line emission at  $\sim 6.7$  keV (both states corresponding to roughly the same 2-30 keV luminosity) over a timescale of  $\sim 1$  year (Serlemitsos et al. 1975). The value of such spectral/temporal measurements is clearly demonstrated by the determination of the binary nature of GX301-2, which resulted directly from the detection of regular variations in the spectrum of that source (Swank et al. 1976). It is apparent, then, that the study of both the spectral and temporal characteristics of X-ray sources is important to a detailed understanding of the nature of these systems.

#### D. Transient X-ray Sources

In early April 1967, a bright ( $S \sim 10 S_{\text{crab}}^{(2)}$ ) new X-ray source was discovered in the constellation Centaurus. A rocket survey of the same region conducted  $\sim 18$  months earlier had failed to detect an observable signal ( $S \approx 0.3 S_{\text{crab}}$ ) at the subsequently reported position. Further observations revealed a steady decline in brightness (see Figure 1.13), with the source (designated Cen X-2) again disappearing below detectable

<sup>2</sup> $S_{\text{crab}} \equiv 2\text{-}6 \text{ keV flux from the Crab nebula} \approx 1.6 \times 10^{-8} \text{ ergs cm}^{-2}\text{s}^{-1}$ .



levels ( $S \approx 0.4 S_{\text{crab}}$ ) by late September. The detection (through mid-1974) of at least three additional sources exhibiting roughly the same temporal behavior as Cen X-2 (Cen X-4, 3U1543-47, and 3U1735-28; see Figures 1.13, 1.14, and Table 1.2) firmly established the existence of the so-called "transient X-ray sources". It is apparent from Table 1.2 that these early sources are relatively bright objects ( $S_{\text{max}} \gtrsim S_{\text{crab}}$ ) located (except for Cen X-4) at low galactic latitude. In addition, although the initial increase phase was not observed in Cen X-2, all of the subsequently detected sources have been characterized by a sudden rise to maximum flux and gradual, nova-like decay.

In 1974 October the GSFC All-Sky Monitor, capable of monitoring the entire X-ray sky on a virtually continuous basis, was launched aboard the Ariel 5 satellite. During the first year of operation, five additional transient sources were detected by instruments onboard Ariel 5 (with several other candidates reported in IAU Circulars), implying a significantly higher rate of occurrence than suggested by the earlier observations. All of the sources (summarized in Table 1.3) for which light curves were obtained exhibit the characteristic nova-like variation of the earlier sources and satisfy the following approximate empirical criteria:

- (1) rapid rise ( $t_{\text{rise}} \lesssim 1 \text{ wk}$ ) to primary maximum ( $\Delta t_{\text{max}} \lesssim 1 \text{ wk}$ ) followed by a gradual decline with characteristic decay times in the range  $\tau_d \sim 1 - 8 \text{ wks}$  (e-folding) or  $t_{1/10} \sim 2 - 18 \text{ wks}$  (10% of maximum);
- (2) magnitude of outburst,  $S_{\text{max}}/S_{\text{min}} \gtrsim 10^3$ , with  $S_{\text{min}} < 1 \text{ UHURU ct s}^{-1}$  ( $\approx 1.7 \times 10^{-11} \text{ ergs cm}^{-2} \text{ s}^{-1}$ , 2-6 keV);
- (3) mean interval between possible recurrent outbursts,  $\bar{T}_{\text{rec}} > 2 \text{ yr}$ ; and

(4) preferential appearance at low galactic latitudes ( $|b| \lesssim 5^\circ$ ). We shall use these observed properties as a rough operational definition of the transient X-ray sources in this thesis. While the majority of "variable" sources are thus excluded by this definition, it will become evident later that a clear-cut distinction between the two source classes (i.e., 'transient' vs. 'variable') is not always possible. Finally, note that the recently discovered "weak, high-latitude transients", i.e., sources characterized by relatively low flux levels at maximum ( $S_{\max} \lesssim 0.1 S_{\text{crab}}$ ), rapid decay ( $\tau_d < 1 \text{ wk}$ ), and occurring at high galactic latitudes (cf. Ricketts, Cooke, and Pounds 1976), are also excluded by the above definition. As discussed in Chapter V, these sources almost certainly represent a distinctly different type of transient phenomenon from that described above.

#### E. Purpose

The limited scope of the early transient source observations (e.g., gaps in source coverage, crude temporal and spectral measurements) left the problem of the nature of these objects largely unresolved. As a consequence of their characteristic nova-like outbursts, thereby apparently distinguishing the transients from the more stable "permanent" X-ray sources, most of the early models attempted to interpret the new phenomenon in terms of analogous stellar objects (e.g., extragalactic supernovae; galactic novae) or more unconventional, hypothetical mechanisms (e.g., black holes traversing dense interstellar clouds, Sofia 1971; association with extragalactic radio outbursts, Pacini and Salvati 1974). In this thesis we attempt to apply observations of the All-Sky Monitor (ASM) to the problem of the nature of the transient X-ray sources. The ASM (described in detail in Chapter II) utilizes a pair of imaging

"pinhole-camera" proportional counters to provide virtually continuous coverage of  $\approx 80\%$  (instantaneously) of the X-ray sky in the 3-6 keV energy range at a sensitivity of  $S \sim 0.1 S_{\text{crab}}$ . With this type of instrument it was hoped to substantially increase our knowledge of the transient X-ray sources in two fundamental ways, viz.: (1) early detection and continued monitoring of the flux over the source evolution yielding comprehensive light curves for comparison with the various models; and (2) extensive sky coverage necessary (to avoid observational selection effects inherent in observations conducted by instruments with limited fields-of-view) in obtaining reliable information on such parameters as spatial distribution, rates of occurrence (and possible recurrence), and peak luminosities.

During the first two years of operation, the ASM and other Ariel 5 experiments have detected and monitored a number of new transient sources and observed highly variable, transient-like behavior in several known galactic sources. In addition, the galactic origin suggested by the earlier transients has been confirmed, with the over-all collection of transients consistent with an approximately uniform distribution in the galactic plane at distances  $d \approx 1$  Kpc. We propose that the observations are consistent with at least two distinct sub-classes of transient X-ray sources, including: (1) intrinsically bright ( $L_{\text{x,max}} \approx 10^{38} \text{ erg s}^{-1} \approx L_E$ )<sup>(3)</sup>, long-lived ( $\tau_d \approx 1$  month) sources occurring at the rate of  $\sim 1-10 \text{ yr}^{-1}$ ;

<sup>3</sup>The Eddington-limited luminosity ( $L_E$ ) is defined as the maximum, accretion-generated source flux, obtained when the radiation pressure becomes equal to the gravitational force on an infalling particle;

$$L_E \approx 1.3 \times 10^{38} \left( \frac{M}{M_\odot} \right) \text{ erg s}^{-1}.$$

and (2) weaker ( $L_{X,\max} \lesssim 10^{38} \text{ erg s}^{-1}$ ), shorter duration ( $\tau_d < 1 \text{ month}$ ) sources with a frequency of occurrence of  $\sim 5\text{-}100 \text{ yr}^{-1}$ . It is suggested that both of these source sub-classes may be reconciled with the standard X-ray binary accretion model, with outbursts attributed to episodic mass exchange resulting from Roche-lobe overflow of the primary, or alternatively, large fluctuations in the density of the stellar wind from the companion.

## CHAPTER II

### EXPERIMENT DESCRIPTION

The Goddard Space Flight Center All-Sky Monitor is one of a complement of six cosmic X-ray experiments aboard the Ariel 5 satellite, the combined fields-of-view of which instantaneously cover most<sup>1</sup> of the X-ray sky (see Figures 2.1 - 2.3). Four experiments are aligned with (or at a small angle to) the spin axis and include: 1) a rotation modulation collimator (RMC), operating in the energy range 0.3 - 20 keV, and capable of determining positions to an accuracy of  $\sim 2$  arc min for bright sources; 2) a high resolution proportional counter spectrometer with a 128 channel pulse height analyzer, sensitive to photons between 2 - 30 keV; 3) a polarimeter/spectrometer operating in the 2-8 keV range and capable of detecting a polarization of  $\sim 3\%$  (for source brightnesses comparable to that of the Crab Nebula) and of conducting searches for pulsar periodicities; and 4) a scintillation telescope (ST) devoted to temporal and spectral studies of sources at energies  $> 40$  keV.

While these four experiments are devoted to a detailed study of the small region within  $\sim 10^\circ$  of the satellite pole, the ASM and Sky Survey Instrument (SSI) cover wide regions of the sky with limited spatial and spectral resolution. This latter experiment consists of a large area proportional counter located in the spacecraft equatorial region and scans an  $\sim 20^\circ \times 360^\circ$  wide band of sky on each satellite rotation. The SSI covers the energy range 1.5 - 20 keV and is capable of conducting a high sensitivity survey of the sky, obtaining source locations, intensities, and spectra.

<sup>1</sup>Except for a small region ( $\theta \sim 8^\circ$ ) centered on the spacecraft South Pole.

The All-Sky Monitor provides coverage of the remainder of the sky in the 3-6 keV band. It is intended primarily for use as an early detection system for transient events in conjunction with the other, more sensitive instruments, and as a continuous monitor of variable and transient phenomena in the relatively bright ( $S \gtrsim 0.2 S_{\text{crab}}$ ) galactic sources. The ASM is the first true imaging experiment to be flown on a satellite, with the imaging accomplished via a pair of X-ray pinhole cameras, (each devoted to 1/2 of the celestial sphere) which utilize position-sensitive anodes together with satellite rotation of the intrinsic fan-beam response to uniquely assign the direction of an incident ionizing event. Gas-filled proportional counters provide the detection medium, with electronic thresholds and an acceptance window defining a maximum response to X-rays in the 3-6 keV band.

Weight and data restrictions imposed on Ariel 5 result in a much lower ASM data rate ( $\sim 1 \text{ bit-s}^{-1}$ ) than that of more sophisticated experiments (e.g., the bit rate on the GSFC OSO-8 X-ray experiments  $> 1 \text{ K bit-s}^{-1}$ ), with a correspondingly low duty cycle for source observations ( $\sim 1\%$ ) and no spectral information obtainable within the 3-6 keV acceptance window. Spatial and temporal resolution have been sacrificed at the expense of all-sky coverage, with an optimal (coarse mode) angular resolution of  $\Delta\theta \sim 5^\circ$  and temporal resolution of  $\Delta t_r \gtrsim 100$  minutes (= one orbit), respectively. The remainder of this Chapter is devoted to a detailed description of the experiment.

#### A. Position Measurement

Several techniques for determining the direction of incoming nuclear particles or high energy photons have been devised in recent years, including measurement of pulse arrival times along a helical cathode

delay line (Lee and Sobottka 1973), and measurement of the risetime (Borkowski and Kopp 1968) and/or amplitude of output voltage pulses from a highly resistive anode (Desai and Holt 1972). While the first two methods dictate relatively complicated electronics and substantial power requirements, simple charge division along a highly resistive anode can be accomplished in a comparatively straightforward fashion with a combination of charge-sensitive preamps and a pulse-height measurement circuit. A simplified schematic circuit diagram illustrating the principle of operation of a position-sensitive anode is shown in Figure 2.4. An event incident at point P along the wire causes charges  $Q_I = \frac{X}{L} Q$  and  $Q_{II} = \frac{L-X}{L} Q$  to be collected in the respective pre-amps, where the total charge  $Q$  is a function of detector gain, photon energy, and anode resistance. The position of the event ( $X/L$ ) is determined by measuring the ratio of the voltage signal (proportional to the charge collected) from one of the pre-amps to the sum of the outputs. Note that the sum is required if the determination of  $X/L$  is to be independent of X-ray energy  $E$  and internal gain and energy resolution of the detector. Pulse rise times and amplitude characteristics for the type of resistive anode proportional counter used in the present experiment are shown in Figure 2.5.

The measurement of the voltage ratio is accomplished via standard ramp rundown analyzing techniques (Streeter 1973), and a block diagram illustrating this part of the circuit is shown in Figure 2.6. To optimize the position resolution of events along the wire, a highly resistive anode of uniform resistivity is essential. Quartz fiber with pyrolytically deposited graphite (diameter  $\approx 25 \mu\text{m}$ ; resistivity/unit length  $\approx 1 \text{ M}\Omega \text{ cm}^{-1}$ ) is capable of position discrimination of better than 1 mm along a 30 cm

(active length) anode ( $\frac{\Delta X}{L} \approx 0.4\%$ , Desai and Holt 1972), and was employed in the detector. The position information (contained in the ratio  $\frac{V_I}{V_I + V_{II}}$ ) is translated via an analog-to-digital converter into a 6-bit spacecraft latitude address with one bit indicating the counter and the remaining five specifying the event position (i.e., a total of  $2^5 = 32$  locations per anode are possible). This information, together with a similar address specifying the spacecraft longitude of the event (discussed below) is then transmitted to the data storage area ("core store") allotted to the ASM. A comprehensive block diagram of the experiment electronics is illustrated in Figure 2.7.

## B. X-Ray Pinhole Camera

### 1. Optimal Geometry and Design

Given the capability to define the position of an ionizing event along the resistive anode to sufficient precision, imaging of the X-ray sky is accomplished via "light-tight" (for X-rays in the energy range of the experiment,  $\sim 2 - 8$  keV) boxes with "pinhole" apertures in one corner, as shown in Figure 2.8. The relative dimensions of anode length ( $l$ ), pinhole area ( $a^2$ ), detector element area ( $b^2$ ), and pinhole-anode separation ( $h$ ) are constrained by considerations of optimum sensitivity<sup>2</sup> and weight restrictions. It can be shown that (cf. Holt 1976) for a total background dominated by contributions from the isotropic, diffuse X-ray "background" ( $D_B = D_{B_0} \frac{a^2 b^2}{h^2}$ ), the sensitivity is optimized by the condition  $a = b$ , dependent only on the aperture-detector distance  $h$

<sup>2</sup>Signal-to-noise ratio,  $S.N. \equiv S/\sqrt{B}$ , where  $S$  and  $B$  represent source and total background counts, respectively.



(and an accumulation time long enough to assure that the source exposure is not quantum-limited, i.e.,  $S > \delta S = \sqrt{S + 2B}$ ). It can be further demonstrated that the condition  $a = b$  results in maximum sensitivity for the case of background which does not arise primarily from incident X-rays (internal background  $I_B = I_{B_0} b^2$ ). We thus have the result that the pinhole camera sensitivity is optimized for  $a \approx b$  whatever the primary source of background.

The final experiment configuration was fixed by satellite constraints (e.g., weight, volume, and data allowances) which dictated an aperture size  $a^2 = 1 \text{ cm}^2$ , aperture-anode distance  $h = 15 \text{ cm}$ , and corresponding active anode length  $l = 30 \text{ cm}$  for a one-dimensional  $90^\circ$  field-of-view (see Figure 2.8). The box enclosing the detector (including a dividing wall between the two cameras) is constructed of  $\sim .1 \text{ mm}$  titanium backed with aluminum (to absorb the K fluorescence of the titanium) in a honeycomb structure. This results in a relatively low-weight, rigid, light-tight ( $E_\gamma \sim 2 - 8 \text{ keV}$ ) enclosure as required by the experiment.

## 2. X-ray Imaging

As the available space aboard the Ariel 5 did not allow a stationary array of multi-anode proportional counters to image the sky, the combined intrinsic fan-beam response of two single-anode pinhole cameras (Figures 2.8 and 2.9) was utilized together with the satellite rotation for this purpose. The celestial sphere is thus scanned by the detector on every rotation of the satellite ( $P_{\text{rot}} \sim 6 \text{ sec}$ ).

The division of the sky into "resolution elements" was again dictated by the space allotted the ASM in the satellite core-store memory. A total of 576 data words were divided into 512 "fine" (8-bit) and 64 "coarse" (16-bit) locations for count accumulation. Incident ionizing

X-ray events are assigned to the appropriate core-store location on the basis of their position in the spacecraft coordinate system. The spacecraft latitude (D) and longitude (A) of an event are defined by its position along the anode as described above, and by the phase of the satellite rotation relative to the sun ( $A_{\text{sun}} \equiv 0^{\circ}$ ), respectively. This latter coordinate is obtained via a system of sensors which are used to determine the position of the sun; the satellite rotation is then divided into equiangular longitudinal sectors by an onboard "sector generator". Although the inherent resolution of the anode and the available electronics allow division into 64 separate, equal-length segments, the tactical decision was made to allocate the 512 fine locations to 16 latitudinal elements (8 per counter) and 32 longitudinal sectors ( $\Delta A = 11^{\circ}.25$ ). The latitudinal elements were defined in such a way as to be generally consistent with a uniform source sensitivity over the anode. This was accomplished by decreasing the latitude extension of elements closer to the satellite equator where source exposure is least to correspondingly lower the internal background. "Dead bands" were introduced at the spacecraft poles and equator (anode extremities) where the pinhole apertures are least efficient (resulting from poor spatial resolution at the poles and minimal source exposure at the equator). In addition, other experiments onboard the spacecraft with higher sensitivity than the ASM view in these regions. The final nominal latitudinal borders were determined as shown in Figure 2.10 and the over-all imaging scheme is illustrated in Figure 2.11, which shows the 512 resolution elements in spacecraft coordinates. The average element subtends a solid angle of  $\sim \frac{4\pi}{512}$  steradians ( $\sim 10^{\circ} \times 10^{\circ}$ ), and the typical source image size of  $\sim 3^{\circ} \times 5^{\circ}$  therefore implies that a source may divide between as many as four elements (but

usually contributes to only one or two). The relative source image-resolution element dimensions are illustrated in Figure 2.11.

### C. Energy Characteristics

#### 1. Detector Response

The energy response of the proportional counters is a function both of the fill-gas (composition and pressure) and of the sealing window. A P10 gas mixture (90% argon, 10% methane) at a pressure of 1 atmosphere was employed, resulting in a peak opacity to X-rays of energy  $E_v \approx 3.2$  keV. A relatively thick (5 mil) Beryllium window was selected. Although this results in a minor sacrifice of efficiency, it reduces the rate of gas diffusion from the counters and also increases the long-term stability of the window response (this is essential as the data limitations do not permit more than a single energy channel). The transmission of photons by the window (thickness =  $x$ , absorption coefficient =  $\mu$ ) varies as  $S_{trans} \sim S_{inc} \exp(-\mu_{Be}(E)x)$ , which when combined with the P10 absorption curve produces the net energy response<sup>3</sup> to a "flat" X-ray beam ( $\frac{dn}{dE} inc = \text{constant}$ ) shown in Figure 2.12. Finally, because of the relatively severe data limitations it was impossible to take advantage of the inherent energy resolution of the proportional counters ( $\frac{\Delta E}{E} \sim 16\%$  FWHM for  $Fe^{55}$  at 5.9 keV).

#### 2. Mean 3 - 6 keV "Efficiency"

One of the primary ASM objectives is to measure detector-independent incident photon fluxes in the nominal (3-6 keV) energy range. Electronic

<sup>3</sup>The detector energy response, i.e., the fraction of incident X-rays detected as a function of energy, is the product of the window transmission and gas ionization efficiency:  $R(E) = \frac{S_{trans} (Be \text{ window}) \times S_{abs} (P10 \text{ gas})}{S_{inc}}$

thresholds are established at 2.5 and 7.5 keV (energy equivalent at nominal gain) by rejecting sum pulses outside of a fixed voltage range. Fluxes may be computed in terms of effective (incident) 3-6 keV photons via a mean efficiency,  $\epsilon$ , obtained by folding known, representative source spectra through the detector energy response. The mean efficiency is formally defined as the ratio of source photons detected to the total number of incident source photons (3-6 keV):

$$S_{\text{inc}}(3-6 \text{ keV}) = \int_{3 \text{ keV}}^{6 \text{ keV}} S(E) dE$$

$$\approx \frac{1}{\epsilon} \int_{\frac{2.5}{A_g} \text{ keV}}^{\frac{7.5}{A_g} \text{ keV}} S(E) R(E, E') dE',$$

where  $S(E)$ ,  $R(E, E')$ , and  $A_g$  are the incident source photon spectrum (photons  $\text{cm}^{-2} \text{sec}^{-1} \text{keV}^{-1}$ ), detector energy response (Figure 2.12), and detector gain (a function of gas pressure and high voltage setting;  $A_{g, \text{nominal}} = 1$ ), respectively. The variation of  $\epsilon$  as a function of detector gain is shown in Figure 2.13 for three representative source spectra, viz.: the Crab Nebula ( $S(E) \propto E^{-2} \text{ cm}^{-2} \text{ s}^{-1} \text{ keV}^{-1}$ , Boldt, Desai, and Holt 1969); Sco X-1 ( $S(E) \propto E^{-1} \exp(-E/5.5 \text{ keV}) \text{ cm}^{-2} \text{ s}^{-1} \text{ keV}^{-1}$ , Holt, Boldt, and Serlemitsos 1969); and the diffuse background ( $S(E) \propto E^{-1.4} \text{ cm}^{-2} \text{ s}^{-1} \text{ keV}^{-1} \text{ steradian}^{-1}$ , Boldt et al. 1969). It is apparent from Figure 2.12 that the gain can change by as much as a factor of  $\sim 2$  (from the nominal value) before noticeable degradation in the detector 3-6 keV efficiency for typical sources may occur.

### 3. Calibration

Due to the diffusion of the counter gas through the Beryllium windows,

the gain will increase slowly in time with a corresponding degradation in detector efficiency. As there are no calibration sources onboard the spacecraft for the purpose of monitoring variations in gain, two natural "calibration" sources are employed. The Crab Nebula, as a result of its stable spectrum and virtually constant flux (over timescales  $\gg$  experiment lifetime), represents one such source. The average internal background is also a useful indicator of the gain since the relatively flat spectrum of charged particles producing pulses in the 3-6 keV band will result in an inverse variation of internal background with gain (the equivalent energy width,  $E_{\text{upper}} - E_{\text{lower}}$ , defined by the electronic thresholds is inversely proportional to  $A_g$ ). If a significant degradation in the detector efficiency is indicated by a long-term decrease in the measured intensity of the Crab Nebula and the average level of internal background, four discrete high-voltage settings are available to return the gain closer to the nominal value in the affected counter(s). As the electronic thresholds are fixed in voltage, switching the high voltage modifies both the region and extent of the energy response curve sampled by the experiment and hence the energy equivalents of the thresholds, as illustrated in Figure 2.14. It can be seen that an increase in gain effectively results in a shift to the lower energy portion of the response curve, thereby requiring a lower high-voltage setting to return to nominal gain and efficiency (see also Figure 2.13).

#### D. Background

As discussed above (optimization of detector geometry), there are primarily two different types of background which interfere with the detection and measurement of sources. Internal background is defined as that component of the noise which arises from triggering of the counters

by high-energy charged particles, and has been minimized in four ways. Two of these are provided by the Ariel 5 satellite and consist of: (1) a relatively clean, near-equatorial, roughly circular orbit (inclination<sup>4</sup>  $2.8^{\circ}$ ; altitude =  $520 \pm 30$  km); and (2) radiation monitors which are used to disable the experiment high-voltage whenever pre-selected threshold levels are exceeded (as occurs regularly within the well-known "South Atlantic Anomaly" low-latitude extension of the trapped radiation belts). The other two techniques employed to maintain a low internal background are designed into the detectors themselves and involve rejection of events at the anode ends (outermost  $\sim 1$  cm) and active anti-coincidence cells which completely surround the position-sensitive volume on all sides except that facing the Beryllium window, as shown in Figure 2.12. Since the internal background rates should be independent of the phase of the satellite rotation (i.e., spacecraft longitude), the mean charged particle contamination per latitudinal element may be measured for each orbit as described in the next Chapter. The "diffuse background" consists of actual X-ray events arising from the approximately isotropic diffuse X-ray background and is a function of the solid angle subtended by a detector element and earth occultation of that element. This component must therefore be computed for each element on an orbit-to-orbit basis as outlined in Chapter III.

The sun occasionally represents an additional source of contamination (when not in the equatorial band of the spacecraft), as solar X-rays may scatter into the pair of longitudinal sectors centered on

<sup>4</sup>Inclination  $\equiv$  angle between earth equatorial and satellite orbit planes.

the sun (see Figure 2.11). However, the solar image is always well-localized and does not introduce appreciable background into the remaining 496 resolution elements. Another sun-related source of X-ray background is that of auroral X-rays originating in the earth's atmosphere, coincident with major solar flares. The presence of occasionally large auroral X-ray fluxes has also been reported from the SSI (Seward et al. 1976). When such contamination is indicated the data is recorded but not included in the analysis procedure. Finally, under the general description of "background" is the possibility of "bit errors" occurring during data collection and/or transmission to the ground tracking stations. The possibility of such errors going undetected is negligible due to the storage of each event into two separate sets of data accumulation registers corresponding to the 512 resolution elements and to 64 longitudinal sector counters (sum of 8 latitudinal elements). As this summing is performed at the front-end (i.e., each ionizing event is registered in both accumulators separately), telemetry errors are easily identified by disagreement of the individual and sum counters. This capability also enables measurement of very strong sources (i.e., > 256 counts/orbit) which would otherwise be limited by the resolution element capacity of  $2^8 - 1 = 255$  counts (a given element recycles to 0 with the 256th count).

#### E. Octant Mode

The preceding description applies to the normal experimental mode of operation ("All-Sky" mode) in which the 512 "fine" core store locations are devoted to nearly the entire sky. Another, finer spatial resolution mode ("Octant" mode), in which the 512 detector elements are restricted to only  $\sim 1/16$  of the sky (see Figure 2.15), is available upon command. The effect is to increase the resolution in both spacecraft latitude

and longitude by a factor of  $\sim 4$ , resulting in a typical Octant mode resolution element of approximately  $2^\circ \times 2^\circ$ . The subsequent ability to resolve sources as close as  $\sim 4^\circ$  and an effective decrease in the local source background result in an increase in the ultimate experimental sensitivity to the approximate level of  $0.05 \text{ cm}^{-2}\text{s}^{-1}$  ( $\sim 40 \text{ UHURU cts s}^{-1}$ ) as compared to the All-Sky mode threshold of  $\approx 0.1 \text{ cm}^{-2}\text{s}^{-1}$  (non-confused regions). As this mode violates the prime objective of continuous full-sky coverage, however, it is used sparingly for the purposes of finer position determination of transient phenomena, detection of emission from weak sources, and resolution of sources in confused sky regions (e.g., Galactic Center).

#### F. Satellite Operation

The Ariel 5 was launched from the San Marco launch platform in the Indian Ocean on 1974 October 15. In lieu of the conventional tape recorder, which frequently limits the satellite useful lifetime, a unique core-store memory unit is employed to collect data during the sunlit portion ( $\sim 3500$  seconds) of each  $\sim 100$  minute orbit. Data cannot be transmitted to the ground in real time, and the core-store is normally "dumped" during passes over tracking stations at Quito, Ecuador or Ascension Island (South Atlantic Ocean) on each orbit. The satellite rotates at an average rate of  $\sim 10 \text{ revolutions min}^{-1}$  and the spacecraft attitude (spin axis pointing direction) is determined on each orbit by a combination of star trackers and sun sensors. A large degree of maneuverability is provided by a gas-jet system and back-up magnetorquer which enables a relatively rapid response of the satellite to transient phenomena in new or existing sources. A long-range viewing program is adopted and



revised each month and is formulated primarily upon objects of interest for viewing by the pole-aligned and SSI experiments. The only constraint upon spacecraft attitude is dictated by the solar cells which must be aligned within  $45^{\circ}$  of the sun for proper charging of the spacecraft's battery supplies. Figure 2.16 represents a block diagram of the major components of the spacecraft systems.

CHAPTER III  
DATA ANALYSIS

In order to accomplish the tasks of detecting new sources and measuring the flux of existing ones, a number of factors must be considered. Several of these have been mentioned above, and the broad group of experimental factors may be divided into the general classifications of:

- (1) computation of effective source exposure time, including correction for variation of source exposure with spacecraft latitude;
- (2) determination of diffuse and internal background levels; and
- (3) calculation of geometrical factors, including the spacecraft location and "splitting" of sources into several resolution elements and correction for possible detector offsets.

A. Source Library

X-ray sources have been compiled into a library which is used as input to the various analysis programs. This library includes sources observed by the UHURU, OSO-7, OAO Copernicus, Ariel 5, SAS-3, and OSO-8 satellites. Other potential X-ray emitting objects (e.g., earlier transient sources, optical novae, radio pulsars) are also entered. As source fluxes are typically specified in units of equivalent UHURU counts  $s^{-1}$ , a conversion factor to incident 3-6 keV photons  $cm^{-2}s^{-1}$  is required.

The computation is performed in Appendix A, with the result

$$\kappa \equiv \frac{\text{ASM 3-6 keV photons } cm^{-2}s^{-1}}{\text{UHURU counts } s^{-1}} = 1.5 \pm .5 \times 10^{-3},$$

where the error arises primarily from uncertainties in source spectral shape. Typical flux levels and variability of the brightest 80 library sources in ASM units are shown in Table 3.1 (for comparison, the UHURU minimum intensities of Sco X-1 and the Crab Nebula are 6800 counts  $s^{-1}$  and 947 counts  $s^{-1}$ , respectively). The source catalog is continuously updated to include

newly discovered transient sources as well as previously undetected quasi-stable weak sources.

## B. Computation Factors

### 1. Source Exposure

The effective exposure time of a source to the ASM during an orbit is a function of the detector on-time (which in turn depends on the orbit duration and the presence of large charged-particle fluxes which trigger high voltage-disabling background rate flags), earth occultation, and source spacecraft latitude. Thus, a particular ( $i^{\text{th}}$ ) source will be 'ON' for a time

$$T_s(i) = [T_{\text{dur}} - T_{\text{dis}}(i)] * \text{LCOR}(D_i),$$

where

$T_{\text{dur}}$  = Orbit duration,

$T_{\text{dis}}(i)$  = "Disable" time of  $i^{\text{th}}$  source

=  $T_{\text{ecl}}$  (Eclipse time) +  $T_{\text{flg}}$  (Background rate flag duration)

+  $T_{\text{occ}}(i)$  (Earth occultation time of  $i^{\text{th}}$  source),

and

$\text{LCOR}(D_i)$  = Latitudinal correction factor for  $i^{\text{th}}$  source (spacecraft latitude  $D_i$ ).

The orbit duration, eclipse time, and duration of background rate flags are computed from an event-time array generated by the various satellite sensors. This array consists of event codes indicating eclipse entry/exit, background rate flag enable/disable, start/end of orbit, power on/off, and the times corresponding to these events. In addition, experiment power, sunlight/eclipse bits, and housekeeping information (high voltage and anticoincidence rate analog parameters) are recorded

at 1000 second intervals throughout the orbit. The computation of the net detector disable time from the event-time array is relatively straightforward, but care must be taken to correct for overlapping disable periods (e.g., source occulted with background rate flags ON).

Intervals within the sunlit portion of an orbit during which a source is occulted by the earth ( $T_{\text{occ}}(i)$ ) will vary from source to source, being a function of the source position (R.A.; Dec.), sun position (R.A.; Dec), and orbit parameters (radius, inclination, and X-ray scale height of atmosphere). The computation of source occultation times consists of finding both the fraction of an orbit that the source is occulted by the Earth and the phase of the occulted portion with respect to the sun. This procedure is outlined in appendix B and results in the generation of another set of source 'OFF' times which are combined with the detector disable times (i.e., experiment high-voltage OFF) from the event-time array to compute the individual source 'ON'-time for the orbit. A plot of the mean unocculted fraction ( $\eta$ ) vs. angular separation from the sun for several sources of interest is shown in Figure 3.1.

The latitudinal correction factor (LCOR) arises from the geometrical property of a scanning aperture that as the elevation of a source approaches the rotation axis it remains in the detector field-of-view for an increasing fraction of the satellite rotation. Using the definition  $\text{LCOR}(D) \equiv \frac{\phi_{1\text{on}}(D)}{2\pi}$ , where  $\phi_{1\text{on}}(D)$  = FWHM of triangular longitudinal "extent"<sup>1</sup> of a source, it is clear that the latitudinal correction factor approaches

<sup>1</sup>Note that this is not the same as the static "fan beam" response,  $\phi_f$  (see Figures 2.8 and 2.9).

the limiting values at the spacecraft equator and pole of LCOR ( $D = 0^\circ$ )  
 $= \frac{\phi_{1on}(0^\circ)}{2\pi} = \frac{\phi_f(0^\circ)/2}{2\pi} = 0.0075$ , and LCOR ( $D = 90^\circ$ )  $= \frac{\phi_{1on}(90^\circ)}{2\pi} \approx$   
 $\frac{2\pi}{2\pi} = 1$ , respectively. It should be noted, however, that for source  
 elevations within the ASM field-of-view (recall  $D_{max} \sim 85^\circ$ ) the effective  
 limiting value is considerably reduced, viz., LCOR ( $D = 85^\circ$ )  $= \frac{\phi_{1on}(85^\circ)}{2\pi}$   
 $\approx \frac{33^\circ}{2\pi} = 0.092$ . A detailed derivation of a general expression for LCOR ( $D$ )  
 is presented in Appendix C and is plotted in Figure 3.2.

## 2. Background Correction

As discussed earlier, background counts arising from the diffuse X-ray background and from energetic charged particles contribute to the net experiment counting rates and must therefore be subtracted from the data. The expected contribution to a resolution element from the diffuse X-ray background (assumed isotropic; see Schwartz, Murray, and Gursky 1976) may be computed from the 3-6 keV efficiency ( $\epsilon$ ), the net ( $j$ th) element ON-time ( $T_e(j)$ ), and the "geometrical factor" ( $G_i \equiv \frac{C_i}{I_0}$ ,  $C_i$  = counting rate of  $i^{th}$  latitudinal element ( $i = 1-8; 9-16$ ) and  $I_0$  = intensity of isotropic source). This latter quantity is proportional to the solid angle subtended by a given resolution element and is thus a function of the aperture and detector element dimensions and aperture-anode separation. As outlined earlier, the spectrum of the diffuse background integrated with the detector response between the nominal 2.5 - 7.5 keV energy thresholds results in a value of  $\epsilon \approx 0.6$ . The net element ON-time ( $T_e(j) = (T_{dur} - T_{dis}(j))/32$ ) is determined as in the preceding section with the "source" coordinates defined by the center of the element. In this case, however, the factor LCOR  $\equiv 1$ , independent of the element spacecraft latitude. Using the geometrical

factors derived for the pinhole cameras in Appendix D and listed in Table 3.2 the expected contribution (detected counts) to an element due to the diffuse background is:

$$N_{db} = G_i * \epsilon I_o * T_e(j), \text{ where}$$

$$I_o = \int_{3 \text{ keV}}^{6 \text{ keV}} 7 E^{-1.4} dE \text{ (cm}^2 \text{ sec keV Sr)}^{-1}$$

$$= 2.73 \text{ (cm}^2 \text{ sec Sr)}^{-1}.$$

For a typical ( $\sim 6000$  second) orbit with  $T_e(j) \approx \frac{3200}{32}$  seconds, elements adjacent to the  $D = 45^\circ$  border ( $G_i \approx 0.01$ ) will receive only  $\sim 2$  diffuse background counts.

"Internal" background (i.e., that component resulting from high energy charged particles) levels vary with a number of factors, including particle densities, anode length corresponding to a detector element, and net detector ON-time. Since this contribution is expected to be independent of the relative phase of satellite rotation, each latitudinal segment of the anode is analyzed individually in both counters on an orbit-to-orbit basis. Evaluation of the mean particle background per latitudinal segment is accomplished by first rejecting any of the 32 longitudinal elements which are expected to receive counts from library sources. The expected diffuse background contribution to the remaining elements is then subtracted from the detected counts and the excess attributed to charged particle contamination. The mean particle background for that latitude is finally calculated in an iterative manner by successively rejecting all elements that deviate from the previous mean by more than  $\pm 3\sigma$ . Typical internal background rates per element (6000 second orbit) vary from  $\sim 7$  counts near the spacecraft pole (longest anode segments) to  $\sim 1-2$  counts in the

near-equatorial elements. A relatively high level of particle contamination ( $\sim 4$  counts/element) has been observed in the equatorial segments and attributed to anode end effects.

### 3. Spatial Response

The technique employed in the ASM for mapping the X-ray sky into a 512 resolution-element ( $\sim 10^\circ \times 10^\circ$  in all-sky mode) image has been described in Chapter II. As sources frequently divide into 2-4 elements, knowledge of the detector latitudinal and longitudinal response is necessary to compute the fraction of the total flux contributed to each element. The source position in spacecraft coordinates is obtained via a simple transformation of its celestial coordinates using the satellite aspect solution and the position of the sun. The spatial response of the detector to point sources is illustrated in Figure 3.3. The latitudinal response is flat, representing simply the "shadow" cast by the pinhole onto the anode. As shown in Table 3.3 the latitudinal extent  $\Delta\theta$  of a source is greatest at spacecraft latitude  $D = 45^\circ$  and decreases toward the pole and equator. It is readily observed with reference to Figure 3.3a that the relative contributions of a source splitting between two latitudinal regions a and b (borderline  $D_{ab}$ ) are

$$F_{lat}^a = \frac{|D_{ab} - \theta_1|}{\Delta\theta} \quad \text{and} \quad F_{lat}^b = \frac{|D_{ab} - \theta_2|}{\Delta\theta}, \quad \text{where } \Delta\theta = |\theta_2 - \theta_1|$$

(note that  $\sum F_{lat} = 1$ ).

Calculation of source splitting in spacecraft longitude is slightly more complicated, since the detector response is now triangular (as opposed to flat) as shown in Figure 3.3b. In addition, the increase in longitudinal extent of sources with increasing spacecraft latitude (see Figure 3.4) must also be taken into account. The fractional source contribution

( $F_{lon}$ ) to a longitudinal element is obtained by taking the ratio of the area under the response curve within the element to the total area,  $\phi_{lon}$  (D). Thus, the total fractional source contribution to a detector element b is given by  $S_{frac}^b = F_{lat}^b * F_{lon}^b$ .

#### 4. Spatial Offsets

During the initial months of ASM operation it became evident that "offsets" ( $< 1^\circ$ ) in the detector geometry (latitude and longitude) exist, as determined from the relative splitting of Sco X-1 and the sun. While the exact origin of these errors is uncertain (aspect errors, experiment misalignment, electronic offsets on the anode, and imprecise sector generator are all possible contributing factors), steps have been taken to empirically compensate for them. To correct for the latitudinal error, permanent offsets for each counter have been estimated and a program which compares the expected and actual latitudinal splitting of Sco X-1 is used to "readjust" the spin axis (up to  $1^\circ$ ) such that agreement is obtained. Longitudinal offsets are introduced when indicated by poor spatial fits to sources (primarily Sco X-1 and the Crab Nebula) and consist of a small "rotation" ( $\sim 1^\circ$ ) of the detector in spacecraft longitude.

#### C. Source Measurement and Detection

##### 1. Flux Measurement

Fluxes are assigned to known X-ray sources on an orbit-to-orbit basis as follows:

1) the source library is mapped into spacecraft coordinates and the exposure and relative splitting of sources within the detector field of view are computed;

2) each of the elements corresponding to the source under examination is checked for the presence of other contributing sources; if less than



90% of the expected counts (based on maximum library intensities) in an element are due to the source in question the element is rejected in the redefinition procedure;

3) the counts (background corrected) from the elements satisfying the 90% criterion are summed, as are the corresponding source fractions;

4) the ( $j^{\text{th}}$ ) source flux is computed from  $S^j = \left( \sum_{i=1}^{M=1,2,\text{or }4} C^i \right) / F^j$ ,

where

$$F^j = \left( \sum_{i=1}^M S_{\text{frac}}^{ji} \right) * T_S^j * \text{LCOR}^j * \epsilon * A_p, \text{ and}$$

$$C^i = O^i - B^i \text{ (Detected-Background counts, } i^{\text{th}} \text{ element),}$$

$A_p$  = Projected pinhole area

$$= 1 \text{ cm}^2 * \cos |D - \pi/4|, \text{ and}$$

$T_S$ ,  $\text{LCOR}$ ,  $\epsilon$ , and  $S_{\text{frac}}$  are as defined earlier;

5) the error in this measurement is taken as the  $1\sigma$  Poisson

statistical uncertainty,  $\text{Err}^j \equiv \left[ \sum_{i=1}^M (O^i + B^i) \right]^{1/2} / F^j$ ; and

6) the measured flux is folded back through the detector response and the resultant expected counts compared to the detected counts; if (due to offsets or other systematic errors) any of the source elements are consequently found to be  $>3\sigma$  below the expected level, the computed flux is successively decreased until this condition is eliminated or until the source is redefined back to its minimum library intensity.

As a result of the intrinsically low single orbit source counting rates ( $\dot{C}$  (Sco X-1)  $\approx$  150 - 500 counts/orbit) the satellite capability of maintaining a fixed orientation ( $\Delta\beta < 0.5^\circ$ ) for periods  $\approx$  1/2 day is utilized for the purpose of combining up to 7 orbits into  $\approx$  1/2 day "accumulations". The resulting factor of  $\approx \sqrt{7}$  improvement in counting

statistics at the expense of temporal resolution correspondingly increases the effective experiment sensitivity with respect to the detection and monitoring of relatively weak sources ( $S \lesssim 0.5 S_{\text{crab}}$ ). Longer accumulation periods, although allowed by the slow drift rate of the satellite spin axis, have not been employed due to the apparent motion of the sun ( $\sim 1^\circ/\text{day}$ ).

## 2. Source Detection

The detection of new sources (or dramatic variations in catalogued sources for which intensities are not normally uniquely assignable due to source confusion) is conducted via daily inspection of the data and use of a computer routine designed to search for significant deviations from the expected counting rates in each resolution element. The array of expected counts ( $E_i$ ) is derived from the estimated contribution of sources (defined at minimum library intensity), the diffuse X-ray background, and the measured internal background. This array is then subtracted from the 512-element matrix of detected counts ( $O_i$ ), and the number of standard deviations computed from  $DEV_i = (O_i - E_i)/\sqrt{E_i}$ . All elements for which  $|DEV_i| \gtrsim 3$  are noted together with the contributing library sources (if any).

On the basis of ASM observations of known weak sources (e.g., Her X-1) an experimental source threshold (all-sky mode accumulations) of  $\sim 0.1 \text{ cm}^{-2} \text{ s}^{-1}$  has been estimated for "clean" sky regions, increasing to  $\sim 0.5 \text{ cm}^{-2} \text{ s}^{-1}$  in moderately confused regions (e.g., Aquila-Serpens). The effective all-sky mode threshold is significantly higher ( $\sim 0.5 - 3 \text{ cm}^{-2} \text{ s}^{-1}$ ) in the proximity ( $\Delta\theta_s \lesssim 5^\circ$ ) of strong, variable sources or in highly confused regions of the galactic plane. As mentioned in Chapter II, the limiting detection threshold is realized by application of the

octant mode (1/2-day accumulations) in relatively unconfused sky regions, at an estimated level of  $\approx 0.05 \text{ cm}^{-2} \text{ s}^{-1}$ .

#### D. Experiment Performance

##### 1. Spatial and Energy Response

Part of the raw data from a representative orbit is shown in Figure 3.5 to demonstrate both the appearance of the X-ray sky image obtained by the ASM and the quantum-limited nature of the data. Although this orbit is of average duration and background levels, it is in reality somewhat atypical in that the five sources indicated happen to be confined almost entirely to single resolution elements. Of particular relevance is the typical counting rate from Sco X-1 of approximately 300 counts/orbit in contrast to the roughly order of magnitude smaller fluxes of the next brightest sources. These statistics underscore the fundamental limitation of a  $1 \text{ cm}^2$  aperture telescope with an average duty cycle (per source) of  $\sim 1\%$  and emphasize the necessity of low counter background and stable energy response for meaningful analysis of the data. A complete computer output for one orbit ("core dump") of data showing the source ON-time and count arrays, spacecraft housekeeping data, etc., is given in Figure 3.6. The improvement in counting statistics and signal-to-noise ratio resulting from integration of the single orbit data is illustrated in Figures 3.7 and 3.8 which represent  $\sim 1/2$  day accumulations of all-sky and octant mode data, respectively. The finer spatial resolution attainable in the octant mode is also demonstrated in Figure 3.8 where the nearby ( $\Delta\theta_s \approx 5^\circ$ ) sources Tau X-1 (Crab Nebula) and A0535+26 are reasonably well resolved.

Evaluation of the empirical response of the detector for comparison with the theoretical value and detection of possible variations in efficiency is clearly important. Good agreement between the computed (nominal gain) and the actual ASM response over the > 2 year lifetime of the experiment is reflected by the fact that the majority of observable UHURU sources monitored by the ASM have been measured within their quoted (3 $\sigma$ ) limits. Long term daily averages for 4 of these sources (Sco X-1, Crab Nebula, Cyg X-2, and Cyg X-1) and the corresponding UHURU flux ranges are shown in Figure 3.9. In addition, consistency has been obtained with several other experiments operating in roughly the same energy range (e.g., SAS-3 and Ariel 5 SSI) during concurrent observations of several flaring and transient sources.

The relative stability of the response is demonstrated by the measured intensity of the Crab nebula plotted in Figure 3.10, which includes data (daily averages) obtained from both counters ("N" and "S" refer to spacecraft northern and southern hemispheres) and at varying spacecraft location (excluding polar, equatorial, and solar elements). While it is clear from this plot that a better fit is obtained by dividing the data into two roughly year-long segments, indicative of an  $\sim 10\%$  increase in detector gain (primarily in the South counter), it is evident that the mean measured flux from the Crab has not varied greatly over the ASM lifetime. In addition, although  $\chi^2$  tests of this data (against the hypothesis of source constancy) over timescales of  $\sim 1$  year yielded unacceptable results, this may be accounted for by the long-term variation in gain, mixture of North and South counter data, and the presence of occasionally large systematic errors on shorter

timescales (due predominantly to low points resulting from spatial offsets)<sup>2</sup>.

As a test for possible differences (North/South) and long-term variations in detector gain, several high-voltage calibrations have been performed at different times in which the intensities of Sco X-1 and the Crab Nebula are measured as a function of detector gain in each of the four high-voltage settings. Reasonable agreement between the observed and expected variation of response with gain was obtained in all but the last calibration of the South counter performed in 1976 July-August, shown in Figure 3.11 (compare with Figure 2.13). The high voltage of that counter was subsequently changed to the next lower setting.

## 2. Sensitivity and Systematic Effects

The effective experimental sensitivity (and relative magnitude of possible systematic errors) may be gauged by analysis of well-studied phenomena in known sources. An excellent test of the experiment performance is afforded by Cygnus X-3 which exhibits a stable (over timescales of years) 4<sup>h</sup>.8 modulation. As its intrinsic weakness ( $S_{\max} \sim 0.5 S_{\text{crab}}$ ), proximity to the strong variable, source Cyg X-1 ( $\Delta\theta_s \approx 10^\circ \approx$  angular separation of adjacent all-sky mode resolution elements), and relatively short period ( $P < 3$  orbits) would all be expected to complicate the measurement of an unambiguous source intensity, the ability to detect this modulation would indicate that systematic effects do not dominate the experiment response. As discussed in Holt (1976), folds of approximately 100 days of single orbit data from Cyg X-3 yield a smooth sinusoidal

<sup>2</sup>This conclusion is supported by the fact that  $\chi^2$  analyses of shorter data segments ( $\sim 1$  month) from a single counter (and with smaller apparent offset errors) have yielded acceptable fits.

light curve which is consistent both in amplitude and phase with the previously reported results of Parsignault et al. (1972), Sanford and Hawkins (1972), Canizares et al. (1973), and Leach et al. (1975), with no significant modulation of Cyg X-1, utilized as a control (see Figure 3.12). Several additional ASM results, including detection of a  $5.6^d$  modulation in Cyg X-1 (Holt et al. 1976a and Fig. 3.13) and the  $35^d$  cycle of Her X-1, which at maximum is just above the experiment (all-sky mode) flux threshold (cf. Holt et al. 1976f and Figure 3.14), confirm the basic reliability of the observations and further illustrate the experiment sensitivity.

Systematic effects arising primarily from uncertainties in the satellite aspect solution, detector offsets, background fluctuations, source confusion, and variations in detector gain are present in the data and must be corrected for where possible. As noted above, several techniques are employed to reduce the magnitude of these errors (e.g., spatial offsets, observed response to Sco X-1, 90% redefinition criterion, high voltage calibration, etc.), but in many cases they are irrecoverable (e.g., imprecision of source ON-time calculation) and can therefore only be estimated. Systematic errors in the measurement of individual sources of interest may also be lessened on an intermittent basis by operating in the octant mode. As mentioned earlier, this mode is particularly useful for the detection of source fluxes near the all-sky mode background level and for identifying sources in a crowded field (cf. Figure 3.8). Finally, utilization of nearby sources as a control and/or well-defined properties of the source under investigation (e.g., an occultation period) represent additional techniques for minimizing systematic effects.

## CHAPTER IV

### OBSERVATIONS

The X-ray light curves obtained for the pre-Ariel 5 transient sources firmly established the nova-like character of the outburst, the magnitude of which apparently differentiated this type of phenomenon from the comparatively stable emission (variability  $\sim$  factor of twenty) of the variable sources. Frequent extended gaps in source coverage, however, severely limited meaningful temporal (and spectral) analyses of the data. As discussed in Chapter I, such studies have been of prime importance in elucidating the nature of the binary X-ray sources (e.g., binary period determination; detection of pulsation periods). In this Chapter, comprehensive X-ray light curves of three new transient X-ray sources which were observable by the ASM are presented, and observations of additional transient sources (not unambiguously measurable by the ASM) from other instruments are summarized. The results of temporal analyses, particularly for the brightest of these sources (A0620-00) are described, as well as observational limits to their frequency of occurrence above an effective detection threshold of  $\approx 0.3 S_{\text{Crab}}$ . In addition, recurrent, transient-like outbursts from known "variable" sources (Aql X-1 and 3U1630-47) apparently intermediate between the transient and variable source classes are examined. The diverse range of variability characteristic of the galactic sources is illustrated in the long-term light curves of several variable sources, ranging from the quasi-regular extended "high" and "low" states ( $S_{\text{high}}/S_{\text{low}} \gtrsim 20$ ) of Cir X-1, through the factor of  $\sim 5$  "transitions" of Cyg X-1, to the gradual, long-term decrease ( $S_{\text{max}}/S_{\text{min}} \gtrsim 5$ ) of Cyg X-3. Finally, the relative constancy of the base-line emission over a two year period from the sources Sco X-1 and Cyg X-2 is contrasted with the previous

behavior.

### A. Transient X-ray Sources

#### 1. A1524-62<sup>(1)</sup>

Shortly after launch of Ariel 5 on 1974 October 15, a relatively bright source appeared in the constellation Triangulum Australe near the highly variable source Cir X-1. It was first reported to be at maximum on 1974 November 22 from the SSI by Pounds (1974), when it was out of the ASM field of view. Figure 4.1 shows the overall 3-6 keV X-ray light curve constructed for A1524-62 via the ASM and SSI, which clearly indicates that the November 22 maximum was only a precursor to a prolonged transient source which was above the ASM threshold for several months (cf. Kaluziński et al. 1975b). While the decline phase of A1524-62 ( $\tau_d \approx 2$  months) is reminiscent of the earlier transients Cen X-4 (Evans, Belian, and Conner 1970) and 3U1543-47 (Matilsky et al. 1972; Li, Sprott, and Clark 1976), the prolonged and variable low-level activity (including the pronounced precursor peak) prior to the onset of the main flare was not observed in those sources. After its discovery by the SSI, a search of earlier ASM data revealed a possible presence of the source as early as 1974 October 28 (day 301), if Cir X-1 (with which it may be confused in the ASM) was truly less than 50 UHURU counts  $s^{-1}$  at this time<sup>2</sup>. Observations of the SSI over the period 1974 November 10 - December 3 (day 314-337) show Cir X-1 at a level of less than 10 UHURU counts  $s^{-1}$  and,

<sup>1</sup>Also designated A1524-61.

<sup>2</sup>The likelihood of such an upper limit to the Cir X-1 flux at this time has been strengthened by the discovery of a strong  $16^d_6$  modulation of the source, characterized by "turnoffs" ( $S_{off} < 50$  UHURU counts  $s^{-1}$ ) lasting in excess of 8 days (see below). The phase of the abrupt downward "transition" of the  $16^d_6$  cycle implies a Cir X-1 turnoff on 1974 day 298.9.



in fact, Cir X-1 was not detected by any Ariel experiment during the entire time displayed.

Periodic modulation of the flux from A1524-62 displayed in Figure 4.1 was searched for by folding the ASM data (with exponential decay subtracted) over trial periods in the range 0.5 - 10 days and noting deviations in the  $\chi^2$ -period distribution (vs. the hypothesis of a constant source intensity). This procedure yielded no significant  $\chi^2$  maxima, with a corresponding upper limit of  $\sim 5\%$  to any source modulation (peak to mean sinusoidal amplitude) in the range of trial periods tested. In addition, a fast fourier transform was performed on the ASM single orbit data (subject to relatively large systematic and statistical uncertainties), with similar results for modulation on shorter time scales ( $\lesssim 10\%$  pulsed power for  $0.2 < P \text{ (days)} < 0.5$ ), consistent with the results of Maraschi et al. (1976). If A1524-62 is an accreting (close) binary system, the absence of X-ray occultations or any lower-level source modulation may indicate a non-negligible orbital inclination and/or extended emission region (relative to the optical companion). Such a conclusion is, in fact, strongly supported by the recent identification of a dwarf-type star as the source optical counterpart (Murdin et al. 1977).

Spectral information over the time of the precursor was obtained by the SSI. In Figure 4.2 these data are plotted differentially in time, with the upper trace the ratio of the low (1.2 - 5.8 keV) to the high (2.4 - 19.8 keV) energy counting rates, and the lower trace their sum. The increasing ratio to approximately 1974 November 22 (day 326) implies a spectral softening of the source up until the precursor peak, after which the ratio measurements are consistent with spectral stability. Four channel pulse-height spectra obtained between days 328-330

(November 24-26) were not fittable with an optically thin isothermal source, but were each consistent with a common power-law approximation to the source spectrum  $dN/dE = (5.2 \pm 0.8) E^{-(2.5 \pm 0.1)} \text{ cm}^{-2} \text{ s}^{-1} \text{ keV}^{-1}$ . No measurable absorption by cold interstellar material at a  $1\sigma$  upper limit of 1.4 keV was detected.

The Triangulum-Circinus region has continued to be monitored in the interval following the last measurements displayed in Figure 4.1. The relatively greater effect of systematic errors at these low flux levels complicated by the proximity to Cir X-1 renders definitive measurements at levels  $\lesssim 0.2 \text{ cm}^{-2} \text{ s}^{-1}$  problematic. An independent measurement of A1524-62 on 1975 June 12 and 15 (1974 days 528 and 531) at a level of  $\sim 0.2 \text{ counts cm}^{-2} \text{ s}^{-1}$  (1 - 10 keV) was reported from SAS-3 (Jernigan 1975). A search of the ASM data in the time between the latter sighting and the last measurements displayed in Figure 4.1 (1975 April 5 - June 12; 1974 day 460-528) yielded frequent upper limits of  $\sim 0.1 - 0.2 \text{ cm}^{-2} \text{ s}^{-1}$ , with a possible<sup>3</sup> detection at these levels commencing on about May 7 (1974 day 492). A source consistent with the position of A1524-62 is evident in the data through 1975 August ( $\sim 1974$  day 600), and A1524-62 has not been re-detected ( $S \lesssim 0.05 \text{ cm}^{-2} \text{ s}^{-1}$ ) in octant mode observations spanning the period 1975 October 29 (1974 day 667) - 1977 January. These results are consistent with the SAS-3 observations and suggest that the latter occurred during an extended low-level ON-state ( $S \approx 0.1-0.2 S_{\text{max}}$ ) of A1524-62 similar to the secondary maxima exhibited by Cen X-4 and 3U1543-47.

<sup>3</sup>Flares of the nearby weak UHURU sources 3U1543-62 ( $S = 0.016 - 0.048 \text{ cm}^{-2} \text{ s}^{-1}$ ) and 3U1510-59 ( $S = 0.01 \text{ cm}^{-2} \text{ s}^{-1}$ ) cannot be entirely ruled out, as well as occasional confusion with Cir X-1.

## 2. A0535+26

During an extended spin axis hold in Taurus between 1975 April 13-29 the transient source A0535+26 was detected by the pole-aligned Rotation Modulation Collimator ('RMC') experiment aboard Ariel 5 (Rosenberg et al. 1975). The nearness of A0535+26 to the bright source Tau X-1 (Crab Nebula) severely limits detection and measurement of this source at low flux levels ( $S \sim 0.2 \text{ cm}^{-2}\text{s}^{-1} \sim 15\% S_{\text{crab}}$ ) in the all-sky mode, as such levels are comparable to the statistical accuracy in the measurement of the Crab. However, the constancy of this latter source allows measurement of the A0535+26 flux, even when source confusion is present, via subtraction of the measured mean flux from the Crab ( $\bar{S}_{\text{crab}} \approx 1.25 \text{ cm}^{-2}\text{s}^{-1}$ , see Figure 3.10). The light curve for A0535+26 obtained by the ASM (Kaluziński et al. 1975a) in this manner is shown in Figure 4.3. Immediately preceding spin axis hold in the Taurus region, the source was not observable at an upper limit ( $1\sigma$ ) of  $\approx 0.2 \text{ cm}^{-2}\text{s}^{-1}$  (the Crab Nebula was simultaneously measured at a flux of  $1.4 \pm 0.2 \text{ cm}^{-2}\text{s}^{-1}$ ), with a comparable upper limit during the period 1974 October - 1975 April. When first observable by the ASM on 1975 April 29 (day 119), A0535+26 was  $\sim 35\%$  more intense than the Crab Nebula, and maintained this level for approximately one week. The time of peak flux has been established to have occurred at approximately this time (April 29 - May 2, Ricketts et al. 1975). The source then decayed with an e-folding time  $\tau_d \approx 19 \text{ d}$  until the Sun was too close for unambiguous separation. When the Sun had moved sufficiently far to allow the source intensity to again be interrogated, it was found to be unobservable (i.e.,  $S \lesssim 0.2 \text{ cm}^{-2}\text{s}^{-1}$ ,  $1\sigma$ ). Recovery phenomena, including at least two secondary maxima, have been reported from the SSI (Pounds 1976a) and SAS-3 (Joss 1975). The most

dramatic of these occurred on approximately 1975 November 8 (day 312), with the 1-6 keV flux reaching  $\sim 10\%$  of primary maximum for several days (Rappaport et al. 1976). As discussed above, detection of A0535+26 at such low flux levels is severely limited due to its proximity to the Crab Nebula, and the source has not been detected above its effective ASM threshold level over the interval 1975 July - 1977 January, during which time no anomalously high measurements of the Crab were made.

It is evident from Figure 4.3 that no occultations of the source were observed. Folds of this data (with the decay trend subtracted) revealed no periodicities in the range  $0.5 \leq P(d) \leq 10$  at an upper limit of  $\sim 10\%$  (fractional sinusoidal amplitude). This is consistent with SAS-3 Doppler shift measurements of the source pulse period (see below), which require binary periods in the range  $17^d \lesssim P \lesssim 77^d$  (Rappaport et al. 1976).

A0535+26 is distinguished from A1524-62 and the earlier transients in several respects. First, the spectrum was characterized by a power-law photon index of  $n \approx -1$  (Ricketts et al. 1975) vs.  $n_{\text{crab}} = -2.1$ , or alternatively by black body temperatures of  $kT \approx 3$  keV and  $kT \approx 8$  keV for the 3-7 keV and 26-73 keV energy ranges, respectively (Coe et al. 1975). Secondly, the source was found to be pulsing with a period of 104 seconds (Rosenberg et al. 1975), with a pulse profile similar to those (on shorter timescales) of Her X-1 and Cen X-3. The consistency of such a modulation in A0535+26 with rapid rotation of the X-ray emitting object clearly favors its identification as a neutron star (vs. white dwarf or black hole). Of additional interest is the tentative optical identification of the source with the B emission star HD245770 (Liller 1975) based on the location of this object within the 1' Ariel 5 error

box (Rosenberg et al. 1975). Finally, UHURU has reported a possible detection of A0535+26 at low flux levels ( $S = 12.7 \pm 3.8$  UHURU counts  $s^{-1} \approx 0.02 \text{ cm}^{-2} s^{-1}$ ) as far back as 1970 December (Forman, Jones, and Tananbaum 1976a).

### 3. A0620-00

The last of the unqualified<sup>4</sup> transient sources to be studied by the ASM is A0620-00 (Nova Monocerotis 1975), discovered by the SSI at  $S \approx 0.005 \times S_{\text{Sco X-1}}$  on 1975 August 3 when the Orion-Monoceros region was exposed to the spacecraft equator. A0620-00 is the first transient to be unambiguously identified optically (Boley et al. 1976) and has also been observed in the infrared and radio bands. As a result of the unprecedented brightness of the source ( $S_{\text{max}} \approx 4 \times S_{\text{Sco X-1}}$ ), a detailed orbit-to-orbit light curve was obtained and sensitive analyses of temporal variability on timescales of hours-months were possible.

#### a. Light Curve

Figure 4.4 is a semi-log display of the ASM A0620-00 data through 1975 November. The points obtained prior to November 21 (day 325) represent single-orbit ( $\sim 0.07$ ) measurements of the flux, while those obtained afterward are  $\sim 1/2$  day averages. Error bars reflect the  $\pm 1\sigma$  statistical uncertainty which generally exceeds any possible systematic error in the analysis of this source. The arrows indicate onset of the emission and approximate commencement of the decline (Elvis et al. 1975), reflecting the relatively brief risetime typical of the transient sources. The source first entered the field-of-view of the ASM on August 20 (day 230),

<sup>4</sup>i.e., satisfying all of the criteria in the operational definition of the transient sources outlined in Chapter I.

and the first group of points is roughly consistent with the fluxes at maximum light recorded by X-ray detectors with thresholds below 3 keV (Elvis et al. 1975; Doxsey et al. 1976). A search for emission from the source in the interval between launch of Ariel 5 and its discovery by the SSI revealed no emission  $\gtrsim 0.1 \text{ cm}^{-2} \text{ s}^{-1}$  during the  $\sim 70\%$  of this time interval that the source region was monitored by the ASM (cf. Kaluziński et al. 1977a). We can thus rule out the type of extended, low-level activity exhibited by A1524-62, since the above limit on early emission from A0620-00 is almost three orders of magnitude below maximum.

It is clear from Figure 4.4 that any attempt to fit the decay with a simple power-law or exponential function yields an unacceptable result, even when the secondary increase occurring in October is excluded. This increase (representing  $\sim 75\%$  higher flux than that expected from an extrapolation of the early September decline) is qualitatively similar to the post-maximum increases observed in Cen X-4 (Evans, Belian, and Conner 1970), 3U1543-47 (Matilsky et al. 1972), and A0535+26 (Pounds 1976a). Shorter intervals, however, could be fit fairly well, and the dashed lines represent best exponential fits to the pre- and post-increase decline phases, with e-folding times of  $28.9^{+1.8}_d$  and  $21.2^{+1.2}_d$  (99% confidence limits), respectively. The acceptable values of  $\chi^2$  resulting from these fits reflect the smoothness of this phase of the decay on timescales from 100 minutes - 1 week. Although this is consistent with other X-ray observations on shorter timescales (Doxsey et al. 1976; Elvis et al. 1975), variations in the optical counterpart of  $\sim 0.5$  magnitudes over  $\sim$  hours - 1 day during this period have been reported by Matsuoka et al. (1976). The solid line in Figure 4.4 is the best  $1/t$  fit to the early September data commencing at maximum light, which is drawn in for comparison with

the similar decay expected in a "colliding shells" model (Brecher and Morrison 1975) of the transient sources. Note, however, that the relatively high ASM low-energy threshold ( $\approx 3$  keV), combined with the progressive softening of the source spectrum (Pounds 1976a), may cause the flux observed by the ASM to decline more rapidly than that which would be measured by a photometer with lower threshold energy.

Figure 4.5 illustrates the ASM data over the final decay phase of A0620-00 from 1975 December until its disappearance below the experimental threshold in late March 1976. All of the points here are  $\sim 1/2$  day averages, and the dashed line is an extrapolation of the post-October exponential fit in Figure 4.4. Although the exponential decline is approximately followed through 1976 mid-January, significant fluctuations on a timescale of  $\approx 1/2$  day are now evident, with the source disappearing below the ASM threshold on several occasions. Similar variations on a timescale of hours-days in the 1.3 - 5 keV flux during the same period have been reported from SAS-3 (Matilsky and Zubrod 1976). A final dramatic increase in flux before disappearance of A0620-00 occurred in early February, representing at least an order-of-magnitude deviation above the level expected from extrapolation of the exponential decline. The subsequent decay is correspondingly more rapid than in the earlier phases (e-folding time  $\approx 10^d$ ), reminiscent of the decay light curves of Cen X-4 (Evans, Belian, and Conner 1970) and 3U1543-47 (Li, Sprott, and Clark 1976).

#### b. Periodicity

Based on SAS-3 observations of A0620-00 during the period 1976 January 7 - February 8 (1975 day 372-404) Matilsky (1976) has reported an  $\sim 50\%$  sinusoidal modulation of the 1.3 - 5 keV flux. Chevalier, Ilovaisky, and Mauder (1976) and Tsunemi, Matsuoka, and Takagishi (1977) have likewise

reported evidence for a similar modulation of the optical counterpart at periods consistent with the SAS-3 value, while Duerbeck and Walter (1976) have suggested a modulation at roughly one half this period ( $P \approx 3.9^d$ ) from B magnitude observations made over the early decline. Since the magnitude of a periodic modulation of the 3-6 keV flux may be correlated with the source intensity, we have analyzed the single-orbit and 1/2-day data in Figures 4.4 and 4.5 separately. In the first case, the best-fit exponentials from the September and October-November data were subtracted out separately, and the residuals folded over trial periods in the range 0.2 - 10 days in intervals fine enough that a regular variation should be revealed by a well-defined peak in the  $\chi^2$  distribution. Neither this procedure, nor a fast fourier transform performed on the single orbit data, succeeded in the detection of any modulation in excess of  $\sim 3\%$ . This is equivalent to an upper limit of 2.3% fractional sinusoidal amplitude on any 3-6 keV modulation in the range searched during this phase of the decay. The 1/2-day data were tested for periodicity in a similar manner. Although the average value of  $\chi^2$  is higher due to random fluctuations (see Figure 4.5,  $\sim 1975$  day 350) and the limited number of cycles at the upper end of the period range, no clear maximum in the vicinity of  $7.8^d$  is evident. A small enhancement in the  $\chi^2$  distribution is present at  $P \approx 8$  days, and we estimate an upper limit of  $\sim 10\%$  to any sinusoidal variation in the range  $7.8^d \pm 0.7^d$ .

The ASM upper limits to periodic modulation for the early light curve are of the same order as results obtained by the Ariel 5 SSI (Elvis et al. 1975) and SAS-3 experiments (Doxsey et al. 1976) at higher frequencies, with reported upper limits on periodicity of 3% (200s - 2d, 2-18 keV) and  $\sim 2\%$  (0.2 ms - 435s, 1 - 10 keV), respectively, during the rise and



early decline phases. The absence of a detectable 3 - 6 keV modulation at the suggested  $\sim 7.8^d$  X-ray or  $\sim 3.9^d$  optical periods during this stage may be indicative of an extended emission region and/or a high orbital inclination, and agrees with B magnitude measurements of Matsuoka et al. (1976) over the same interval who found an upper limit of 0.05 magnitudes on any periodicities in the 2 - 64 day range. With respect to the later decline we note that the SAS-3 period is based on observations during an interval in which the ASM source coverage is only  $\sim 30\%$  and does not include the February increase (see Figure 4.5). The absence of a clear  $7.8^d$  modulation in our data may be reconciled with the  $\sim 50\%$  sinusoidal modulation (1.3 - 5 keV) reported by Matilsky (1976) if the effect is more conspicuous below the ASM low energy threshold, or if it was present at that level only during the time that the ASM coverage was incomplete.

#### c. Comparison with Optical Observations

Since the identification of V616 Monocerotis as the optical counterpart of A0620-00 (Boley et al. 1976), several observers have monitored the source in the optical band. Of considerable interest are observations made in the vicinity of the 3-6 keV increases during October 1975 and February 1976. B magnitude measurements of Matsuoka et al. (1976) during September-October clearly show an increase in the optical emission of  $\sim 0.6$  magnitudes concurrent (to an accuracy of  $\approx 1$  week due to a gap in ASM coverage, see Figure 4.4) with the October X-ray increase. Their data also show a roughly exponential decay (e-folding time  $\approx 1$  month) in B magnitude during September in good agreement with the 3-6 keV X-ray observations, but somewhat more rapid than the  $\sim 60$  day decay time observed in UBV by Duerbeck and Walter (1976) over the same time span. The February increase is again apparently reflected in the optical data, with an increase

of  $\sim 50\%$  between 19 January - 16 March implied by the visual magnitude estimates of Bortle (1976a,b). A final rapid optical decline commenced at about the time of this last observation, the source brightness decreasing approximately one magnitude by 31 March (Bortle 1976c), and another  $\sim 2$  magnitudes during April (Martynov 1976). Since the corresponding X-ray decrease commenced on  $\sim$  March 1 with an order-of-magnitude drop in flux by March 16, the apparent correlation between the X-ray and optical features of the decline suggests a time lag of  $\sim 2$  weeks during this stage of the decay. The discrepancy between the mean decay time constants over the initial decline (August - January) of the optical ( $\tau_o \approx 2 \frac{1}{2}$  months) and 3-6 keV ( $\tau_x \approx 1$  month) fluxes should also be noted. As the measured effective temperature is just below the 3-6 keV band of the ASM (Doxsey *et al.* 1976), the observed spectral softening during the decay would tend to make the ASM-measured and optically determined decay time constants underestimate and overestimate, respectively, of the true luminosity decay time. This disagreement can not arise entirely from the high threshold of the ASM, however, as SAS-3 measured a flux (1.3 - 5 keV) of  $S \approx 0.2 S_{\text{crab}}$  on January 7 (Matilsky 1976) in good agreement with the ASM data. Both the slower decay rate and the possible "lag" of the optical emission with respect to the final rapid disappearance at X-ray energies are apparently consistent with a mechanism in which X-ray and UV heating contribute significantly to the production of the optical emission.

Combination of the X-ray or optical decay time constant with the X-ray flux at maximum light allows estimates of the total energy and corresponding mass exchange responsible for the primary source outburst

(i.e., excluding secondary increases)<sup>5</sup>. These two limiting timescales and  $S_{\text{max}} \approx 1.7 \times 10^{-6} \text{ erg cm}^{-2}\text{s}^{-1}$  (1-10 keV, Doxsey et al. 1976) yield a total energy output of  $E(1-10 \text{ keV}) \approx 5-14 \times 10^{44} d_1^2 \text{ erg}$  ( $d_1 \equiv d/1 \text{ Kpc}$ ). Assumption of a mass-to-radiation conversion efficiency of  $\sim 10\%$  implies a corresponding mass exchange of  $3 \times 10^{-9} d_1^2 M_{\odot} \lesssim \Delta M \lesssim 9 \times 10^{-9} d_1^2 M_{\odot}$ .

#### 4. Norma "Transient"

An X-ray flare in the Norma region was detected by the ASM in 1975 October, occurring within  $5^{\circ}$  of the bright UHURU source 3U1636-53 (Kaluziński et al. 1975c). Octant mode observations permitted determination of an approximate source position of  $l^{\text{II}} = 330^{\circ}.7$ ,  $b^{\text{II}} = -1^{\circ}.1$  (R.A. =  $16^{\text{h}}09^{\text{m}}$ , Dec =  $-52^{\circ}.6$  [1950]), with an estimated error radius (90% confidence) of  $2^{\circ}$ . Due to its proximity to 3U1636-53 (which has exhibited a moderate degree of variability, in contrast to its constancy in the Third UHURU (3U) catalog, Giacconi et al. 1974), the only definitive measurements of this source were obtained in the octant mode. However, assumption of a maximum flux for 3U1636-53 at its UHURU value ( $S \approx 0.4 \text{ cm}^{-2}\text{s}^{-1}$ ; octant mode observations frequently yield  $S \approx 0.3 \text{ cm}^{-2}\text{s}^{-1}$ ) indicates that the Norma transient attained maximum light during the period 1975 day 303-313 (October 30 - November 9) with a peak flux in the range  $0.4 \lesssim S_{\text{max}} (\text{cm}^{-2}\text{s}^{-1}) \lesssim 1.0$ . The ASM data for both sources is shown in Figure 4.6. Octant mode observations conducted approximately 11 months prior and 2 1/2 months after apparent maximum yielded upper limits of  $0.1 \text{ cm}^{-2}\text{s}^{-1}$  to the flux and the source has not been detected in subsequent octant mode observations of this region. While this flare may thus represent

<sup>5</sup>The binary accretion process is assumed as the mechanism underlying the X-ray outburst in this calculation. Note that  $1 M_{\odot} \equiv \text{Solar mass} = 1.99 \times 10^{33} \text{ gm}$ .

a relatively short-lived transient X-ray source, it is interesting to note that its position is consistent with that of the so-called "Norma X-ray Burster" (Grindlay and Gursky 1976; Belian, Conner, and Evans 1976), the highly variable ( $\approx 20\times$ ) UHURU source 4U1608-52 (Matilsky, Gursky, and Tananbaum 1973; Tananbaum et al. 1976), and the relatively hard-spectral ( $kT \approx 30$  keV) OSO-7 source X1608-52 (Li 1976). If these sources correspond to the same object (as appears likely from the positional coincidence), the transient-like behavior observed by the ASM suggests a strong connection between the transient and "variable" X-ray sources. In view of its closer resemblance to the latter class of objects, the Norma "transient" is not included within the transient source classification in the following discussion.

#### 5. A1118-61 and A1742-28

A1118-61 and A1742-28 represent two additional transients detected in the first year of Ariel 5 operation for which X-ray light curves have been constructed, but which were unobservable by the ASM. At maximum light on 1974 December 26 ( $S \approx 0.10 \text{ cm}^{-2}\text{s}^{-1}$ , 3-9 keV; Eyles et al. 1975a), A1118-61 was still below the ASM all-sky mode flux threshold. In any event, its proximity to the bright, variable source Cen X-3 would have made unambiguous flux measurements at levels  $S \approx 0.5 \text{ cm}^{-2}\text{s}^{-1}$  possible only during an extended low state of the latter source. A relatively hard spectrum ( $n \approx -1$ ) and pulse period ( $P = 6.75$  min) have been reported (Eyles et al. 1975a; Ives, Sanford, and Bell-Burnell 1975), similar to those later observed in A0535+26. Characteristics of the light curve include a well-defined precursor peak, e-folding decay time of  $\sim 1$  week, and possible low-level recovery phenomena up to 1 month after primary

maximum (cf. Eyles et al. 1975a and Figure 4.7). While a possible optical identification with the Mira variable RS Cen has been suggested (Fabian, Pringle, and Webbink 1975), additional expected X-ray outbursts at the 164.<sup>d</sup>51 period of that system have not been detected (Davison and Sanford 1976), nor has the source been observed in previous or subsequent observations of the Centaurus region of which we are aware. Interestingly, in view of the similarities of its X-ray properties to those of A0535+26, A1118-61 has also been tentatively identified with a highly reddened,  $\sim$  12th magnitude B emission star (Chevalier and Ilovaisky 1975).

A1742-28, though a fairly bright source at maximum ( $S_{\max} \approx 3.5 \text{ cm}^{-2} \text{ s}^{-1}$ , 3-8 keV; cf. Eyles et al. 1975b and Figure 4.8), is situated in the extremely crowded region of Galactic Center and therefore virtually indistinguishable by the ASM from large variations in those sources<sup>6</sup>. A1742-28 was characterized by a relatively soft spectrum ( $n \approx -3$ ) and an apparent three-component decay similar to that of 3U1543-47 (Branduardi et al. 1976). It thus appears to more closely resemble A1524-62 and A0620-00 as opposed to the hard, pulsing transients. Furthermore, this object is probably among the most luminous X-ray sources in the galaxy, as low energy absorption implies a neutral hydrogen column density of  $n_{\text{H}} \approx 10^{23} \text{ atom cm}^{-2}$ , consistent with a source near the galactic nucleus radiating at a rate of  $L_{\text{x,max}} \approx 3 \times 10^{38} \text{ erg s}^{-1}$ .

## 6. Additional Transient Sources and Candidates

As evident from Table 1.3, there remain an additional four sources

<sup>6</sup>We note that an emission excess was evident in this region when exposed to the ASM field of view in the time intervals immediately adjacent to the cited observation.

(A1246-58, A1745-36, A1743-29, and MX1803-24) which, although detailed light curves were not obtained, clearly exhibited the sudden appearance and initial decay characteristic of the transient sources (and were not observed in previous surveys). Therefore, while a definitive classification cannot be made, these sources are included within the class of transient sources in the following discussion. Finally, a number of transient source "candidates", i.e., sources which may belong to this class but for which an insufficient amount of data exists (e.g., A0025+59, Skinner 1975; MX0656-07, Clark 1975), have been reported during 1975-76 (see Table 4.1).

#### 7. Null Transient Source Observations

Of equal importance to the above observations are the "null" results for transient sources during the two years of Ariel 5 monitoring of the sky. In particular, estimates of the ASM threshold to sources of the type discussed above are necessary for the determination of the occurrence rate and spatial and luminosity-lifetime distribution of the transients addressed in Chapter V. The sensitivity of the ASM to transients is a strong function of their galactic location, with an estimated source threshold ( $\tau_d \gtrsim 2$  weeks) for  $|b^{II}| \gtrsim 10^\circ$  (limited primarily by the quantum counting statistics and fluctuations in background) of  $S_{\text{thresh}} \sim 0.2 \text{ cm}^{-2} \text{ s}^{-1}$ . While this limit is also attainable in uncrowded regions of the plane (e.g., Galactic Anticenter), it increases to  $\sim 0.5 - 1.0 \text{ cm}^{-2} \text{ s}^{-1}$  in the vicinity ( $\Delta\theta \sim 5^\circ$ ) of strong sources (e.g., Centaurus, Norma, and Cygnus complexes). The efficiency is clearly a minimum in the region of Galactic Center, where the detection threshold may approach  $S_{\text{thresh}} \sim 2 S_{\text{crab}} (\sim 3 \text{ cm}^{-2} \text{ s}^{-1})$ . The corresponding octant mode sensitivity is about a factor of two greater, but its infrequent use and limited sky coverage

lessens the probability of detecting new sources in that mode. The combined fields-of-view of the Ariel 5 instruments ( $\Omega_{\text{tot}} \gtrsim 3.95\pi$  Sterad) insures that few, if any, transient events will be missed as a result of incomplete sky coverage. Furthermore, the small blind spot centered on the spacecraft south pole is not fixed in space for periods exceeding  $\sim 2$  weeks. The ASM/Ariel 5 observations of the transient X-ray sources may thus be summarized as follows (see also Table 1.3):

(1) No sources ( $\tau_d \gtrsim 2$  weeks) were observed at latitudes  $|b^{\text{II}}| > 8^\circ$ , at a source threshold of  $S_{\text{thresh}} \approx 0.2 \text{ cm}^{-2}\text{s}^{-1}$ . The scarcity of bright sources in this region suggests that few ( $\lesssim 2$ ) transients went undetected as a result of source confusion; and

(2) A total of nine unqualified transients (including one from SAS-3) were detected within  $8^\circ$  of the plane, with peak (3-6 keV) fluxes in the range  $0.1 - 50 \text{ cm}^{-2}\text{s}^{-1}$ . Although difficult to estimate, an upper limit of  $\sim 10$  sources  $\text{yr}^{-1}$  to the rate at which transient sources ( $S_{\text{max}} \gtrsim 0.5 \text{ cm}^{-2}\text{s}^{-1}$ ,  $\tau_d > 2$  weeks) may have been missed due to confusion with bright sources in the disk (including Galactic Center) appears conservative. This is roughly consistent with the extended galactic plane surveys conducted by the SSI on several different occasions which failed to detect any additional transient sources, with a flux threshold considerably below that of the ASM ( $S_{\text{thresh}}(\text{SSI}) = 0.001 - 0.01 \text{ cm}^{-2}\text{s}^{-1}$ ). As discussed in Chapter V, these "null" measurements are important in determining the spatial, luminosity, and frequency distributions of the transient X-ray sources.

## B. Variable Sources

### 1. Aquila X-1

#### a. History

Aql X-1 (3U1908+00) exhibits the most extreme long-term variability of the quasi-stable sources, with an observed luminosity range of  $L_{\max}/L_{\min} \approx 500$ . This volatility was evident from early rocket surveys of the region in which Aql X-1 was detected only on an occasional basis (cf. Seward 1970). A moderate degree of variability was also observed by UHURU, as reflected in the 3U Catalog record ( $S \approx 0.1 - 0.3 \text{ cm}^{-2} \text{ s}^{-1}$ , Giacconi et al. 1974). Markert (1974) has reported OSO-7 observations over three intervals during 1971-73 which suggest the existence of well-defined "high" ( $S \sim 0.6 \text{ cm}^{-2} \text{ s}^{-1}$ ) and "low" ( $S \approx 0.01 \text{ cm}^{-2} \text{ s}^{-1}$ ) intensity states. Aql X-1 was subsequently observed by OAO Copernicus at levels at least an order of magnitude below the UHURU range in intermittent observations over a two-year period through 1975 May (Davidsen et al. 1975). This apparent quiescent state was interrupted in 1975 June by a sudden flare (factor of  $\approx 20$  increase, Buff 1975) to the level of the Crab nebula, followed by a gradual ( $\tau_d \sim 1$  month) decay back to the pre-flare state. The succeeding "low" state was again punctuated in 1976 June by a similar outburst (Kaluziński et al. 1976b; Watson 1976b; Kaluziński et al. 1977b).

#### b. ASM Observations

The proximity of Aql X-1 ( $l^{\text{II}} = 35.7^{\circ}$ ,  $b^{\text{II}} = -4.0^{\circ}$ ) to the sources Ser X-1 (3U1837+04) and 3U1901+03 ( $S_{\max} \approx 0.4$  and  $0.1 \text{ cm}^{-2} \text{ s}^{-1}$ , respectively) make unambiguous detection of a low Aql X-1 flux ( $\lesssim 0.2 \text{ cm}^{-2} \text{ s}^{-1}$ ) problematic in the all-sky resolution mode. Consequently, occasional fluctuations in detector background and other systematic effects could conceivably result in "accidental" flux measurements (with low



probability) as high as  $\sim 0.3 \text{ cm}^{-2} \text{ s}^{-1}$  for this particular source. The data obtained during the 1975 and 1976 flares of Aql X-1 are illustrated in Figures 4.9 and 4.10, and represent the only unambiguous detections of the source over the  $\sim 25$  months of ASM operation during which the duty cycle for daily monitoring of the Aquila-Serpens region was  $> 75\%$ . These plots consist of 1/2-day accumulations with corresponding  $\pm 1\sigma$  statistical error bars (estimated  $1\sigma$  systematic errors are smaller than the statistical uncertainties). The upper limits obtained ( $0.1 \text{ cm}^{-2} \text{ s}^{-1}$ ) immediately prior to the 1975 flare are consistent with the SAS-3 observations (Buff 1975), and no positive detections of the source above  $\sim 0.2 \text{ cm}^{-2} \text{ s}^{-1}$  were made during the preceding 7 1/2 months. A similar search of the ASM data over the period between the flares yielded no unambiguous source sightings through 1976 April, with a possible detection at  $\sim 0.3 \text{ cm}^{-2} \text{ s}^{-1}$  (for  $\sim 1$  day) two weeks prior to the 1976 outburst. We note finally that the apparently differing peak flux levels of the flares are actually consistent with a single limiting value ( $S_{\text{max}} \approx S_{\text{crab}}$ ), as degradation in the effective 3-6 keV detector efficiency of  $\sim 10\%$  between the two flare observations can not be excluded (cf. § III.D.1).

### c. Periodicity

As a 1.3-day modulation has been reported (Watson 1976a) from the 1975 SSI flare data (obtained during the time interval in Figure 4.9 labelled "equator"), we have investigated both the 1975 and 1976 ASM data for periods in the range 0.3 - 3 days. The standard technique, i.e., folding the data (the 1975 and 1976 data were analyzed separately) over the range of trial periods and noting deviations in the  $\chi^2$ -period distribution to the hypothesis of source constancy, was employed. The most prominent peak in the 1975 ASM data, is indeed, consistent with

the SSI result. As the two experiments have mutually exclusive fields-of-view, the ASM result at a level of  $3\% \pm 1\%$  is an independent measure of the same effect, but cannot be claimed to be an independent detection owing to its marginal statistical significance. Assuming its reality, we can refine the period estimation to  $1.28 \pm 0.02$  days. No such modulation is evident at this period in the 1976 data, however, with statistical errors comparable to those in 1975.

A summary of the totality of the 1971-76 data for Aql X-1 is displayed in Figure 4.11, from which there is a clear indication that the OSO-7 data are consistent with flaring episodes similar to those in 1975-76. As there is no exact period which can be fit to the four flares for which there is observational evidence, we have derived a mean flare interval of 435 days with an rms scatter of  $\sim 10\%$ , and have indicated a possible history of identical flares which satisfy all of the observations<sup>7</sup>. The implications of the irregularity of the proposed flare cycle for models of the transient sources is discussed in the following Chapter.

## 2. 3U1630-47 (Norma XR-1)

Another source which apparently undergoes repeated outbursts similar to those of Aql X-1 is 3U1630-47. Jones et al. (1976) have reported a flare cycle for 3U1630-47 of  $P = 615 \pm 5$  days based on an analysis of UHURU and Ariel 5 data (see Figure 4.12). This source is located in the relatively crowded Norma region and its angular separation from the bright, variable

<sup>7</sup>An additional transient-like outburst from Aql X-1 was observed in 1977 January (Watson 1977), characterized by a peak flux of roughly one-third that of the 1975 and 1976 flares ( $S_{\max} \approx 0.4 \text{ cm}^{-2} \text{ s}^{-1}$ , Holt and Kaluziński 1977).

UHURU source 3U1642-45 ( $\Delta\theta_s \sim 3^\circ$ ) is at the octant mode spatial resolution limit. Several octant mode observations near the time of the last reported flare are available, however, and an effort was made to measure the source intensity at those times. The resultant points are consistent with the results of Jones et al. (1976) and are plotted in Figure 4.13. 3U1630-47 has not been observed at levels exceeding  $\sim 0.2 \text{ cm}^{-2}\text{s}^{-1}$  in prior or subsequent octant mode observations of the Norma region.

### 3. Cyg X-1

Yet another type of long-term variability which is reminiscent of both the transient sources and the extended "high" and "low" intensity states exhibited by Cen X-3 is evident in the ASM observations of Cyg X-1 (see Figure 3.9). A sharp (factor of  $\sim 4$ ) increase commencing on 1975 April 23 (day 113) is shown in Figure 4.14. As shown there, no visible decay from this highly variable emission state was observed for at least ten days after onset, at which time the source left the ASM field of view (at the spacecraft pole). Subsequent observations by the collimated proportional counter experiment on Ariel 5 reveal a gradual decline back to the pre-"transition" intensity by 1975 May 14 (day 134), implying a decay time  $\tau_d \lesssim 8$  days.

A smaller increase was reported in 1975 September (Primini 1975), which displayed the same temporal variability and a decay time of  $\sim 1$  week. In 1975 November a third increase was observed (Kaluziński et al. 1975d; Grindlay and Schreier 1975), with a peak flux at the level of the April event and characterized by similar variability. As demonstrated in Figure 4.15, however, this "high" state was maintained for  $\sim 3 \frac{1}{2}$  months, terminating relatively abruptly ( $\tau_d < 1$  week) in 1976 mid-February.

Spectral information on the April flare indicates a steepening of the spectrum in the "high" state (power-law photon index  $n \approx -4$ ) relative to that characterizing the low state ( $n \approx -2$ ). While spectral data on the November transition has not been reported, the type of spectral variation observed in the April event was also associated with a transition occurring in 1971 April (Tananbaum et al. 1972).

#### 4. Circinus X-1

##### a. ASM Observations

Cir X-1 (3U1516-56) exhibits a high degree of variability (factor of  $\gtrsim 20$ ) on timescales ranging from seconds to years. Eclipse-like behavior has been reported by several observers (Tuohy and Davison 1973; Jones et al. 1974), but no period consistent with all observations had been found, with difficulties resulting from the long-term variability of the source (e.g., "extended lows" similar to those of Cen X-3) and the relatively short observing time possible with most instruments prior to Ariel 5.

From the launch of Ariel 5 through 1975 August, Circinus X-1 was not unambiguously detected above the all-sky mode threshold ( $\sim 0.1 \text{ cm}^{-2} \text{ s}^{-1}$  in this region), and observations conducted by other experiments on Ariel 5 in 1974 November and again in 1975 March failed to detect the source above a level of  $\sim 0.01 \text{ cm}^{-2} \text{ s}^{-1}$  in the 1.2-19.8 keV range (Kaluziński et al. 1975b). In 1975 October Cir X-1 exhibited a significant increase ( $\gtrsim$  factor of 10) in the 3-6 keV flux, signaling the commencement of a new phase of heightened activity (cf. Kaluziński et al. 1976c). The source subsequently fluctuated between approximately  $\lesssim 0.05$  and  $1.5 \text{ cm}^{-2} \text{ s}^{-1}$  through 1976 February, after which the peak intensity gradually declined to  $\lesssim 0.1 \text{ cm}^{-2} \text{ s}^{-1}$  by 1976 late April. It is evident from Figures

4.16 and 4.17 that the bulk of the emission is confined to relatively brief, flarelike episodes occurring at fairly regular intervals. Order-of-magnitude variations over time scales  $\gtrsim 1$  day are not uncommon, and the light-curve bears little resemblance to that of any known occulting X-ray binary.

b. Periodicity

Periodic modulation of the flux was searched for by folding the data in Figure 4.16 over trial periods between  $\sim 14$  and 20 days, the range below  $14^{\text{d}}.3$  having been effectively ruled out by UHURU (Jones *et al.* 1974) and OSO-7 (Canizares, Li, and Clark 1974) observations. A significant peak in the  $\chi^2$  versus period distribution occurred near  $16^{\text{d}}.55$ , with a corresponding light curve characterized by a relatively short interval ( $\lesssim 5$  days) of high-level emission followed by an abrupt falloff to minimal flux. To improve the precision of our determination of the period, transition epoch, and duration of a possible occultation, the single-orbit data were inspected and revealed six clear instances in which the Cir X-1 count rate dropped from relatively high to low levels in adjacent orbits. Two such transitions are illustrated in Figure 4.18, where the sharpness of the decrease in flux is apparent, occurring over a time scale of  $\lesssim$  one orbit ( $\approx 0^{\text{d}}.07$ ). Taking the end-time of the last ON orbit for the time of transition and an accuracy of  $\pm$  one orbit, a least-squares fit to a constant period yielded  $P = 16^{\text{d}}.585 \pm 0^{\text{d}}.01$ , and transition epoch  $\text{JD } 2,442,877.181 \pm 0.07^{(8)}$ , where the quoted errors are  $\approx 3/2$  the square root of the respective fit variances. Since the effective ASM single-orbit (coarse-mode) sensitivity is  $\sim 0.3 \text{ cm}^{-2} \text{ s}^{-1}$

<sup>8</sup>JD = Julian date; JD 2,442,327.5 = 1974 day 280.0.

in a region as confused as Circinus, the points following the transition in Figure 4.18 are not definitive. A fine-mode observation of a transition on 1976 April 8 showed a possible detection ( $2\sigma$ ) at  $\approx 0.05 \text{ cm}^{-2} \text{ s}^{-1}$  as early as four orbits ( $0.^{\text{d}}33$ ) later, but was followed by another six orbits ( $0.^{\text{d}}42$ ) in which no detectable signal at this level was observed.

Figure 4.19 shows the data of Figure 4.16 folded modulo  $16.^{\text{d}}585$ , with phase 0.0 centered on the epoch of rapid transition from high to low intensity. The asymmetric nature of the emission over the cycle is again quite evident, with the bulk of the source activity occurring at phase  $> 0.75$ . No sharp emergence from an eclipse is apparent, in contrast to the UHURU observation of 1972 May 9-17 (Jones *et al.* 1974) and to the behavior of the occulting X-ray binaries Cen X-3, Her X-1, and Vela X-1<sup>(9)</sup>. Note that the scatter of points at phase  $> 0.75$  in Figure 4.19 is due primarily to the folding of cycles of differing peak intensity, and not to variations within each cycle (see Figure 4.16).

With regard to the long-term behavior of Cir X-1, Clark, Parkinson, and Caswell (1975) have proposed a young runaway binary model in which the ON state occurs near periastron of a highly elliptical, long-period orbit. Davison and Tuohy (1975) found that an interval of  $\approx 220$  days between times of high emission was consistent with the available X-ray data. This is difficult to reconcile with the observations reported here since the absence of emission at more than 10 percent of maximum between 1974 October and 1975 August implies an extended low state (at

<sup>9</sup>Forman (1977) has recently reported that a re-analysis of the 1971-72 UHURU data for Cir X-1 has yielded an eclipse-like light curve at a period of  $16.^{\text{d}}605$  with an eclipse duration of  $\approx 1.^{\text{d}}25$ .

energies  $< 6$  keV) of  $\approx 300$  days. In addition, the relatively regular "envelope" of the long-term emission evident in Figure 4.16 is not present in the later data, with a clearly irregular modulation of maxima in the  $16.6^d$  cycle apparent after about 1974 day 830 (1976 April 9; see Figure 4.17). It thus appears that while the long-term variability of Cir X-1 at relatively low X-ray energies can sometimes be characterized by fairly well defined "high" and "low" states, no regular long-term pattern may exist. Finally, note the transient-like decay ( $\tau_d \approx 1$  month) of the successive  $16.6^d$  maxima which commenced between 1976 January 30 - February 19 (1974 day 760 - 780).

#### 5. Cygnus X-3

As discussed earlier, the  $4.8^h$  periodicity of Cyg X-3 affords an excellent test of the experiment sensitivity. The long-term light curve of this source is also interesting, as shown in Figure 4.20. In particular, a source modulation at the period  $P \approx 17^d$  emerged from folding of this data (cf. Holt et al. 1976d). In addition to significant fluctuations on timescales of days-weeks, a clear over-all declining trend is evident, with a roughly five-fold decrease in flux occurring over a period of  $\sim 1$  year. As changing gain and spacecraft orientation during this time could conceivably result in systematic errors as large as  $\sim 20\%$ , a gradual, long-term decay of the source emission (3-6 keV) is clearly indicated. Whether this variation represents a decrease in the total X-ray luminosity or reflects a gradual spectral variation of the source (cf. Serlemitsos et al. 1975) cannot be determined from our data. Subsequent observations have shown Cyg X-3 at levels  $\approx 0.2 \text{ cm}^{-2} \text{ s}^{-1}$  except for occasional, short-lived, enhanced intervals where the flux may reach a level of  $\sim 0.4 \text{ cm}^{-2} \text{ s}^{-1}$ .

## 6. Sco X-1 and Cyg X-2

We conclude this Chapter with a short discussion of two sources which have exhibited little, if any, long-term variations during the  $\sim 2$  years of Ariel 5 operation. Sco X-1 and Cyg X-2 have been likened in several respects, including their X-ray variability (factor of  $\sim 3$  on timescales of hours-days, Giacconi et al. 1974) and identification with short period ( $P_{\text{opt}} = 0.^{\text{d}}787$  and  $0.^{\text{d}}92$  for Sco X-1 and Cyg X-2, respectively) binaries with late-type, low-mass optical companions.

The ASM light curves of these sources are shown in Figure 3.9. While dramatic long-term variations are not apparent in the records of these sources, both have been shown to exhibit distinctive variations on shorter timescales. Holt et al. (1976c) have shown that the observed fluctuations of Sco X-1 are consistent with shot-noise dominated emission, characterized by flares (duration  $\approx .3\text{d}$ ) occurring at a rate of  $\approx 200 \text{ d}^{-1}$ . Cyg X-2, on the other hand, has been found to vary quasi-regularly by a factor of  $\sim 5$  with a cycle of  $11.^{\text{d}}2$  (Holt et al. 1976e). Interestingly, neither of these sources exhibits an observable modulation of the 3-6 keV flux at the proposed optical periods (Holt et al. 1976b,e).

It is clear from the ASM observations that the vast majority of galactic X-ray sources exhibit some degree of variability over time scales of hours-years. A number of UHURU sources listed as "non-variable" have been observed to fluctuate (e.g., 3U1636-53) while others of low (quoted) variability have exhibited major outbursts (e.g., Aql X-1, 4U1608-52). In addition, several sources observed at relatively high flux levels during the UHURU era have shown marked reductions in intensity



from recent observations (S (1975-76)  $\approx$  0.05 - 0.01  $S_{UHURU}$ , Villa et al. 1976). It would thus appear that all binary X-ray sources are variable at some sensitivity level over a wide range of time scales, with the transient sources representing the most extreme manifestation of the intrinsically chaotic accretion process.

## CHAPTER V

### DISCUSSION AND CONCLUSIONS

We now turn to the discussion of the nature of the transient X-ray sources. Inasmuch as the extreme variations of these sources observationally distinguishes them from the majority of variable X-ray sources, it is desirable to examine whether they may represent a new type of astrophysical phenomenon (as suggested, for example, in some models for the  $\gamma$ -ray bursts), or may be explained in terms of more conventional mechanisms. In the latter case, we must distinguish between a number of a priori possibilities, including sources characterized by similar variability in the optical band (novae and supernovae) and extreme variations in relatively stable X-ray emitting systems (X-ray binaries). The observations of Chapter IV may be utilized in two fashions to attack this problem. First, the results of § IV.A.7 may be employed to constrain the various parameters (spatial distribution, rate of occurrence, and peak luminosity) of the over-all transient source population. Secondly, the implications of the individual temporal and spectral characteristics of each source may be combined with the preceding information and investigated in the context of specific source mechanisms. We shall demonstrate that both classes of observational constraints are consistent with a source interpretation in terms of the standard X-ray binary model, with outbursts caused by large variations in the mass transfer rate to the compact object resulting from temporary increases in the stellar wind density or episodic Roche-lobe overflow of the companion. Note, however, that no a priori assumptions are made as to the spatial and luminosity distributions of the transient sources.

As noted in Chapter I, the pre-Ariel 5 transients (Table 1.2) are characteristically bright ( $S_{\max} \gtrsim S_{\text{crab}}$ ), long-lived ( $\tau_{\text{avg}} \gtrsim 1$  month) sources appearing (except for Cen X-4) within  $5^\circ$  of the galactic plane. The relative insensitivity of the earlier instruments to transient events resulting from incomplete and non-uniform sky coverage make those observations of limited value for quantitative estimates of the aforementioned transient source parameters. Indeed, the detection of at least nine additional transients (with peak fluxes ranging from  $\sim 0.1 - 40 S_{\text{crab}}$ ) during the first 2 years of Ariel 5 operation suggests that the predominance of bright, long-duration transients in the earlier data may be reasonably attributed to observational selection effects. In the following discussion, the virtually continuous all-sky coverage ( $\gtrsim 80\%$  of the 3-6 keV X-ray sky at a level  $\approx 1/3$  Crab) of the ASM is combined with that of the other (limited field-of-view, higher sensitivity) Ariel 5 experiments, with an expected considerable reduction in such effects.

#### A. Spatial Distribution

While a galactic origin for the transient sources was demonstrated by Silk (1973) on the basis of the pre-Ariel 5 sources (cf. Appendix E), their apparent concentration at low galactic latitude may plausibly be ascribed to observational bias in the plane. Citing this possibility, Silk in fact concluded that the early observations favored a galactic halo population. It is quite clear from Tables 1.3 and 4.1, and Figures 1.6 and 5.1 (the latter representing a galactic map of "unqualified" transient sources, proposed candidates, transient/variable sources<sup>1</sup>,

<sup>1</sup>This classification includes sources which exhibit relatively frequent, transient-like outbursts (e.g., Aql X-1 and 3U1630-47).

and long-term variable ( $\gtrsim 10x$ ) UHURU sources), however, that the transients must constitute a disk population similar to that of the brighter UHURU sources. An upper limit to the mean displacement from the galactic plane ( $|\bar{z}|$ ) may be obtained on purely probabilistic grounds, independent of whether the transients represent a local (low luminosity) phenomenon or are located at galactic distances (i.e.,  $d \gtrsim 1$  Kpc). Including only the sources observed over the two year period from 1974 October (Table 1.3), we find a mean galactic latitude of  $|\bar{b}| = 3.1^\circ$ . The probability of observing all nine sources within  $7^\circ$  of the plane from a spherically-distributed source population is  $P \lesssim 10^{-5}$ . If we now assume the worst possible case (for establishing an upper limit to  $|\bar{z}|$ ) of a galactic distribution for the transients, a mean distance from the sun of  $\bar{d} \lesssim 15$  Kpc is implied, and the observed latitude distribution (excluding Cen X-4, which is probably much closer) yields the result  $|\bar{z}| \lesssim 0.78$  Kpc. Note that even for the anomalously high latitude source Cen X-4, ( $b = 23^\circ$ ), the distance from the plane may be reconciled with the above half-thickness if  $L \gtrsim 10^{38}$  erg s $^{-1}$  ( $z \gtrsim 0.57$  Kpc). The observed source galactic longitudes may also be employed to effectively rule out a local origin ( $\bar{d} \lesssim 1$  Kpc), since the probability of detecting only two sources out of nine with galactic longitude  $90^\circ \lesssim \ell \lesssim 270^\circ$  from a uniform angular distribution is  $P \approx 0.07$  ( $P \approx 0.01$  if the pre-Ariel 5 transients are included).

Another estimate of the scale height of the disk occupied by the transient sources is obtainable from their direction in the galaxy (i.e., galactic longitude) and the observed fluxes at maximum. Anticipating the characteristic range of peak luminosities ( $L$ ) of the transients derived in the next section,  $2 \times 10^{36} \lesssim L$  (erg s $^{-1}$ )  $\lesssim 2 \times 10^{39}$ , it is instructive to tabulate the distance to the sources as a function of  $L$ . Table 5.1

shows this dependence and includes the maximum distance to each source in the Milky Way (i.e., to the galactic edge), where we assume values for the galactic radius ( $R$ ) and sun-galactic center distance ( $R_s$ ) of 15 and 10 Kpc, respectively. On the basis of these sources, we find an average displacement from the galactic plane of  $|\bar{z}| \approx 0.3 \times (L_{38})^{1/2}$  Kpc, ( $L_{38} \equiv L/10^{38} \text{ erg s}^{-1}$ ), and it is apparent that the transients must reside in a relatively thin disk ( $0.002 \lesssim |\bar{z}|/R \lesssim 0.06$ ). While it is therefore possible to exclude only a Halo Population II ( $|\bar{z}| \approx 2$  Kpc, Allen 1963) origin for the transient sources at this point, evidence for the existence of two distinct spatial distributions is discussed in the following Section.

As can be seen from Figures 1.6 and 5.1, the spatial distribution of the "unqualified" transients is entirely consistent with that of the variable ("permanent") sources, even to the extent of an apparent concentration near galactic center, which has been associated with a physical concentration of sources in the nuclear bulge ( $320^\circ < \ell < 20^\circ$ , Salpeter 1973; Gursky 1973). While we cannot rule out an enhancement in the space density of the transient sources in the inner nuclear region, an approximately uniform distribution throughout the remainder of the disk is clearly implied by the appearance of two sources in the vicinity of Galactic Anticenter. It is interesting to note in this regard that Matilsky et al. (1973) concluded that the UHURU data on low-latitude sources ( $|b| < 20^\circ$ ) is consistent with at least two types of objects: (1) a small number of intense sources in the central galactic region with  $|\bar{z}| \approx 650$  pc; and (2) a larger number of less intense sources more uniformly dispersed through the Galaxy with  $|\bar{z}| \approx 200$  pc. Although the statistics do not allow exclusion of additional systematic variations of the space density

(for example, clumping in the spiral arms), such effects will not significantly affect the conclusions of the next section in which a roughly uniform spatial distribution is assumed.

### B. Occurrence Rates and Luminosities

A rough determination of the characteristic luminosity (at maximum) of the transient sources may be obtained based upon the above spatial distribution and the observed fluxes<sup>2</sup>. As illustrated in Table 5.1, the majority of sources would lie beyond the boundary of the galaxy for  $L \gtrsim 2 \times 10^{39} \text{ erg s}^{-1}$ , while most would be located within  $\sim 1 \text{ Kpc}$  of the Sun for  $L \lesssim 10^{36} \text{ erg s}^{-1}$  (in contrast to the non-local origin suggested from the galactic longitude distribution). Given the consistency of the spatial characteristics of the transient sources with a roughly homogeneous distribution in the galactic plane, we may define more precisely the range of allowed luminosities following the procedure of Silk (1973). As outlined in Appendix E, the assumption that the transients may occur anywhere in the galactic plane (scale height  $h \ll R$ ) with roughly equal probability and peak absolute luminosity ( $L$ ), gives the relation:

$$N(>S_0, t) = \frac{1}{4\pi} \left( \frac{L}{S_0 R^2} \right) \left( \frac{t}{\tau} \right), \text{ or} \quad (5-1a)$$

$$\frac{L}{\tau} \left( \frac{\text{erg s}^{-1}}{\text{yr}} \right) = 4.3 \times 10^{38} \left( \frac{N(>S_0, t)}{t} \right) \left( \frac{S_0}{S_{\text{crab}}} \right) \left( \frac{R}{15 \text{ Kpc}} \right)^2 \quad (5-1b)$$

where  $N(>S_0, t)$  is the number appearing above a threshold flux  $S_0$  in time  $t$ , with a mean time  $\tau$  between all source occurrences in the galaxy (of radius  $R$ ). Note that this equality holds only under the conditions that:

<sup>2</sup>We assume throughout this discussion spherically symmetric X-ray emission, i.e.,  $S = \frac{L}{4\pi d^2}$ . Any beaming or non-spherically symmetric emission over a solid angle  $\Omega$  will correspondingly lower the deduced luminosities by a factor  $\Omega / 4\pi$ .

(a) no sources are missed (due to source confusion, for example) whose fluxes exceed  $S_0$ , and (b) the characteristic luminosity is such that  $S < S_0$  for  $d \gtrsim R$ <sup>(3)</sup>. If either condition is violated the quantity  $N(>S_0, t)$  will be under-estimated, and Equation (5-1b) can only give a lower limit to the ratio  $L/\tau$ . We also note that Equation (5-1a) is just the "size distribution" for equi-luminous sources located uniformly in a thin disk  $N(>S, t) = \left(\frac{L}{4\pi R^2}\right) \left(\frac{t}{\tau}\right) S^{-1}$  evaluated at flux level  $S_0$ . If the number of sources were sufficiently large, one could use the observed size distribution to discriminate between a uniform and inhomogeneous spatial distribution (for example,  $N(>S, t) = \left(\frac{L}{4\pi R^2}\right)^{1/2} \left(\frac{t}{\tau}\right) S^{-1/2}$  for M spiral arms, cf. Appendix E). However, as shown in the log N-log S plot of Figure 5.2 and as discussed in Appendix E, the paucity of transients does not allow resolution of this problem at the present time, although a spherical distribution (extragalactic or galactic halo) is clearly irreconcilable with the observations.

We now relax the assumption of a single characteristic transient source luminosity and investigate the possible existence of at least two source sub-classes, distinguished primarily in terms of luminosity, and to a lesser extent, other characteristics such as spectrum and lifetime. Examination of Tables 1.2 and 1.3 suggest that the transients may be divided into two main classes: (1) bright ( $S_{\max} \gtrsim S_{\text{crab}}$ ), soft spectral ( $\alpha \gtrsim \alpha_{\text{crab}}$ ), long-duration ( $\tau_d \gtrsim 1$  month) sources exemplified by A0620-00

<sup>3</sup>This condition implies that we are sensitivity-limited to the sources; i.e.,  $R_0 < R$ , where  $R_0 = \left(\frac{L}{4\pi S_0}\right)^{1/2}$ , see Appendix E.

(henceforth designated Type I), and (2) weaker ( $S_{\max} \lesssim S_{\text{crab}}$ ), harder spectral ( $\alpha \lesssim \alpha_{\text{crab}}$ ), short-lived ( $\tau_d < 1$  month) sources typified by A1118-61 ("Type II"). It is also interesting to recall that the two Ariel 5 transients which presumably belong to this latter category (A1118-61 and A0535+26) have both been shown to be pulsating with relatively long periods (104s and 6.75m, respectively) and have been tentatively associated (Chevalier and Ilovaisky 1975; Liller 1975) with massive early-type giant companions (OB stars). While these sources must be characterized by luminosities  $L \lesssim 5 \times 10^{37} \text{ erg s}^{-1}$  and  $10^{38} \text{ erg s}^{-1}$ , respectively (in order to insure confinement to the Galaxy), sources such as A0620-00 and A1742-28 apparently represent a more luminous phenomenon ( $L \gtrsim 10^{38} \text{ erg s}^{-1}$ ) in view of their observed brightness and probable distances ( $d \gtrsim 1$  and 5 Kpc, respectively). Given the evidence for a two-component transient source population, a more rigorous determination of the corresponding peak luminosities and rates of occurrence may now be attempted.

#### 1. High Luminosity Sources (Type I)

It is clear from the log N-log S plot (Figure 5.2) that there exists a predominance of bright sources with a corresponding deficiency of sources at fluxes  $S < S_{\text{crab}}$  (with respect to the assumed plane distribution, curve II). Although a fraction of this deficiency (especially in the range  $0.1 \lesssim S/S_{\text{crab}} \lesssim 0.5$ ) may be attributed to sources missed as a result of confusion in the plane, the magnitude of the discrepancy is such that some portion of it must arise from a physical absence of sources in this flux range. As the majority of sources with fluxes  $S > S_{\text{crab}}$  are reconcilable with Type I transients, this conclusion implies that the ASM is not sensitivity-limited to the bright, long-duration sources, and Equation 5-1b therefore provides only a lower limit on the



ratio  $L/\tau$ . The detection of three sources of the Type I variety during the first year of Ariel 5 operation (A1524-62, A1742-28, and A0620-00 all exceeded  $S_{\text{crab}}$  at maximum, compared to an effective experiment threshold  $S_{\text{thresh}} \approx 1/3 S_{\text{crab}}$ ) implies a value of  $\tau_I \gtrsim 0.1 \text{ yr}$  (i.e.,  $f_I = \tau_I^{-1} \lesssim 10 \text{ yr}^{-1}$ , on the average), and a corresponding characteristic peak luminosity  $L_I \gtrsim 10^{38} \text{ erg s}^{-1}$ (4).

As discussed above, the maximum allowable luminosity for these sources is specified by the requirement of containment within the Galaxy. The potentially great distance ( $d_{\text{max}} \sim 20 \text{ Kpc}$ ) and relative brightness of A1742-28 make this source particularly useful in this regard, yielding  $L \lesssim 2 \times 10^{39} \text{ erg s}^{-1}$ . In addition, the peak luminosity of A0620-00, for which a good upper limit to the distance is known ( $d \lesssim 3 \text{ Kpc}$ , Wu et al. 1976; Whelan et al. 1976),  $L \lesssim 9 \times 10^{38} \text{ erg s}^{-1}$ , is consistent with the above value. Furthermore, the rough agreement of this upper limit to  $L_I$  with that derived from Equation 5-1b with  $\tau_I < 1 \text{ yr}$  ( $L_I \lesssim 10^{39} \text{ erg s}^{-1}$ ), suggests that we have not seriously underestimated  $N(>S_0, t)$  in that Equation. It is interesting to note that the derived range of Type I peak luminosities,  $10^{38} \lesssim L_I \text{ (erg s}^{-1}\text{)} \lesssim 2 \times 10^{39}$ , is consistent with that expected from a class of  $M_X \approx 1 - 10 M_\odot$  Eddington-limited sources ( $L_E \approx 1.3 \frac{M_X}{M_\odot} \times 10^{38} \text{ erg s}^{-1}$ ). Note also that this argument is self-consistent as virtually all sources of this type will appear at intensities above the ASM level of detectability (i.e., even at  $d_{\text{max}} \sim 20 \text{ Kpc}$ ,  $S \gtrsim 0.1 S_{\text{crab}}$ ), and that the sensitivity-limitation condition (b) above is

<sup>4</sup>Note that we have chosen  $S_0 = S_{\text{crab}}$  in this case to minimize the effects of violation of condition (b) (sensitivity-limitation) above. Note also that a comparable lower limit ( $L \gtrsim 9 \times 10^{37} \text{ erg s}^{-1}$ ) is obtained if we include MX 1803-24 as a Type I source ( $N(>S_{\text{crab}}, t=2\text{yr}) = 4$ ).

not satisfied ( $R_0 \approx 10 - 30$  Kpc). This latter situation is further accentuated by the Sun-Galactic Center offset, as discussed in Appendix E. Finally, as a consequence of their intrinsic brightness, proximity to the plane, and longevity, earlier sources belonging to this class (Cen X-2, Cen X-4, and 3U1543-47) were detectable with relatively high efficiency even without continuous all-sky coverage.

## 2. "Low Luminosity Sources (Type II)

In contrast to the Type I transients, the harder-spectral, shorter-duration sources are consistent with a source population that is intrinsically less luminous at maximum. The upper limits to the luminosities of A1118-61 and A0535+26 ( $L \lesssim 5 \times 10^{37}$  erg s $^{-1}$  and  $10^{38}$  erg s $^{-1}$ , respectively) indicate that the ASM is indeed sensitivity-limited to this class of transient sources. Note also that the short-lived UHURU transient 3U1735-28 is consistent with a source of luminosity  $L \sim 5 \times 10^{37} - 10^{38}$  erg s $^{-1}$  residing in or near the Galactic Nucleus ( $d \approx 7-10$  Kpc). In this case, the relative brevity of the outburst only contributes to the problem of source detection, suggesting that all such sources above an effective threshold of  $S_0 \approx 1/3 S_{\text{crab}}$  will not be observed, in general. Thus, condition (a) on Equation 5-1b will not be satisfied, and this relation again can only specify a crude lower limit for the ratio  $L/\tau$ :

$$L_{\text{II}}/\tau_{\text{II}} \left( \frac{\text{erg s}^{-1}}{\text{yr}} \right) \gtrsim 2 \times 10^{38} \left( \frac{S_0}{S_{\text{crab}}} \right) \left( \frac{R}{15 \text{ Kpc}} \right) \quad (5-1c)$$

where we have used  $N(>S_0 = S_{\text{crab}}, t = 2 \text{ yr}) \approx 1$  (A0535+26) since the efficiency for detection is so poor at the level of A1118+61. Although the galactic longitude distribution of the over-all source sample is irreconcilable with a local origin (§V.A), we cannot rule out a priori

the possibility that the subclass of Type II transients represents an intrinsically weak phenomenon with a correspondingly greater rate of occurrence (i.e.,  $L_{II} < 10^{35}$  erg s<sup>-1</sup>,  $\tau_{II} < 10^{-3}$  yr, Equation 5-1c). Such an extreme situation can effectively be ruled out, however, in view of the following considerations (we include the UHURU transient 3U1735-28 as a Type II source in this discussion):

(1) As for the over-all sample, a local spherical distribution of these sources may be ruled out on probabilistic grounds (Prob (N = 3,  $|b| < 5^\circ$ )  $\approx 5 \times 10^{-3}$ ). The source horizon<sup>(5)</sup> ( $L < 10^{35}$  erg s<sup>-1</sup>,  $S > 0.1 S_{\text{crab}}$ ) of  $r_h \approx 0.7$  Kpc and the observed latitude constraint ( $|b| < 5^\circ$ ) then yield a maximum disk half-thickness of  $|\bar{z}| \lesssim 100$  pc;

(2) The condition  $\tau \lesssim 10^{-3}$  implies a total number of (Type II) sources instantaneously 'ON' in the Galaxy of  $N_i \approx \frac{T_{\text{ON}}}{\tau} \lesssim \frac{0.10 \text{ yr}}{\tau}$ , ( $T_{\text{ON}}$  is the average source ON-time  $T_{\text{ON}} \lesssim 2 \tau_d$ ,  $\tau_d \lesssim 3$  weeks), or  $N_i \lesssim 100$ . Such a relatively large number of transients could contribute an unresolved source component to the observed upper limit to a galactic ridge ( $L_n < 8 \times 10^{-30}$  erg s<sup>-1</sup> cm<sup>-3</sup>,  $\ell^{II} = 60^\circ$ , (5-2); Holt et al. 1974). Assuming the source density in relation (5-2) to be composed entirely of Type II transient sources in the ON state ( $n_s = \frac{N_i}{2\pi R^2 h}$ ) gives an independent upper limit on  $(L/\tau)$  of:

$$L_{II}/\tau_{II} \left( \frac{\text{erg s}^{-1}}{\text{yr}} \right) < 4 \times 10^{38} \left( \frac{R}{15 \text{ Kpc}} \right)^2 \left( \frac{h}{0.1 \text{ Kpc}} \right) \left( \frac{0.10 \text{ yr}}{T_{\text{ON}}} \right), \quad (5-2a)$$

<sup>5</sup>The source horizon is the maximum observable distance for which sources of luminosity  $L$  will appear above a threshold flux  $S_{\text{thresh}}$ ;  $r_h = (L/4\pi S_{\text{thresh}})^{1/2}$ .

where we note that this relation is useful only if the number of instantaneous sources is sufficiently large (i.e.,  $\tau \lesssim 10^{-3}$  yr);

(3) The assumption of a roughly uniform spatial distribution in the galactic disk ( $N(>S) \propto S^{-1}$ ) and the detection of one source brighter than the Crab over a two year interval implies a yearly rate of occurrence at fluxes exceeding  $S = .01 S_{\text{crab}}$  of  $N(>.01 S_{\text{crab}}, t = 1 \text{ yr}) \approx 50$ , or  $\dot{N}(>.01 S_{\text{crab}}) \approx 4 \text{ month}^{-1}$ . The extended galactic plane observations of the SSI are interesting in this regard (total observing time  $> 2 \frac{1}{2}$  months), as that instrument ( $S_{\text{thresh}} \approx .005 S_{\text{crab}}$ ) would be expected to detect  $\gtrsim 10$  of these sources during that time. While a number of weak, previously undetected sources have been discovered by the SSI during such scans (Villa et al. 1976), most of these sources cannot be associated with the transients, as the continuous 3-4 week observing time of each survey would allow identification of a decaying trend. The apparent deficiency of weak ( $S < 0.1 S_{\text{crab}}$ ) transients indicated by this observation thus strongly suggests that the Type II transients occur less frequently than permitted by the ridge constraint (i.e.,  $\tau_{\text{II}} \gtrsim 10^{-2}$ ). In fact, the possibility that the SSI is not sensitivity-limited to these sources (at  $S_0 \approx .01 S_{\text{crab}}$ ) would imply  $L \gtrsim 4 \times 10^{36} \text{ erg s}^{-1}$ , roughly consistent with that defined by the estimated lower limit on  $\tau_{\text{II}}$  and Equation (5-1c),  $L \gtrsim 2 \times 10^{36} \text{ erg s}^{-1}$ .

An upper limit to  $\tau_{\text{II}}$  may be estimated from the rate of detection of the Type II sources (at least two unambiguous sightings were made in the first year of Ariel 5 operation, with several additional candidates reported in IAU Circulars (cf. Table 4.1), and the fact that the marginal sensitivity of the ASM to such short-lived, weaker sources suggests that

we have not observed a significant fraction of those at a maximum flux in excess of  $\sim 1/3 S_{\text{crab}}$ . Thus, a reasonable estimate for the longest mean interval between source occurrences is  $\tau_{\text{II}} \lesssim 0.2 \text{ yr}$  and Equation (5-1c) now implies (allowing for a non-detected source rate ( $S > S_{\text{crab}}$ ) of  $\sim 1 \text{ yr}^{-1}$ ) an approximate (conservative) upper limit to the Type II peak luminosity of  $L_{\text{II}} \lesssim 1 \times 10^{38} \text{ erg s}^{-1}$ , in rough agreement with that derived above on the basis of the observed fluxes and galactic longitudes of A1118-61, A0535+26, and 3U1735-28. It is interesting to note that the deduced range of  $2 \times 10^{36} \lesssim L_{\text{II}} (\text{erg s}^{-1}) \lesssim 1 \times 10^{38}$  is reconcilable with the tentative identification of both A1118-61 and A0535+26 with OB stars ( $V$  (A1118-61)  $\sim 12$ , Chevalier and Ilovaisky 1975;  $m_B$  (HDE245770/A0535+26)  $\sim 9.5$ , Liller 1975) at distances  $d > 1 \text{ Kpc}$  ( $d_1 \gtrsim 10$  and 3;  $L_{37} \gtrsim 2$  and 4, respectively, assuming absolute magnitudes and interstellar absorption of  $M_V \approx -5$  and  $A_V \approx 2$ ). As shown in the galactic model (from 21 cm observations, Simonson 1975) of Figure 5.3, the luminosity ranges for both classes of transient sources are roughly consistent (except for an apparent deficiency at longitudes  $0^\circ < \ell < 180^\circ$ ) with the initial assumption of an approximately homogeneous spatial distribution.

Although the total number of instantaneous ('ON') transient sources is too small to contribute an unresolved source component to a galactic ridge ( $N_{i,I} \lesssim 2$ ,  $N_{i,II} \lesssim 10$ ), the total number of quiescent, potential transient sources ( $N_q$ ) may be estimated from the observed mean recurrence times ( $\bar{T}_{\text{rec}}$ ) and upper limits on  $\tau$ , and compared with the ridge upper limit (Equation 5-2). The approximate number of transient sources in the quiescent state is simply  $N_q \approx \bar{T}_{\text{rec}}/\tau$ , yielding limits on the total Type I and II source populations of  $10 \lesssim N_{qI} \lesssim 500$  and  $100 \lesssim N_{qII} \lesssim 5000$ , where we have taken  $10 \lesssim \bar{T}_{\text{rec}} (\text{yr}) \lesssim 50$  as a conservative range to the

mean recurrence period of the transients (well within the mean of Aq1 X-1 ( $T_{\text{rec}} \sim 1$  yr) and A0620-00 ( $T_{\text{rec}} \sim 58$  yr) and the average frequency of the recurrent novae,  $T_{\text{rec}} \sim 10$ -80 yr). Such a large number of weak sources ( $L_q \lesssim 10^{35}$  erg s $^{-1}$  since  $L_{\text{max}}/L_{\text{min}} \gtrsim 10^3$ ) could contribute an unresolved source component to the ridge, and Equation 5-2 may now be used to obtain a crude upper limit to the product of the quiescent state luminosity and number of sources in that state:

$$\frac{L_q N_q}{2\pi R^2 h} < L_n \lesssim 8 \times 10^{-30} \text{ erg s}^{-1} \text{ cm}^{-3};$$

$$L_q N_q \lesssim 2.6 \times 10^{37} \left(\frac{R}{15 \text{ Kpc}}\right)^2 \left(\frac{h}{.5 \text{ Kpc}}\right) \text{ erg s}^{-1}. \quad (5-2b)$$

The estimated lower limits to the quiescent state populations then imply quiescent state luminosities  $L_{qI} \lesssim 2 \times 10^{36}$  erg s $^{-1}$  and  $L_{qII} \lesssim 2 \times 10^{35}$  erg s $^{-1}$  ( $h \sim 0.3$  Kpc), roughly consistent with the observed ratio  $L_{\text{max}}/L_{\text{min}} \gtrsim 10^3$  and  $L_{\text{max}}$  (I;II)  $\sim 2 \times 10^{39}; 1 \times 10^{38}$  erg s $^{-1}$ . Note also that an actual mean recurrence time  $\bar{T}_{\text{rec}}$  larger than the estimated lower limit and values of  $\tau$  smaller than the derived upper limits ( $\tau_I < 1$  yr;  $\tau_{II} < 10^{-1}$  yr) will both tend to decrease the upper limit on  $L_q$ . Thus, the approximate number of dormant transient X-ray sources in a roughly uniform galactic disk distribution is reconcilable with the deduced maximum luminosities, peak/quiescent luminosity ratio, and the observed upper limit to a galactic ridge.

It is interesting to note the similarity of the suggested luminosity sub-classes for the transients to the proposed bi-modal luminosity distribution of the more permanent X-ray sources (cf. Margon and Ostriker 1973 and Figure 5.4), with the brighter group emitting at a luminosity consistent

with an Eddington-limited  $1 M_{\odot}$  secondary, and the weaker group radiating at a luminosity which is at least an order of magnitude lower. It is clear from the derived spatial distribution and peak luminosities of the Type I/II transients that neither class can be closely related to the "weak, high-latitude" transients. In addition to the short-lived nature (minutes - days) and low fluxes at maximum ( $S_{\max} \lesssim 0.1 S_{\text{crab}}$ ), the mean galactic latitude ( $|b| \sim 40^{\circ}$ ) of four sources identified with this group (A1103+38, MX2346-65, A0000+28, and A0353-40; Cooke 1976) implies a source population comprised of weak, local objects ( $d_1 \lesssim 3$ ;  $L_x \lesssim 10^{35} \text{ erg s}^{-1}$ ) and/or strong extragalactic sources ( $d_1 \gtrsim 500$ ,  $L_x \gtrsim 10^{40} \text{ erg s}^{-1}$ ).

We conclude this Section with a re-examination of the transient source spatial distribution. On the basis of the luminosity ranges for the two source subclasses, we now obtain mean displacements from the galactic plane of  $0.3 \lesssim |\bar{z}_I| \text{ (Kpc)} \lesssim 1.3$  (Cen X-2, Cen X-4, 3U1543-47, A1524-62, A1742-28, A0620-00) and  $0.04 \lesssim |\bar{z}_{II}| \text{ (Kpc)} \lesssim 0.3$  (3U1735-28, A1118-61, A0535+26). This suggests that the Type I/II subclasses may be further differentiated in terms of the thickness of their respective disk scale heights, although a larger sample is clearly required for a more reliable estimate of  $|\bar{z}|$ . With regard to stellar population subdivisions, we note that the Type II sources are consistent with Population I objects (Extreme Population I:  $|\bar{z}| \approx 120 \text{ pc}$ ; Older Population I:  $|\bar{z}| \approx 160 \text{ pc}$ , Allen 1963), while the Type I transients are reconcilable with a Disk Population ( $|\bar{z}| \approx 400 \text{ pc}$ ) or Intermediate Population II ( $|\bar{z}| \approx 700 \text{ pc}$ ) distribution (cf. Allen 1963; Oort 1958), and that of the older population "permanent" X-ray sources<sup>6</sup>. Note that this further supports our assumption

<sup>6</sup>According to Gursky and Schreier (1974) sources belonging to this group are Sco X-1, Her X-1, Cyg X-2, and Cyg X-3, with displacements from the plane ranging from  $z \sim 0.1 - 4.0 \text{ Kpc}$ .

of a roughly uniform disk distribution (vs. spiral arms) for the over-all transient source sample as the spiral arms are characterized by a scale height  $|\bar{z}| \lesssim 160$  pc (Extreme/Older Population I, Allen 1963). It is further interesting to note, finally, that this apparent spatial differentiation is also consistent with the association of the Type I/II transients with low-mass, late-type binary systems, and massive, early-type companions, respectively.

### C. Observational Constraints on Source Models

A variety of mechanisms have been suggested to interpret the phenomenon of the transient X-ray sources. In this section, we critically evaluate the proposed models in the context of the characteristic temporal and spectral properties from the individual source observations (Chapter IV), and the additional constraints imposed by the results of the two preceding sections. In view of the latter, we confine this discussion to systems capable of producing X-ray luminosities on the order of  $L_x \sim 10^{36} - 10^{39}$  erg s<sup>-1</sup> and consistent with a galactic disk distribution. Notwithstanding the close similarity of the transient X-ray source light curves to the optical variations of the classical<sup>7</sup> novae, we shall attempt to demonstrate that the observations are best explained in terms of episodic accretion in normally weak (quiescent-state luminosity  $L_x \lesssim 10^{35}$  erg s<sup>-1</sup>) X-ray binary systems. It is further suggested that the proposed differentiation of the transients into two sub-classes may arise from the nature of the optical companion, with late (dwarf, main sequence, sub-giant) vs. early (OB giant, B emission) type stars associated with Types I and II, respectively.

<sup>7</sup>i.e., objects in which the outburst results from explosive thermonuclear burning on the surface of a white dwarf, as distinguished from accretion mechanisms associated with some dwarf and recurrent novae.



## 1. Classical Novae

### a. Models

The classical nova phenomenon, characterized by a rapid rise ( $t_{\text{rise}} \sim \text{hrs-days}$ ) by  $\sim 10$ - $12$  magnitudes ( $L_{\text{max}}/L_{\text{min}} \approx 10^4$ - $10^5$ ) followed by a gradual decline back to the pre-nova state (see Figure 1.5), is quite similar to the phenomenology of the transient X-ray sources. Interestingly, the total energy released ( $E_{\text{tot}} \approx 10^{44} - 10^{45}$  ergs, Schatzmann 1965) in the nova outburst is comparable to the X-ray energy output of the transient sources ( $E_x \approx L_x \tau_d \approx 10^{42} - 10^{46}$  ergs), and the observed nova spatial distribution (Disk Population, Allen 1973) is not irreconcilable with that of the Type I transients. Additionally, the interaction of the expanding shell of gas ejected in the initial thermonuclear runaway with the surrounding medium provides a natural mechanism for X-ray production similar to that of the supernova remnants. Indeed, Edwards (1968) suggested that the roughly monotonic cooling observed in Cen X-2 could be accounted for by expansion of the circumstellar envelope surrounding a nova shortly after outburst, with the X-rays originating in an expanding shell of shock-heated gas. In a modification of the nova model, Van Horn and Hansen (1974) replaced the accreting white dwarf with a low-mass ( $M \lesssim 0.15 M_{\odot}$ ) neutron star, with the outburst resulting from thermonuclear shell flash of accreted hydrogen ( $\dot{M} \sim 10^{-12} M_{\odot} \text{ yr}^{-1}$ ) on the neutron star surface. We note immediately that a serious objection to this model on theoretical grounds is raised by the conclusion of Borner and Cohen (1973) that the occurrence of such low mass neutron stars in nature is highly improbable ( $M_{\text{ns}} \gtrsim 0.2 M_{\odot}$ ). Two additional nova-related models similar to that of Edwards were invoked to interpret the early observations of A0620-00, particularly in light of its identification with the recurrent nova V616

Monocerotis. In the "colliding shells" hypothesis (Brecher and Morrison 1975) and the nova model of Gorenstein and Tucker (1976) the X-ray emission is hypothesized to arise from interaction of the expanding shell with previously ejected shells or the ambient circumstellar material, respectively. Finally, a nova-like model in which the outburst results from isothermal expansion of a dense H II cloud (unspecified ejection mechanism) was proposed by Manley (1967) to explain the early observations of Cen X-2.

#### b. Comparison with Observations

The hypothesized association of the transient X-ray sources with ordinary optical novae is contradicted by several general observations, which may be summarized as follows:

(1) The lack of nova counterparts ( $m_V \gtrsim 15$ ) for all of the transients except A0620-00 (which is probably not a classical nova, as discussed below). This implies an absolute visual magnitude at maximum of  $M_V \gtrsim 5 - 5 \log d_1 - A_V$  (recall that  $d_1 \equiv d/1\text{Kpc}$ ), which for distances  $d_1 = 1-10$  (and modest interstellar absorption), requires the optical counterparts to be  $\sim 5-10$  magnitudes fainter than the observed range for novae ( $\bar{M}_V \approx -5$ );

(2) The absence of detectable X-ray emission from optical novae. The upper limit to such emission for the eight novae reported since 1974 October from the ASM ( $S_X \lesssim 0.1 \text{ cm}^{-2} \text{ s}^{-1}$ ,  $1\sigma$ ) implies an approximate upper limit on the ratio of the optical to X-ray (3-6 keV) luminosity (assuming  $M_V = -5$ ) of  $L_X/L_{\text{opt}} \lesssim .01 d_1^2$ . A more stringent upper limit was obtained by SAS-3 for Nova Cygni 1975 ( $L_X/L_{\text{opt}} \lesssim 10^{-4}$ , Hoffman et al. 1976), which may be contrasted with that measured for A0620-00 ( $L_X/L_{\text{opt}} \approx 10^3$ , Doxsey et al. 1976); and

(3) The estimated frequency of occurrence of galactic novae ( $\sim 100 \text{ yr}^{-1}$ , Allen 1973), vs. that deduced for the transients, particularly the Type I sources ( $\tau_I^{-1} \lesssim 10 \text{ yr}^{-1}$ ).

It is clear from these considerations that ordinary classical novae cannot be directly connected with the transient X-ray sources.

In addition to the difficulties encountered by the nova association listed above, a number of the individual transient source observations are also inconsistent with nova mechanisms. The identification of A0620-00 with a recurrent nova last erupting in 1917 (Eachus, Wright, and Liller 1976) renewed speculation that some of the transient sources might originate in nova outbursts occurring under "unusual" circumstances (e.g., presence of previously ejected shells or dense circumstellar material). A number of difficulties with this association in the case of A0620-00 have been pointed out, however, such as the absence of stellar absorption and emission lines (Gull et al. 1975; Boley et al. 1976), the high X-ray to optical luminosity ratio, the inconsistency of optically thin bremsstrahlung in producing the observed optical and infrared radiation (Kleinmann, Brecher, and Ingham 1975), and physically distinct radio emission from that observed in several novae (Owen et al. 1976). With regard to the X-ray observations, in Chapter IV we noted an apparent discrepancy between the observed exponential decay and the  $1/t$  fall-off expected in several nova models (Edwards 1968; Brecher and Morrison 1975). The correlation of the X-ray and optical emission during the October and February increases represents additional, convincing evidence against a traditional optical nova origin for A0620-00, since in the nova models the X-ray and optical emission is hypothesized to originate in two well-separated regions (i.e., hot, expanding gas shell vs. surface of a white dwarf). For the same reason, the possible

existence of a modulation of the X-ray and optical emission of A0620-00 at the suggested  $\sim 7.8^d$  period represents additional evidence against a nova model.

Although A0620-00 is the only transient source for which comprehensive, concurrent optical observations exist, the characteristic X-ray behavior exhibited by several earlier sources is apparently inconsistent with the nova mechanism, as well. For example, the extended, low-level pre-flare emission from A1524-62 and the pronounced precursor peak in the rise phase of this and other transients is inconsistent with the very sudden rise ( $t_{\text{rise}} \sim \text{hrs}$ ) observed in some common novae and that expected in the thermonuclear shell flash model of Van Horn and Hansen ( $t_{\text{rise}} \sim \text{minutes}$ ). The substantial secondary maxima exhibited months to years after primary maximum by the sources A0535+26 (Joss 1975), 3U1543-47 (Li, Sprott, and Clark 1976), 3U1735-28 (Pounds 1976a), and A0620-00, and the relatively short recurrence time inferred from Aql X-1 and A0620-00 further distinguish these objects from the "one-shot" behavior (i.e.,  $\bar{T}_{\text{rec}} > 10^3 \text{ yr.}$ ) of the classical novae. In addition, the typical decay light curves are better fit by an approximately exponential fall-off, as opposed to the power-law decay ( $L = L_0 \left\{ \frac{t - t_0}{t_0} \right\}^{-\alpha}$ ) expected in the expanding shell ( $\alpha = 1$ ) or cloud ( $\alpha = 3$ ) mechanisms. Finally, the spectral observations are also inconsistent with the expected initially rapid cooling of an expanding nova shell ( $T = T_0 \left\{ \frac{t - t_0}{t_0} \right\}^{-2/3}$  for an Edwards-type model), although a more gradual cooling over the decline has been observed in several sources (Pounds 1976b). In conclusion, there appears to be sufficient evidence at this time to allow rejection of the hypothesized association of the transient X-ray sources with the classical nova phenomenon.

## 2. Binary Accretion Models

We now discuss the evidence in favor of the standard binary accretion mechanism underlying the X-ray emission of the more stable galactic sources. As demonstrated in the preceding sections both the characteristic peak luminosities and spatial distribution of the transients are completely consistent with those of the variable galactic sources. In addition, the transient behavior of several "permanent" sources, (e.g., Aql X-1) and the less extreme, long-term variability of other catalogued sources (e.g., Cyg X-1, Cir X-1, Cyg X-3) evident in the ASM observations suggest that the transient X-ray sources may be understood in terms of similar systems, differentiated only in the greater instability of the mass-exchange process.

A number of mechanisms have been proposed to explain the characteristic variability of the transients within the basic accretion hypothesis, including:

- (1) Modulation of the flux analogous to the 35<sup>d</sup> cycle of Her X-1; and
- (2) Episodic variations in the rate of mass transfer to the compact object resulting from:
  - a) orbital-phase-related variations in an eccentric-orbit binary;
  - b) intrinsic variability of the optical companion (e.g., dwarf and recurrent novae; Mira variables; OB giants; B emission stars);
  - c) relatively steady mass-exchange interrupted by "discharge" of an accretion disk due to triggering of an instability;
  - d) temporary decrease in a supercritical accretion rate (i.e., totally self-absorbed in the X-ray region); or
  - e) presence in a globular cluster.

In the remainder of this Chapter the above models are compared with the ASM and other available observations.

a. Her X-1 Type Modulation

The a priori possibility that the "outbursts" of the transient X-ray sources may actually represent the modulation of a (normally invisible) "permanent" source analogous to the 35<sup>d</sup> cycle<sup>8</sup> of Her X-1 may be effectively ruled out on the following grounds:

(1) the irregularity of the transient source phenomenon, including possible aperiodic recurrence (e.g., Aql X-1), secondary maxima, and extended, recurrent, low-level emission is in direct contrast to the high regularity of the 35<sup>d</sup> cycle (cf., Figure 1.12);

(2) the fractional Her X-1 ON-time ( $T_{ON}/P_{35} \sim 0.3$ ) over the 35<sup>d</sup> cycle implies, assuming a roughly similar geometry, a modulation cycle for the transients ( $T_{ON} \lesssim .5$  yr) of  $P_{Mod} \lesssim 2$  yr, as opposed to the estimated mean recurrence period  $\bar{T}_{rec} \gtrsim 10$  yr;

(3) the concurrent optical/X-ray variations of V616 Mon/A0620-00 indicate a physical variation in the X-ray/optical emission (Hz Her does not vary with the 35<sup>d</sup> cycle, as Her X-1 is continuously ON)<sup>9</sup>; and

(4) the expected increase in low-energy cutoff with declining flux (i.e., increasing obscuration by the accretion disk) has not been observed in the transient sources.

<sup>8</sup>see Brecher (1972), Katz (1973), Roberts (1974) and Petterson (1975) for precession-related models of the 35<sup>d</sup> cycle.

<sup>9</sup>Note that the long-term ( $\sim 10$  yr) variation of Hz Her is reconcilable with changes in the accretion rate to Her X-1 (optical emission linked to X-ray flux via heating effects; Jones, Forman, and Liller 1973).

While a Her X-1-like modulation is irreconcilable with the majority of transient sources observed to date, such a mechanism cannot be ruled out for the regularly recurrent "transient" 3U1630-47 (cf. Chapter IV). In addition, Brecher (1975) has suggested that the slow "pulsation" periods of the transient sources A1118-61 and A0535+26 may represent the free precession of a neutron star with spin periods in the range 0.01 - 0.1s, and in this sense may exhibit a Her X-1-like ( $35^d$ ) modulation.

b. Episodic Accretion

i) Eccentric Orbit Binary Hypothesis

The standard scenario of the formation of an X-ray binary system involves evolution of the more massive star to the point of a supernova explosion, leaving behind the less evolved companion and a newly formed neutron star/black hole (cf. de Loore et al. 1974). Since the explosion may occur assymmetrically, a non-negligible eccentricity of the resulting orbit would be expected initially, followed by a gradual re-circularization due to the effect of tidal forces (Stutantyo 1975). Indeed, the X-ray pulsars Her X-1 and Cen X-3 have both been shown (via measurement of the Doppler-shifted pulse periods) to be in nearly circular orbits about the companion. On the other hand, a non-negligible eccentricity ( $\epsilon \approx 0.14 \pm 0.05$ ; Hutchings, 1974) has been derived<sup>10</sup> for the slowly pulsating source Vela X-1. Several authors (Clark and Parkinson 1975, and references therein) have suggested that the observed outbursts of the transient X-ray sources may signal the sudden turn-on of accretion during the approach of periastron in a long-period, eccentric orbit binary. As discussed

<sup>10</sup>Milgrom and Avni (1976) have recently noted, however, that this value may be significantly overestimated, and the orbit essentially circular.

earlier, only three sources are known which have undergone repetitive, transient-like outbursts. The regularity of the proposed period of 3U1630-47 ( $P = 615 \pm 5d$ ) is consistent with the relatively precise timing required in this model, but is also reconcilable with alternative periodic mechanisms such as the expansion-contraction cycle of the long period (Mira) variables or the presumably precession-related  $35^d$  modulation of Her X-1.

The irregular flare cycle ( $\bar{P} = 435d \pm 10\%$ ) proposed for Aql X-1 (Kaluziński et al. 1977b), on the other hand, is very difficult to interpret with such a mechanism, as are the secondary maxima and irregular, low-level emission exhibited by several transients. Another serious constraint placed on this hypothesis are the eccentricities implied by the duration and recurrence rate of the outbursts. Avni, Fabian, and Pringle (1976) have shown that lower limits on the eccentricity of transient source orbits can be estimated from the observable parameters  $f \equiv L_{\max}/L_{\min}$  and  $g \equiv \frac{2t_1}{P}$ , where  $2t_1$  is the total outburst duration and  $P$  is the orbital period ( $P > t_2 \equiv$  observed interval for which  $L < L_{\min}$ ). The implied resultant eccentricities are, in general, prohibitively large (viz.,  $\epsilon \gtrsim 0.9$ ; cf. Table I of Avni, Fabian and Pringle), and in the case of A0620-00,  $\epsilon > 0.99$ . These authors have therefore concluded that, since the probability of production of such large eccentricities in a supernova scenario is extremely small and because circularization of the orbit should produce a uniform distribution of eccentricities (which has not been observed), the association of the majority of transient X-ray sources with eccentric orbit binaries is unlikely.

#### ii) Variable Companions

As discussed in Chapter I and summarized in Table 1.1, a wide range of temporal variability, indicative of stellar pulsations, explosions,



and chaotic mass exchange, has been observed in the optical region of the spectrum. In particular, the quasi-regular variations of the "eruptive" variables (e.g., dwarf and recurrent novae), semi-regular expansion of the long-period variables (e.g., Mira variables), strong, variable stellar winds of early type giants (e.g., OB stars), and erratic mass ejection episodes of B emission stars make these objects attractive candidates for binary companions in transient X-ray sources. We now illustrate the consistency of such associations with observation.

#### X-ray Dwarf Nova Model (Type I Sources)

The existence of a class of binaries exhibiting nova-like optical outbursts and consisting of a red and blue dwarf pair (hence, "dwarf novae") has been known for some time. In contrast to the standard nuclear burning interpretation of traditional novae, several dwarf nova models have been proposed in which the outburst is attributed to episodic mass transfer from the red to blue component (Bath et al. 1974; Osaki 1974; see Figure 5.5). The optical emission is presumed to arise from reprocessing of UV and soft X-ray radiation in an accretion disk, at a "hot spot" where the accreting matter intercepts the disk, and from X-ray heating of the red star's atmosphere. Avni, Fabian, and Pringle (1976) have suggested that A0620-00 may represent a dwarf nova-type system with a neutron star or black hole as the accreting object. In this model, the gravitational energy released via accretion onto the collapsed member resulting from episodic overflow of the red companion's Roche-lobe is responsible for the X-ray outburst. While in "normal" dwarf novae the bulk of the radiation emerges in the optical and UV bands, X-ray emission dominates in the red dwarf-neutron star/black hole system and a transient X-ray source is produced. The authors showed that for a distance of

1-3 Kpc, the optical observations are compatible with X-ray heating of an optical primary of spectral class later than G5V, and therefore mass transfer must occur by Roche-lobe overflow. The accretion rate required to generate the observed X-ray luminosity of A0620-00 ( $L_x \approx 2 \times 10^{38} d_1^2$  erg s<sup>-1</sup>, 1-10 keV) is (assuming 10% mass-energy conversion efficiency)  $\dot{M}_{\text{max}} \approx 4 \times 10^{-8} d_1^2 M_{\odot}\text{-yr}^{-1}$ . Interestingly, this rate (for  $d_1 \approx 2$ ) is within the limits of that predicted for self-excited mass transfer in dwarf novae ( $\dot{M} \approx 1.5 \times 10^{-7} M_{\odot}\text{yr}^{-1}$ , Bath et al. 1974). We note that Endal, DeVinney and Sofia (1976) have proposed a similar model for A0620-00 in which an Algol-type binary undergoes sporadic mass transfer from a sub-solar mass companion (dwarf or subgiant) onto a white dwarf, citing the difficulty in forming neutron stars or black holes in low mass systems. Calculations of Fabian, Pringle, and Rees (1976), however, have shown that luminosities exceeding  $\sim 10^{36}$  erg s<sup>-1</sup> are problematic via accretion onto white dwarfs, which is apparently well below the peak luminosity of A0620-00. Furthermore, the established existence of low-mass X-ray binaries (e.g., Her X-1, Sco X-1) and the possibility of their formation via modes other than supernova explosions (Whelan and Iben 1973; Gursky 1975; Flannery and Van den Heuvel 1975; Canal and Schatzmann 1976) lessen the objection to A0620-00 as such a system.

The X-ray dwarf nova analogy is consistent with other aspects of A0620-00. In particular, the correlation of the X-ray and optical increases is expected in such a system where the optical and X-ray emission originate in a common region (i.e., accretion disk) or are connected via a reprocessing mechanism (e.g., X-ray heating of the "normal" star). In addition, the reported optical period at 3.<sup>d</sup>92 during the early decline and periods at approximately twice this value from X-ray and optical observations

during the later decay may be indicative of a binary system in which the optical variability is initially dominated by an extended emission region viewed from differing aspects (similar to the double-maximum light curves of HDE 226868 or Hz Her in the long-term X-ray 'OFF' state), followed by predominance of X-ray heating of the contracting star at the orbital period ( $\sim 7.8^d$ ), reminiscent of the Her X-1 - Hz Her system in the long-term X-ray 'ON' state. The absence of X-ray eclipsing (the  $7.8^d$  modulation reported by Matilsky (1976) is sinusoidal rather than eclipse-like, and the present data indicate that this modulation is certainly not present at the reported level of  $\sim 50\%$  during most of the observable lifetime of the source) is not surprising with the relatively small optical star (Avni, Fabian, and Pringle (1976) have computed an eclipse probability of  $\approx 37\%$  for reasonable system parameters). We should also point out here, however, that the existence of a  $7.8^d$  binary period is difficult to account for in the dwarf nova model where the longest expected period is  $\sim 3$  days (Avni, Fabian, and Pringle 1976), independent of the mass of the X-ray component. The nature of the optical companion in A0620-00 is thus still uncertain, as the evidence is apparently inconsistent with both a dwarf and giant class star.

Several characteristics of A0620-00 are consistent with cataclysmic accretion models in general. Ricketts, Pounds, and Turner (1975), for example, have pointed out that a marked softening in the X-ray spectrum during the rise phase is consistent with a growing accretion disk, and Stoeger (1976) has discussed a scenario in which an instability in the developing disk accounts for the observed "pre-cursor" peak (Elvis *et al.* 1975). The resemblance of A0620-00 to other established X-ray binaries is also significant. Several observers have noted a resemblance between

V616 Monocerotis and Sco X-1, especially in the colors (Eachus, Wright, and Liller 1976), B magnitude, and ratio of X-ray to optical radiation at maximum light (Boley et al. 1976), and the appearance  $\sim$  3 weeks after maximum of weak emission at NIII  $\lambda\lambda$ 4634-4640 and He II  $\lambda$ 4686 (Peterson, Jauncey, and Wright 1975). Cowley and Crampton (1975) have reported evidence for a "hot spot" on the accretion disk in Sco X-1, analogous to that expected in the dwarf nova models, and have noted the similarity of the implied masses and  $0.787^d$  period of the latter source to those of old novae and cataclysmic variables. The A0620-00 transient radio event has been compared by Owen et al. (1976) to similar episodes in Cyg X-3, which has also been likened to a dwarf nova system (Davidsen and Ostriker 1974). Finally, Citterio et al. (1976) have pointed out that measurements of the infrared flux made in 1975 October are consistent with a source that is self-absorbed in that band, similar to the case of Sco X-1. The similarities of the optical, infrared, radio, and X-ray characteristics of A0620-00 to known galactic X-ray sources clearly favor models involving sudden changes in the rate of mass transfer in binary systems as the triggering mechanism in the transient X-ray sources.

The problem of divergent distance estimates for A0620-00 can also be resolved within the context of accretion models. Eachus, Wright, and Liller (1976) have derived a distance of  $d = 11 \pm 3$  Kpc based on the typical rate of fading of other recurrent novae, while a more conservative estimate of  $.5 \lesssim d \lesssim 3$  is consistent with the sharp interstellar absorption lines observed by Gull et al. (1976), and an Eddington-limited luminosity at maximum for a  $1 - 10 M_{\odot}$  accreting object. Although the optical evolution of the "X-ray dwarf novae" may resemble that of recurrent novae, the peak optical luminosity will be considerably less since the radiation

emerges primarily in the X-ray region. The assumption of an accretion rate comparable to that of ordinary recurrent novae and the observed ratio of  $L_X/L_{opt} \approx 10^3$  imply an absolute visual magnitude at maximum of  $M_V \sim 1$  instead of the typical value of  $M_V \approx -6$  (Payne-Gaposchkin 1964). The corresponding distance of  $d \approx 500$  pc should be taken only as a rough lower limit, since effects such as self-excited mass transfer will tend to increase the rate of mass exchange in the X-ray system (Bath et al. 1974). We note in this regard that Wu et al. (1976) have derived a distance to A0620-00 of  $d \approx 630$  pc from UV observations of the 2200 Å interstellar absorption feature, while Wickmrasinghe and Warren (1976) have found a value (based upon interstellar reddening) of  $d > 2$  Kpc.

The irregularity of the proposed flare cycle for Aql X-1 has several obvious implications for models of that source, which are particularly relevant to the present discussion in view of its similarity to the Type I transient sources. As noted above, the observed scatter in the presumed flare period is inconsistent with the relatively precise timing expected from a binary phase-related variation in the accretion flow. The same consideration decreases the likelihood of a mechanism involving expansion of the red giant component in a Mira Variable-type binary as proposed for the transients 3U1543-47 (Li, Sprott, and Clark 1976) and A1118-61 (Fabian, Pringle, and Webbink 1975), or of a Her X-1 like precession-governed modulation (as opposed to actual flares). As the observed X-ray phenomenology is not unlike that of the optical light curves of dwarf novae (and some recurrent novae; compare Figures 1.4 and 4.9 - 4.11), we suggest that these observations are most easily interpreted in terms of an X-ray dwarf nova binary model. Applying the empirical period-amplitude relation for U Gem stars and recurrent novae of Payne-Gaposchkin (1964), the inferred

ratio  $L_{\max}/L_{\min} \sim 500$  (assuming that most of the radiation emerges in X-rays) yields an expectation value for the interval between flaring episodes of  $\sim 465$  days. The excellent agreement between the predicted and observed mean flare cycles should not be taken literally, as the uncertainty in  $L_{\max}/L_{\min}$  implies a correspondingly wide dispersion in the expectation flare interval. Recognizing further that X-ray dwarf novae may deviate significantly from period-amplitude relations describing their optical analogues (Avni, Fabian, and Pringle 1976), we can only conclude that the observed flare interval is not inconsistent with that which might be expected from such a source.

The close similarity of the two ASM flare light curves for Aql X-1 is another model constraint, as it suggests detailed reproducibility. This characteristic of the source behavior can be reconciled with accretion dwarf nova models invoking relatively continuous mass transfer to an accretion disk which is eventually "dumped" by an instability (Osaki 1974) or, alternatively, quasi-periodic unstable Roche-lobe overflow of the red star (Bath *et al.* 1974)<sup>(11)</sup>. In the former model, the similarity of the flares results from the comparable amounts of material accumulated between episodes, while in the latter a high regularity of the magnitude of Roche-lobe spills and/or a feedback loop (regulated first by self-excited transfer and later by Eddington-limited flow) may be implied. Finally, we note that the non-flaring source behavior observed by UHURU (Jones 1976) may be analogous to the "standstills" observed in several dwarf novae including Z Cam ( $S_{\text{standstill}} \sim 0.3 - 0.5 S_{\max}$ , Osaki 1974).

<sup>11</sup>The recent report of an additional, lower-level outburst (Watson 1977; Holt and Kaluziński 1977) in 1977 January would apparently favor the latter mechanism.

We conclude this sub-section with a few general comments on the dwarf nova analogy to the Type I transient X-ray sources. While the probability of observing eclipses in these sources is relatively low ( $\approx 0.37$  for A0620-00-type systems), the probability of observing no occultations for the three sources of this class for which detailed temporal analyses on time scales of hrs-days were possible is only  $P \approx (.63)^3 \approx 0.25$  ( $\approx 0.06$  including Cen X-2, Cen X-4, and 3U1543-47). While this is not unreasonably low, it may indicate the presence of an extended X-ray emission region if these systems are indeed close, low-mass, Roche-lobe overflow binaries. Finally, we note the consistency of the detection rate of the Type I transients ( $\sim 1-3 \text{ yr}^{-1}$ ) with that deduced by Whelan *et al.* (1976) for detectable outbursts of the A0620-00 type ( $0.2 < f(\text{yr}^{-1}) < 20$ ), based on the initial conditions, mass-ratio distributions, space-density of dwarf novae (Kraft 1967), and relative eruption intervals of dwarf novae and A0620-00-like objects. Although we have concentrated on the dwarf nova analogue, similar systems with variable, late-type companions (i.e., not strictly limited to red dwarfs) are also reconcilable with the observations. In particular, some of the objects classified as "recurrent novae" (in addition to V616 Monocerotis) may actually be more closely related to the phenomenon of the Type I transient X-ray sources than that of the classical novae.

#### Mira Variables

An alternative mode of mass exchange via Roche-lobe overflow, as would result from expansion of a Mira variable in orbit about a compact object, has been proposed as a possible mechanism for several of the transient X-ray sources. This association was suggested by the presence of variable, M-type giants within the X-ray error boxes of 3U1543-47 (Forman and Liller

1973), and A1118-61 (Fabian, Pringle, and Webbink 1975). In addition, the overlapping error boxes ( $\sim 10^{-15}^0$  in diameter) of two early transient source candidates in the constellation Cetus (Cet X-1, Barnden and Francey 1969; Cet X-2, Shukla and Wilson 1971) are centered on Mira (0 Ceti) itself (cf. Davison and Sanford 1976). Li, Sprott, and Clark (1976) have shown that the X-ray luminosity of 3U1543-47 could be produced if a fraction  $\delta$  of the surface of the expanding giant is accreted onto the collapsed object, where  $\delta \sim 10^{-2} - 10^{-3}$ . These authors have further suggested that the observed erratic, smaller fluctuations superposed on the major quasi-periodic optical variations could cause smaller Roche-lobe overflow events and thereby account for the secondary X-ray maxima of 3U1543-47.

A Mira variable mechanism is apparently inconsistent, however, with several individual source observations. For instance, this association can apparently be ruled out for A0620-00, as B magnitude measurements (Ward et al. 1975) of V616 Monocerotis in the quiescent state (Palomar Observatory Sky Survey Charts, circa 1955) imply a distance of  $d \approx 15$  Kpc (for an assumed red giant), which would place the source well outside of the galaxy and imply an unrealistic X-ray luminosity in excess of  $\sim 2 \times 10^{40}$  erg  $s^{-1}$ . Additionally, the correlation of the 3-6 keV and optical fluxes of A0620-00 makes a red giant primary improbable in that the optical emission should be dominated by the giant, and relatively insensitive to variations in the X-ray luminosity. In the case of Aql X-1, although we cannot conclusively rule out a Mira variable association, the observed irregularity of the flare cycle favors the more chaotic behavior characteristic of the dwarf novae-type variables. The absence of an optical counterpart for Aql X-1 ( $M_B > 17.5$  during the 1975 June flare, Davidsen et al. 1975) would further tend to favor a less luminous



optical companion. The suggested identification of the red variable RS Cen with A1118-61 has also been weakened by Copernicus observations occurring two cycles ( $P \approx 163^d$ ) before and one cycle after its appearance, in which no X-ray emission was detected<sup>12</sup> (Davison and Sanford 1976). Similarly, the failure of the ASM to detect X-ray emission ( $S \lesssim 0.1 \text{ cm}^{-2} \text{ s}^{-1}$ ,  $\approx .005$  of the maximum flux of Cen X-2) from O Ceti over three maxima of the 331d light cycle apparently lessens the likelihood of an identification of the Cetus sources with that object<sup>13</sup>. Finally, the spatial distribution of at least the shorter period Mira variables ( $P < 250 \text{ d} = \text{Intermediate Pop. II, Allen 1963}$ ) is in contrast to that of the Type II transients. Thus, while expansion of a red giant in a binary system is an attractive mechanism for transient mass-exchange episodes, no firm evidence for the association of such systems with the transient X-ray sources has yet been obtained.

#### Early-type Giant Variables (Type II Sources)

The proposed existence of a class of weak, short-duration transients (Type II) attaining peak luminosities approximately 1-2 orders of magnitude less than those of the bright, long-lived sources may be indicative of a smaller-amplitude mode of mass transfer. The identification of several "permanent" sources (e.g., Cyg X-1, Cen X-3, Vela X-1) with early-type giant optical primaries and the fact that all three exhibit

<sup>12</sup> $S \lesssim 2\%$  and  $10\%$  of the Ariel 5 maximum flux, respectively.

<sup>13</sup>Li, Sprott, and Clark (1976) have pointed out, however, that the observed variability of the magnitude of the red giant pulsations could cause the absence of X-ray outbursts at some of the optical maxima.

high and low states ( $S_{\text{high}}/S_{\text{low}} \sim 5 - 20$ ) suggests that large fluctuations in the density of the stellar wind emanating from such a companion could conceivably account for the outbursts of the Type II transients. The lesser amount of mass transferred and correspondingly smaller accretion disk might explain the lesser magnitude, shorter lifetime, and harder spectrum (optically thin vs. optically thick emission region; cf., Pounds 1976b) of these sources in comparison to those of the Type I, Roche-lobe overflow transients.

Several authors (Fabian 1975; Wickmrasinghe and Whelan 1975) have proposed that a steady stellar wind can account for the presumed slowdown of the initially rapid pulsar spin period to time scales of  $\sim$  minutes as observed for A1118-61 and A0535+26, and that sporadic enhancements in this wind (from  $\dot{M} \approx 10^{-10} - 10^{-6} M_{\odot} \text{yr}^{-1}$ ) could produce a transient source of luminosity  $L_x \approx 10^{36} \text{ erg s}^{-1}$ . In the model of Wickmrasinghe and Whelan (1975) the optical counterparts of these transients are OB stars which, because the weak-wind ("sleeping phase", Van den Heuvel 1974) stage lasts  $\sim 100$  times longer than the intense stellar wind phase, leads to the conclusion that there could exist  $\sim 100$  times as many of these dormant transients as the quasi-stable stellar wind sources (i.e., of the Vela X-1 variety). If we estimate the total number of these "stable" stellar wind sources in the galaxy ('SW') at  $N_{\text{SW}} \sim 10 - 100^{(14)}$ , then the total

<sup>14</sup>This estimate is based on the assumption that the UHURU survey is essentially complete for sources with luminosities  $L_x \approx 10^{36} \text{ erg s}^{-1}$  (cf. Blumenthal and Tucker 1974; Sofia and Wesemael 1976).

number of such inactive systems is  $N_{qSW} \approx 10^3-10^4$  (15), which is within the range expected for the population of quiescent Type II transients ( $N_{qII} \sim 100-5000$ ).

The proposed identification of A1118-61 and A0535+26 with B emission (Be) stars has led Maraschi, Treves, and Van den Heuvel (1976) to speculate that these objects could give rise to the transient X-ray emission via sudden variations<sup>(16)</sup> in the rate of mass ejection, which could recur over a time scale of years (as does the optical emission observed from typical stars of this type). As the authors point out, the total amount of accreted matter (for a neutron star companion) is  $\Delta M \approx 5 \times 10^{-9} M_{\odot}$ , or only a few percent of the amount of mass in the envelopes of Be stars required for producing the observed emission lines. Interestingly, the identification of a Be star counterpart for the weak ( $L_x \approx 10^{33} \text{ erg s}^{-1}$ ) source X Per (3U0352+30) suggests that this object may represent the quiescent state of these transients and is observable only because of its proximity ( $d \sim 170 \text{ pc}$ ). Since the frequency of active periods in Be stars is known to be approximately  $10^{-1} \text{ yr}^{-1}$  (i.e.,  $\bar{T}_{rec} \sim 10 \text{ yr}$ ), our upper limit on the frequency of short-duration transients ( $\tau^{-1} \approx 100 \text{ yr}^{-1}$ ) would imply, in this case, that the total number of Be transients in the quiescent phase is  $N_{qBe} \lesssim 1000$ , or about 10-100 times the number of observed

<sup>15</sup>This number is consistent with the estimated number of massive close binaries in the Galaxy,  $N \sim 3 \times 10^3$  (De Cuyper et al. 1976).

<sup>16</sup>These stars have been observed to be losing mass as a result of very high rotational rates, with material ejected from the equatorial region.

"permanent" galactic sources with massive early-type companions. Thus, as for the case of OB stellar wind sources, the estimated number of quiescent Be transients is consistent with the rates of occurrence and recurrence of the Type II transient sources. Finally, the absence of occultations in the two sources representative of the Type II class is not inconsistent<sup>17</sup> with their association with massive ( $M_* \gtrsim 10 M_\odot$ ) systems with binary periods comparable to those of the "permanent"<sup>18</sup> stellar wind sources. However, the reported lower limit of 17d to the binary period of A0535+26, if the observed change in pulse period is due to binary motion (Rappaport *et al.* 1976), implies that we cannot exclude the possibility that some of the Type II transients may be characterized by relatively longer periods than their "permanent" stellar wind counterparts. Until positive optical identifications are obtained, however, one cannot conclusively demonstrate that either variable OB or B emission stars are the progenitors of the weak, short-duration transients.

### iii) Disk Instabilities

Other models for the transient sources based on sudden accretion episodes involving an essentially non-variable companion in an X-ray binary have been proposed. Amnuel, Guseinov, and Rakhamimov (1974) pointed out a long-term, transient-like behavior exhibited by nine

<sup>17</sup>The probability of observing eclipses from neither A1118-61 and A0535+26 is  $P \approx (1 - r/a)^2 \approx 0.4$  for  $r = 10 R_\odot$  (B0 star),  $M = 10 M_\odot$ , and binary period  $P_b = 5d$ .

<sup>18</sup>For example, the binary periods of Cen X-3, Cyg X-1, Vela X-1, and Cir X-1 are 2.1, 5.6, 8.9, and 16.6d, respectively.

galactic sources, the entire "outburst" occurring over a timescale of  $\sim 4$  years. They suggested that a very slow, steady build-up of an accretion disk fed by a companion of spectral class later than F over a time of  $\sim 10^3$  years until triggered by an instability could account for these "slow" transients as well as the Type I/II transients. This type of mechanism can clearly not be reconciled with the sources for which recurrence periods have been established, including A0620-00 ( $T_{\text{rec}} \approx 58$  yr), Aql X-1 ( $T_{\text{rec}} \approx 435 \text{ d} \pm 10\% \text{ rms}$ ), and 3U1630-47 ( $T_{\text{rec}} \approx 615 \pm 5 \text{ d}$ ), and also has difficulty explaining the secondary maxima and irregular, low-level emission observed for many of the transient sources. In addition, the proposed early-type companions for the Type II transients are inconsistent with those hypothesized in the above model.

#### iv) Supercritical Accretion: Smothering

Another binary accretion mechanism has been suggested as an alternative explanation of the relatively slow "rotation" periods of A1118-61 and A0535+26. Pringle and Webbink (1975) have proposed that the 6.75 minute period of A1118-61 may represent the orbital period of a close white dwarf-neutron star/black hole binary system. In this model the transient outburst is associated with a temporary decrease in the supercritical mass transfer rate which ordinarily smothers the X-ray object. Consequently, the luminosity at maximum should be Eddington-limited, with a corresponding distance ( $M_x = 1 M_{\odot}$ ) of  $d \sim 26$  Kpc for that source. As mentioned earlier, this is difficult to reconcile with the galactic longitude of A1118-61 (see Table 5.1). The same apparent difficulty applies to A0535+26, where the distance of  $\sim 6$  Kpc would place it close to the "edge" of the galactic disk. While the observed softening of the spectra of several transients is consistent with a progressive lessening of the line-of-sight

obscuring material, this effect is also consistent with a cooling accretion disk expected in the other accretion models. We can rule out, however, a reversion back to the original, "smothered" state, since the expected increase in low energy cutoff with decreasing flux has not been observed in any of the transients for which temporally separated spectral measurements were obtained.

Large fluctuations in a supercritical stellar wind density, with corresponding variations in X-ray self-absorption (or optical thickness) similar to those presumably responsible for the long-term modulation of several "permanent" sources (e.g., Cen X-3, Cir X-1), are similarly unlikely as a possible mechanism for the production of transient X-ray sources. Clearly, the phenomenology of these sources, including the ratio of maximum to minimum luminosities ( $\frac{L_{x,max}}{L_{x,min}} \approx 100$ ), relatively frequent transitions between "low" (smothered) and "high" (lower wind density) states, and duration of the roughly steady "high" state emission (weeks-months), differs significantly from that of the transients. It is not inconceivable, however, that some of the weaker candidate transients (e.g., MX0656-07) may represent such systems. In contrast, the flares of early, massive-type binaries such as Cyg X-1 (in particular, the 1974 April increase), presumably triggered by increases in the stellar wind density (Holt et al. 1976a), and hence accretion rate (as opposed to decreases in the wind density), more closely resemble, on a smaller scale, the outbursts of the transient X-ray sources. Indeed, Coe, Engel, and Quenby (1976) have pointed out the similarity of the spectral evolution of the 1974 April flare of Cyg X-1 and the outburst of A0620-00.

## v) Globular Clusters

The proposed identification of the transient source candidate MX1746-20 with the globular cluster NGC 6440 (Forman, Jones, and Tananbaum 1976b) has suggested the possible existence of yet another class of "transient" X-ray sources. This source was observed by UHURU in 1971-72, remaining approximately 20 times higher than the average flux in the preceding and following year for a time of  $\sim 1\ 1/2 - 3$  months (with no visible declining trend during that time). As Forman, Jones, and Tananbaum have pointed out, this transient-like behavior may be reconciled with two prominent models for globular cluster X-ray sources: (1) a supermassive accreting black hole at the cluster center (Bahcall and Ostriker 1975; Silk and Arons 1975), or (2) collapsed, stellar-mass objects at the cluster core accreting either from an orbiting companion (similar to the binary accretion models above) or during near-encounters (Clark 1975b). This latter binary model is interesting in its possible implications for the transient sources (as defined in Chapter I), as Gursky and Schreier (1975) have noted that the companion of the X-ray object in a globular cluster must be an extreme Population II (i.e., highly evolved) object. The similarity of the proposed "globular cluster transients" to the Type I transients is thus understandable if the latter are indeed associated with late-type companions as we have suggested above (i.e., the former objects represent Type I binary transients which are preferentially formed in globular clusters). In addition, the overlapping spacial error boxes of the transient A1742-28 with an X-ray burster<sup>19</sup> (Lewin 1976) is also interesting, as the two different types of variability can be reconciled

<sup>19</sup>Several "bursters" have been positively identified with globular clusters.

within the same accreting binary framework. In particular, one model for the burst sources (Lewin 1976) utilizes plasma instabilities in a filling accretion disk surrounding a neutron star to produce the X-ray flashes. Note, however, that the relatively thin disk spatial distribution characteristic of the transient sources is inconsistent with the  $\sim$  spherical distribution (Halo Pop. II) of the globulars. Thus, while it has been shown that some transients may reside in globular clusters, these objects do not represent a necessary requirement for the production of a transient X-ray source.

#### D. Summary

Based upon the increasing body of observations, a consistent picture of the phenomenon of the transient X-ray sources can be constructed. It has been demonstrated that these sources are reconcilable with the basic binary accretion mechanism underlying the more stable galactic sources, distinguished from this latter class of objects primarily by the episodic nature of the mass exchange process. As with the "permanent" sources, good evidence exists for two distinct transient source sub-classes, differentiated primarily according to the mode of mass transfer: (1) Roche-lobe overflow in dwarf nova-type (low mass companion) binaries, or (2) enhancements in the stellar wind emanating from a massive, early-type companion. The characteristic parameters of the two source groups are summarized in Table 5.2. It further appears that, in contrast to a sharp division of galactic binary X-ray sources into "permanent" and "transient" categories, a relatively broad spectrum of temporal variability exists as outlined in Table 5.3.



The All-Sky Monitor has played an important role in the study of the transient sources, establishing the galactic disk spatial distribution, allowing estimates of the characteristic frequencies and luminosities which are relatively free from observational selection effects, and providing detailed light curves of several transient sources and flaring "permanent" sources. A number of questions remain relatively unexplored, however. For example, the mechanism underlying the outbursts of the optical companion itself has not been specified, although several models for such variability have been proposed (dynamical instability of a red dwarf envelope, Bath *et al.* 1974; magnetic variability of a subgiant, Hayakawa 1976; thermal instability in a weak stellar wind situation (early giant-type stars), Buff and McCray 1974). In view of their description in terms of episodic accretion in normally inactive X-ray binaries, it has been suggested that the transient sources represent a potential astrophysical laboratory for such studies as the investigation of time-dependent phenomena in accretion disks (Pounds 1976a) and the evaluation of numerical models of stellar atmospheres irradiated by an external X-ray flux (Endal, De Vinney, and Sofia 1976). Further observations are required to confirm the suggested association of early-type giant stars and Type II transients and to improve upon the rough estimates of the transient source population parameters ( $|\bar{z}|$ ,  $L$ ,  $\tau$ ) obtained from the first two years of ASM observations. We note in this latter regard the expected additional lifetime ( $\sim 2$  yrs) of Ariel 5 and the proposed launch in the early 1980's of a second generation All-Sky Monitor, with improved spatial resolution (comparable to current octant-mode resolution) and sensitivity (factor of  $\sim 10$  improvement in counting statistics).

## APPENDIX A

### UHURU-ASM FLUX CONVERSION

As the first satellite to comprehensively survey the X-ray sky, the UHURU count rate has been adopted as a standard unit for cosmic X-ray flux measurement. This standard count rate may be related to incident 2 - 6 keV energy fluxes via a nominal<sup>1</sup> conversion factor, given by 1 UHURU count s<sup>-1</sup> = 1.7 x 10<sup>-11</sup> erg cm<sup>-2</sup>s<sup>-1</sup> (2-6 keV). To convert these rates to the ASM units of incident 3-6 keV photons we may write the following:

$$A \equiv \kappa U ; \tag{A-1}$$

$$A = \int_3^6 \frac{dN}{dE} dE(\text{keV}) \text{ cm}^{-2}\text{s}^{-1}; \tag{A-2}$$

$$U_E = \int_2^6 E \frac{dN}{dE} dE \text{ erg cm}^{-2}\text{s}^{-1},$$

$$U_E = 1.7 \times 10^{-11} \text{ erg cm}^{-2}\text{s}^{-1} \times U (\text{count s}^{-1}), \tag{A-3}$$

$$= 1.06 \times 10^{-2} \text{ keV cm}^{-2}\text{s}^{-1} \times U.$$

Combination of these equations yields:

$$\begin{aligned} \kappa &\equiv \frac{A}{U} \\ &= 1.06 \times 10^{-2} \text{ keV cm}^{-2}\text{s}^{-1} \frac{\int_3^6 \frac{dN}{dE} dE}{\int_2^6 E \frac{dN}{dE} dE} \end{aligned}$$

To obtain the "best" value for  $\kappa$ , we have evaluated these integrals for "representative" power-law and exponential spectra, with the results shown in Table A.1. It can be seen that a value of  $\kappa = 1.5 \pm 0.5 \times 10^{-3}$  represents a reasonable conversion for a relatively wide range of incident spectra.

<sup>1</sup>Obtained for an "average" source spectrum, and usually accurate to + 30% (see Giacconi et al. 1974); the unit so defined has been designated  $\overline{U}$  UHURU flux unit (UFU).

APPENDIX B  
EARTH OCCULTATION

A cosmic X-ray source of declination  $|\delta_x|$  less than some critical declination ( $\delta_c$ ) will be occulted by the earth during some fraction of each satellite orbit. Since the spacecraft operates only in sunlight, both the duration and phase (relative to the sun) of the source occultation must be computed to obtain the correct source exposure time to the detector. In the following derivation, an equatorial, circular orbit is assumed, and the magnitude of errors resulting from the non-zero inclination ( $\theta_i \approx 2.9^\circ$ ) and eccentricity ( $\epsilon \approx 0.0033$ ) of the actual orbit are estimated.

1. Computation of Occultation Angle ( $\theta_{occ}(\delta_x)$ ):

From Figure B.1, it can be seen that a source will never be occulted if  $|\delta_x| \geq \delta_c$ , where

$$\begin{aligned}\delta_c &= \phi \\ &= \sin^{-1}(R_x/R_o) \\ &= 70.87^\circ.\end{aligned}$$

For  $|\delta_x| < \delta_c$  the extent of occultation increases with decreasing declination, reaching a maximum at  $\delta_x = 0^\circ$ . The occultation angle, defined as the angle traversed by the satellite during which the source is earth-occulted<sup>1</sup>, is given by (see Figure B.2):

$$\begin{aligned}\sin\left[\frac{\theta_{occ}(\delta_x)}{2}\right] &= \frac{R'(\delta_x)}{q}, \text{ where} \\ q &= R_o/\cos \phi \text{ and} \\ R'(\delta_x) &= (R_o^2 \tan^2 \phi - r_{\delta_x}^2)^{1/2} \\ &= \frac{R_o}{\cos \phi} (\sin^2 \phi - \sin^2 \delta_x)^{1/2}. \text{ Hence,}\end{aligned}$$

<sup>1</sup>This is equivalent to the angle traversed by the occulted source in its apparent motion relative to an observer moving with the spacecraft, and is so illustrated in Figure B.2.

$$\theta_{\text{occ}}(\delta_x) = 2 \sin^{-1} \left( \sin^2 \phi - \sin^2 \delta_x \right)^{1/2}. \quad (\text{B-1})$$

Note that this reduces to the two limiting values

$$\begin{aligned} \theta_{\text{occ}}(\phi) &= 0 \text{ and} \\ \theta_{\text{occ}}(0) &= 2\phi, \text{ as required.} \end{aligned}$$

## 2. Determination of Source Occulted Phase Relative to the Sun:

As illustrated in Figure B.3, the times of occultation commencement/termination during the orbit may be obtained from the time of eclipse entry ( $T_{\text{ee}}$  = event 7 in time-event code housekeeping array) as:

$$T_{\text{occ}} \left( \begin{array}{c} \text{start} \\ \text{end} \end{array} \right) = T_{\text{ee}} + \left[ \frac{(\pi/2 - \psi) + \alpha_{\text{rel}} \mp \theta_{\text{occ}}(\delta_x)/2}{2\pi} \right] P_{\text{orb}},$$

where

$$\begin{aligned} \alpha_{\text{rel}} &= |\alpha_x - \alpha_{\odot}|, \\ \delta_x &= \text{Source DEC.}, \\ \alpha_x &= \text{Source R.A.}, \text{ and} \\ \alpha_{\odot} &= \text{Sun R.A.} \end{aligned}$$

## 3. Mean Unocculted Fraction

As  $\alpha_{\odot}$  varies during the year, the phase of the occulted region relative to the sun (and hence eclipse entry) will rotate, with a corresponding variation in the "mean unocculted fraction" defined by

$$\eta \equiv \frac{\theta_{\text{sun}} - f\theta_{\text{occ}}(\delta_x)}{\theta_{\text{sun}}}, \text{ where}$$

$\theta_{\text{sun}}$  = Angle subtended by sunlit fraction of orbit

$$\theta_{\text{sun}}(\delta_{\odot}) = \left( 2\pi - \sin^{-1} \left[ \frac{\cos^2 \psi - \sin^2 \delta_{\odot}}{\cos^2 \delta_{\odot}} \right]^{1/2} \right), \text{ and}$$

$f$  = fraction of  $\theta_{\text{occ}}$  lying within  $\theta_{\text{sun}}$ .

Thus,  $\eta$  will vary smoothly between the values

$$\eta = \eta_{\min} = \frac{\theta_{\text{sun}}(\delta_{\theta}) - \theta_{\text{occ}}(\delta_X)}{\theta_{\text{sun}}(\delta_{\theta})} \\ \approx \frac{\pi + 2\psi - \theta_{\text{occ}}(\delta_X)}{\pi + 2\psi}$$

in the interval

$$\alpha_{\text{rel}} \geq \pi - \alpha_{\min},$$

$$\alpha_{\min} \approx \frac{\pi + 2\psi - \theta_{\text{occ}}(\delta_X)}{2}; \text{ and}$$

$$\eta = \eta_{\max} = \begin{cases} 1, & \text{when } \theta_{\text{occ}}(\delta_X) \approx 2\pi - (\pi + 2\psi) \\ \approx \frac{2\pi - \theta_{\text{occ}}(\delta_X)}{\pi + 2\psi}, & \text{otherwise} \end{cases}$$

in the interval  $\alpha_{\text{rel}} \leq \alpha_{\max}$ ,  $\alpha_{\max} \approx \frac{\pi - 2\psi - \theta_{\text{occ}}(\delta_X)}{2}$ . The function  $\eta(\alpha_X, \delta_X, \alpha_{\theta}, \delta_{\theta})$  has been plotted vs.  $\alpha_{\text{rel}}$  for several different sources in Figure 3.1.

#### 4. Estimated Error

An upper limit to the error in occultation angle resulting from the non-zero inclination of the satellite orbit is obtained by evaluating equation B-1 for  $\delta_X \pm \theta_i = \delta_X \pm 3^{\circ}$ :

$$\underline{\delta_X = 0^{\circ}}: \quad \Delta\theta_{\text{occ}} < 2 \left[ \sin^{-1} (\sin^2 70.87^{\circ} - \sin^2 3^{\circ})^{\frac{1}{2}} - 70.87^{\circ} \right] < 0.5^{\circ};$$

Thus, the possible error in fractional source exposure

$$\text{time is: } \frac{\Delta T_s}{T_s} \leq \frac{\Delta\theta_{\text{occ}}}{\theta_{\text{occ}} - \theta_{\text{sun}}} < .006;$$

$$\underline{\delta_X = \Phi = 70.87^{\circ}}:$$

$$\Delta\theta_{\text{occ}} < 2 \sin^{-1} \left[ \sin^2 70.87^{\circ} - \sin^2 67.87^{\circ} \right]^{\frac{1}{2}} < 21.4^{\circ}, \text{ or}$$

$$\frac{\Delta T_s}{T_s} \leq \frac{\Delta\theta_{\text{occ}}}{\theta_{\text{occ}} - \theta_{\text{sun}}} < .11.$$

The error in  $\theta_{\text{occ}}$  resulting from non-zero orbital eccentricity may be estimated from

$$\Delta\theta_{\text{occ}} < 2 \sin^{-1} \left[ \sin^2(\phi \pm \Delta\phi) - \sin^2\delta_x \right]^{1/2},$$

where

$$\Delta\phi < \sin^{-1} \frac{R_x}{R_0} - \sin^{-1} \frac{R_x}{R_0 \pm \Delta R_0},$$

$$\Delta R_0 = 30 \text{ Km};$$

$$\Delta\phi < .75^\circ.$$

Since this is less than the maximum error due to orbital inclination, it is clear that the greatest systematic errors ( $\frac{\Delta T_s}{T_s} \approx 10\%$ ) will occur for sources with  $|\delta_x| \sim \delta_c$ .

APPENDIX C

COMPUTATION OF SOURCE LATITUDINAL CORRECTION FACTOR (LCOR)

As discussed in Chapter III, as the elevation of a source increases (i.e., increasing spacecraft latitude, D), the source is exposed to the detector for an increasing fraction of the satellite rotation. This effect is corrected for by defining a source latitudinal correction factor as:

$$LCOR(D) \equiv \frac{\phi_{1on}(D)}{2\pi},$$

$$\phi_{1on}(D) \equiv \text{FWHM of triangular longitudinal spatial response (cf. Figure 3.4),}$$

with the property that

$$T_s = LCOR(D) \times TIMON,$$

$$TIMON \equiv \text{Net detector ON-time } (=T_{dur} - T_{dis}(i)), \text{ and}$$

$$T_s = \text{Effective source exposure time.}$$

This factor may now be computed as follows (refer to Figure C.1a):

$$\hat{S} \equiv \text{Source position vector (chosen in } yz \text{ plane)}$$

$$\hat{N} \equiv \text{Pinhole normal vector}$$

$$\phi \equiv \text{Angle between } xy \text{ plane projections of } \hat{N} \text{ and } \hat{S}.$$

Hence,

$$\hat{N} = -\sin\phi \cos D \hat{x} + \cos\phi \cos D \hat{y} + \sin D \hat{z},$$

$$\hat{S} = \cos D \hat{y} + \sin D \hat{z},$$

and

$$\begin{aligned} \cos\phi_{NS} &= \hat{N} \cdot \hat{S} \\ &= \cos\phi \cos^2 D + \sin^2 D, \text{ or} \end{aligned}$$

$$\phi_{NS} = \cos^{-1} (\cos\phi \cos^2 D + \sin^2 D). \quad (C-1)$$

The static "fan-beam" detector response is also latitude-dependent, and as shown in Figure C.1b,

$$\phi_f(D) = \tan^{-1} \left[ \frac{a \cos(D-\pi/4)}{h} \right], \quad (C-2)$$

where

$$a = 1 \text{ cm} \quad \text{and}$$

$$h = 15 \text{ cm.}$$

Now, a source will be exposed to the detector as long as the condition

$$|\phi_{NS}(D)| \leq \phi_f(D)$$

is satisfied. Thus, one-half of the longitudinal extent (i.e.,  $\phi_{1/2} = \phi(\text{response} = 1) \rightarrow \phi(\text{response} = 0)$ ) is given by:

$$|\phi_{NS}| = \phi_f$$

$$\cos^{-1} \left[ \cos \phi_{1/2} \cos^2 D + \sin^2 D \right] = \tan^{-1} \left[ \frac{a \cos(D-\pi/4)}{h} \right];$$

or

$$\phi_{1/2}(D) = \cos^{-1} \left\{ \frac{\cos \left[ \tan^{-1} \left( \frac{a \cos(D-\pi/4)}{h} \right) \right] - \sin^2 D}{\cos^2 D} \right\}. \quad (C-3)$$

Finally, for a triangular response function,

$$\text{FWHM} = 1/2 \times \text{Longitudinal extent};$$

$$\phi_{1on}(D) = \phi_{1/2}(D), \text{ and}$$

$$\text{LCOR}(D) = \frac{\phi_{1/2}(D)}{2\pi}, \text{ with } \phi_{1/2}(D) \text{ as given in Equation C-3.}$$



APPENDIX D

COMPUTATION OF "GEOMETRICAL FACTORS"

Recall that the geometrical factor is defined to relate the counting rate of a detector to an isotropic source flux:  $C \equiv G I_0$ , where

$C$  = Detector count rate ( $\text{sec}^{-1}$ ),

$I_0$  = Isotropic source intensity ( $\text{photons cm}^{-2}\text{s}^{-1}\text{sr}^{-1}$ ), and

$G$  = Geometrical factor.

In the case of the All-Sky Monitor, there exist eight independent detector elements (corresponding to the eight electronically-divided anode segments) for which geometrical factors must be computed to obtain the expected contribution from the isotropic diffuse X-ray background.

Following Sullivan (1971), we may write (see Figure D.1):

$$G = \int_{\Omega} d\omega \int_S d\vec{\sigma} \cdot \hat{r} = \int_{\Omega} d\omega A(\omega), \quad (\text{D-1})$$

where

$d\omega$  = element of solid angle,

$d\vec{\sigma}$  = element of surface area of the last detecting sensor to be penetrated, and

$\hat{r}$  = unit vector in direction  $\omega$ .

For an ideal, cylindrically symmetric detector with two planar detecting areas (consisting in the present case of the pinhole aperture and anode detecting strip), the geometrical factor is given by Equation D-1, with the domain  $\Omega$  limited by the top detector:

$$G = \int_{\Omega} \int_{S_2} (d\vec{\sigma}_2 \cdot \hat{r}) d\omega ;$$

$$d\omega = \frac{\hat{r} \cdot d\vec{\sigma}_1}{r^2},$$

$$G = \int_{S_1} \int_{S_2} (\hat{r} \cdot d\vec{\sigma}_1)(\hat{r} \cdot d\vec{\sigma}_2). \quad (\text{D-2})$$

For the geometry shown in Figure D.1a (two rectangular detecting areas with sides  $(c_1, d_1)$  and  $(c_2, d_2)$  where  $c_1$  and  $d_1$  are parallel to  $c_2$  and  $d_2$ , respectively), Equation D-2 may be integrated to yield:

$$\begin{aligned}
 G = & h^2 \ln \frac{h^2 + \alpha^2 + \delta^2}{h^2 + \alpha^2 + \beta^2} \frac{h^2 + \gamma^2 + \beta^2}{h^2 + \gamma^2 + \delta^2} + \\
 & +2 \left[ \alpha(h^2 + \beta^2)^{\frac{1}{2}} \tan^{-1} \frac{\alpha}{(h^2 + \beta^2)^{\frac{1}{2}}} + \beta(h^2 + \alpha^2)^{\frac{1}{2}} \tan^{-1} \frac{\beta}{(h^2 + \alpha^2)^{\frac{1}{2}}} \right] + \\
 & -2 \left[ \alpha(h^2 + \delta^2)^{\frac{1}{2}} \tan^{-1} \frac{\alpha}{(h^2 + \delta^2)^{\frac{1}{2}}} + \beta(h^2 + \gamma^2)^{\frac{1}{2}} \tan^{-1} \frac{\beta}{(h^2 + \gamma^2)^{\frac{1}{2}}} \right] + \\
 & -2 \left[ \gamma(h^2 + \beta^2)^{\frac{1}{2}} \tan^{-1} \frac{\gamma}{(h^2 + \beta^2)^{\frac{1}{2}}} + \delta(h^2 + \alpha^2)^{\frac{1}{2}} \tan^{-1} \frac{\delta}{(h^2 + \alpha^2)^{\frac{1}{2}}} \right] + \\
 & +2 \left[ \gamma(h^2 + \delta^2)^{\frac{1}{2}} \tan^{-1} \frac{\gamma}{(h^2 + \delta^2)^{\frac{1}{2}}} + \delta(h^2 + \gamma^2)^{\frac{1}{2}} \tan^{-1} \frac{\delta}{(h^2 + \gamma^2)^{\frac{1}{2}}} \right], \quad (D-3)
 \end{aligned}$$

where

$$\alpha \equiv \frac{1}{2}(c_1 + c_2), \quad \beta \equiv \frac{1}{2}(d_1 + d_2),$$

$$\gamma \equiv \frac{1}{2}(c_1 - c_2), \quad \text{and} \quad \delta \equiv \frac{1}{2}(d_1 - d_2).$$

For the ASM detector,  $c_1 = d_1 = d_2 = a$  ( $c_2$  varies according to latitudinal segment), and Equation D-3 is correspondingly simplified. Instead of performing the integration for each of the eight anode segments, however, we may utilize the symmetry of the detector and the property of the geometrical factor that  $G_{\text{Tot}} = \sum_i G_i$  (resulting from its integral nature), where in this case  $G_{\text{Tot}}$  = Geometrical factor for the entire anode, and

$$G_i = \text{Geometrical factor for the } i^{\text{th}} \text{ anode segment (latitudinal element),}$$

to compute each of the  $G_i$ . Thus (see Figure D.1b),

$$G_{\text{Tot}} = G_{nn'} \quad (\text{D-4a})$$

$$G_n + G_{n'} = 2 G_n = G_{nn'} - G_{mm'} \quad (\text{D-4b})$$

$$G_{nm} + G_{n'm'} = 2(G_n + G_m) = G_{nn'} - G_{11'} \quad (\text{D-4c})$$

$$G_{n1} + G_{n'1'} = 2(G_n + G_m + G_1) = G_{nn'} - G_{kk'} \quad (\text{D-4d})$$

$$G_{nk} + G_{n'k'} = 2(G_n + G_m + G_1 + G_k) = G_{nn'} - G_{jj'}, \text{ and} \quad (\text{D-4e})$$

$$G_j + G_{j'} = 2 G_j = G_{jj'} \quad (\text{D-4f})$$

Equations D-4 may now be solved for the eight geometrical factors, upon evaluation of the expressions for  $G_{nn'}$ ,  $G_{mm'}$ ,  $G_{11'}$ ,  $G_{kk'}$ , and  $G_{jj'}$ :

$$G_8 = G_n = (G_{nn'} - G_{mm'})/2$$

$$G_7 = G_m = (G_{nn'} - G_{11'})/2 - G_8$$

$$G_6 = G_1 = (G_{nn'} - G_{kk'})/2 - (G_7 + G_8)$$

$$G_5 = G_k = (G_{nn'} - G_{jj'})/2 - (G_6 + G_7 + G_8)$$

$$G_4 = G_j = G_{jj'}/2$$

$$G_3 = G_4$$

$$G_2 = G_5, \text{ and}$$

$$G_1 = G_6 + G_7 + G_8.$$

The five (sum) geometrical factors are computed from Equation D-3, with

$$\alpha = \frac{1}{2}(a + \ell'), \quad \beta = a, \quad \gamma = \frac{1}{2}(a - \ell'), \quad \text{and} \quad \delta = 0, \text{ where}$$

$$\ell' = \ell, \frac{7\ell}{8}, \frac{3\ell}{4}, \frac{\ell}{2}, \text{ and } \frac{\ell}{4} \text{ for } G_{nn'}, G_{mm'}, G_{11'}, G_{kk'}, \text{ and } G_{jj'},$$

respectively. The factors  $G_i$  thus computed are listed in Table 3.3.

## APPENDIX E

### CONSTRAINTS ON THE LUMINOSITIES, FREQUENCY, AND SPATIAL DISTRIBUTION OF THE TRANSIENT X-RAY SOURCES<sup>1</sup>

We begin by making the following simplifying assumptions:

- (1) Transient sources may occur at random anywhere within a given galaxy, with a mean time  $\tau$  between occurrences (per galaxy);
- (2) The outburst is characterized by a sharp turn-on and exponential decay (time constant  $\tau_d = T_{ON}$ ), with  $L(t < 0) = 0$  and  $L(t > 3 T_{ON}) = 0$ .
- (3) All sources appearing above a minimum detectable flux,  $S_0$ , are detected (limiting radius  $R_0 \equiv (\frac{L}{4\pi S_0})^{1/2}$ ).

It follows (see, for example, Bevington 1969, page 38) from assumption (1) that the probability (per galaxy) of at least one source occurring in the interval  $(0, t)$  is given by

$$\begin{aligned}
 P(t, \tau) &= 1 - e^{-t/\tau} \\
 &\approx \frac{t}{\tau} \quad \text{for } t \ll \tau.
 \end{aligned}
 \tag{E-1}$$

#### A. Extragalactic Origin

For a uniform spherical distribution of sources (density =  $n_s$ ), the number  $N_r$  within a radius  $r$  is

$$N_r = 4\pi \int_0^r n_s r'^2 dr'.
 \tag{E-2}$$

Thus, the total number of sources appearing above  $S = S_0$  in time  $t$  ( $\ll \tau$ ) is:

<sup>1</sup>The basic approach followed herein is taken from Silk (1973).

$$\begin{aligned}
 N(>S_0, t) &= 4\pi \int_0^{R_0} n_g P(t, \tau) r^2 dr \\
 &= \frac{4\pi}{3} n_g \left(\frac{t}{\tau}\right) R_0^3 \\
 N(>S_0, t) &= \frac{4\pi}{3} n_g \left(\frac{L}{4\pi S_0}\right)^{3/2} \left(\frac{t}{\tau}\right) \quad (E-3)
 \end{aligned}$$

where

$n_g$  = number density of galaxies.

We may also evaluate the contribution ( $I_s$ ) of the population of unresolved transient sources to the diffuse X-ray background as follows:

$$I_s = \frac{1}{\Omega} \int_0^{R_H} \frac{dE}{dt} \frac{n_g P(t, \tau)}{4\pi r^2} 4\pi r^2 dr;$$

where

$R_H$  = Hubble radius =  $\frac{c}{H_0}$ , ( $R_H \gg R_0$ ),

$c$  = speed of light

and

$H_0$  = Hubble's constant;

$$I_s = \frac{1}{4\pi} \int_0^{R_H} \frac{LT_{ON}}{t} n_g \frac{t}{\tau} dr$$

$$I_s \approx \frac{n_g c}{4\pi H_0} \frac{LT_{ON}}{\tau} \text{ erg (cm}^2 \text{ s sterad)}^{-1} < I_x, \quad (E-4)$$

where

$I_x$   $\equiv$  isotropic diffuse X-ray background.

Equations E-3 and E-4 may be solved for  $L$  and  $\tau$  in terms of known or observable parameters:

$$L \geq \frac{9}{4\pi} \left(\frac{c}{H_0}\right)^2 \frac{(N(>S_0, t))^2}{I_x} S_0^3 \frac{T_{ON}^2}{t^2} \quad (E-5)$$

and

$$\tau \geq \frac{9}{16\pi^2} n_g \left(\frac{c}{H_0}\right)^3 \frac{(N(S_0, t))^2}{I_x^3} S_0^3 \frac{T_{ON}^3}{t^2} \quad (E-6)$$

Adopting the values:

$$I_x = 7.6 \times 10^{-8} \text{ erg (cm}^2 \text{ s sterad)}^{-1} \text{ (1-13 keV, Gorenstein et al. 1969),}$$

$$H_0 = 50 \text{ km s}^{-1} \text{ Mpc}^{-1}, \text{ and}$$

$$n_g = 1 \times 10^{-75} \text{ cm}^{-3}, \text{ Equations E-5 and E-6 yield:}$$

$$L \geq 1.3 \times 10^{45} \left[ \frac{N(>S_0, t)}{5} \right]^2 \left( \frac{2}{t} \right)^2 \left( \frac{S_0}{8 \times 10^{-9}} \right)^3 \left( \frac{T_{ON}}{0.1} \right)^2 \text{ erg s}^{-1},$$

and

$$\tau \geq 2.5 \times 10^3 \left[ \frac{N(>S_0, t)}{5} \right]^2 \left( \frac{2}{t} \right)^2 \left( \frac{S_0}{8 \times 10^{-9}} \right)^3 \left( \frac{T_{ON}}{0.1} \right)^3 \text{ yr},$$

where the parameters  $t$ ,  $N(>S_0, t)$ ,  $S_0$ , and  $T_{ON}$  are taken from the Ariel 5 observations:

$$t = 2 \text{ yr},$$

$$S_0 \approx S_{\text{crab}}/2 = 8 \times 10^{-9} \text{ erg cm}^{-2} \text{ s}^{-1},$$

$$N(>S_0, t) = 5$$

$$T_{ON} = 0.1 \text{ yr}.$$

While these values for  $L$  and  $\tau$  are approximately 1-2 orders of magnitude below those derived by Silk on the basis of the pre-Ariel 5 observations, the result  $\tau \approx 2.5 \times 10^3 \text{ yr}$  is still irreconcilable with the known rate of occurrence of supernovae ( $\tau_{\text{SN}} \approx 10^2 \text{ yr per galaxy}$ ), thereby ruling out the hypothesis that the transient sources are related to extragalactic supernova explosions (Sofia 1972). As further noted by Silk, an extragalactic origin in general for the transient sources would require the

occurrence of catastrophic events in some fraction  $f$  of all galaxies at a mean interval  $\Delta t = f\tau(>2.5 \times 10^3 f)$  yr with total X-ray energy outputs of  $E \sim 4 \times 10^{51}$  ergs. As these properties are so extreme compared to the known properties of extragalactic sources (e.g.,  $E_{SN} \leq 4 \times 10^{49}$  ergs, Allen 1963), such an origin is extremely improbable.

### B. Galactic Origin

Proceeding as in (A) Equation E-2 now becomes:  
(in the following we have ignored the offset of the sun from the galactic center)

For a uniform spherical halo distribution of sources we obtain:

$$N(>S_0, t) = \int_0^{R_0} n_s (4\pi r^2 dr); \quad n_s = \frac{P(t, \tau)}{\frac{4}{3} \pi R^3},$$

where

$n_s$  = number density of transients in the Galaxy

and

$R$  = galactic radius; hence,

$$\begin{aligned} N(>S_0, t) &= \left(\frac{R_0}{R}\right)^3 \frac{t}{\tau} \\ &= \frac{1}{R^3} \left(\frac{L}{4\pi S_0}\right)^{3/2} \frac{t}{\tau}. \end{aligned} \quad (E-7)$$

As noted in Chapter V, the observed absence of transients outside of a narrow band along the galactic equator allows us to rule out a spherical halo distribution for the transient sources. We thus pursue the case of a uniform spatial distribution of sources in a disk of scale-height  $h \ll R$ , and Equation E-2 becomes:

$$N(>S_0, t) \approx \int_0^{R_0} n_s (2\pi r' dr'); \quad n_s = \frac{P(t, \tau)}{2\pi R^2 h}$$

$$\approx \left(\frac{R_0}{R}\right)^2 \frac{t}{\tau},$$

$$N(>S_0, t) = \frac{L}{4\pi S_0 R^2} \frac{t}{\tau}, \text{ yielding the ratio}$$

$$\frac{L}{\tau} \approx 4\pi N(>S_0, t) S_0 \frac{R^2}{t}. \quad (\text{E-8})$$

This expression can only provide a lower limit on the ratio  $\frac{L}{\tau}$  for three reasons:

(1) we have assumed a sensitivity-limited situation, i.e.,  $R_0 < R$ ; since, in some cases we expect  $R_0 \geq R$ , the number observed will be  $\leq$  the number expected ( $N(>S_0, t)$ ) in Equation E-8;

(2) in a similar fashion, the offset of the sun from the center of the Galaxy ( $R_s \approx 10$  Kpc) will result in fewer sources being observed as  $r'$  increases from  $r' = R - R_s$  to  $r' = R_0$  (see Figure E.1); and

(3) some fraction of sources with  $S > S_0$  may be missed due to source confusion in crowded regions of the plane.

Note that these effects will cause the  $\log N - \log S$  curve to "turn over" with respect to that expected from an ideal uniform disk distribution ( $\Delta N (\equiv \text{expected-observed})$  increases with decreasing flux), and hence the  $\log N - \log S$  plot shown in Figure 5.2 cannot be used to distinguish between the uniform disk vs. (thin, narrow) spiral arms distributions (arm width,  $w \ll R$ , and thickness  $t \ll w$ ; For this case  $N(>S_0, t) = M \int_0^{R_0} \sigma_s w dl$ ,

$$\sigma_s = \frac{P(t, \tau)}{MRw} \quad (M = \text{no. of arms}); \quad N(>S_0, t) = \left(\frac{R_0}{R}\right) \frac{t}{\tau} = \frac{1}{R} \left(\frac{L}{4\pi S_0}\right)^{\frac{1}{2}} \frac{t}{\tau}.$$



Adopting values of

$$S_0 = S_{\text{crab}}/2 = 8 \times 10^{-9} \text{ erg cm}^{-2} \text{ s}^{-1},$$

$$R = 15 \text{ Kpc},$$

and

$$t = 2 \text{ yr},$$

Equation E-8 becomes:

$$\frac{L}{\tau} \geq 4.3 \times 10^{38} N(>S_0, t) \left( \frac{S_0}{S_{\text{crab}}} \right) \left( \frac{R}{15 \text{ Kpc}} \right)^2 \left( \frac{t}{2 \text{ yr}} \right).$$

## REFERENCES

- Allen, C. W. 1963, Astrophysical Quantities (London: Athlone Press).
- Allen, C. W. 1973, Astrophysical Quantities (London: Athlone Press).
- Amuel, P. R., Guseinov, O. H., and Rakhimov, Sh. Ju. 1974, Ap. and Space Sci., 29, 331.
- Ariel 5 Group, University of Birmingham 1976, IAU Circ., No. 2934.
- Avni, Y., Fabian, A. C., and Pringle, J. E. 1976, M.N.R.A.S., 175, 297.
- Bahcall, J., and Ostriker, J. 1975, Nature, 256, 23.
- Barnden, L. R., and Francey, R. J. 1969, Proc. Astr. Soc. Australia, 1, 236.
- Bath, G. T., Evans, W. D., Papaloizou, J., and Pringle, J. E. 1974, M.N.R.A.S., 169, 447.
- Belian, R. D., Conner, J. P., and Evans, W. D. 1976, Ap. J. (Letters), 207, L33.
- Bevington, P. R. 1969, Data Reduction and Error Analysis for the Physical Sciences (New York: McGraw-Hill).
- Blumenthal, G. R., and Tucker, W. H. 1974, Ann. Rev. Astr. and Ap., 12, 23.
- Boldt, E. A., Desai, U. D., Holt, S. S., and Serlemitsos, P. J. 1969, Nature, 224, 677.
- Boldt, E. A., Desai, U. D., and Holt, S. S. 1969, Ap. J., 156, 427.
- Boley, F., Wolfson, R., Bradt, H., Doxsey, R., Jernigan, G., and Hiltner, W. A. 1976, Ap. J. (Letters), 203, L13 (see also IAU Circ. No. 2819).
- Bolton, C. T. 1975, Ap. J., 200, 269.
- Borkowski, C. J., and Kopp, M. K. 1968, Rev. of Scientific Instr., 39, 1515.
- Borner, G., and Cohen, J. M. 1973, Ap. J., 185, 959.
- Bortle, J. 1976a, IAU Circ., No. 2918.

- Bortle, J. 1976b, IAU Circ., No. 2935.
- Bortle, J. 1976c, IAU Circ., No. 2941.
- Brecher, K. 1972, Nature, 239, 325.
- Brecher, K. 1975, Nature, 257, 203.
- Brecher, K., and Morrison, P. 1975, Bull. Am. Astr. Soc., 7, 538.
- Branduardi, G., Ives, J. C., Sanford, P. W., Brinkman, A. C., and  
Maraschi, L. 1976, M.N.R.A.S., 175, 47P.
- Buff, J. 1975, IAU Circ., No. 2788.
- Buff, J., and McCray, R. 1974, Ap. J., 189, 147.
- Canal, R., and Schatzmann, E. 1976, Ap. and Space Sci., 46, 229.
- Canizares, C. R., McClintock, J. E., Clark, G. W., Lewin, W. H. G.,  
Schnopper, H. W., and Sprott, G. F. 1973, Nature Phys. Sci., 241, 28.
- Canizares, C. R., Li, F. K., and Clark, G. W. 1974, Ap. J. (Letters), 191,  
L75.
- Carpenter, G. F., Eyles, C. J., Skinner, G. K., Willmore, A. P., and  
Wilson, A. M. 1975, IAU Circ., No. 2852.
- Chevalier, C., and Ilovaisky, S. A. 1975, IAU Circ., No. 2778.
- Chevalier, C., Ilovaisky, S. A., and Mauder, H. 1976, IAU Circ., No. 2957.
- Chodil, G., Mark, H., Rodrigues, R., and Swift, C. D. 1968, Ap. J. (Letters),  
152, L45.
- Citterio, O., Conti, G., Di Benedetto, P., Tanzi, E. G., Perola, G. C.,  
White, N. E., Charles, P. A., and Sanford, P. W. 1976, M.N.R.A.S.,  
175, 35p.
- Clark, D. H., Parkinson, J. H., and Caswell, J. L. 1975, Nature, 254, 674.
- Clark, D. H., and Parkinson, J. H. 1975, Nature, 258, 408.
- Clark, G. W. 1975a, IAU Circ., No. 2843.
- Clark, G. W. 1975b, Ap. J. (Letters), 199, L143.

- Coe, M. J., Engel, A. R., and Quenby, J. J. 1976, Nature, 259, 544.
- Coe, M. J., Carpenter, G. F., Engel, A. R., and Quenby, J. J. 1975, Nature, 256, 631.
- Cooke, B. A. 1976, Preprint SSI 21.
- Cooke, B. A., Pounds, K. A., Stewardson, E. A., and Adams, D. J. 1967, Ap. J., 150, 189.
- Cowley, A. P. and Crampton, D. 1975, Ap. J. (Letters), 201, L65.
- Davidson, A., and Ostriker, J. P. 1974, Ap. J., 189, 331.
- Davidson, A., Sanford, P., Davison, P., and Mason, K. 1975, IAU Circ., No. 2793.
- Davison, P. J. N., and Tuohy, I. R. 1975, M.N.R.A.S., 173, 33P.
- Davison, P. J. N., and Sanford, P. W. 1976, Nature, 259, 98.
- Davison, P., Burnell, J., and Ives, J. 1976, IAU Circ., No. 2925.
- De Cuyper, J. P., De Greve, J. P., De Loore, C., and Van den Heuvel, E. P. J. 1976, Astron. Astrophys. 52, 315.
- De Loore, C., De Greve, J. P., Van den Heuvel, E. P. J., and De Cuyper, J. P. 1974, Proc. of the 2nd IAU Regional Meeting at Trieste.
- Desai, U. D., and Holt, S. S. 1972, IEEE Trans. Nucl. Sci., NS-19, 592.
- Doxsey, R., Jernigan, G., Hearn, D., Bradt, H., Buff, J., Clark, G. W., Delvaille, J., Epstein, A., Joss, P. C., Matilsky, T., Mayer, W., Mc Clintock, J., Rappaport, S., Richardson, J., and Schnopper, H. 1976, Ap. J. (Letters), 203, L9.
- Duerbeck, H. W., and Walter, K. 1976, Astron. Astrophys., 48, 141.
- Eachus, L., Wright, E., and Liller, W. 1976, Ap. J. (Letters), 203, L17.
- Edwards, P. J. 1968, Nature, 217, 43.
- Elvis, M., Page, C. G., Pounds, K. A., Ricketts, M. J., and Turner, M. J. L. 1975, Nature, 257, 656 (see also IAU Circ., No. 2814).

- Endal, A. S., De Vinney, E. J., and Sofia, S. 1976, Astrophys. Lett., 17, 131.
- Epstein, A. 1976, presented at meeting of HEAD/AAS, Cambridge, Mass.
- Evans, W. D., Belian, R. D., and Conner, J. P. 1970, Ap. J. (Letters), 159, L57.
- Eyles, C. J., Skinner, G. K., Willmore, A. P., and Rosenberg, F. D. 1975a, Nature, 254, 577.
- Eyles, C. J., Skinner, G. K., Willmore, A. P., and Rosenberg, F. D. 1975b, Nature, 257, 291.
- Fabian, A. C. 1975, M.N.R.A.S., 173, 161.
- Fabian, A., Pringle, J. E., and Webbink, R. F. 1975, Nature, 255, 208.
- Fabian, A. C., Pringle, J. E., and Rees, M. J. 1976, M.N.R.A.S., 175, 43.
- Flannery, B. P., and Van den Heuvel, E. P. J., 1975, Astron. Astrophys., 39, 61.
- Forman, W., and Liller, W. 1973, Ap. J. (Letters), 183, L117.
- Forman, W., Jones, C., and Tananbaum, H. 1976a, Ap. J. (Letters), 206, L29.
- Forman, W., Jones, C., and Tananbaum, H. D. 1976b, Ap. J. (Letters), 207, L25.
- Forman, W. 1977, presented at the 149th meeting of the American Astronomical Society, Honolulu, Hawaii.
- Francey, R. J., Fenton, A. G., Harries, J. R., and McCracken, K. G. 1967, Nature, 216, 773.
- Giacconi, R. 1976, Am. Journal of Phys., 44 (No. 2), 121.
- Giacconi, R., Murray, S., Gursky, H., Kellogg, E., Schreier, E., Matilsky, T., Koch, D., and Tananbaum, H. 1974, Ap. J. Suppl., No. 237, 27, 37.
- Glasby, J. S. 1969, Variable Stars (Cambridge, Mass.: Harvard University Press).

- Gorenstein, P., and Tucker, W. H. 1976, Annual Review of Astronomy and Astrophysics, 14, to be published.
- Grindlay, J., and Schreier, E. 1975, IAU Circ., No. 2863.
- Grindlay, J. E., and Gursky, H. 1976, Ap. J. (Letters), 209, L61.
- Gull, T. R., York, D. G., Snow, T. P., Jr., and Henize, K. G. 1976, submitted to Ap. J. (Letters); see also IAU Circ. No. 2819.
- Gursky, H. 1973, in DeWitt and DeWitt (eds.), Black Holes, (New York: Gordon and Breach).
- Gursky, H. 1975, IAU Symposium No. 73, 'Structure and Evolution of Close Binaries', Cambridge, England.
- Gursky, H., and Schreier, E. 1974, CFA preprint No. 119.
- Gursky, H. and Schreier, E. 1975, in IAU Symposium No. 67, 'Variable Stars and Stellar Evolution', eds. V. Sherwood and L. Plant (Dordrecht: Reidel).
- Harries, J. R., McCracken, K. G., Francey, R. J., and Fenton, A. G. 1967, Nature, 215, 38.
- Harries, J. R., Tuohy, I. R., Broderick, A. J., Fenton, K. B., and Luyendyk, A. P. J. 1971, Nature Phys. Sci., 234, 149.
- Harwit, M. 1973, Astrophysical Concepts (New York: Wiley).
- Hayakawa, S. 1976, Preprint CSR-P-76-22.
- Hayakawa, S., and Matsuoka, M. 1964, Prog. Theoret. Phys. Suppl. Japan, No. 30, 204.
- Hoffman, J. A., Lewin, W. H. G., Brecher, K., Buff, J., Clark, G. W., Joss, P. C., and Matilsky, T. 1976, Nature, 261, 208.
- Holt, S. S., Boldt, E. A., and Serlemitsos, P. J. 1969, Ap. J. (Letters), 158, L155.

- Holt, S. S., Boldt, E. A., Serlemitsos, P. J., Murray, S. S., Giacconi, R., Kellogg, E. M., and Matilsky, T. A. 1974, Ap. J. (Letters), 188, L97.
- Holt, S. S. 1976, Astrophys. Space Sci., 42, 123.
- Holt, S. S., Boldt, E. A., Serlemitsos, P. J., and Kaluzienski, L. J. 1976a, Ap. J. (Letters), 203, L63.
- Holt, S. S., Boldt, E. A., Serlemitsos, P. J., and Kaluzienski, L. J. 1976b, Ap. J. (Letters), 205, L27.
- Holt, S. S., Boldt, E. A., Serlemitsos, P. J., and Kaluzienski, L. J. 1976c, Ap. J. (Letters), 205, L79.
- Holt, S. S., Boldt, E. A., Serlemitsos, P. J., Kaluzienski, L. J., Pravdo, S. H., Peacock, A., Elvis, M., Watson, M. G., and Pounds, K. A. 1976d, Nature, 260, 592.
- Holt, S. S., Boldt, E. A., Serlemitsos, P. J., and Kaluzienski, L. J. 1976e, Ap. J. (Letters), 205, L143.
- Holt, S. S., Boldt, E. A., Kaluzienski, L. J., Serlemitsos, P. J., and Swank, J. H. 1976f, Nature, 263, 484.
- Holt, S. S., and Kaluzienski, L. J. 1977, IAU Circ., No. 3031.
- Hutchings, J. B. 1974, Ap. J., 192, 685.
- Ives, J. C., Sanford, P. W., and Bell-Burnell, S. J. 1975, Nature, 254, 578.
- Jernigan, G. 1975, IAU Circ., No. 2817.
- Jernigan, G. 1976, IAU Circ., No. 2957.
- Jones, C. 1976, private communication.
- Jones, C. A., Forman, W., and Liller, W. 1973, Ap. J. (Letters), 182, L109.
- Jones, C., Giacconi, R., Forman, W., and Tananbaum, H. 1974, Ap. J. (Letters), 191, L71.

- Jones, C., Forman, W., Tananbaum, H., and Turner, M. J. L. 1976, CFA preprint No. 589.
- Joss, P. C. 1975, IAU Circ., No. 2863.
- Kaluziński, L. J., Holt, S. S., Boldt, E. A., and Serlemitsos, P. J. 1975a, Nature, 256, 633.
- Kaluziński, L. J., Holt, S. S., Boldt, E. A., Serlemitsos, P. J., Eadie, G., Pounds, K. A., Ricketts, M. J., and Watson, M. 1975b, Ap. J. (Letters), 201, L121.
- Kaluziński, L. J., Holt, S. S., Boldt, E. A., and Serlemitsos, P. J. 1975c, IAU Circ., No. 2859.
- Kaluziński, L. J., Holt, S. S., Boldt, E. A., and Serlemitsos, P. J. 1975d, IAU Circ., No. 2863.
- Kaluziński, L. J., Holt, S. S., Boldt, E. A., and Serlemitsos, P. J. 1976a, IAU Circ., No. 2935.
- Kaluziński, L. J., Holt, S. S., Esfandiari, M., Boldt, E. A., and Serlemitsos, P. J. 1976b, IAU Circ., No. 2965.
- Kaluziński, L. J., Holt, S. S., Boldt, E. A., and Serlemitsos, P. J. 1976c, Ap. J. (Letters), 208, L71.
- Kaluziński, L. J., Holt, S. S., Boldt, E. A., and Serlemitsos, P. J. 1977a, Ap. J. 212, 203.
- Kaluziński, L. J., Holt, S. S., Boldt, E. A., and Serlemitsos, P. J. 1977b, Nature, 265, 606.
- Katz, J. I. 1973, Nature, 246, 87.
- Kellogg, E., Gursky, H., Murray, S., Tananbaum, H., and Giacconi, R. 1972, Ap. J. (Letters), 169, L99.
- Kitamura, T., Matsuoka, M., Miyamoto, S., Nakagawa, N., Oda, M., Ogawara, Y., and Takagishi, K. 1969, Nature, 224, 784.



- Kleinmann, S. G., Brecher, K., and Ingham, W. H. 1975, preprint.
- Kraft, R. P. 1967, Publ. Astr. Soc. Pacific, 76, 431.
- Kraft, R. P. 1975, in H. Gursky and R. Ruffini (eds.), 'Neutron Stars, Black Holes and Binary X-ray Sources', Astrophysics and Space Science Library, Vol. 48, 235 (Boston: D. Reidel).
- Leach, R. W., Murray, S. S., Schreier, E. J., Tananbaum, H. D., and Ulmer, M. P. 1975, Ap. J., 199, 184.
- Lee, D. M., and Sobottka, S. E. 1973, Nucl. Instr. and Meth., 109, 421.
- Lewin, W. H. G., Doty, J., Hoffman, J. A., Clark, G. W., Jernigan, J. G., Li, F. K., and McClintock, J. E. 1976, Preprint No. CSR-P-76-14.
- Lewin, W. H. G. 1976, Preprint CSR-P-76-24.
- Li, F. K. 1976, IAU Circ., No. 2936.
- Li, F. K., Sprott, G. F., and Clark, G. W. 1976, Ap. J., 203, 187.
- Liller, W. 1975, IAU Circ., No. 2780.
- Manley, O. P. 1967, Phys. Rev. Letters, 19, 1144.
- Maraschi, L., Treves, A., and Van den Heuvel, E. P. J. 1976, Nature, 259, 292.
- Maraschi, L., Huckle, H. E., Ives, J. C., and Sanford, P. W. 1976, Nature, 263, 34.
- Margon, B., and Ostriker, J. P. 1973, Ap. J., 186, 91.
- Markert, T., 1973, Ap. J. (Letters), 184, L67.
- Markert, T. H. 1974, Ph.D. Thesis.
- Martynov, D. Ya. 1976, IAU Circ., No. 2953.
- Matilsky, T. 1976, IAU CIRC., No. 2949.
- Matilsky, T., and Zubrod, D. 1976, presented at meeting of HEAD/AAS, Cambridge, Mass.

- Matilsky, T., Giacconi, R., Gursky, H., Kellogg, E., and Tananbaum, H. 1972, Ap. J. (Letters), 174, L53.
- Matilsky, T. A., Gursky, H., and Tananbaum, H. 1973, presented at 141st Meeting of the American Astronomical Society, Tucson.
- Matilsky, T., Gursky, H., Kellogg, E., Tananbaum, H., Murray, S., and Giacconi, R. 1973, Ap. J., 181, 753.
- Matsuoka, M., Tsunemi, H., Eiraku, M., Inoue, H., Koyama, K., Maeda, Y., Takagishi, K., and Watanabe, E. 1976, preprint (ISAS RN12).
- Mc Cluskey, G. E., and Kondo, Y. 1971, Ap. and Space Sci., 10, 464.
- Milgrom, M., and Avni, Y. 1976, Astron. Astrophys., 52, 157.
- Murdin, P., Griffiths, R. E., Pounds, K. A., Watson, M. G., and Longmore, A. J. 1977, M.N.R.A.S., 178, 27P.
- Oort, J. H. (et al.), 1958, Stellar Populations, ed. O'Connell, pp. 414, 533, Vatican Ob.
- Osaki, Y. 1974, Publ. Astron. Soc. Japan, 26, 429.
- Owen, F., Balonek, T., Dickey, J., Terzian, Y., and Gottesman, S. 1976, Ap. J. (Letters), 203, L15 (see also IAU Circ. No. 2823).
- Pacini, F., and Salvati, M. 1974, Ap. J. (Letters), 188, L55.
- Pacini, F., and Shapiro, S. L. 1975, Nature, 255, 618.
- Parsignault, D. R., Gursky, H., Kellogg, E. M., Matilsky, T., Murray, S., Schreier, E., Tananbaum, H., Giacconi, R., and Brinkman, A. C. 1972, Nature Phys. Sci., 239, 123.
- Payne-Gaposchkin, C. 1964, The Galactic Novae (New York: Dover).
- Peterson, B., Jauncey, D. L., and Wright, A. E. 1975, IAU Circ., No. 2837.
- Petterson, J. A. 1975, Ap. J. (Letters), 201, L61.
- Pounds, K. A. 1974, IAU Circ., No. 2729.

- Pounds, K. A. 1976a, presented at meeting of HEAD/AAS, Cambridge, Mass.
- Pounds, K. A. 1976b, submitted to Comments in Astrophysics and Space Science, June 1976.
- Prendergast, K. H., and Burbidge, G. R. 1968, Ap. J. (Letters), 151, L83.
- Primini, F. 1975, IAU Circ., No. 2833.
- Pringle, J. E. and Webbink, R. F. 1975, M.N.R.A.S., 172, 493.
- Rappaport, S., Joss, P. C., Bradt, H., Clark, G. W., and Jernigan, J. G. 1976, Ap. J. (Letters), 208, L119.
- Ricketts, M. J., Pounds, K. A., and Turner, M. J. L. 1975, Nature, 257, 657.
- Ricketts, M. J., Cooke, B. A., and Pounds, K. A. 1976, Nature, 259, 546.
- Ricketts, M. J., Turner, M. J. L., Page, C. G., and Pounds, K. A. 1975, Nature, 256, 631.
- Roberts, W. J. 1974, Ap. J., 187, 575.
- Rosenberg, F. D., Eyles, C. J., Skinner, G. K., and Willmore, A. P. 1975, Nature, 256, 628.
- Rothschild, R. E., Boldt, E. A., Holt, S. S., and Serlemitsos, P. J. 1974, Ap. J. (Letters), 189, L13.
- Salpeter, E. 1973, in H. Bradt and R. Giacconi (eds.), X-and Gamma-Ray Astronomy, IAU Symp. 55, 135.
- Sanford, P. W., and Hawkins, F. H. 1972, Nature Phys. Sci., 239, 135.
- Schatzmann, E. 1965, Stellar Structure, eds. H. Aller and D. McLaughlin (Chicago: University of Chicago Press).
- Schreier, E. J., Swartz, K., Giacconi, R., Fabbiano, G., and Morin, J. 1976, Ap. J., 204, 539.
- Schwartz, D. A., Murray, S. S., and Gursky, H. 1976, Ap. J., 204, 315.

- Serlemitsos, P. J., Boldt, E. A., Holt, S. S., Rothschild, R. E., and Saba, J. L. R. 1975, Ap. J. (Letters), 201, L9.
- Seward, F. 1970, An Illustrated Catalog of Cosmic X-ray Sources, LLL Report UCID-15622.
- Seward, F. D., Horton, B., Pollard, G., and Sanford, P. W. 1976, Nature, 264, 421.
- Shklovski, I. 1967, Ap. J. (Letters), 148, L1.
- Shukla, P. G., and Wilson, B. G. 1971, Ap. J., 164, 265.
- Silk, J. 1973, Ap. J., 181, 747.
- Silk, J., and Arons, J. 1975, Ap. J. (Letters), 200, L131.
- Simonson, S. C. III 1975, CNRS Paris Colloquium, 1974 Sept., ed. L. Weliachew.
- Skinner, G. K. 1975, private communication.
- Smith, J. F., and Courtier, G. M. 1976, Proc. R. Soc. Lond. A. 350, 421.
- Sofia, S. 1971, Acta Cien. Ven., 22, 124.
- Sofia, S. 1972, Ap. J. (Letters), 175, L113.
- Sofia, S., and Wesemael, F. 1976, Ap. J., 205, 233.
- Stoeger, W. R. 1976, Nature, 261, 211.
- Streeter, G. R. 1973, 'UK-5 Final Electrical Configuration', Spacetic Inc.
- Strohmeier, W. 1972, Variable Stars, ed. A. J. Meadows (Oxford: Pergamon Press).
- Stutantyo, W. 1975, Astron. Astrophys., 35, 251.
- Sullivan, J. D. 1971, Nucl. Instr. and Meth., 95, 5.
- Swank, J. H., Becker, R. H., Boldt, E. A., Holt, S. S., Pravdo, S. H., Rothschild, R. E., and Serlemitsos, P. J. 1976, Ap. J. (Letters), 209, L57.
- Tananbaum, H., Gursky, H., Kellogg, E., Giacconi, R., and Jones, C. 1972, Ap. J. (Letters), 177, L5.

- Tananbaum, H., Chaisson, L. J., Forman, W., Jones, C., and Matilsky, T. A. 1976, Ap. J. (Letters), 209, L125.
- Thorne, K. S., and Price, R. H. 1975, Ap. J. (Letters), 195, L101.
- Tsunemi, H., Matsuoka, M., and Takagishi, K. 1977, Ap. J. (Letters), 211, L15.
- Tuohy, I. R., and Davison, P. J. N. 1973, Nature Phys. Sci., 244, 121.
- Turner, M. J. L. 1976, presented at meeting of HEAD/AAS, Cambridge, Mass.
- Ulmer, M. P., Baity, W. A., Wheaton, W. A., and Peterson, L. E. 1973, Ap. J., 184, L117.
- Van den Heuvel, E. P. J. 1974, Proc. 16th Solvay Conf. Physics, (Editions de l'Universite de Bruxelles, Brussels).
- Van Horn, H. M., and Hansen, C. J. 1974, Ap. J., 191, 478.
- Villa, G., Page, C. G., Turner, M. J. L., Cooke, B. A., Ricketts, M. J., Pounds, K. A., and Adams, D. J. 1976, M.N.R.A.S., 176, 609.
- Ward, M. J., Penston, M. V., Murray, C. A., and Clements, E. D. 1975, Nature, 257, 660.
- Watson, M. G. 1976a, M.N.R.A.S., 176, 19P.
- Watson, M. G. 1976b, private communication.
- Watson, M. G. 1977, private communication.
- Wheaton, W. A., Baity, W. A., and Peterson, L. E. 1975, IAU Circ., No. 2761.
- Whelan, J. and Iben, I. 1973, Ap. J., 186, 1007.
- Whelan, J. A. J., Ward, M. J., Allen, D. A., Danziger, I. J., Fosbury, R. A. E., Murdin, P. G., Penston, M. V., Peterson, B. A., Wampler, E. J., and Webster, B. L. 1976, preprint.
- Wickmrasinghe, D. T., and Whelan, J. A. J. 1975, Nature, 258, 503.
- Wickmrasinghe, D. T., and Warren, P. R. 1976, M.N.R.A.S., 177, 59P.

Wu, C. C., Aalders, J. W. A., Van Duinen, R. J., Kester, D., and Wesselius, P. R. 1976, Astron. Astrophys., 50, 445.

Wyatt, S. P. 1964, Principles of Astronomy (Boston: Allyn and Bacon).

Zel'dovich, Ya. B., and Guseinov, O. 1965, Ap. J., 144, 841.

Zel'dovich, Ya. B., and Novikov, I. D. 1967, Relativistic Astrophysics, Vol. 1 (Moscow: Izdatel'stvo Nauka), English edition by K. S. Thorne and W. D. Arnett, 1971, (Chicago: University of Chicago Press).

Nature	Class	Designation, description, prototype	Period	Amplitude	Type
Pulsating (periodic)	C	Cepheids I = classical cepheids ( $\delta$ Cep)	$1^d.5-80^d$	$0^m.1-2^m$	F-K
	CW	Cepheids II = W Virginis stars	1-50		
	RRa	asymmetric light curve (RR Lyr)	0.5		
	RRc	RR Lyrae stars, sinusoidal light curve (SX UMa)	0.3	0.5-1.5	A
	M	Mira stars ( $\alpha$ Cen = Mira)	80-1000	2.5-8	M, N
	RVa	constant mean brightness (AC Her)			
	RVb	RV Tauri stars, varying mean brightness (RV Tau)	30-150	0.5-3	G-M
	C	Beta Canis Majoris stars, Giants	0.1-0.3	0.1	gB2
	Sc	Delta Scuti stars, Dwarf cepheids	0.6	0.2	dF
	CV	Alpha Canum Venaticorum stars, with variable magnetic fields	1-25	0.1	Ap
Semi-regular (cyclic)	SRa	appreciable periodicity (Z Aqr)			
	SRb	Red stars, poor periodicity (AF Cyg)	30-1000	1-2	M
	SRc	Supergiants ( $\mu$ Cen)			
	SRd	Yellow Giants and Supergiants (S Vul)	30-1000	1-2	F-K
Irregular Eruptive	Ia	early Spectral type (BO Cep)	50-300		A, F
	Ib	Variables, red Giants ( $\zeta$ Cyg)	80-200	many	K, M
	Ic				
	SN	Supernovae (CM Tau = Crab Nebula)			
	Na	Fast novae (GK Per = Nova 1901)		20	
	Nb	Slow novae (RR Pic = Nova 1909)		7-16	
	Nc	Very slow novae (RT Ser = Nova 1952)			
	Nd	Recurrent novae (T CrB = Nova 1866/1946)	$10^d-80^d$	4-8	dF, dG
	Ne	Nova-like stars (P Cyg = Nova 1600)			very heterogeneous class
	UG	U Geminorum stars, Dwarfs, frequent outbursts	20-600	2-6	dG
Z	Z Camelopardalis stars, generally constant	10-40	2-5	dG	
RCB	R Coronae Borealis stars, high luminosity	10-300	1-9	F-R	
Twitchety	RW	RW Aurigae stars, { in diffuse nebulae	1-2	3	B-M
	T	T Tauri stars, { or in associations			
Symbiotic	UV	UV Ceti stars, Dwarfs, rare flares	$10^{m.1}$	1-6	dMe
		Combination spectra stars (Z And, AG Peg)	700	2-4	gM + Ae
		Spectroscopic doubles, hot and cool component?			
Eclipsing	EA	Algol = Beta Persei stars, spheres	$0^d.2-6^d$	0-4	A-G
	EB	Beta Lyrae stars, spheroids	1-10	0-2	B-F
	EW	W Ursae Majoris stars	0.2-1	0-0.8	F-K

REPRODUCIBILITY OF THE ORIGINAL PAGE IS POOR

Table 1.2

## PRE-ARIEL 5 TRANSIENT X-RAY SOURCES

SOURCE DATE OF OBS. COORDINATES	$S_{\text{max}}/S_{\text{crab}}^+$ ENERGY BAND (keV)	TEMPORAL CHARACTERISTICS	SPECTRAL CHARACTERISTICS	REFERENCES
Cen X-2 4 Apr - 18 May 1967 $l^{\text{II}} = 305^{\circ}3$ $b^{\text{II}} = 0^{\circ}5$	9.9 2-5	Initial appearance uncertain to 1 1/2 yr. Exponential decay with $\tau \sim 23^{\text{d}}$ . No fluctuations on timescales of 100 sec. (Recurrent outbursts up to $\sim$ one year after maximum?) See Figure 2.	Consistent with thermal bremsstrahlung with decreasing temperature over decline $(4.2 - 1.8) \times 10^7$ °K in 40 days.	Harries et al. (1967) Francey et al. (1967) Cooke et al. (1967) Chodil et al. (1967)
Cen X-4 6 July-24 Sep 1969 $l^{\text{II}} = 331^{\circ}0$ $b^{\text{II}} = 23^{\circ}0$	24.8 3-12	Abrupt rise to maximum flux ( $\sim$ 2 days). Two decline phases: Initial $\sim$ .025 mag per day decrease ( $\tau \approx 43^{\text{d}}$ ) for $\sim$ 50 days, fol- lowed by a steeper decay to disappearance in $\sim$ 30 days. Possible recovery phenomena evident. See Figure 2.	Spectral hardness index (6-12 keV: 3-6 keV) decreased sharply in first few days, then remained nearly constant at an average value of .5. During this phase, the spectrum was similar to Sco X-1 (exponential), with $T =$ $4.5 \times 10^7$ °K.	Evans et al. (1970) Kitamura et al. (1969)
3U1735-28 13 & 19 Mar. 1971 $l^{\text{II}} = 359^{\circ}6$ $b^{\text{II}} = 2^{\circ}1$	0.6 2-10	Observed on only two days $\sim$ one week apart; not seen five days earlier or twenty days later. No large ( $\geq 20\%$ ) changes in intensity apparent. Re- detected $\sim$ 5 yrs. after maximum.	Best fitted by a thermal bremsstrahlung spectrum with parameters: $A = (2.2 \pm 0.1) \times 10^{-9}$ $B = (2.2 \pm 0.3)$ keV $kT = (4.8 \pm 0.9)$ keV	Kellogg et al. (1971) Turner (1976)
3U1543-47 26 July 1971 - 1 Feb 1972 $l^{\text{II}} = 330^{\circ}94$ $b^{\text{II}} = 5^{\circ}37$	1.9 2-10	Observed rise time of $\sim$ 3-4 days. Exponential decay similar to early phase of Cen X-4 ( $\tau = 50^{\text{d}}$ ). Daily variations present, but no significant changes on times of $\sim$ 1 sec- $\sim$ 3 hr. Recovery peaks evident. Observed at $\sim$ 2% of maximum $\sim$ 5 yrs. later. See Figure 3.	Steep spectrum, best fit by power law with average energy spectral index of $-3.0 \pm 0.2$ . No indication of low-energy cut-off to 1.7 keV. Sudden change in spectral index observed, implying $\sim$ 30% drop in $T^{**}$ in time of $\sim$ 90 min.	Matilsky et al. (1971) Belian et al. (1973) Li et al. (1976) Pounds (1976)

$$^+ S_{\text{crab}} = 1.6 \times 10^{-8} \text{ erg cm}^{-2} \text{ sec}^{-1} \text{ (2-6 keV)}$$

$$^* \text{dn/dE} = A \exp(-(B/E)^{8/3}) \times \exp(-E/kT) \text{ ergs-cm}^{-2} \text{ s}^{-1} \text{ keV}^{-1}$$

\*\* Isothermal Bremsstrahlung fit



Table 1.3

## POST-UHURU TRANSIENT X-RAY SOURCES

SOURCE DATE OF OCCURRENCE COORDINATES	$S_{\text{max}}/S_{\text{crab}}$ ENERGY BAND	TEMPORAL CHARACTERISTICS	SPECTRAL CHARACTERISTICS	REFERENCES
A1524-62 Nov. 1974 $i_{\text{II}} = 32022$ $b_{\text{II}} = -475$	0.9 3-6 keV	$\tau_R^* \approx 20^{\text{d}}$ $\tau^{**} \sim 2$ months. Precursor peak ( $\sim 70\% \times S_{\text{max}}$ ) $\sim 10^{\text{d}}$ prior to primary maximum.	Best fit by power law spectrum with photon index = -2.5. Spectral softening evident through precursor peak.	Pounds (1975) Kaluziński et al. (1975a)
A1118-61 Dec. 1974 $i_{\text{II}} = 29225$ $b_{\text{II}} = -078$	0.10 3-9 keV	$\tau_R \sim 3^{\text{d}}$ $\tau \sim 1$ week Precursor peak $\sim 5^{\text{d}}$ prior to maximum ( $\sim 40\% \times S_{\text{max}}$ ). "Pulsing" at P = 6.75 min.	Best fit spectrum: Power law with index = -1.0. Significant absorption < 4 keV (local to source).	Ives et al. (1975) Eyles et al. (1975a)
A1742-28 Feb. 1975 $i_{\text{II}} = 359296$ $b_{\text{II}} = -0514$	2.3 3-10 keV	$\tau_R \approx 2^{\text{d}}$ $\tau_1 \sim 12^{\text{d}}$ (for 40 days after maximum). $\tau_2 \sim 90^{\text{d}}$ (for next 140 days).	Power law spectrum with photon number index = -3 and neutral hydrogen column density $N_{\text{H}} = 10^{23}$ atom-cm <sup>-2</sup> . Variations in hardness and degree of absorption on timescale of $\sim$ days.	Eyles et al. (1975b) Branduardi et al. (1976)
A0535+26 Apr. 1975 $i_{\text{II}} = 18125$ $b_{\text{II}} = -227$	$\sim 2.0$ 3-7 keV	$\tau_R \sim 11^{\text{d}}$ $\tau \sim 19^{\text{d}}$ Low-level emission ( $\sim 12\% \times S_{\text{max}}$ ) $\geq 5$ days prior to onset. Recurrent emission $\sim 7$ months after maximum. Pulsing at P = 104 sec.	Best fit by power law with index = -0.8 - -1.1. Initial strong low energy attenuation, followed later by no noticeable cutoff to $\sim 1.2$ keV. If spectrum is thermal, considerable cooling during decay is implied.	Rosenberg et al. (1975) Ricketts et al. (1975a) Kaluziński et al. (1975b) Rappaport et al. (1976)
A0620-00 Aug. 1975 $i_{\text{II}} = 20921$ $b_{\text{II}} = -655$	$\sim 4.0$ 1.5-5 keV	$\tau_R \sim 7^{\text{d}}$ $\tau$ (3-6 keV) $\sim 25^{\text{d}}$ Secondary increases $\sim 2$ and 7 months after maximum followed by final rapid decline ( $\tau \leq 10^{\text{d}}$ ). Similar decay of recurrent nova optical counterpart (V616 Monocerotis).	Best fit by variable power law or thermal spectra with high energy excess. Initially hard through precursor peak, with marked softening ( $\alpha = -0.6$ - -3.0; $kT \approx 30$ - 1.5 keV), during rise to primary maximum. Gradual softening and increasing low energy attenuation afterwards.	Elvis et al. (1975) Ricketts et al. (1975b) Doxsey et al. (1976) Kaluziński et al. (1976)
A1246-56 Dec. 1974 $i_{\text{II}} = 302$ $b_{\text{II}} = 3.5$	(0.2) 3-6 keV	$\tau < 1$ month		Pounds (1976)
A1745-16 Feb. 1976 $i_{\text{II}} = 35421$ $b_{\text{II}} = -472$	(0.3)			Davison et al. (1976)
A1743-29 Mar. 1976 $i_{\text{II}} = 35926$ $b_{\text{II}} = -0542$	(0.2)			Ariel 5 Group Univ. of Birmingham (1976)
MX1803-24 May 1976 $i_{\text{II}} = 621$ $b_{\text{II}} = -179$	(1.0)			Jernigan (1976)

\*  $\tau_R$  = Rise-time\*\*  $\tau$  = e-folding decay time constant

Table 3.1

				CATALOGUED X-RAY SOURCES	LIBRARY NUMBER 1 241 SOURCES			
		NAME		CELESTIAL COORDINATES	GALACTIC COORDINATES			INTENSITY VAR
				LONGITUDE	LONGITUDE	LATITUDE	COUNTS/SQ.-CM-SEC	
1	3U	1617-15	SCO X-1	244.278	-15.537	359.087	23.747	10.200 2.5
2	3U	0531+21	TAU X-1	82.864	-21.995	184.538	-5.790	1.420 1.0
3	3U	1758-25	GX 5-1	269.530	-25.079	5.084	-1.032	0.845 2.0
4	2U	1813-14	GX 17+2	273.290	-14.060	16.424	1.280	0.588 1.5
5	3U	1702-36	GX 349+2	255.580	-36.359	349.093	2.756	0.536 2.0
6	3U	1758-20	GX 9+1	269.643	-20.537	9.071	1.147	0.446 2.0
7	3U	1636-53		249.225	-53.650	332.914	-4.811	0.391 1.0
8	3U	1656+35	CYG X-1	259.092	35.059	71.318	3.084	0.352 5.0
9	3U	1811-17	GX 13+1	272.927	-17.185	13.516	0.082	0.348 1.6
10	3U	2142+38	CYG X-2	325.648	38.086	87.322	-11.316	0.324 2.5
11	3U	1735-44		263.799	-44.420	346.044	-6.974	0.315 1.0
12	3U	1820-30	SGR XR-4	275.107	-30.388	2.784	-7.907	0.250 1.5
13	3U	1744-26	GX 3+1	266.185	-26.562	2.272	0.800	0.230 3.0
14	3U	1728-16	GX 9+9	262.208	-16.947	8.493	9.027	0.229 1.7
15	3U	1837+04	SER X-1	279.330	4.990	36.099	4.881	0.202 2.0
16	3U	1642-45	GX 340+0	250.525	-45.524	339.578	-0.075	0.190 3.0
17	3U	1658-48	GX 339-A	254.739	-48.726	338.925	-4.322	0.172 3.0
18	3U	1705-44		256.348	-44.050	343.322	-2.363	0.140 3.0
19	3U	1908+00	AQL X-1	287.030	0.050	35.666	-4.002	0.099 3.0
20	3U	2030+40	CYG X-3	307.639	40.784	79.836	0.710	0.097 3.0
21	3U	1728-24	GX 1+4	262.207	-24.716	1.914	4.817	0.090 1.0
22	3U	2321+58	CAS A	350.303	58.557	111.750	-2.116	0.080 1.0
23	3U	1630-47	NOR XR-1	247.543	-47.272	336.903	0.282	0.075 3.0
24	3U	0316+41	PER X-1	49.146	41.352	150.578	-13.234	0.071 1.0
25	3U	1743-29	GCX	265.900	-29.130	359.951	-0.327	0.060 1.0
26	3U	1822-00		275.716	-0.035	29.951	5.782	0.055 1.0
27	3U	1516-56	CIR X-1	229.182	-56.902	322.111	0.046	0.054 20.0
28	3U	1700-37		255.110	-37.770	347.745	2.193	0.051 3.0
29	3U	1702-42	ARA XR-1	255.579	-42.980	343.837	-1.272	0.051 1.0
30	3U	1746-37		266.699	-37.010	353.554	-4.989	0.046 1.0
31	3U	1254-69		193.590	-69.018	303.483	-6.425	0.038 1.0
32	3U	1228+12	VIR XR-1	167.020	12.700	283.555	74.507	0.033 1.0
33	3U	1901+03		285.420	3.020	37.141	-1.420	0.033 4.0
34	3U	1512+07		288.150	7.700	42.550	-1.649	0.032 1.0
35	3U	0539-64	LMC X-3	84.841	-64.078	273.537	-32.007	0.031 1.0
36	3U	0352+30		88.091	30.909	163.093	-17.113	0.030 1.0
37	3U	0540-69	LMC X-1	55.241	-69.798	280.232	-31.438	0.029 1.0
38	3U	1556+11		299.200	11.600	51.303	-9.265	0.026 1.0
39	3U	1556-60	NOR 2	239.227	-60.628	324.132	-5.967	0.025 1.0
40	3U	1653+35	HER X-1	253.301	35.599	58.258	38.120	0.025 6.0
41	3U	1822-37		275.560	-37.189	356.787	-11.300	0.025 1.0
42	3U	1755-33	SCO XR-6	268.890	-33.800	357.240	-4.907	0.023 3.0
43	3U	0521-72	LMC XR-1	80.401	-72.018	283.103	-32.665	0.022 1.0
44	3U	1145-61		176.379	-61.889	295.597	-0.204	0.022 5.0
45	3U	1257+28	COMA X-1	194.371	28.190	56.334	87.964	0.022 1.0
46	3U	1704-32		256.129	-32.110	352.763	4.960	0.021 1.0
47	3U	1953+31		298.480	31.939	66.390	1.885	0.019 5.0
48	3U	1643-62		235.751	-62.409	321.708	-6.293	0.018 3.0
49	3U	1812-12		273.020	-12.110	18.009	2.447	0.018 1.0
50	3U	1538-52	NOR XR-2	234.500	-52.179	327.398	2.238	0.017 1.0
51	3U	1714-39		258.730	-39.300	348.207	-0.992	0.017 1.0
52	3U	2129+47		322.490	47.029	91.596	-3.106	0.017 1.0
53	3U	1022-55		155.619	-55.489	283.237	1.400	0.016 1.0
54	3U	1223-62	GX 301+0	185.960	-62.558	300.106	-0.101	0.016 3.0
55	3U	1632-64		248.200	-64.138	324.632	-11.379	0.016 1.0
56	3U	1736+43		264.101	43.050	68.826	31.081	0.016 1.0
57	3U	0900-40	VELA X-1	135.064	-40.359	263.065	-3.933	0.015 10.0
58	3U	1624-49	NOR 1	246.080	-49.090	334.915	-0.267	0.015 5.0
59	3U	1626-67		246.670	-67.360	321.745	-13.057	0.015 1.0
60	3U	0115+63		18.870	63.558	125.943	1.111	0.015 7.0
61	3U	0614+09		93.560	9.170	200.849	-3.387	0.015 1.0
62	3U	0022+63	CEP X-1	5.560	63.898	120.105	1.448	0.014 1.0
63	3U	0532-66	LMC X-4	83.080	-66.618	276.596	-32.555	0.014 1.0
64	3U	0750-49		117.600	-49.449	263.250	-11.355	0.014 1.0
65	3U	0833-45	VEL XR-1	128.401	-45.049	263.584	-2.823	0.014 1.0
66	3U	1258-61	GX 304-1	194.512	-61.334	304.085	1.245	0.014 5.0
67	3U	1134-61		173.610	-61.598	294.256	-0.269	0.013 1.0
68	3U	0449+66		72.380	66.838	143.620	14.431	0.012 1.0
69	3U	1118-60	CEN X-3	169.730	-60.316	292.067	0.361	0.012 20.0
70	3U	1322-42	CEN A	200.549	-42.789	309.448	19.395	0.012 1.0
71	3U	1709-23	OPH XR-2	257.360	-23.359	0.534	9.240	0.012 5.0
72	3U	0143+61		25.820	61.328	129.464	-0.589	0.011 1.0
73	3U	0821-42		125.390	-42.659	260.370	-3.169	0.011 1.0
74	3U	1906+09		286.600	9.720	43.621	0.649	0.011 1.0
75	3U	0032+24		8.200	24.200	118.295	-38.252	0.010 1.0
76	3U	0042+32		10.710	32.779	121.508	-29.802	0.010 1.0
77	3U	1231+07		187.900	7.140	290.693	69.324	0.010 1.0
78	3U	1510-59		227.530	-58.998	320.310	-1.214	0.010 1.0
79	3U	1727-33	GX 354+0	261.839	-33.700	354.235	0.129	0.010 10.0
80	3U	1832-23		278.000	-23.219	10.406	-6.948	0.010 1.0

REPRODUCIBILITY OF TIME  
ORIGINAL PAGE IS POOR

"GEOMETRICAL" FACTORS FOR DIFFUSE  
BACKGROUND COMPUTATION

ANODE SEGMENT (i)	$G_i$
1 ; 9	0.013484
2 ; 10	0.010338
3 ; 11	0.011997
4 ; 12	0.011997
5 ; 13	0.010338
6 ; 14	0.007901
7 ; 15	0.003052
8 ; 16	0.002532

Table 3.3

SOURCE LATITUDINAL EXTENT ( $\Delta\theta$ )  
AS A FUNCTION OF  
SPACECRAFT LATITUDE (D)

D (degrees)	$\Delta\theta$ (degrees)
0; 90	1.91
10; 80	2.56
20; 70	3.14
30; 60	3.56
45	3.82

Table 4.1

## TRANSIENT SOURCE CANDIDATES AND TRANSIENT-LIKE VARIABLES\*

SOURCES	COORDINATES	EPOCH	PEAK FLUX ( $S/S_{CRAB}$ )	COMMENTS	REFERENCES
CET X-1	145° -60° ERROR CIRCLE RADIUS = 15°	DECEMBER, 1967	~0.6 1.5-6 keV	UV CETI (MIRA) IN ERROR BOX	BARNDEN AND FRANCEY, 1969
CET X-2	159°±10° -52°±5°	OCTOBER, 1969	~10 1.5-5 keV	UV CETI (MIRA) IN ERROR BOX	HARRIES et al, 1971 SHUKLA AND WILSON, 1971
CEP X-4	99° 3.4°	JUNE-JULY, 1972	~0.2 7-26 keV	NOT DETECTED ~6 MONTHS PRIOR AND ~7 MONTHS SUBSEQUENT. HARD SPECTRUM.	ULMER et al, 1973
3UI901+03	37.1° -1.4°	JAN.-MAR., 1971	~0.1 2-6 keV		FORMAN et al, 1976a
3U0115+63	125.9° 1.1°	JAN.-FEB., 1971	~0.1 2-6 keV		FORMAN et al, 1976a
MX1746-20	7.7° 3.8°	DECEMBER, 1971- MARCH, 1972	~0.2 3-6 keV	GLOBULAR CLUSTER NGC 6440 IN ERROR BOX	FORMAN et al, 1976 b
MX0656-07	220.2° -1.7°	20 SEPT 1975; MARCH, 1976	~0.1 3-6 keV	SPECTRAL HARDNESS (1.3-13 keV) ≈ CRAB NEBULA	CLARK, 1975 CARPENTER et al, 1975 KALUZIENSKI et al, 1976a
CENTAURUS TRANSIENT	313°±5° 0°±5°	DECEMBER, 1971- APR., 1972; JUNE, 1972	4x10 <sup>-3</sup> CM <sup>-2</sup> S <sup>-1</sup> keV <sup>-1</sup> 10 keV	VERY HARD SPECTRUM (35 keV THERMAL BREM.)	WHEATON et al, 1975
AQL X-1 * (3UI908-100)	35.7° -4°	1971-1976	~1 3-6 keV	MEAN FLARE INTERVAL ~435 DAYS ± 10%	KALUZIENSKI et al, 1977 b MARKERT, 1974
3UI630-47 *	336.9° 0.3°	1971-1976	~0.4 2-6 keV	PERIOD=615 ± 5 DAYS	JONES et al, 1976
NORMA TRANSIENT * (4UI608-48)	330.9° -0.8°	1971-1976	~0.4 3-6 keV	NORMA BURSTER ? GX331-1 ? 4UI608-52 ? MX1608-52 ?	KALUZIENSKI et al, 1976 b TANANBAUM et al, 1976 GRINDLAY AND GURSKY, 1976
GX339-4 * (3UI658-48)	339° -4°	1971-1973	~0.3	VARIABLE BY ≥ 60X OVER ~MONTHS	MARKERT et al, 1973
A0025+59	120.1° -3.2°	1975	≤ 0.1		SKINNER, 1975

Table 5.1

## DISTANCE AND Z-DISPLACEMENT OF TRANSIENT SOURCES vs. LUMINOSITY

SOURCE	$r_e^*$ (kpc)	$L(\text{ERG-S}^{-1})=10^{36}$ (d; z) in kpc	$10^{37}$ (d; z)	$10^{38}$ (d; z)	$10^{39}$ (d; z)
CEN X-2	18.3	0.23 ; .002	0.73 ; .006	2.30 ; 0.02	7.30 ; 0.06
CEN X-4	22.9	0.15 ; .057	0.47 ; 0.18	1.50 ; 0.57	4.70 ; 1.80
3U1735-28	25.0	0.95 ; .035	3.00 ; 0.11	9.50 ; 0.35	30.0 ; 1.10
3U1543-47	22.9	0.52 ; .049	1.64 ; 0.15	5.20 ; 0.49	16.4 ; 1.50
A1524-62	21.2	0.82 ; .065	2.60 ; 0.21	8.20 ; 0.65	26.0 ; 2.10
A1118-61	15.6	2.24 ; .030	7.10 ; .095	22.4 ; 0.30	71.0 ; 0.95
A0535+26	5.0	0.51 ; .025	1.62 ; .079	5.10 ; 0.25	16.2 ; 0.79
A1742-28	25.0	0.48 ; .001	1.51 ; .003	4.80 ; 0.01	15.1 ; 0.03
A0620-00	5.5	0.10 ; .012	0.33 ; .038	1.00 ; 0.12	3.30 ; 0.38
A1246-58	17.7	1.61 ; .098	5.09 ; 0.31	16.1 ; 0.98	50.9 ; 3.10
A1745-36	24.9	1.31 ; .095	4.16 ; 0.30	13.1 ; 0.95	41.6 ; 3.00
A1743-29	25.0	1.61 ; .012	5.09 ; .037	16.1 ; 0.12	50.9 ; 0.37
MX1803-24	24.9	0.72 ; .024	2.28 ; .075	7.20 ; 0.24	22.8 ; 0.75
AQL X-1	22.0	0.72 ; 0.05	2.28 ; 0.16	7.20 ; 0.50	22.8 ; 1.60
3U1630-47	23.7	1.14 ; .006	3.60 ; .018	11.4 ; 0.06	36.0 ; 0.18

$$* r_e = r_s \cos \angle^x + (R^2 - r_s^2 \sin^2 \angle^x)^{1/2}, \quad r_s = 10 \text{ kpc} \quad R = 15 \text{ kpc}$$

TABLE 5.2

## TRANSIENT X-RAY SOURCES

<u>CLASSIFICATION</u>	<u>TYPE I</u>	<u>TYPE II</u>
Spatial Distribution	$0.3 \lesssim  \bar{z} $ (Kpc) $\lesssim 1.3$ ; Disk Pop. - Intermed. Pop. II	$0.04 \lesssim  \bar{z} $ (Kpc) $\lesssim 0.3$ ; Population I
Frequency	$1 \lesssim \tau^{-1}(\text{yr}^{-1}) \lesssim 10$	$5 \lesssim \tau^{-1}(\text{yr}^{-1}) \lesssim 100$
Lifetime	$\tau_d \gtrsim 1$ month	$\tau_d \lesssim 1$ month
Peak Luminosity	$10^{38} \lesssim L(\text{erg s}^{-1}) \lesssim 2 \times 10^{39}$	$2 \times 10^{36} \lesssim L(\text{erg s}^{-1}) \lesssim 10^{38}$
Additional Characteristics	Relatively soft, $\alpha^* \gtrsim \alpha_{\text{crab}}$	Hard spectrum $\alpha \lesssim \alpha_{\text{crab}}$ Slowly pulsating
Mechanism	Roche-lobe overflow of low-mass, late type companion	Stellar wind increase of massive early-type optical companion
Examples	Cen X-2, Cen X-4, 3U1543-47, A1524-62, A1742-28, A0620-00	3U1735-28, A1118-61, A0535+26
"Stable" Counterparts	Aql X-1	Vela X-1 (3U0900-40), Cyg X-1

---


$$* E \frac{dn}{dE} = E^{-\alpha}$$

TABLE 5.3  
LONG-TERM VARIABILITY OF GALACTIC X-RAY SOURCES

<u>TYPE</u>	<u>VARIABILITY</u>	<u>TIMESCALE</u>	<u>EXAMPLES</u>
Quasi-Stable	$\approx 3$	yrs	Sco X-1; Cyg X-2
Variable	$\sim 5$	yrs	Cyg X-3*
Flaring	$\sim 5 - 10$	$T_{ON} \sim$ months	Cyg X-1
High/Low States	$\sim 20 - 100$	$T_{ON} \sim$ months - yrs	Cen X-3, Cir X-1, Vela X-1, Her X-1 ( $\sim 10$ yr optical cycle)
Regular modulation	$\sim 20$	$T_{MOD} \sim$ months	Her X-1 (35d cycle)
Highly variable	$\approx 100$	months - yrs	See Villa <u>et al.</u> 1976
Recurrent transients (Transient/Variable)	$\sim 50 - 500$	$\tau_d \sim 1$ month $\bar{T}_{rec} \approx 5$ yrs	Aql X-1, 3U1630-47
"Slow" transients	$\approx 100$	$\tau_d \sim 3$ yrs	See Amnuel, Rakhimov, and Guseinov (1974)
Transient Sources	$\approx 10^3$	$\tau_d \sim 1$ month $\bar{T}_{rec} \approx 10$ yrs	This work

\* 3-6 keV



Table A.1

 **$\kappa$  vs INCIDENT SOURCE SPECTRUM**

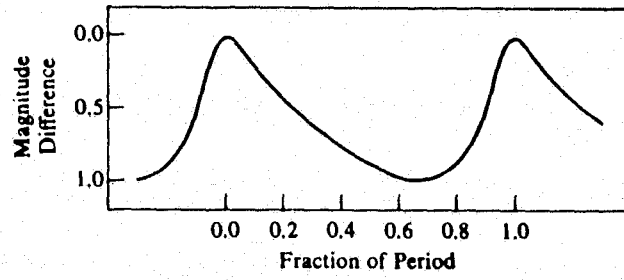
$n^*$	$kT^{**}(\text{keV})$	$\kappa^+ (\times 10^3)$
1	—	1.84
2	—	1.61
3	—	1.33
4	—	0.99
—	3	0.97
—	4	1.34
—	5	1.53
—	6	1.63

$$* \frac{dN}{dE} = a E^{-n}$$

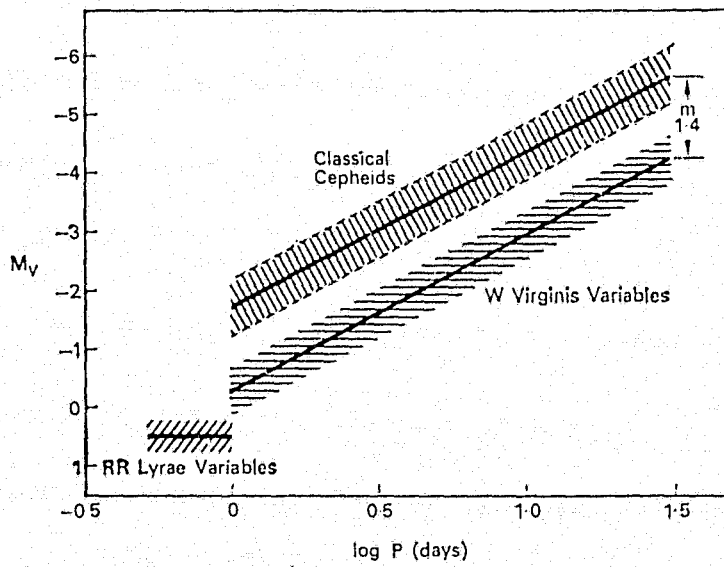
$$** \frac{dN}{dE} = b E^{-1} e^{-E/kT}$$

$$A (3-6 \text{ keV photons cm}^{-2} \text{ s}^{-1}) = \kappa \times U (\text{UHURU counts s}^{-1})$$



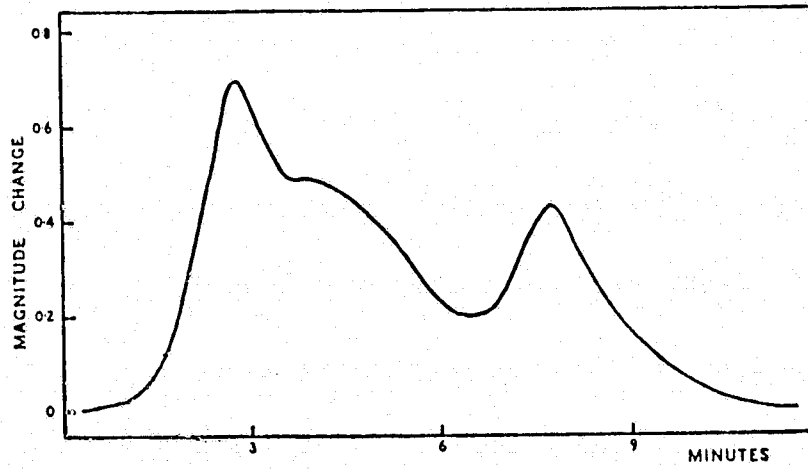


(a)

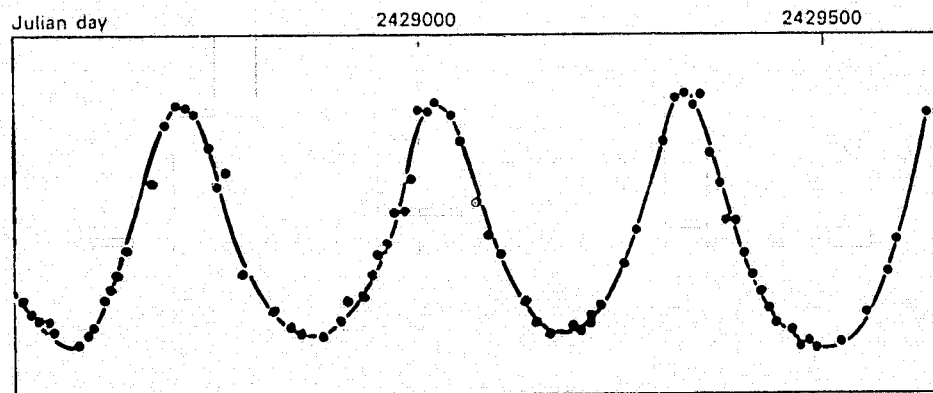


(b)

Figure 1.2

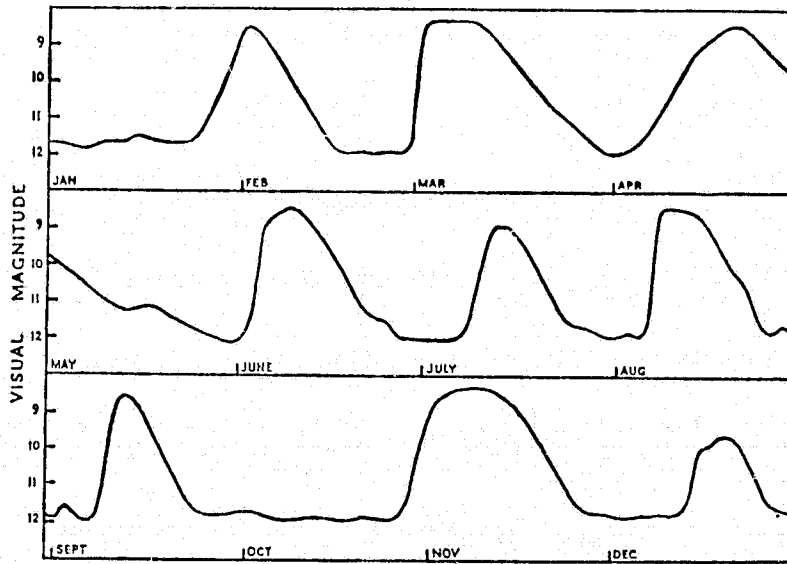


(a)

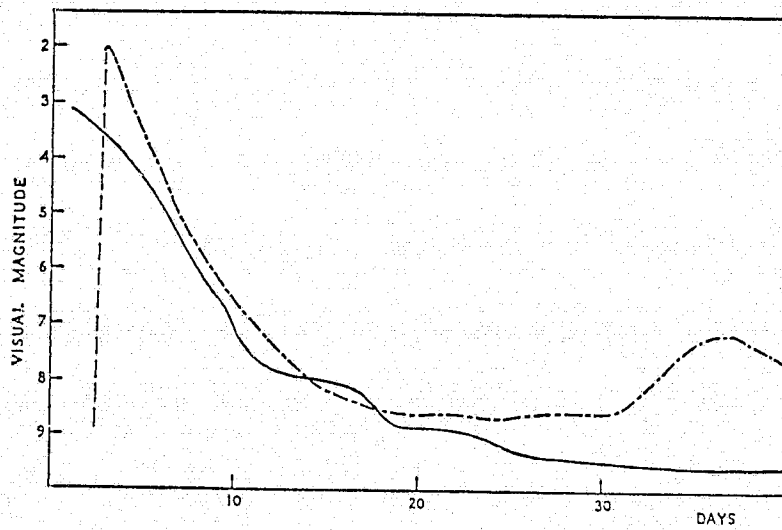


(b)

Figure 1.3



(a)



(b)

Figure 1.4

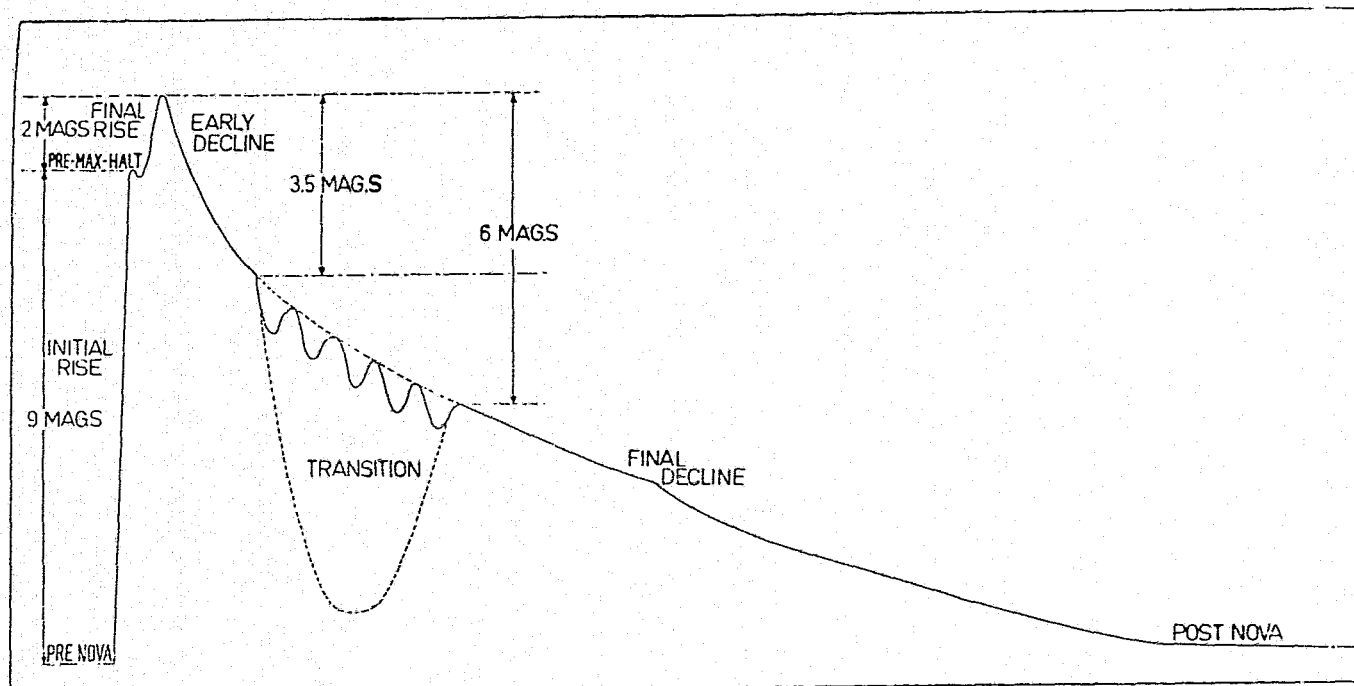


Figure 1.5

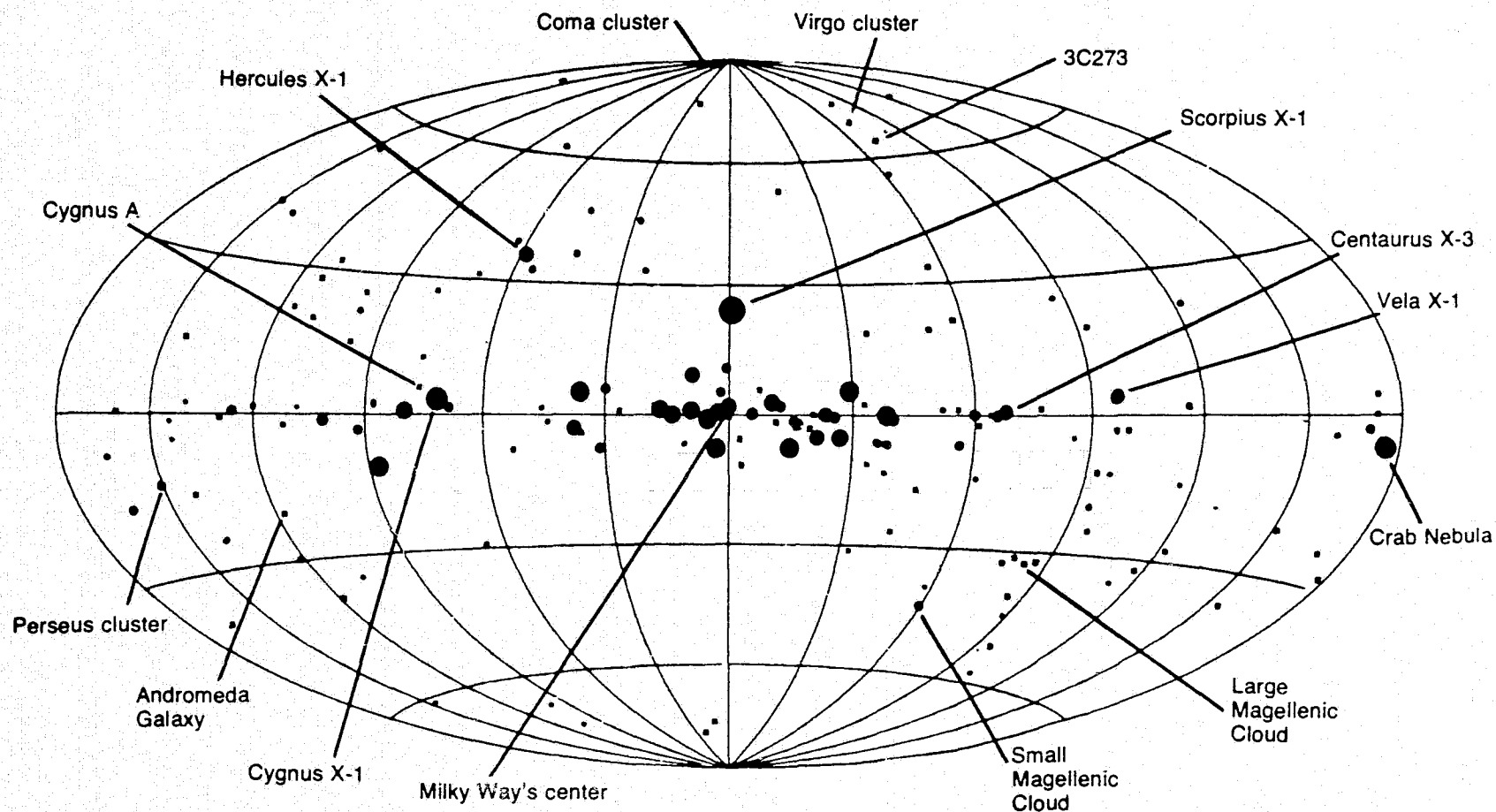
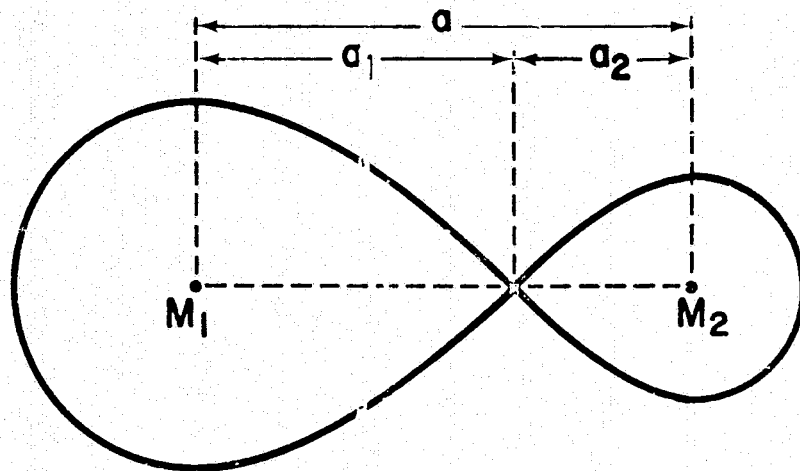


Figure 1.6



ALWAYS:  $P = 2\pi \sqrt{\frac{a^3}{G(M_1 + M_2)}} \quad v_2^3 = \frac{2\pi G}{P} \frac{M_1^3}{(M_1 + M_2)^2}$

X-RAYS:  $10^{36} \text{ erg/sec} < L \sim \frac{1}{10} \frac{GM_2}{R_2} \dot{M}_2 < 10^{38} \left(\frac{M_2}{M_\odot}\right)$

$R_1 < a_1$ :  $-\dot{M}_2 \sim 10^{-3} \dot{M}_1$ ,  $M_1 \gtrsim 20 M_\odot$  FOR  $L \gtrsim 10^{36}$

$R_1 > a_1$ :  $-\dot{M}_2 \sim \dot{M}_1$ ,  $M_1 \lesssim 2 M_\odot$  FOR  $L \lesssim 10^{38}$

Figure 1.7



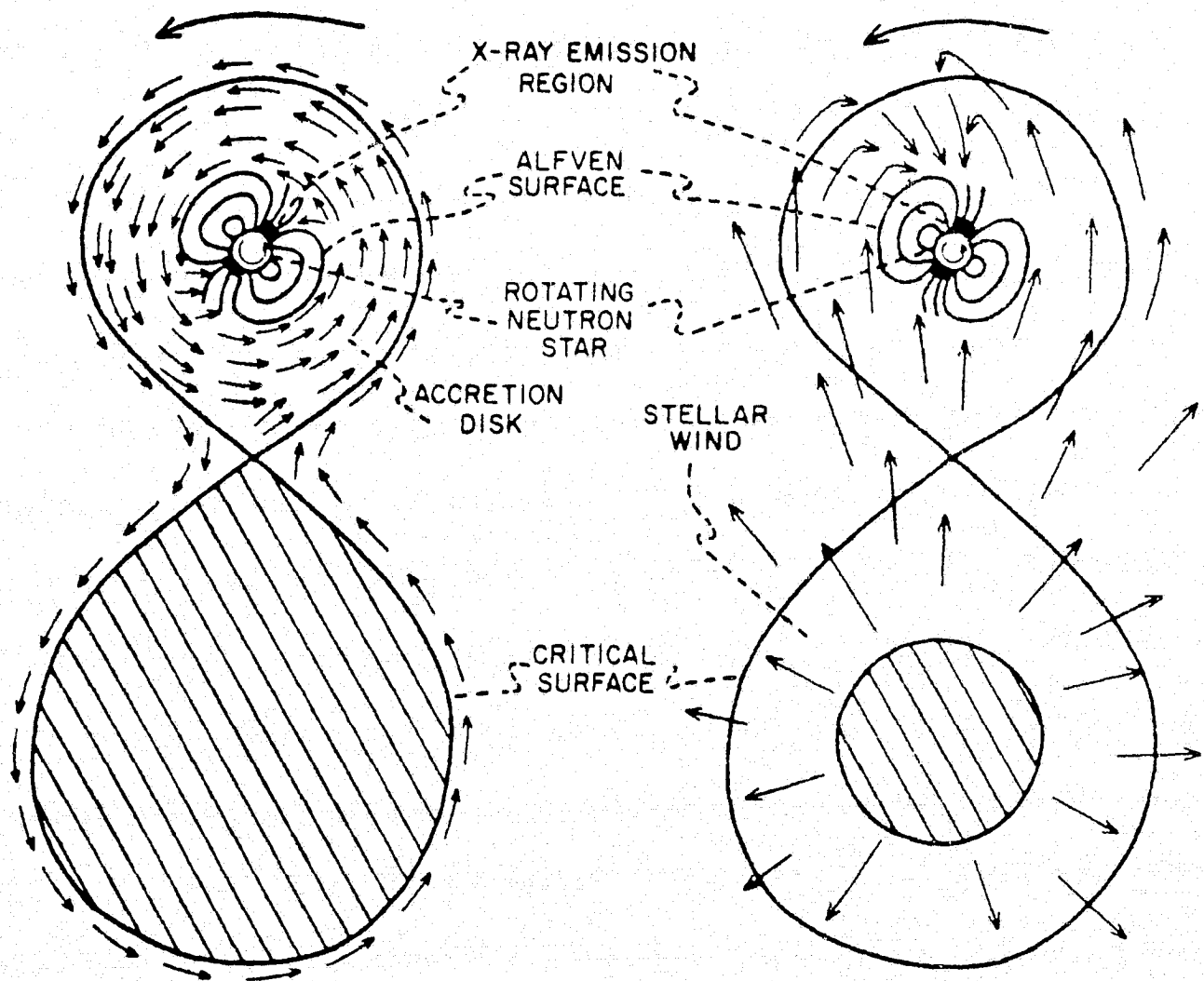


Figure 1.8

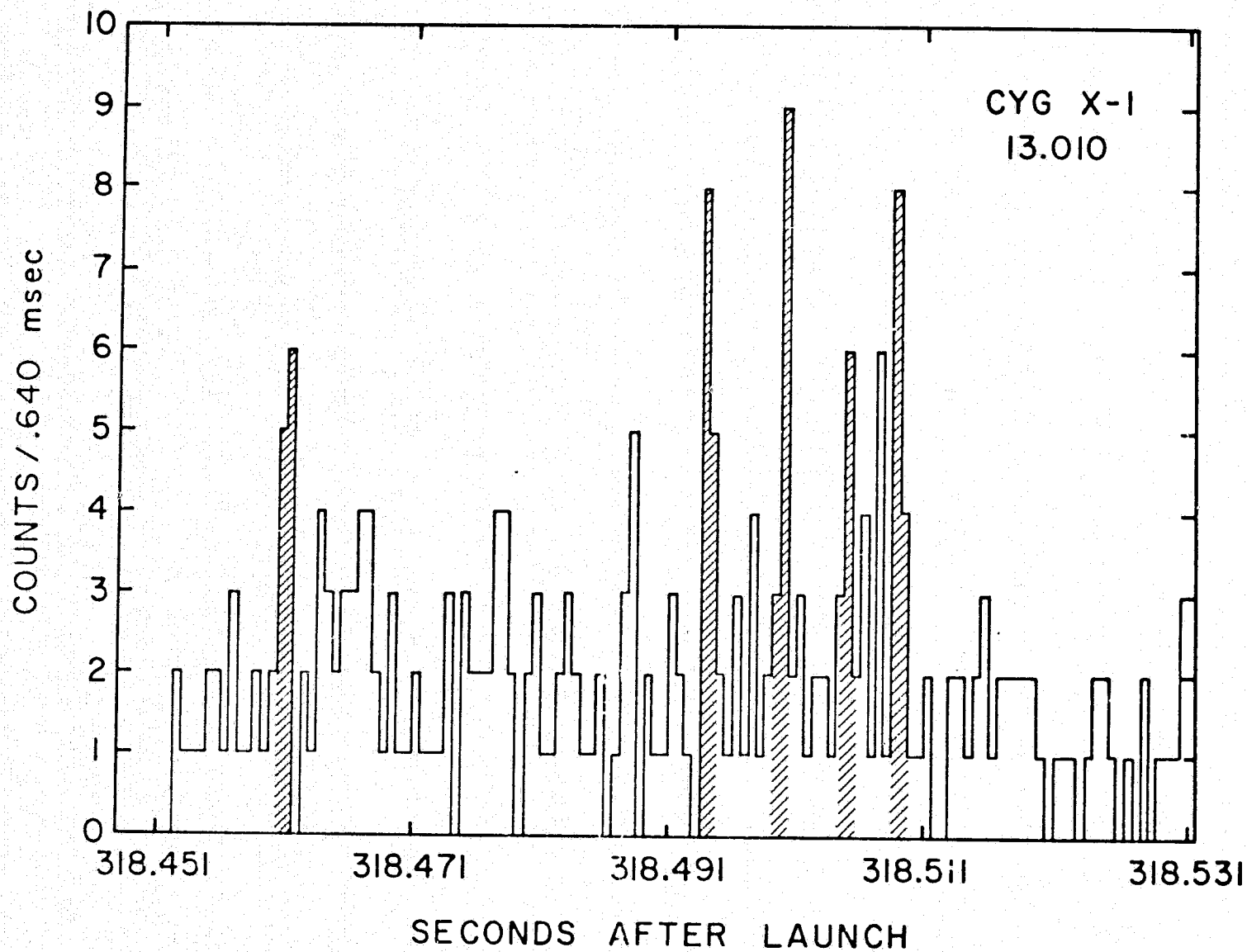


Figure 1.9

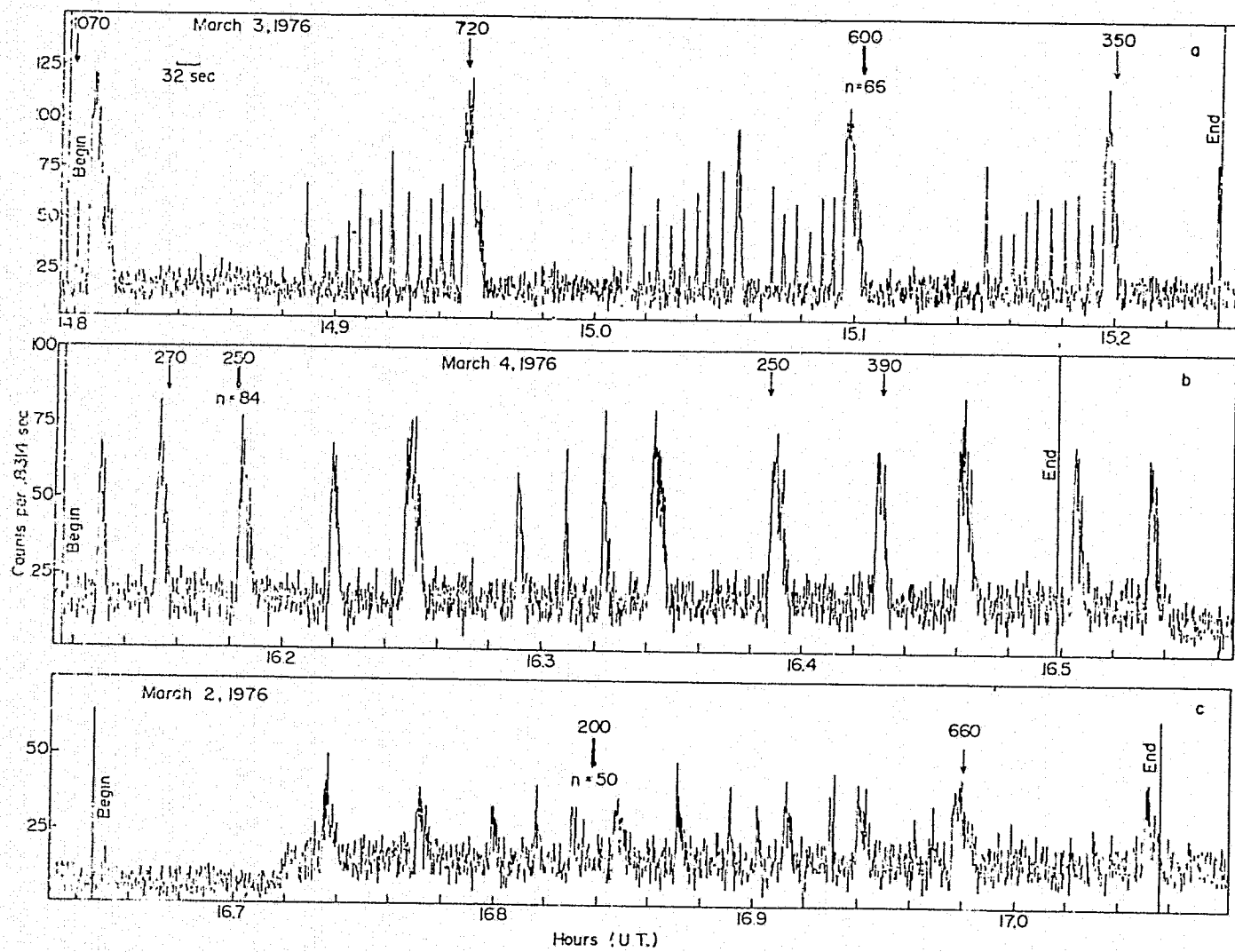


Figure 1.10

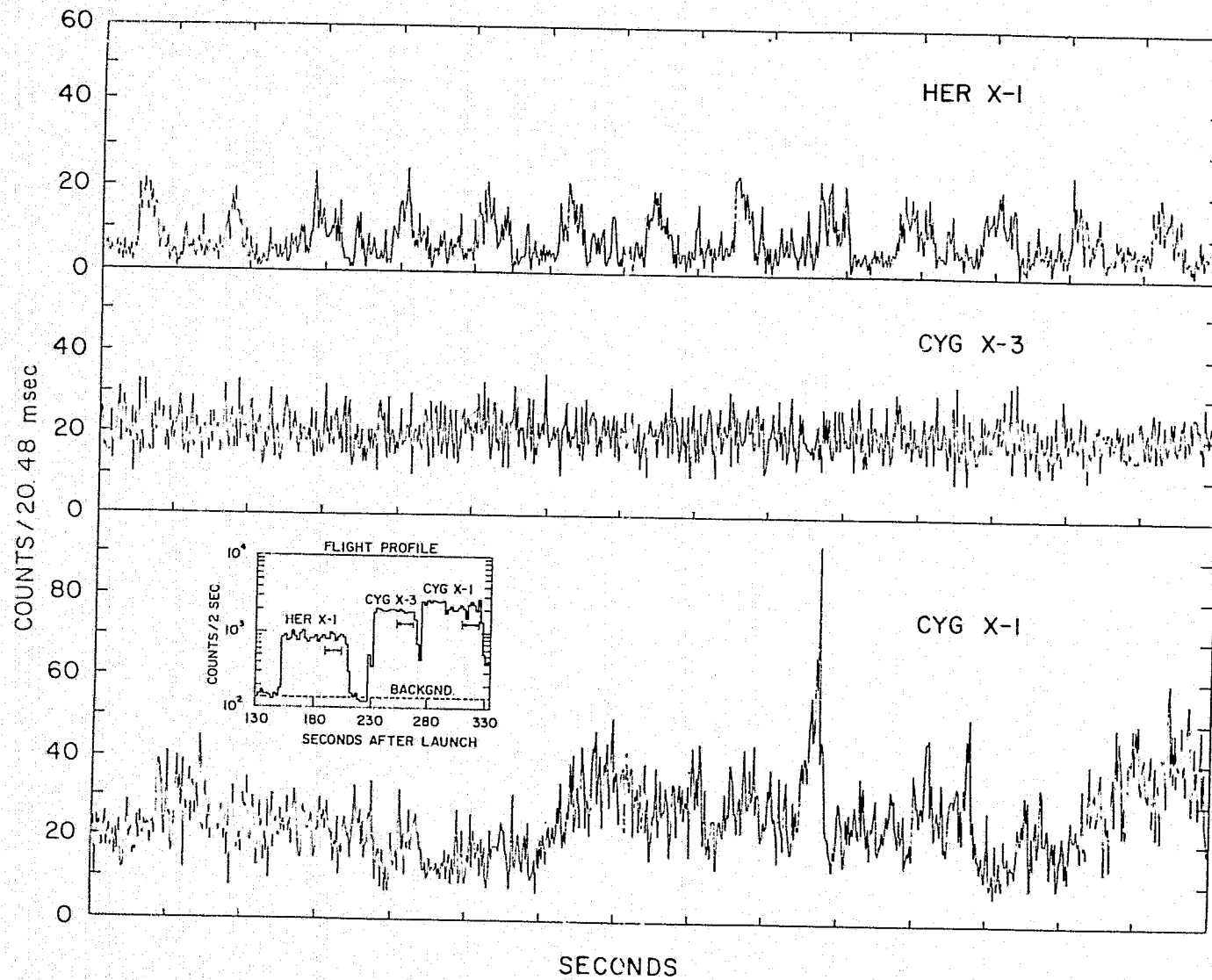


Figure 1.11

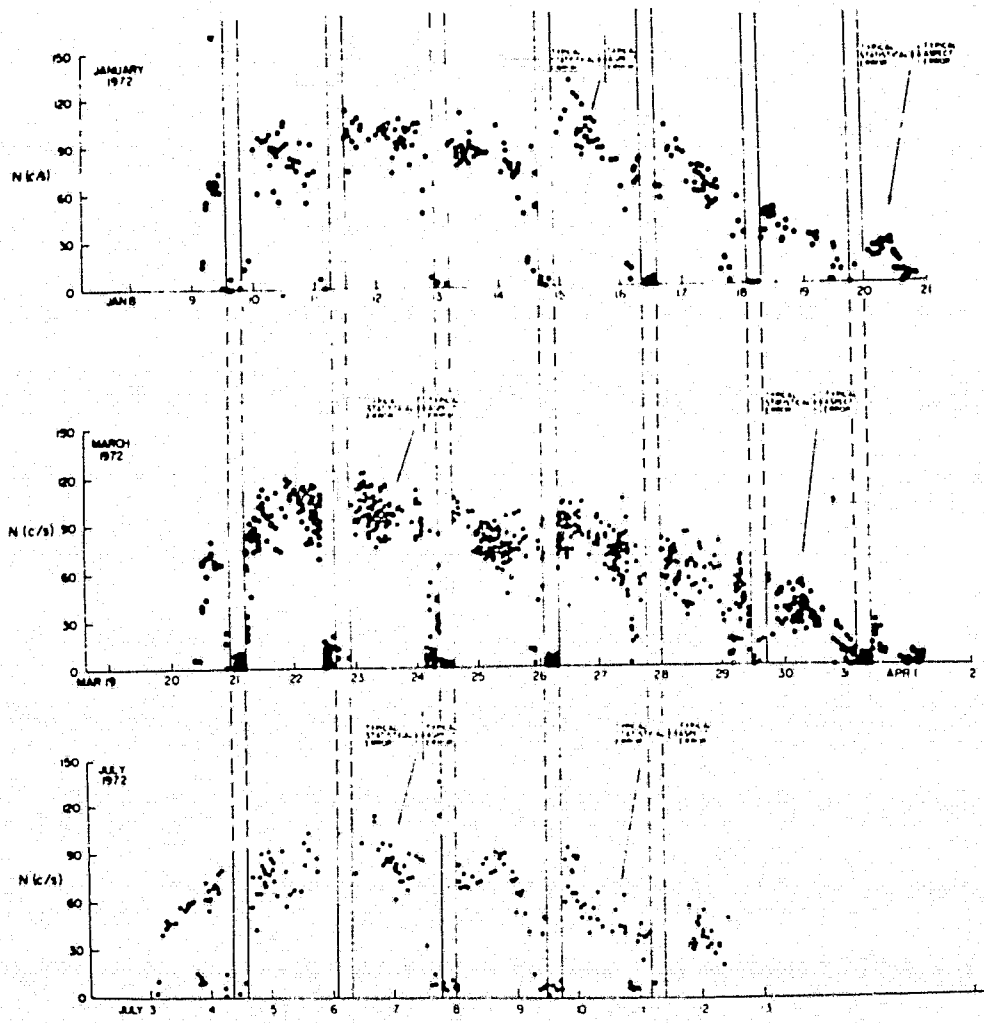


Figure 1.12

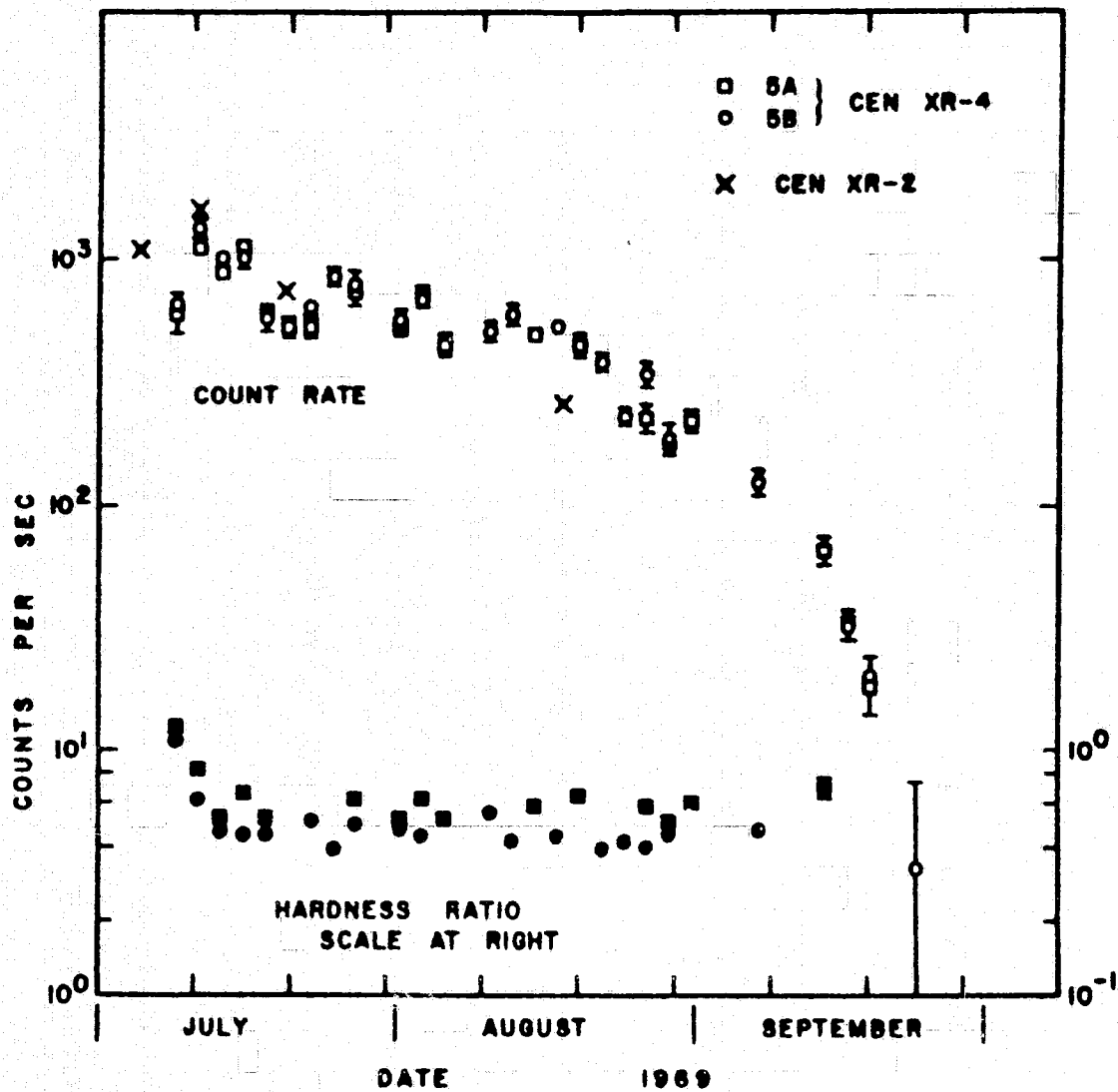


Figure 1.13

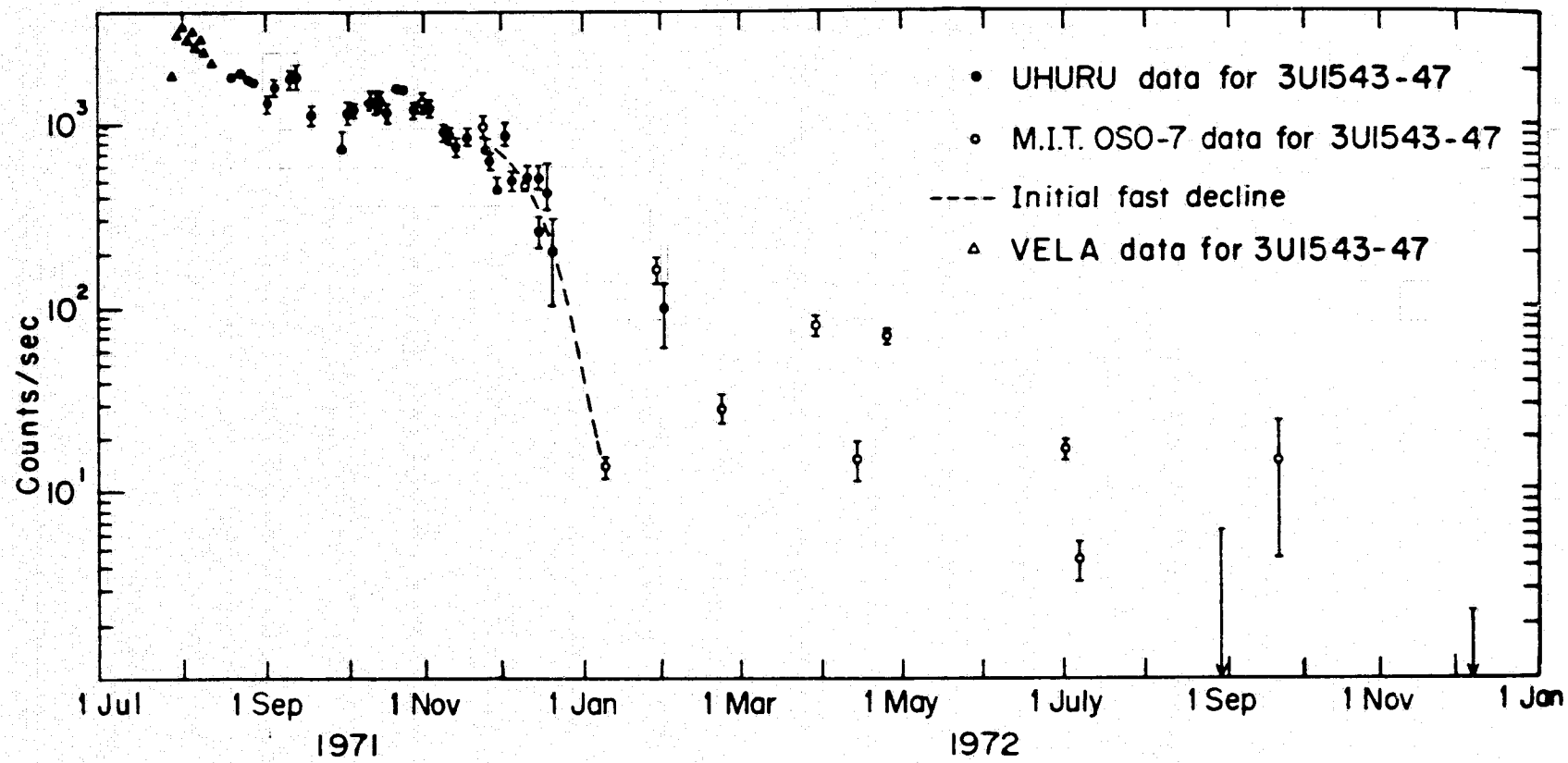


Figure 1.14

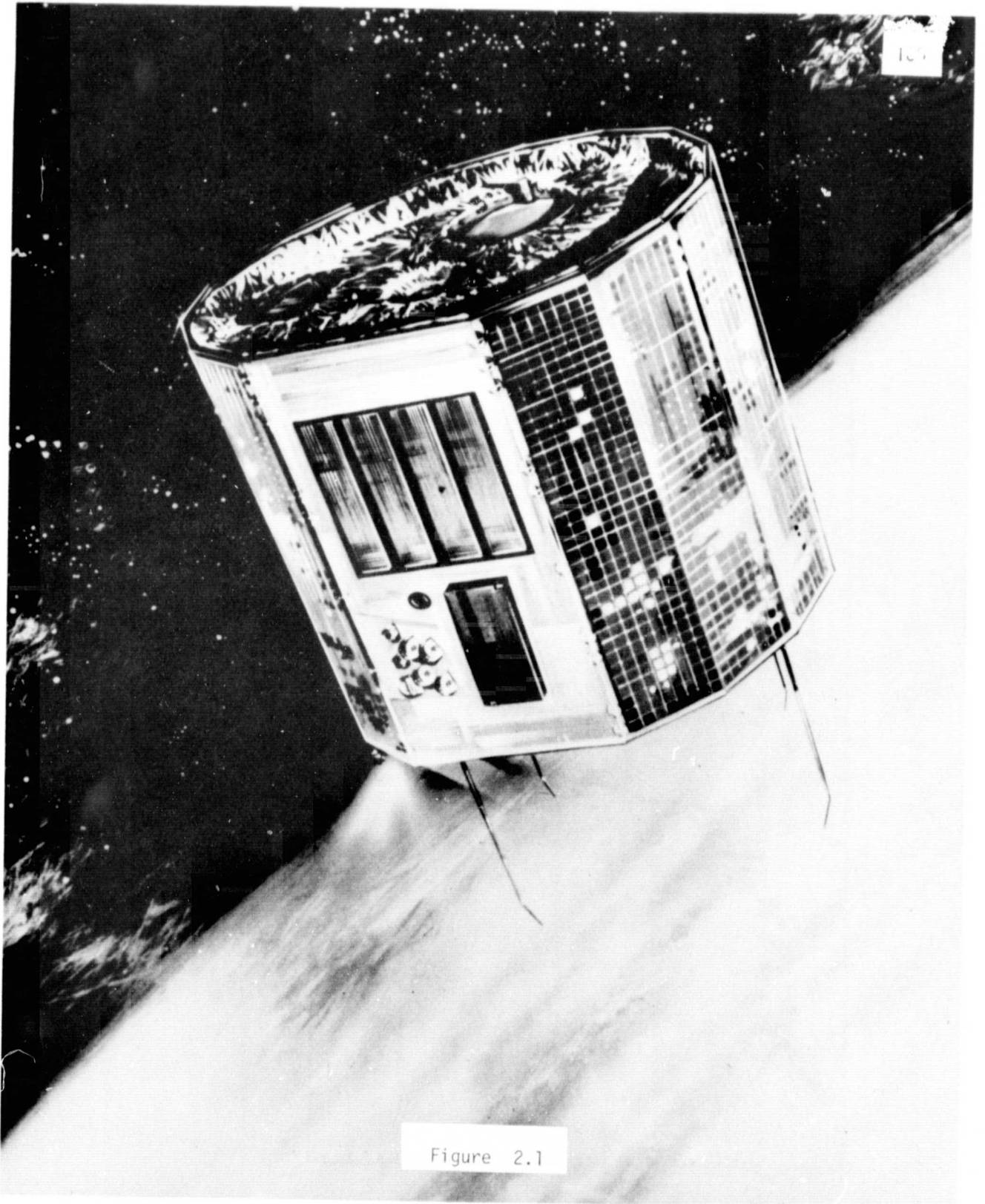


Figure 2.1



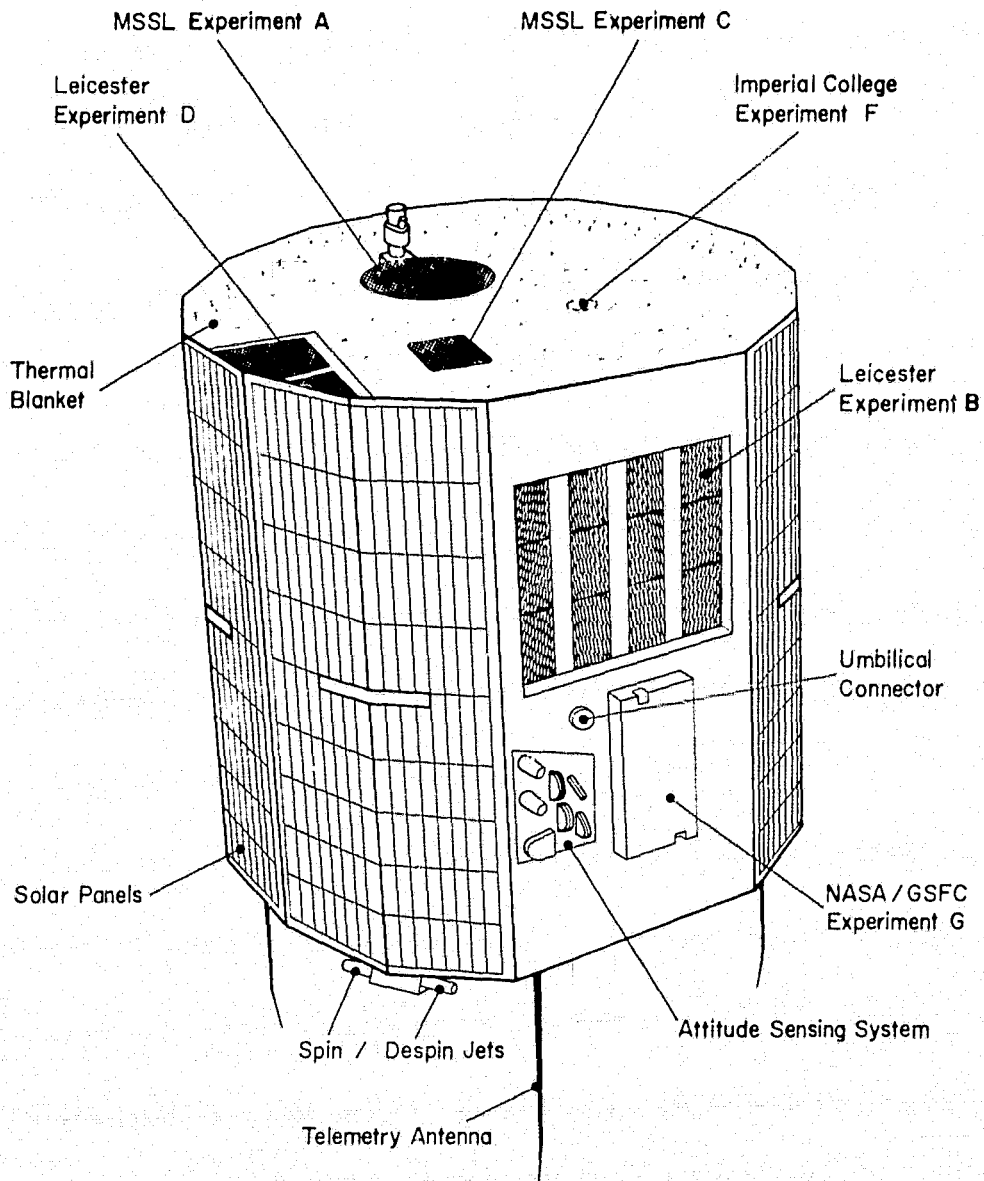


Figure 2.2

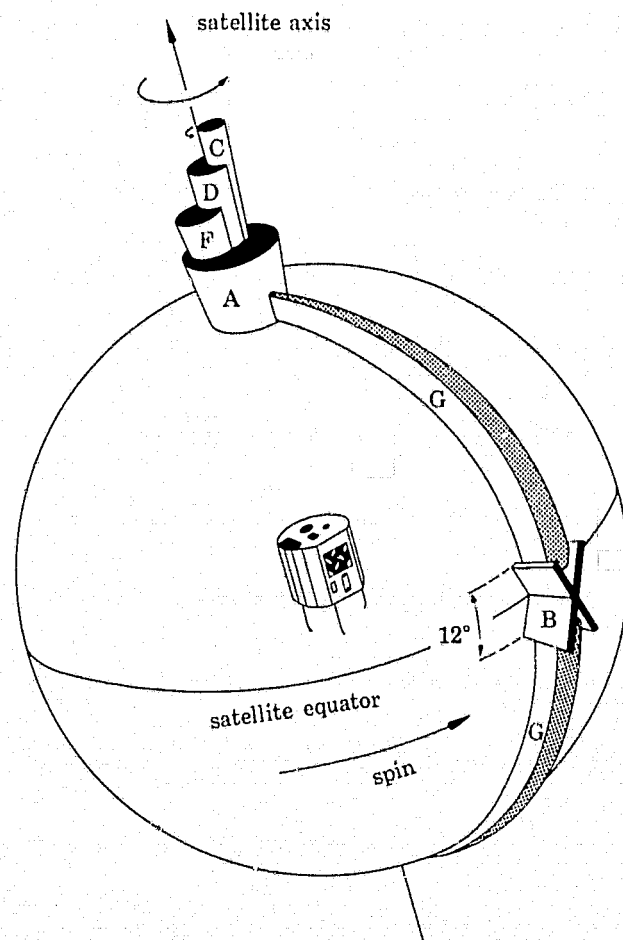
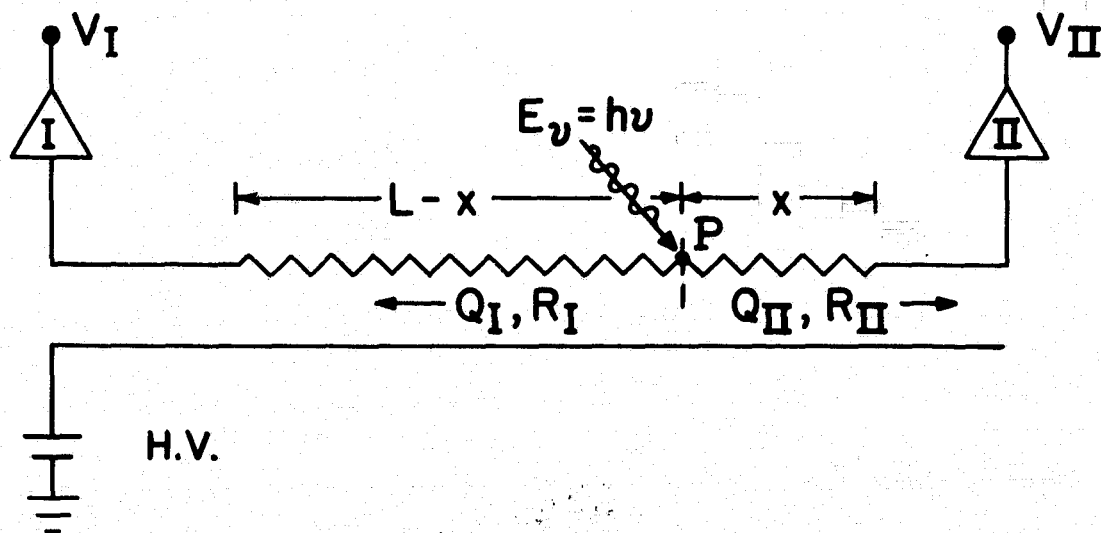


Figure 2.3



$$Q = Q_I + Q_{II}$$

$$Q_I R_I = Q_{II} R_{II} \quad (1)$$

$$\left. \begin{aligned} R_I &= \left(\frac{\rho}{\alpha}\right)(L-x) \\ R_{II} &= \left(\frac{\rho}{\alpha}\right)x \end{aligned} \right\} \quad (2)$$

$L$  = ANODE LENGTH

$\rho$  = ANODE RESISTIVITY

$\alpha$  = ANODE CROSS-SECTIONAL AREA

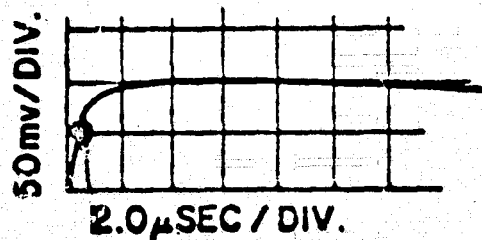
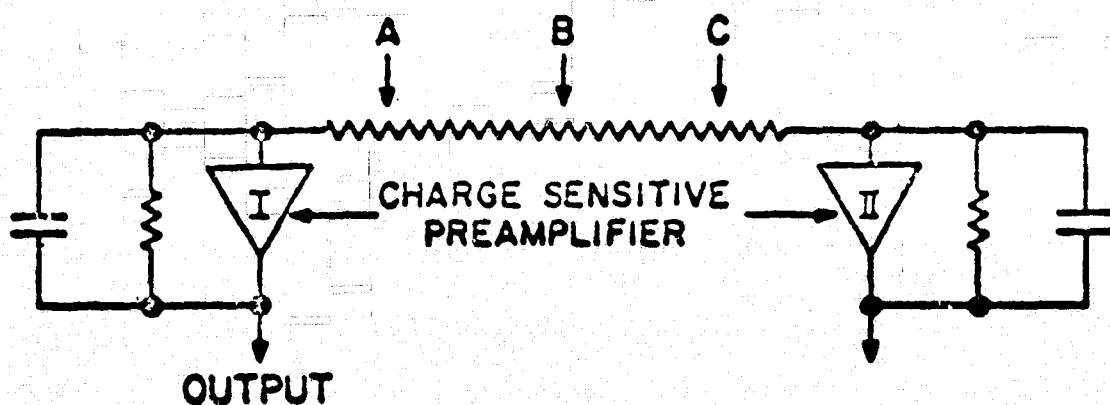
$V_{I,II}$  = VOLTAGE OUTPUTS OF PRE-AMPS I, II

(1) AND (2)  $\Rightarrow$

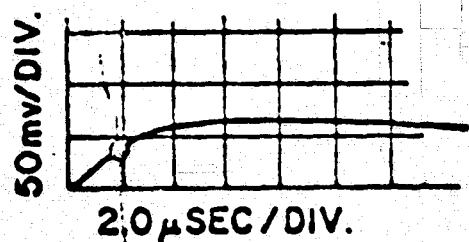
$$\frac{x}{L} = \frac{Q_I}{Q} = \frac{V_I}{V_I + V_{II}}$$

Figure 2.4

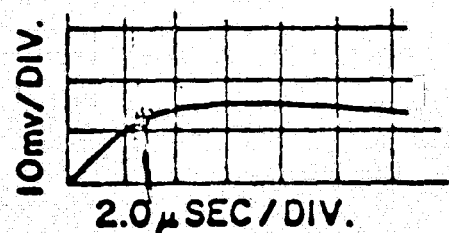
3



OUTPUT FROM AMP I  
DUE TO  
EVENT AT A ALONG THE ANODE



EVENT AT B ALONG THE ANODE



EVENT AT C ALONG THE ANODE

Figure 2.5

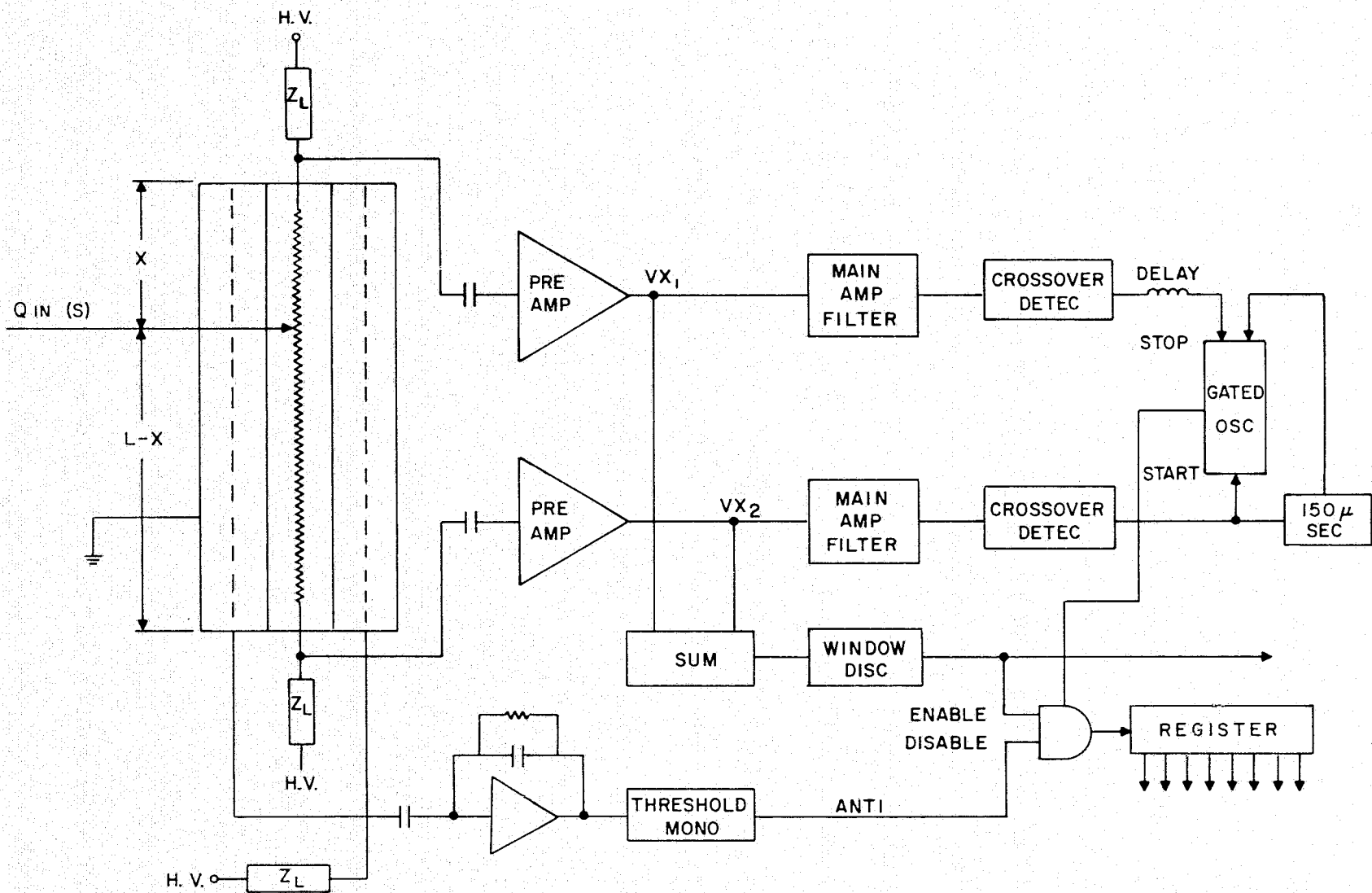
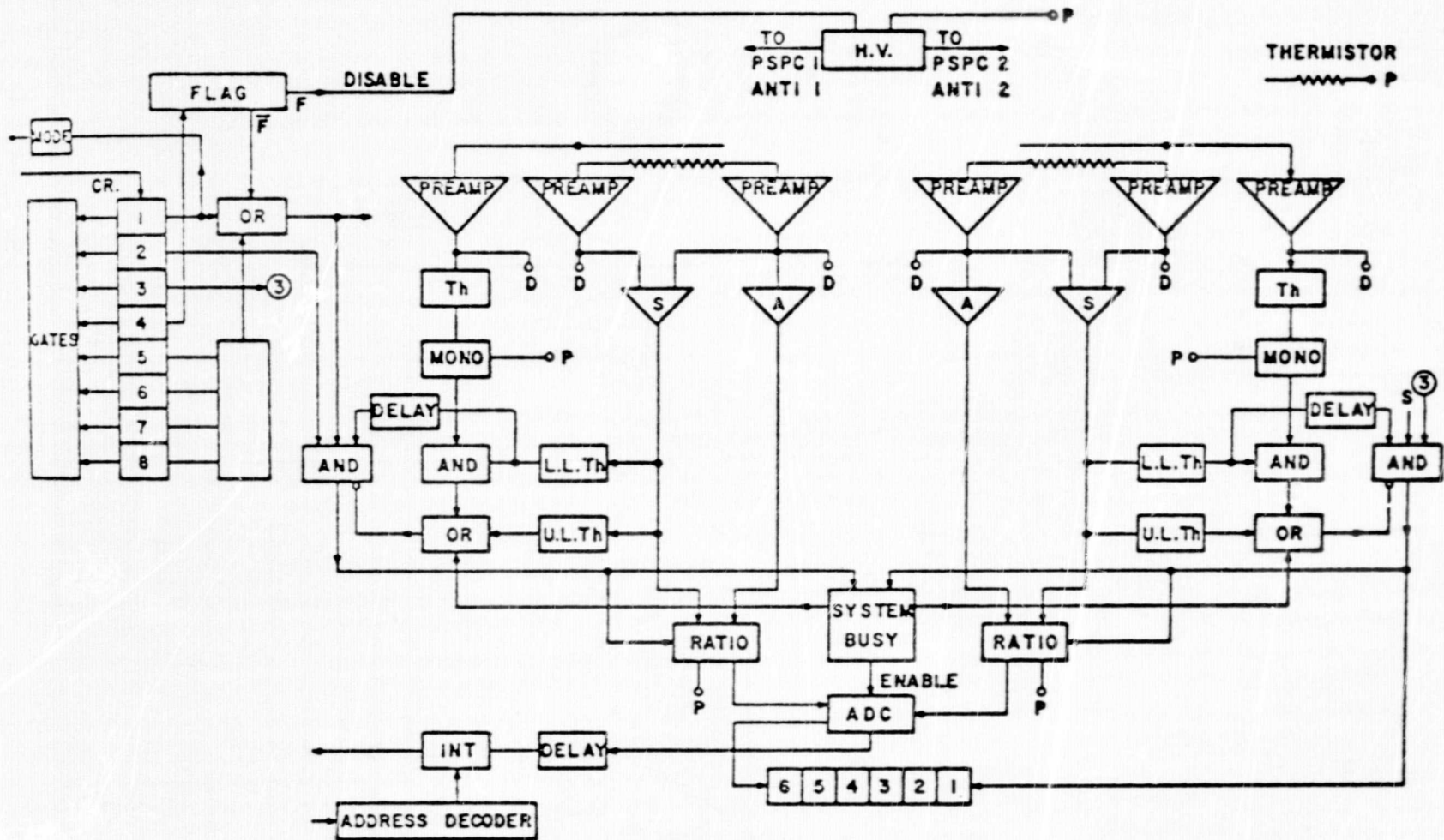


Figure 2.6



D - TO DIAGNOSTIC CONNECTOR  
P - ANALOG OUTPUTS FOR MONITORING

**BLOCK DIAGRAM**

Figure 2.7

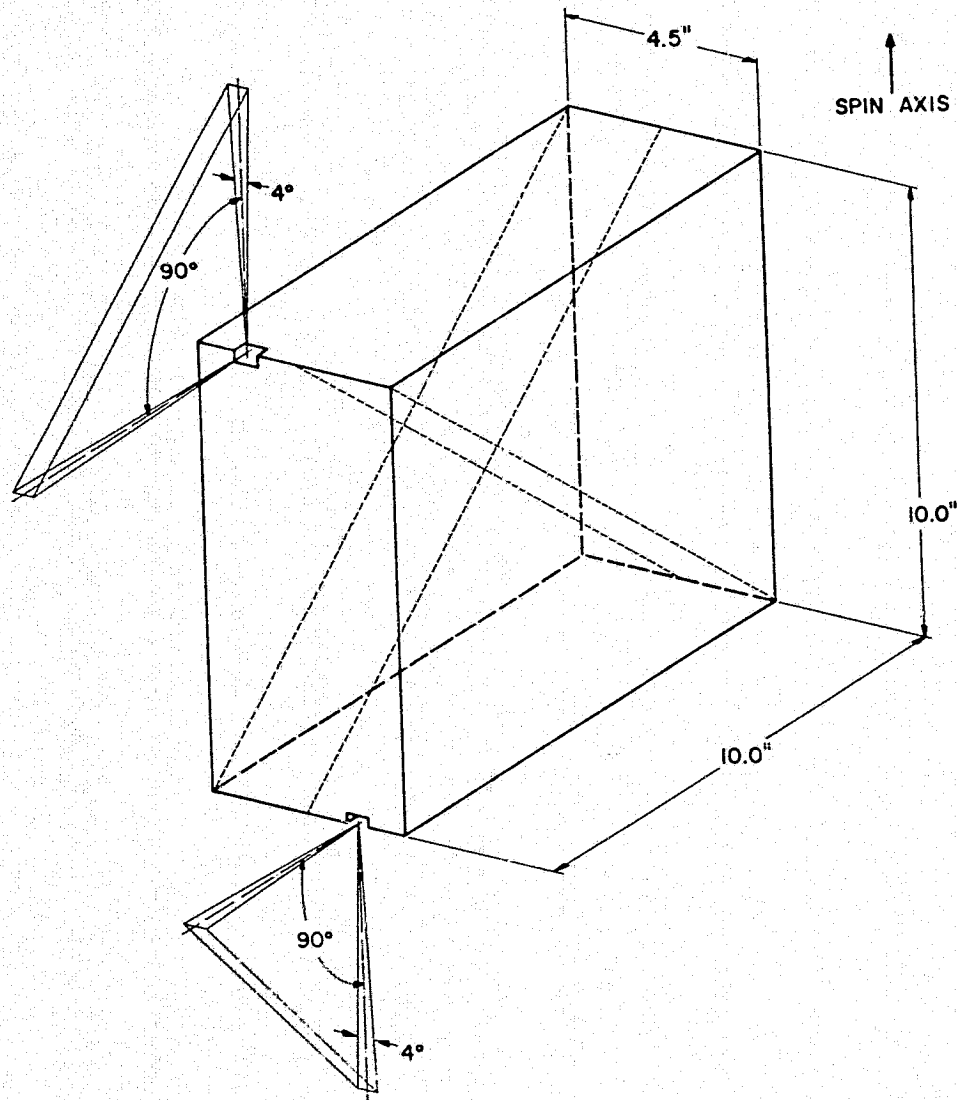


Figure 2.8

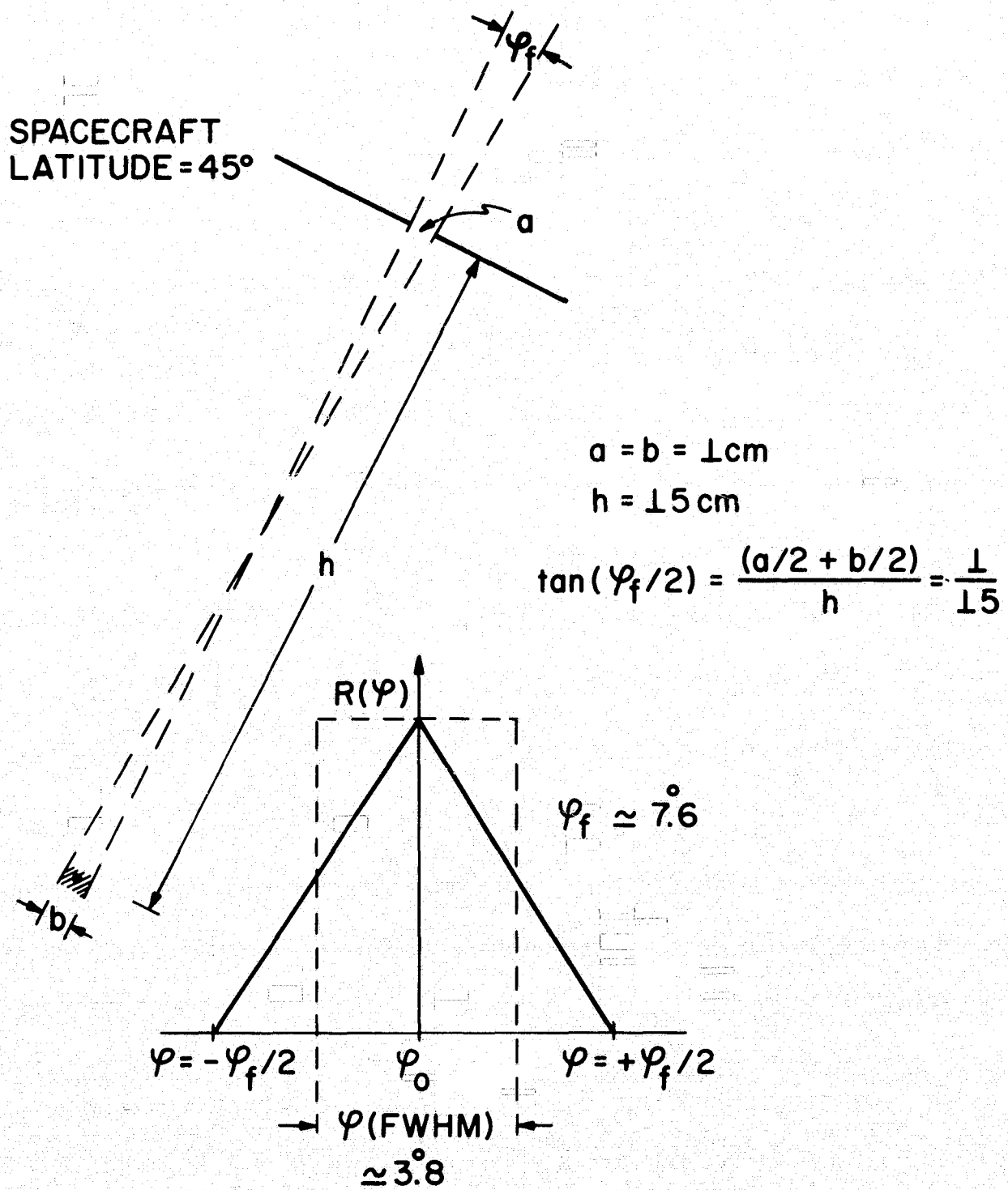


Figure 2.9



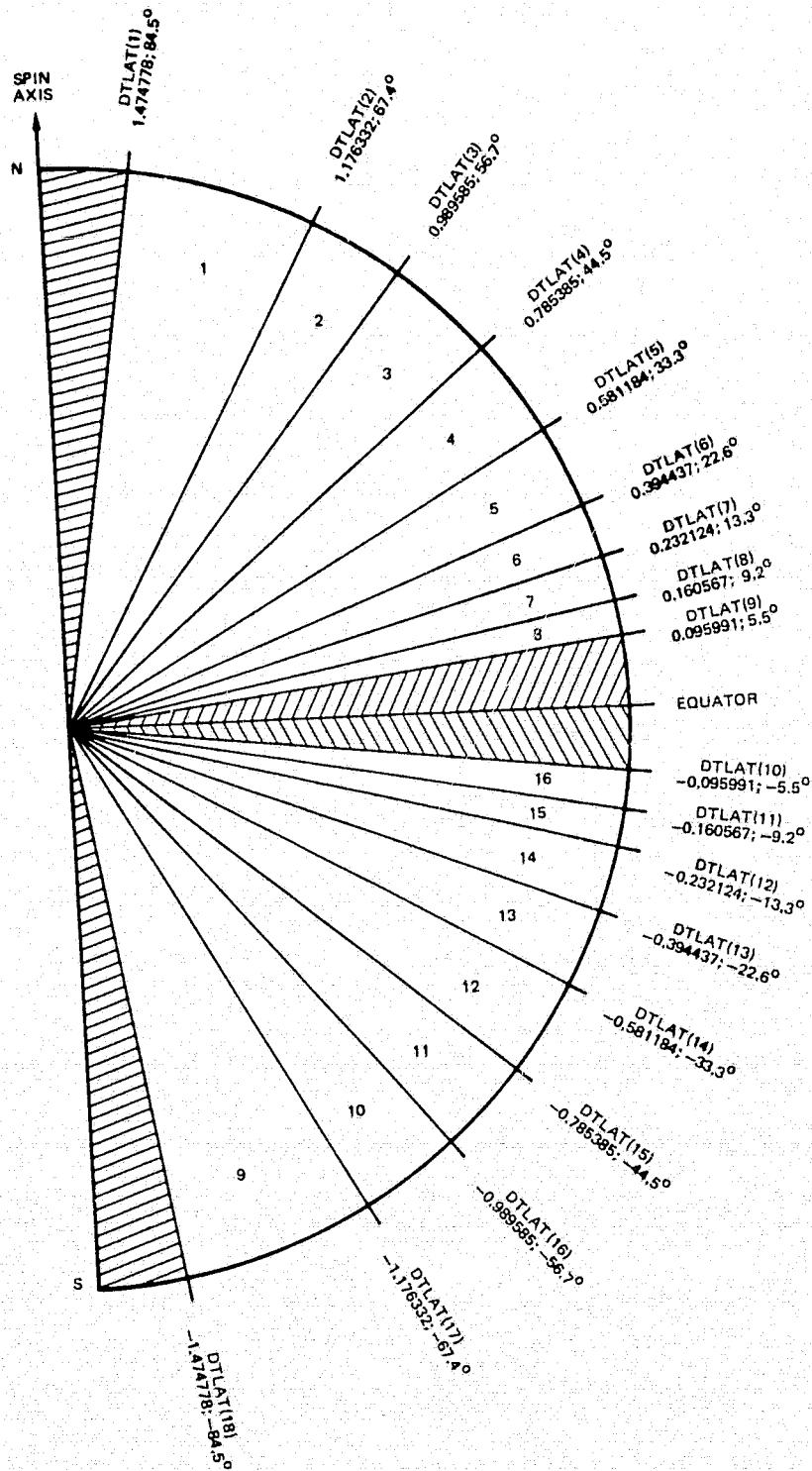


Figure 2.10

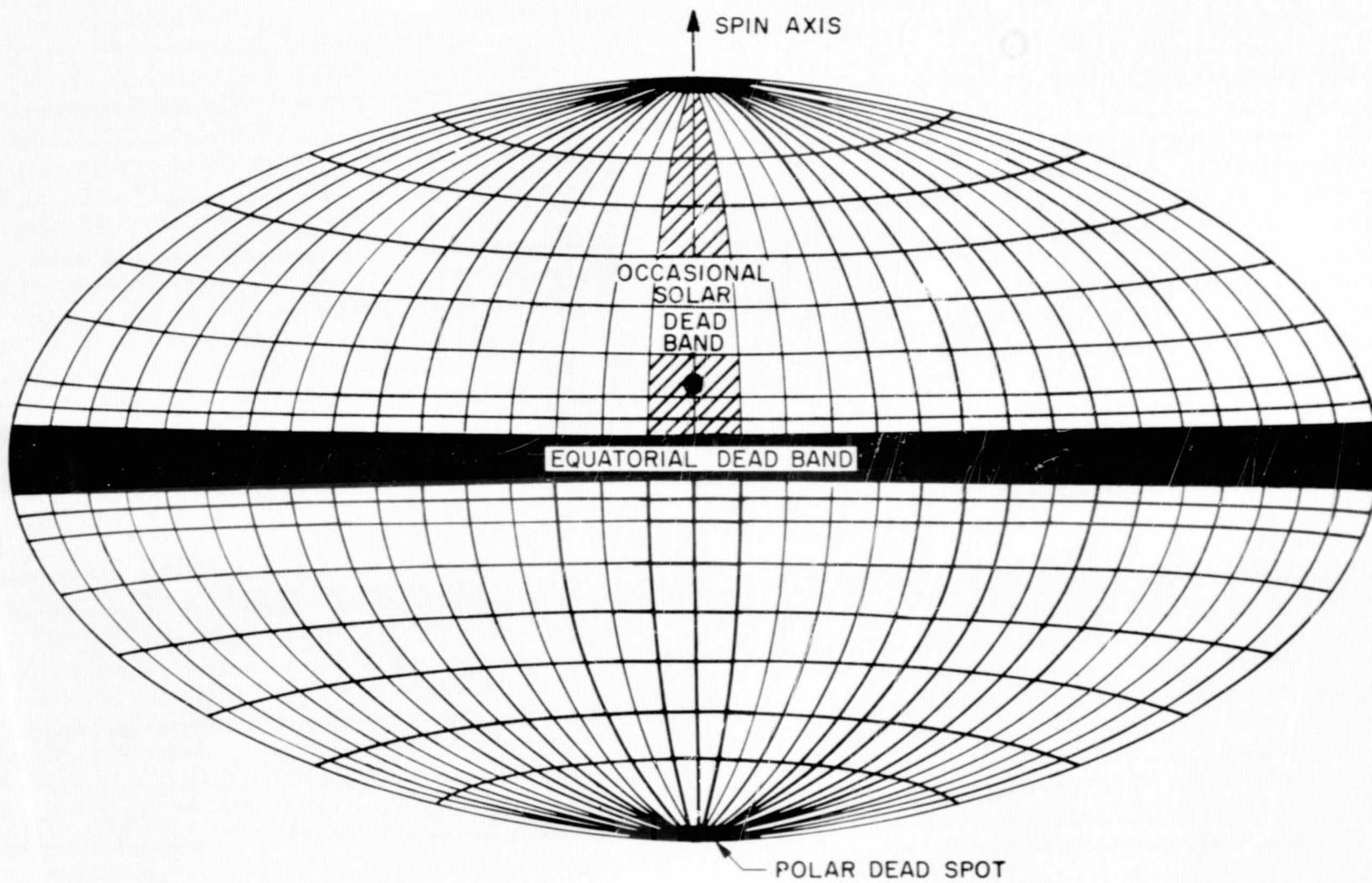


Figure 2.11

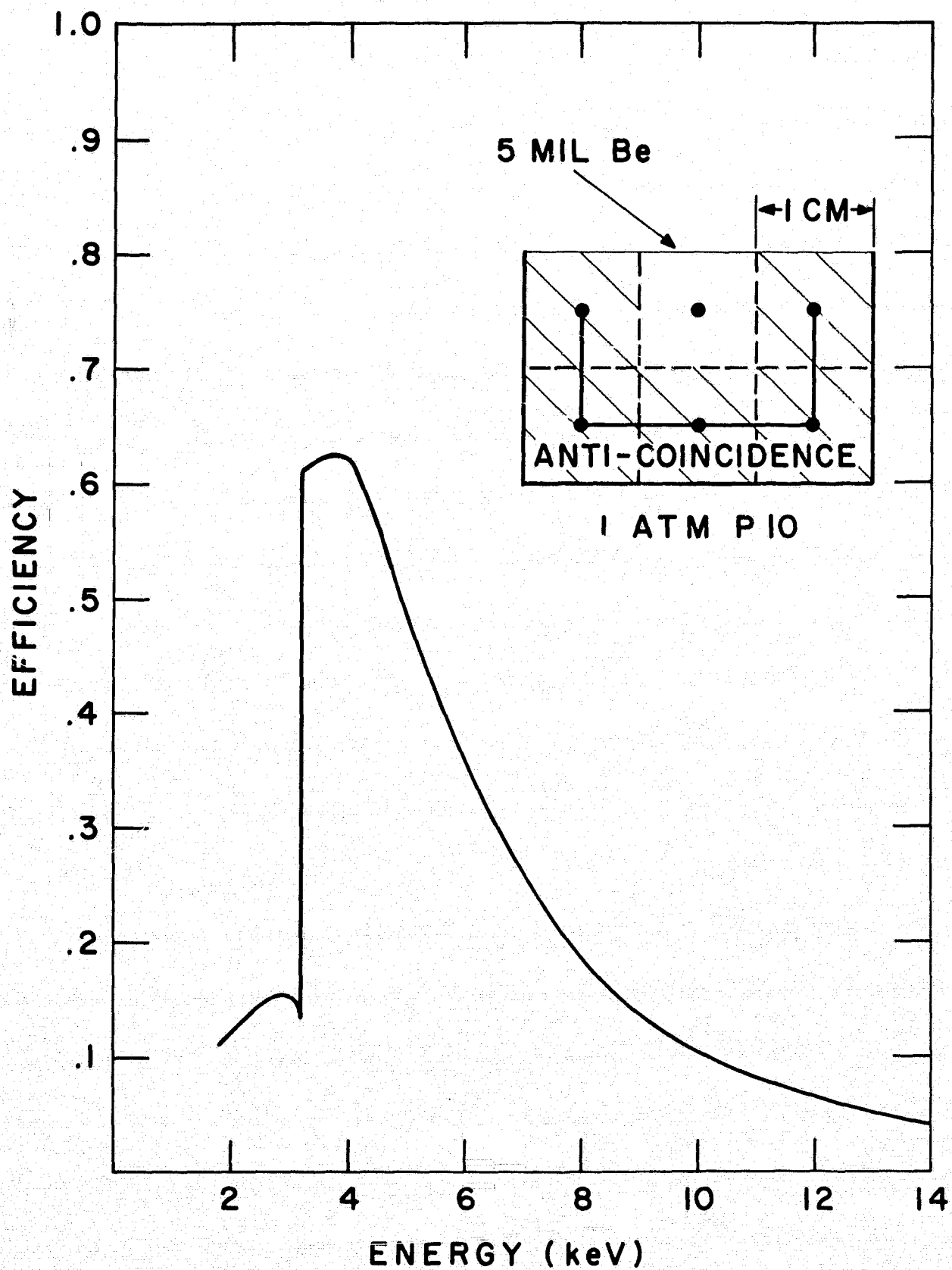


Figure 2.12

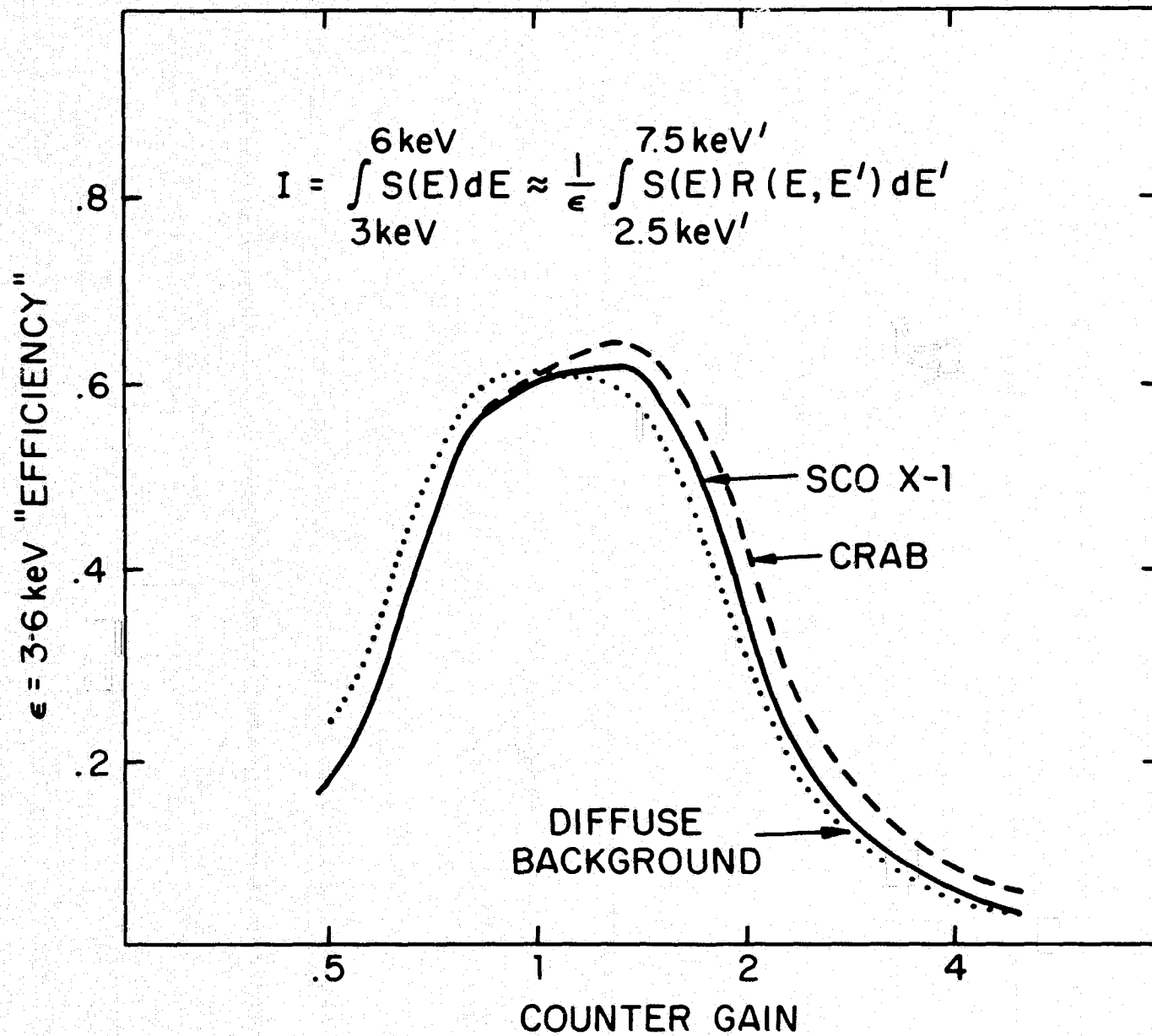


Figure 2.13

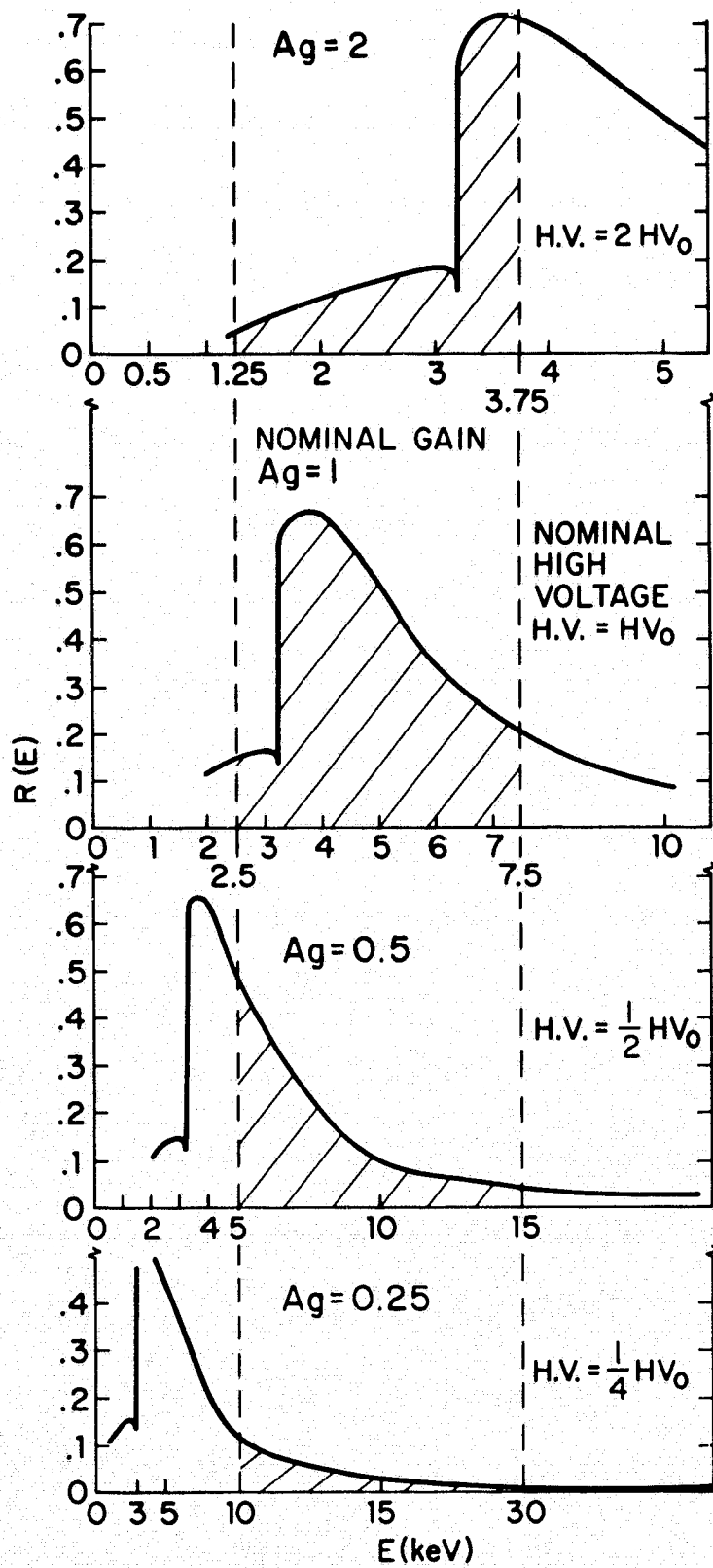


Figure 2.14

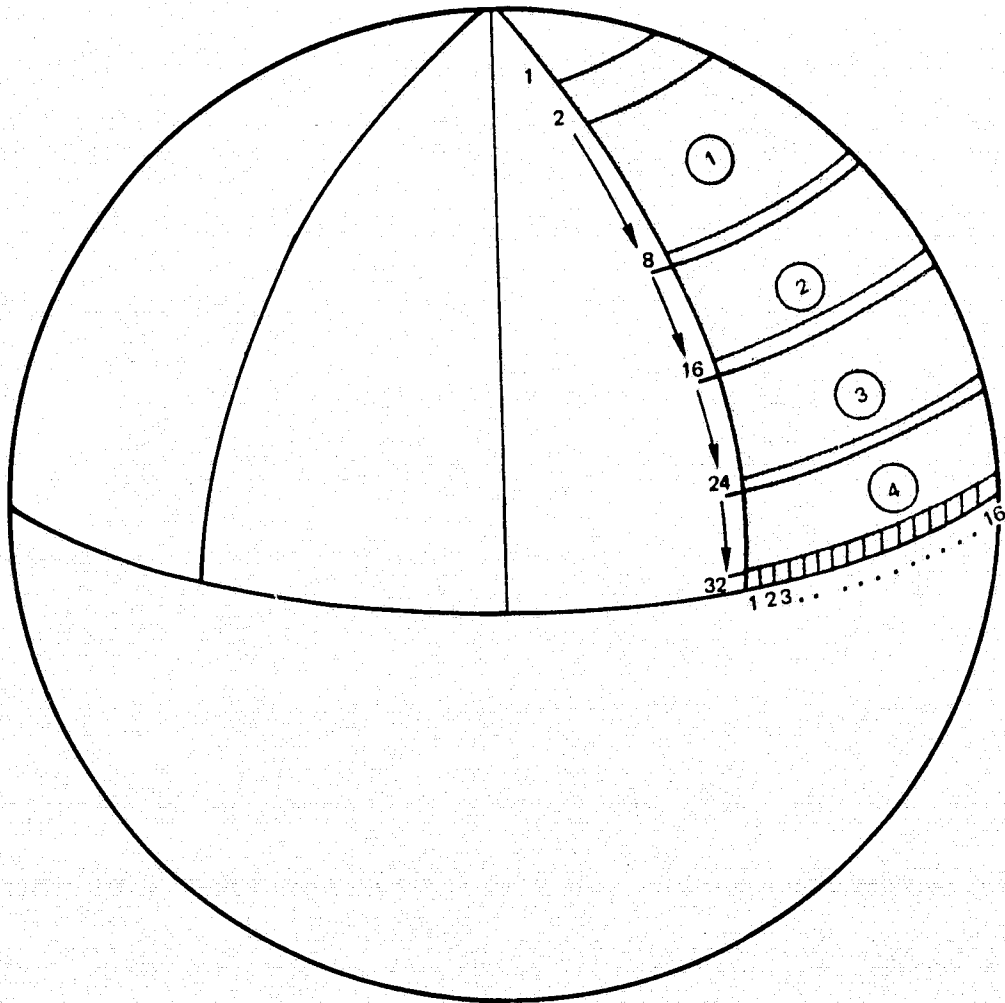


Figure 2.15

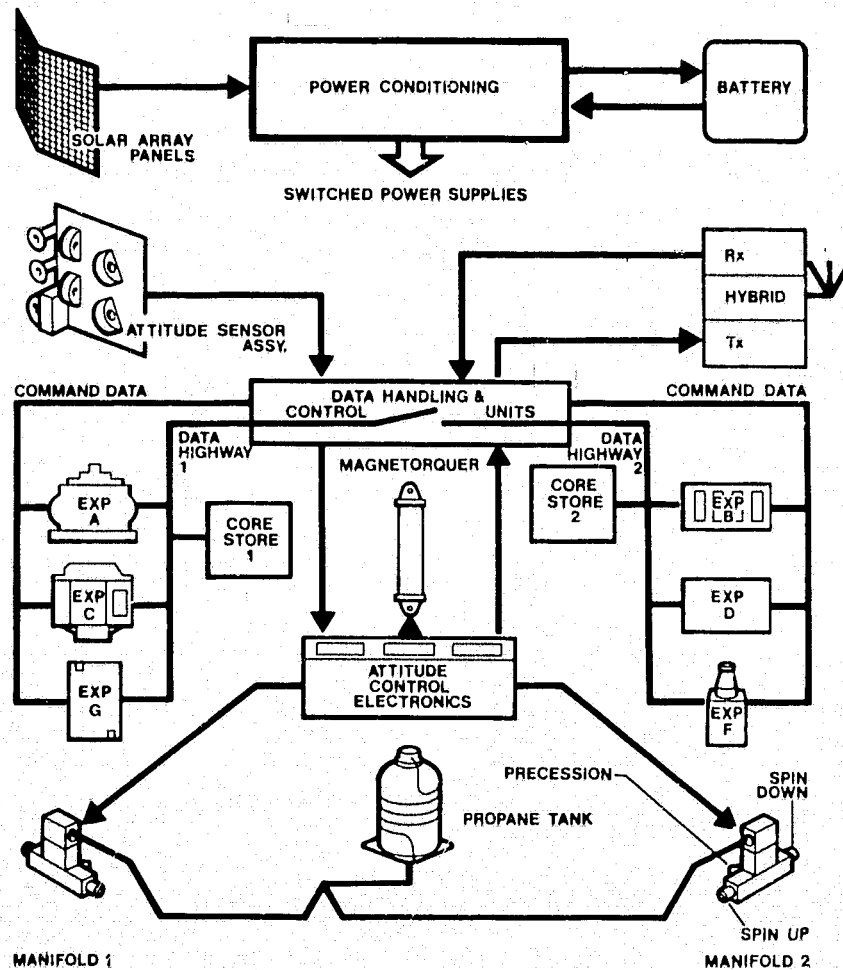


Figure 2.16

MEAN UNOCCULTED SOURCE FRACTION ( $\eta$ ) VS. POSITION

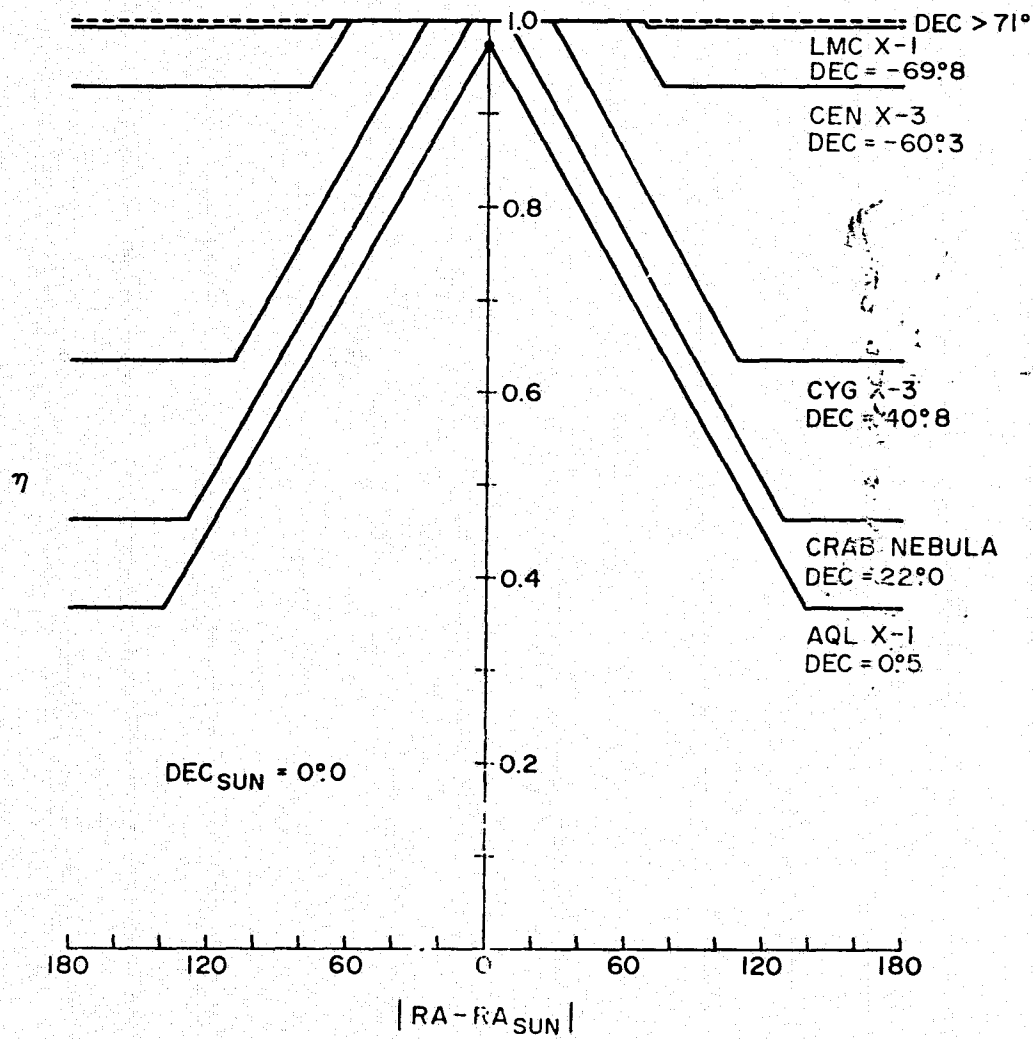


Figure 3.1



LATITUDINAL CORRECTION FACTOR VS SOURCE SPACECRAFT LATITUDE

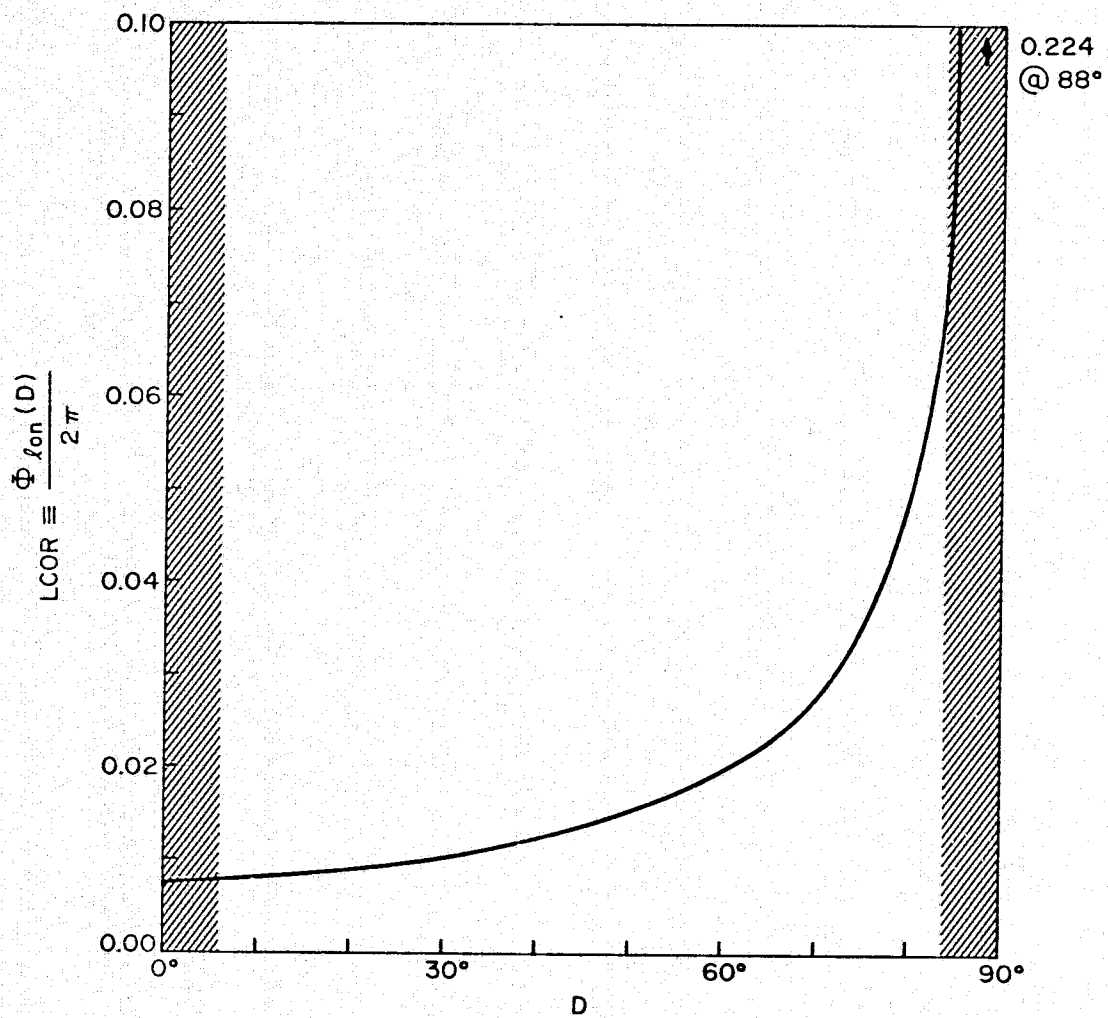
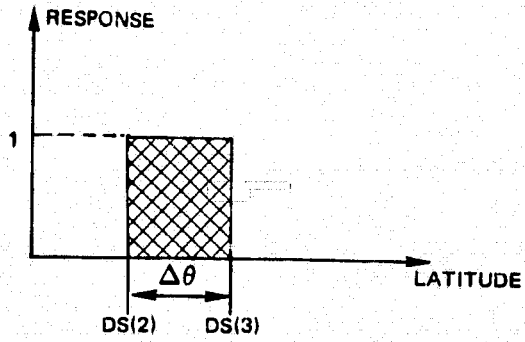
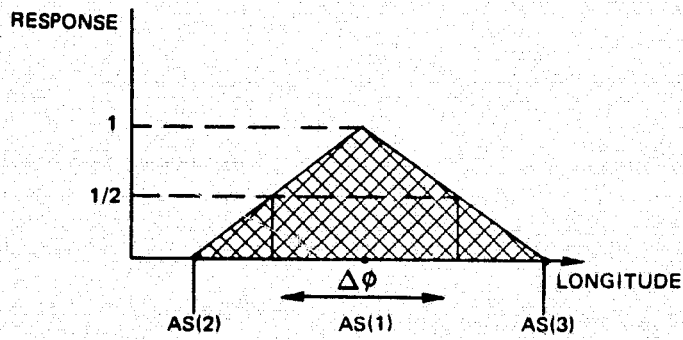


Figure 3.2



Response Versus Latitude

(a)



Response Versus Longitude

(b)

Figure 3.3

LONGITUDINAL RESPONSE AS A FUNCTION OF SPACECRAFT LATITUDE

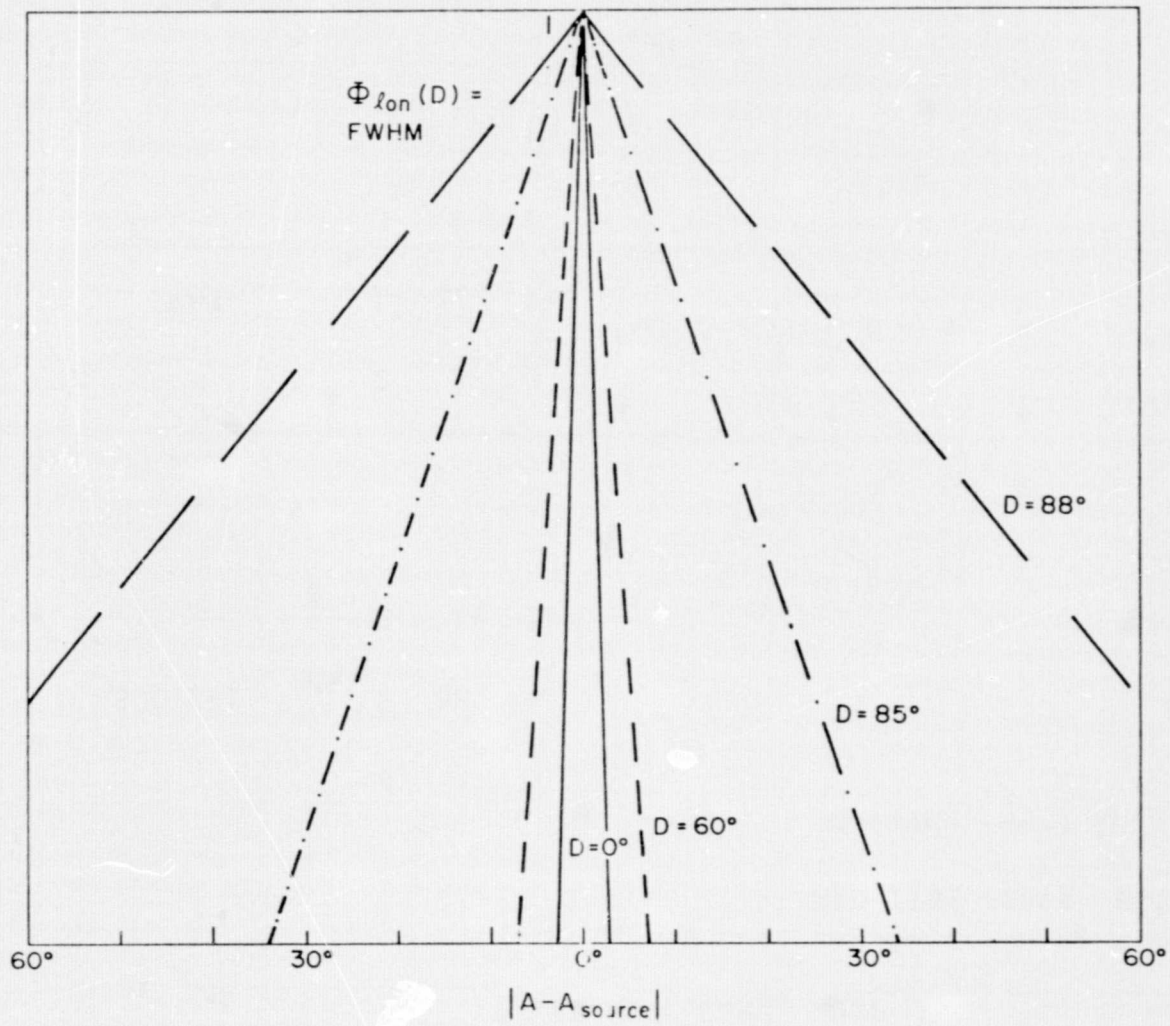


Figure 3.4

"TYPICAL" CORE DUMP

MID-TIME 1975 6.0885d

ON-TIME 3552 sec

	6	3	4				
SCO X-1	2	287	4				
	2	1	1		4	3	5 7
					1	4	19 6 CYG X-2
					3	4	6 7
	2	2	3		4	20	17 7 CYG X-1,3
CRAB	1	11	1		0	6	5 5
	3	2	1				

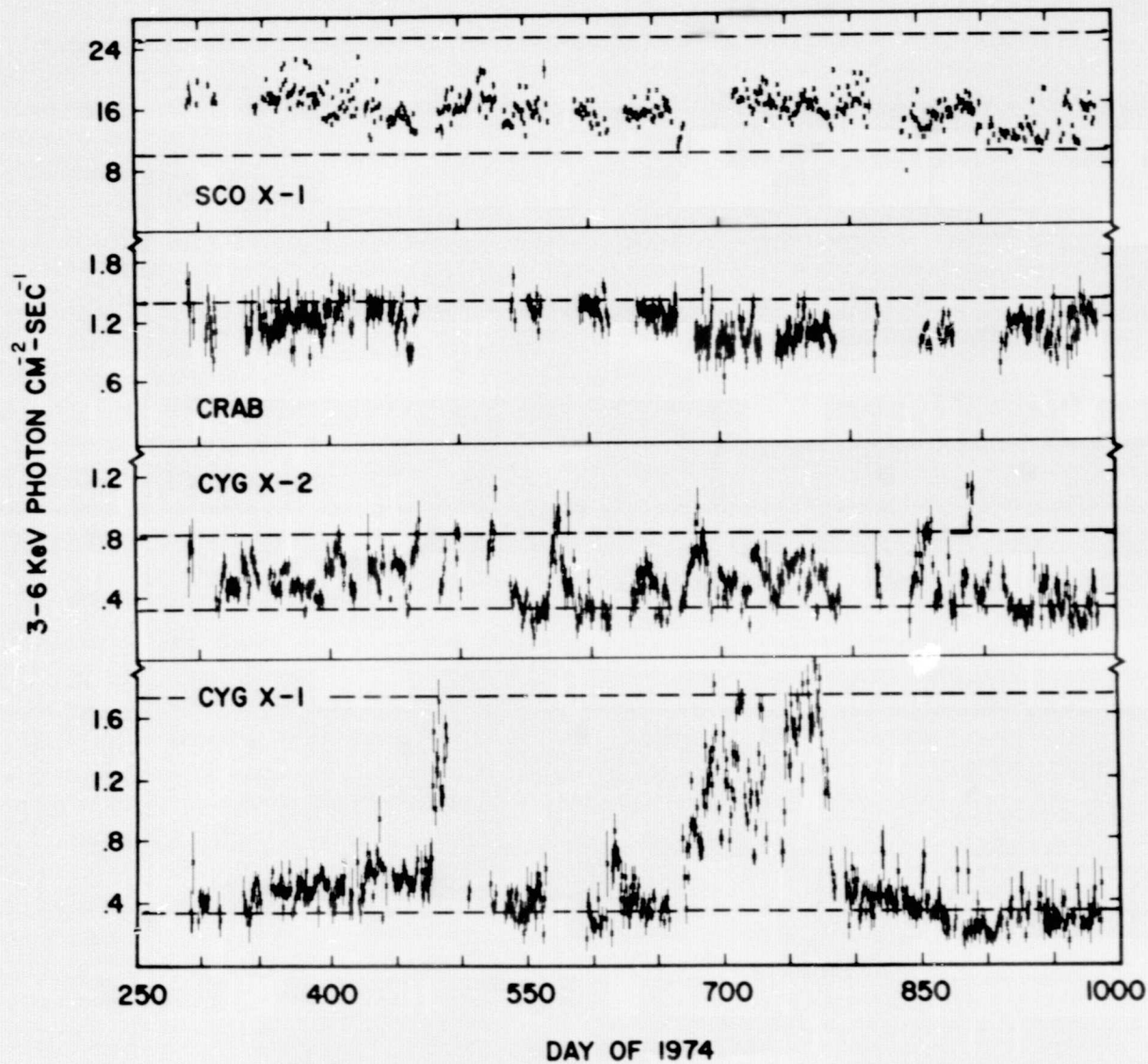
Figure 3.5











REPRODUCIBILITY OF THIS  
ORIGINAL PAGE IS POOR

Figure 3.9



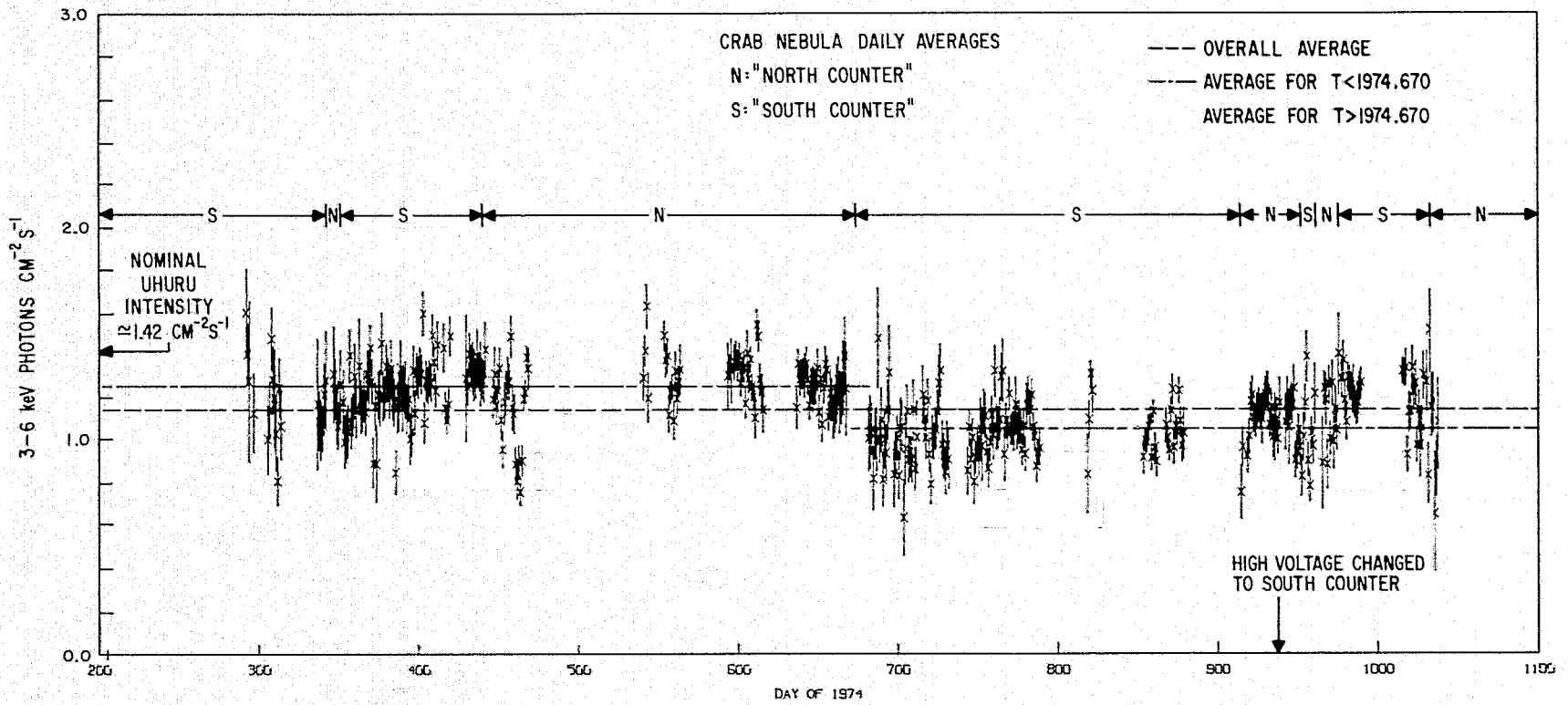


Figure 3.10

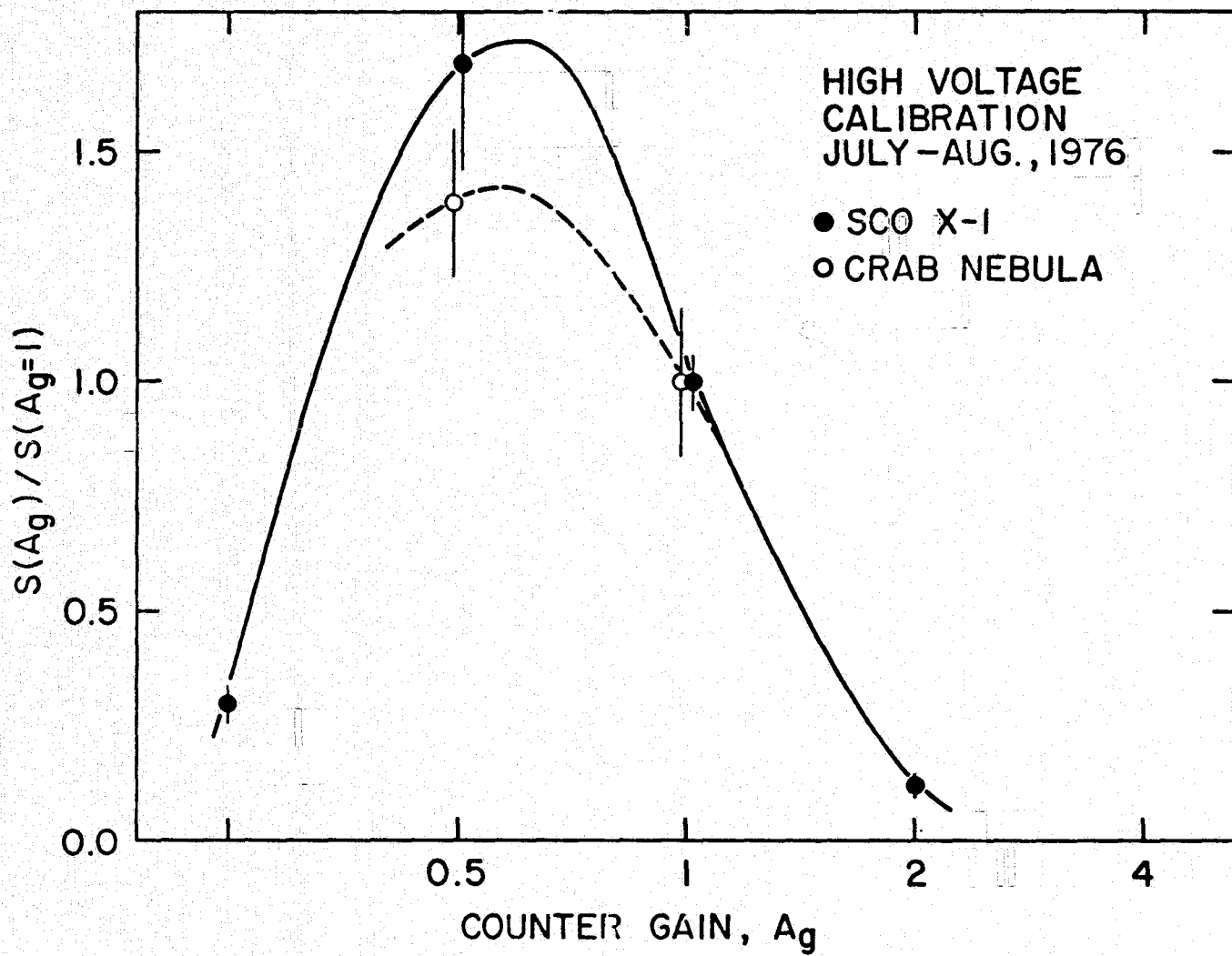


Figure 3.11

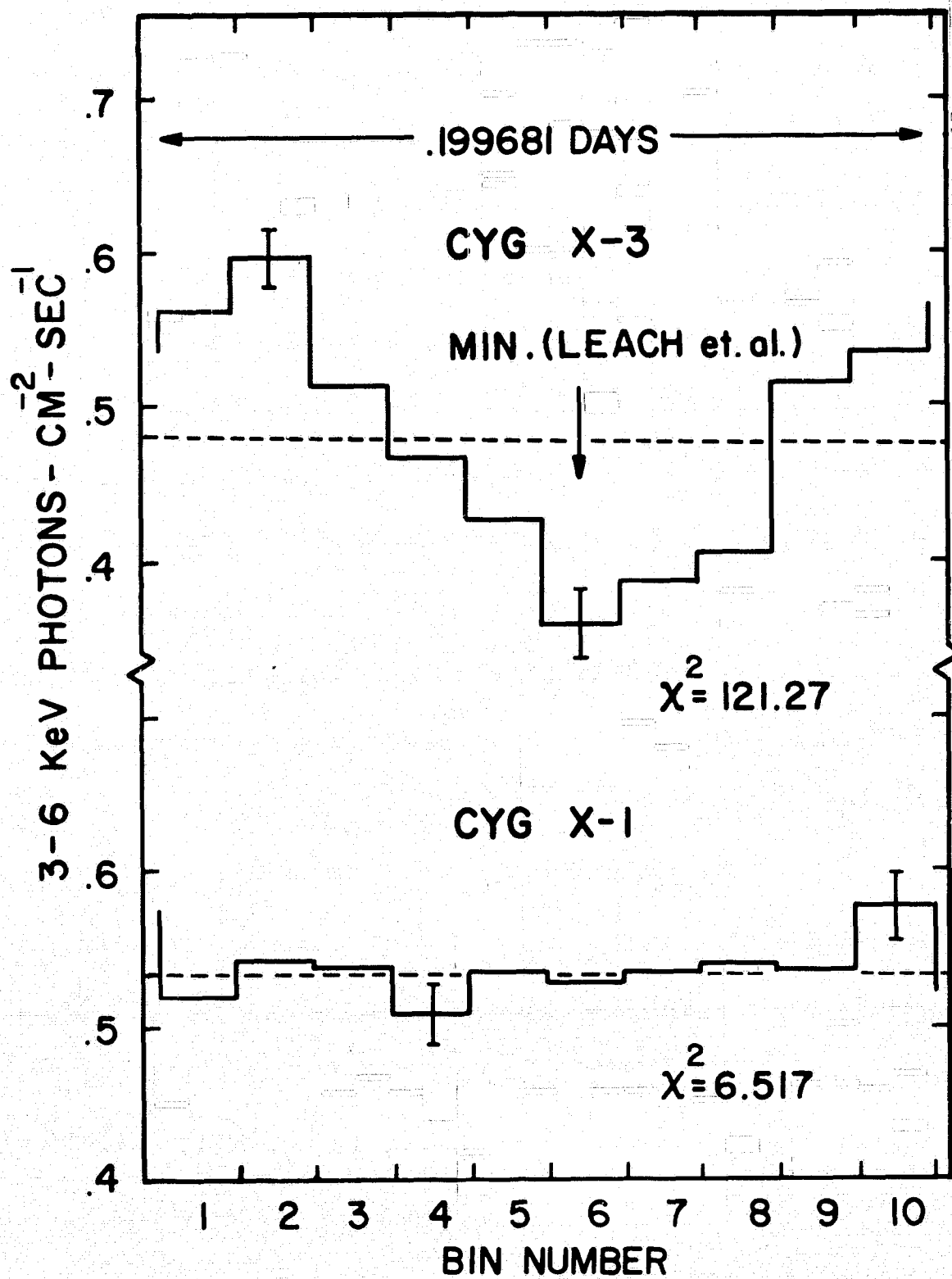


Figure 3.12

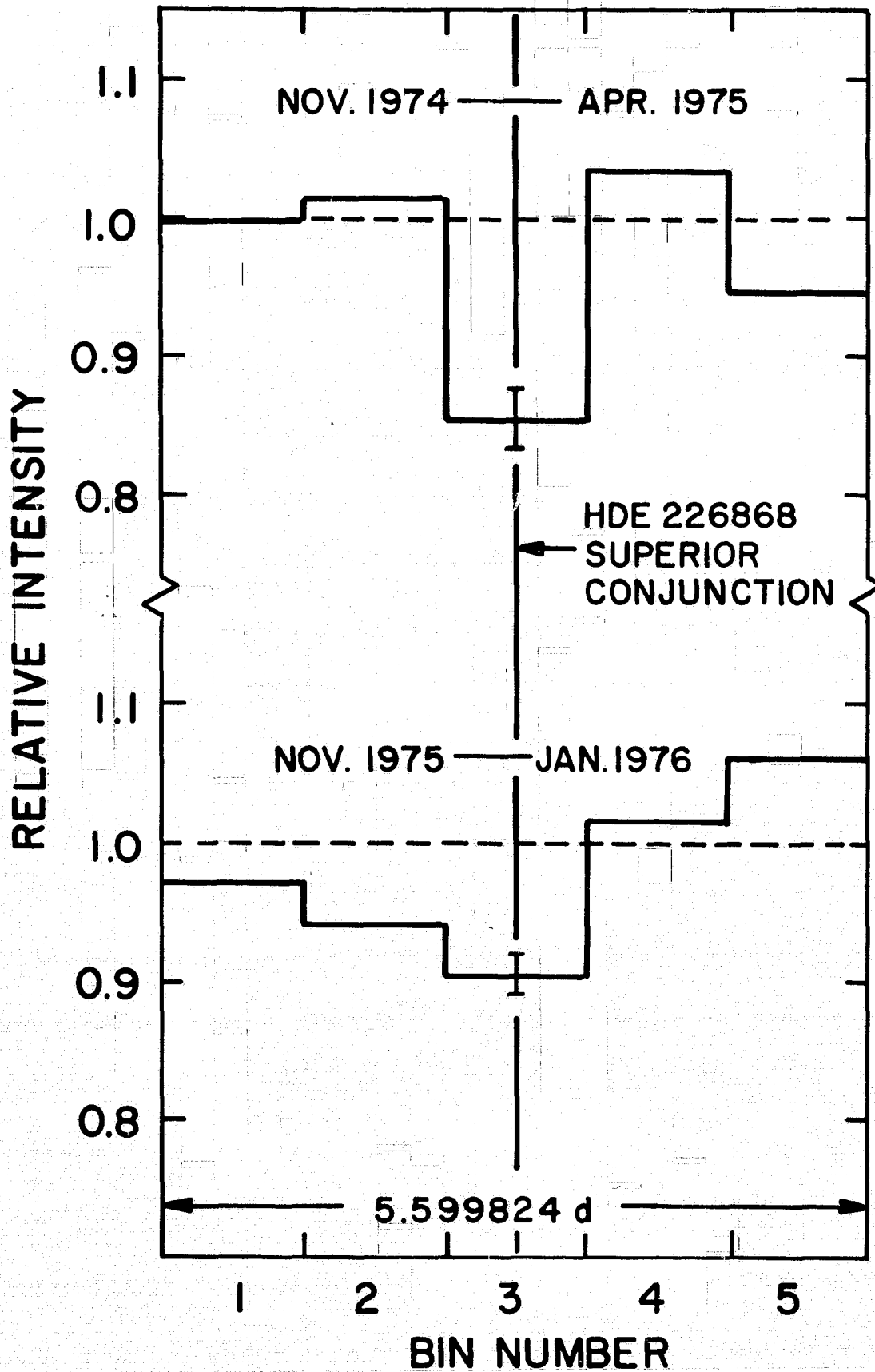


Figure 3.13

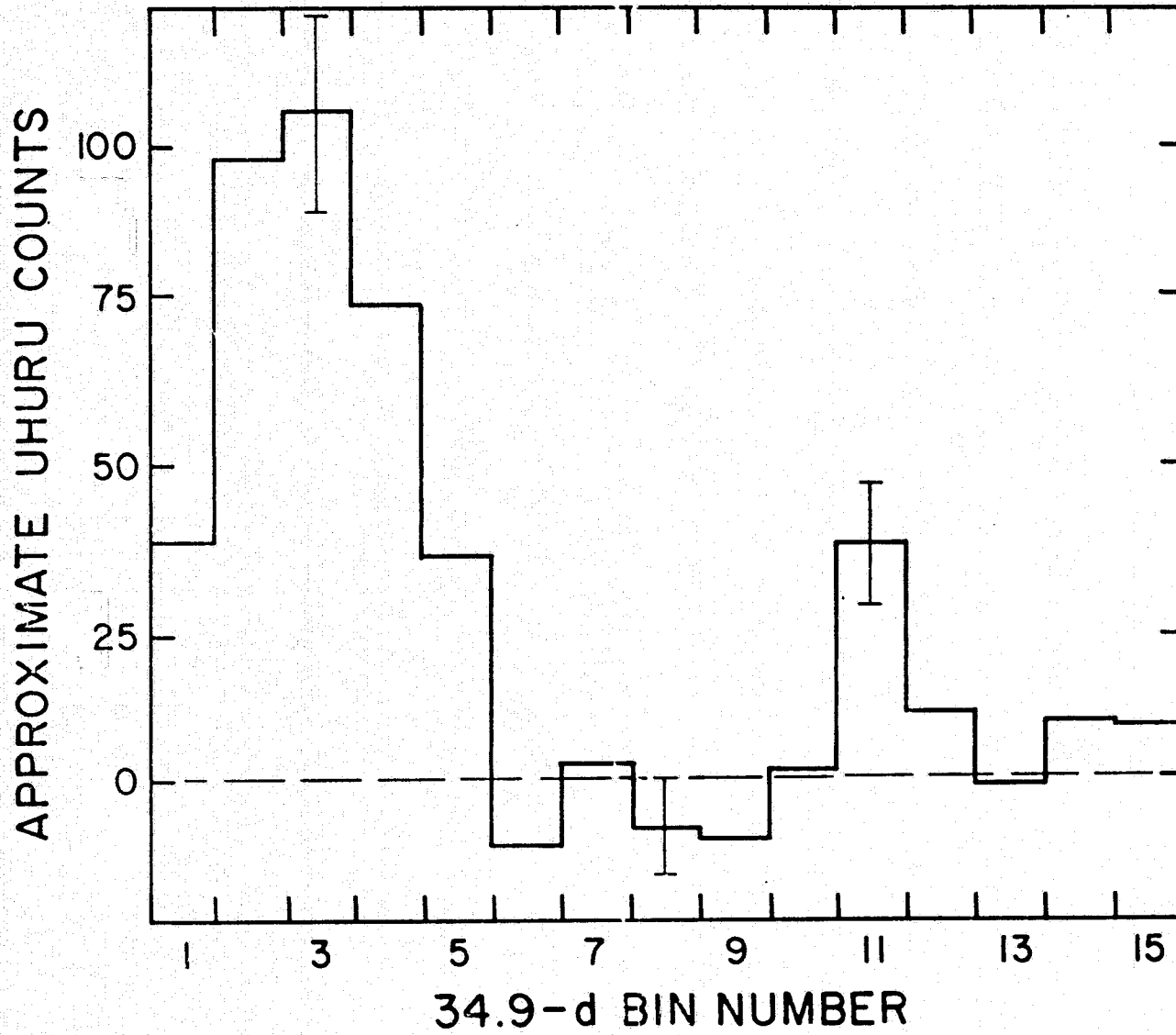


Figure 3.14

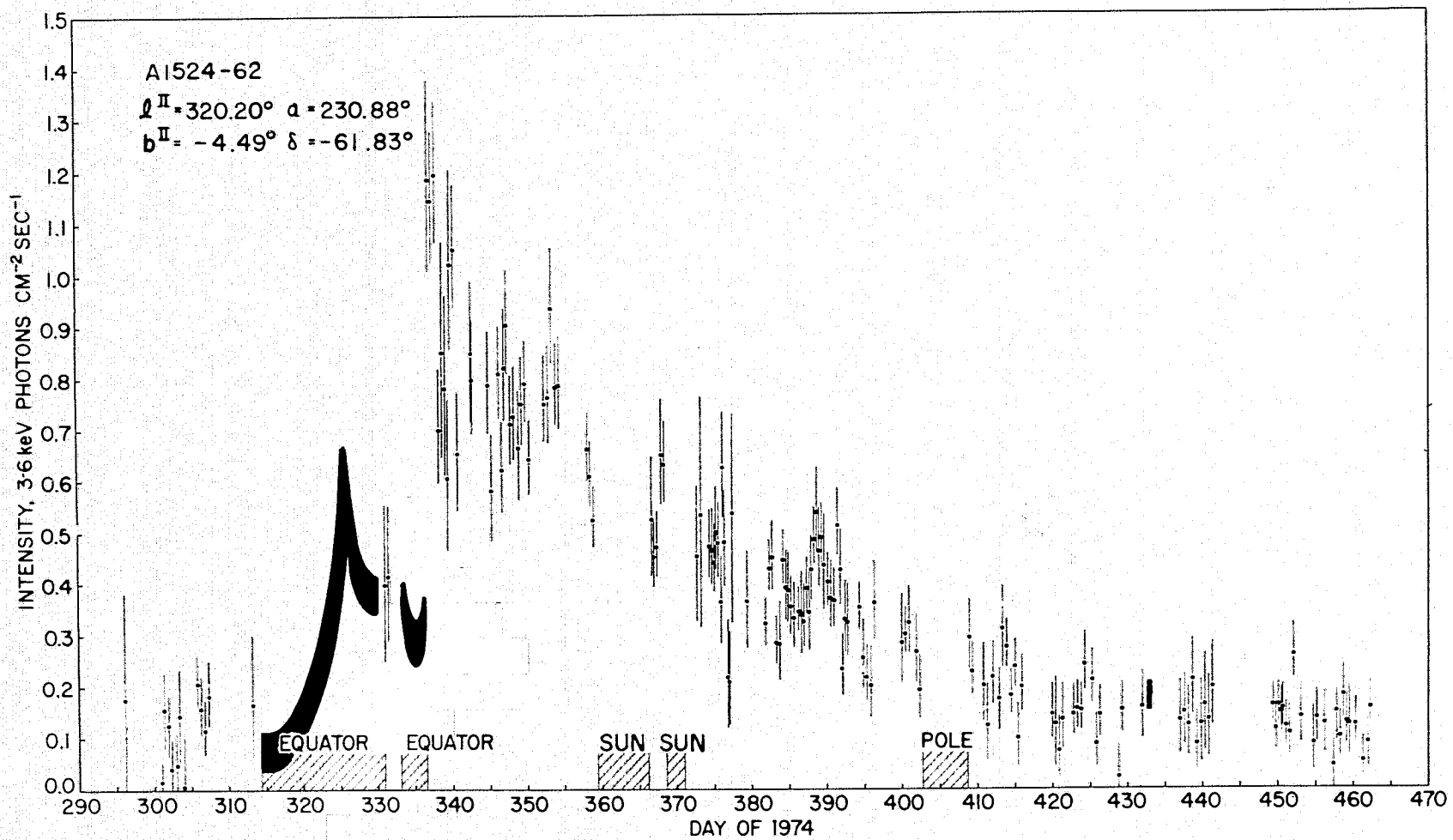


Figure 4.1

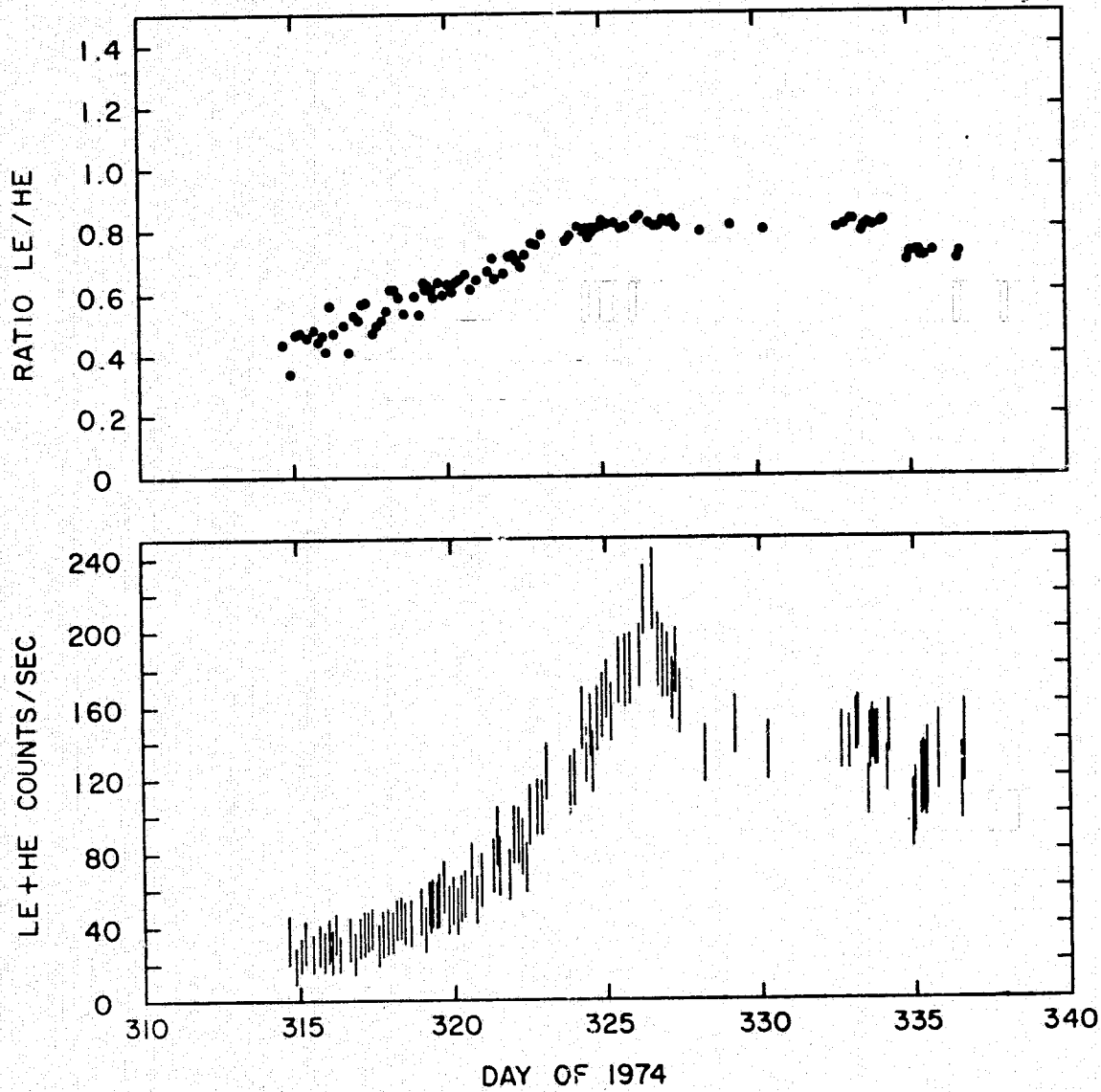


Figure 4.2

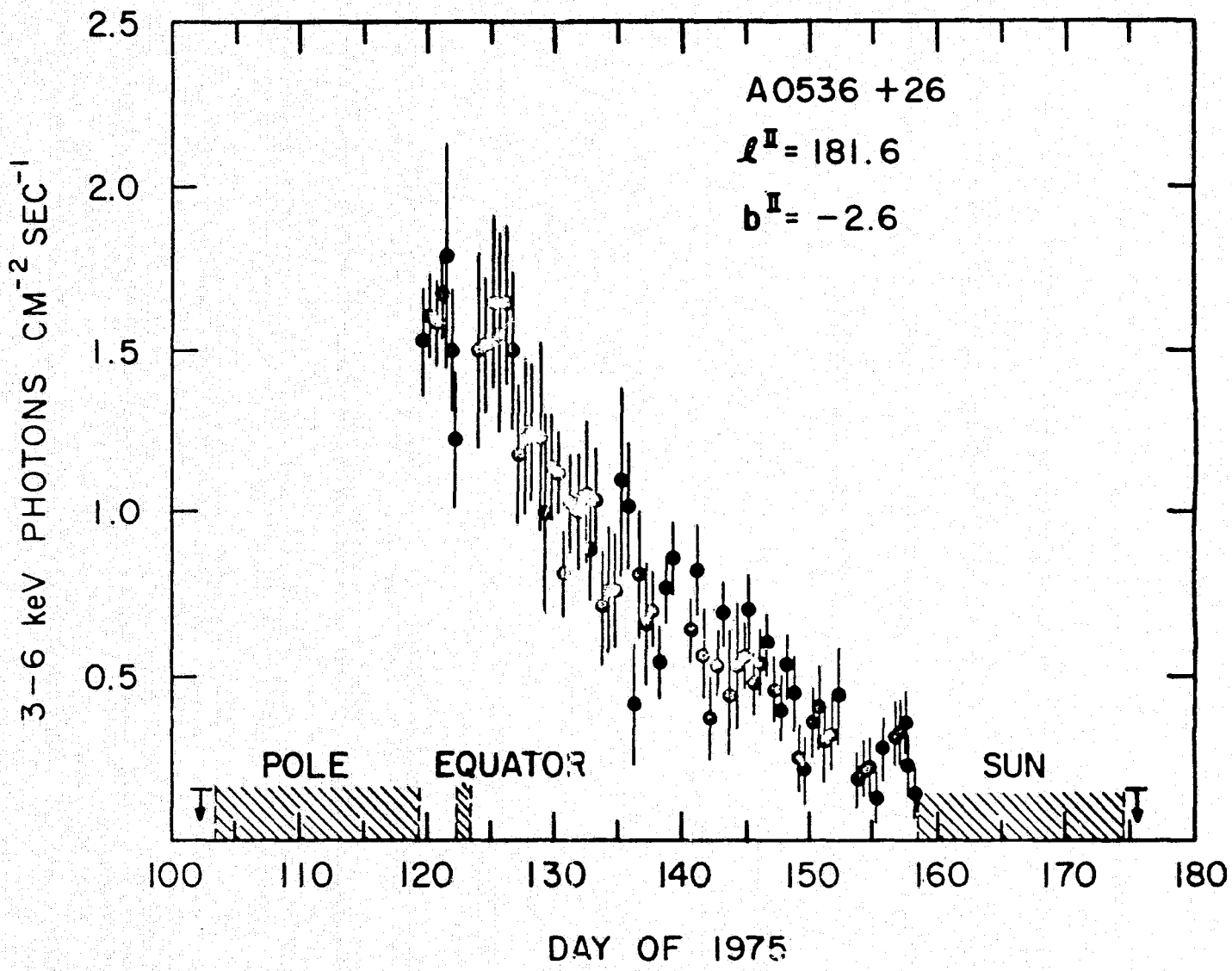


Figure 4.3



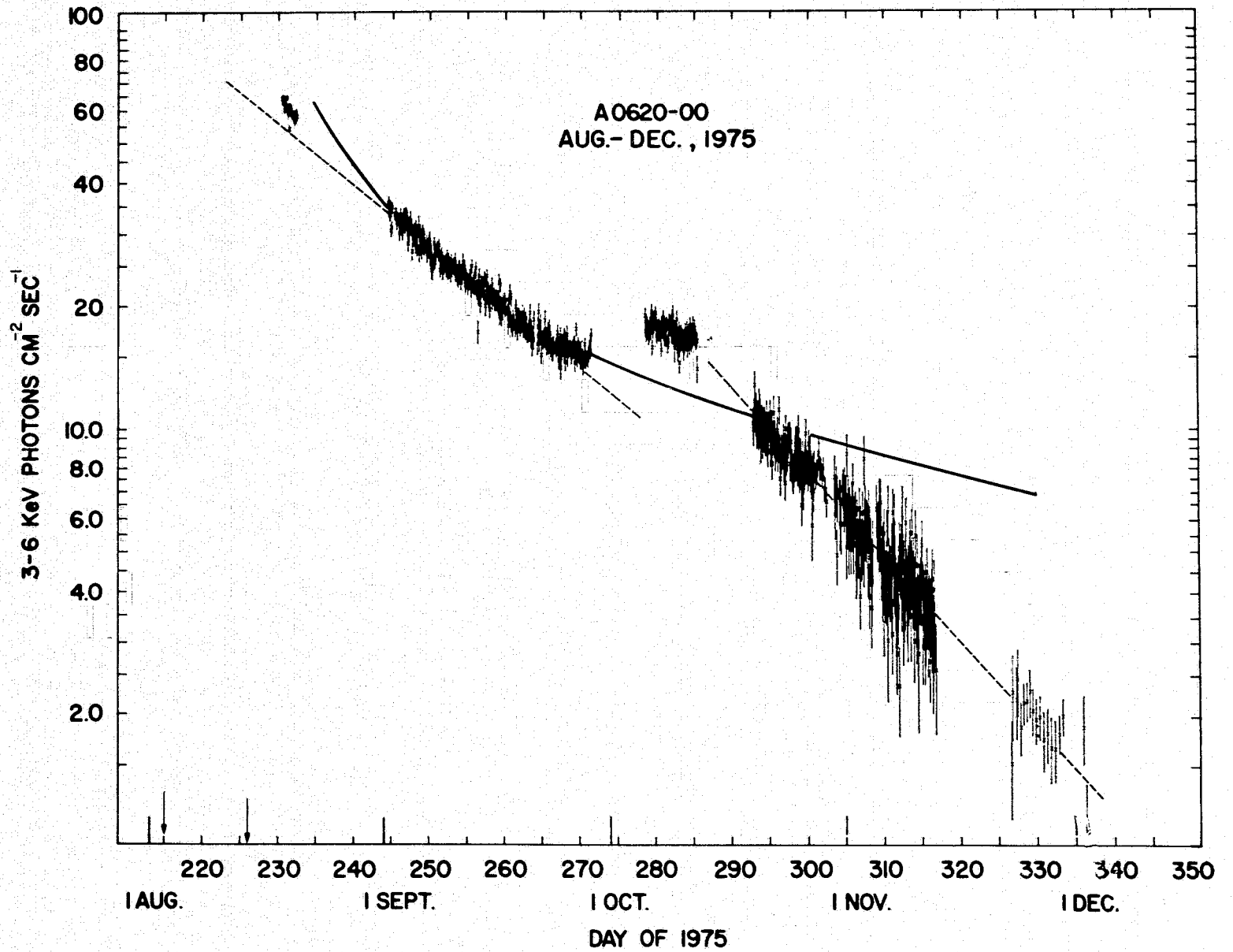


Figure 4.4

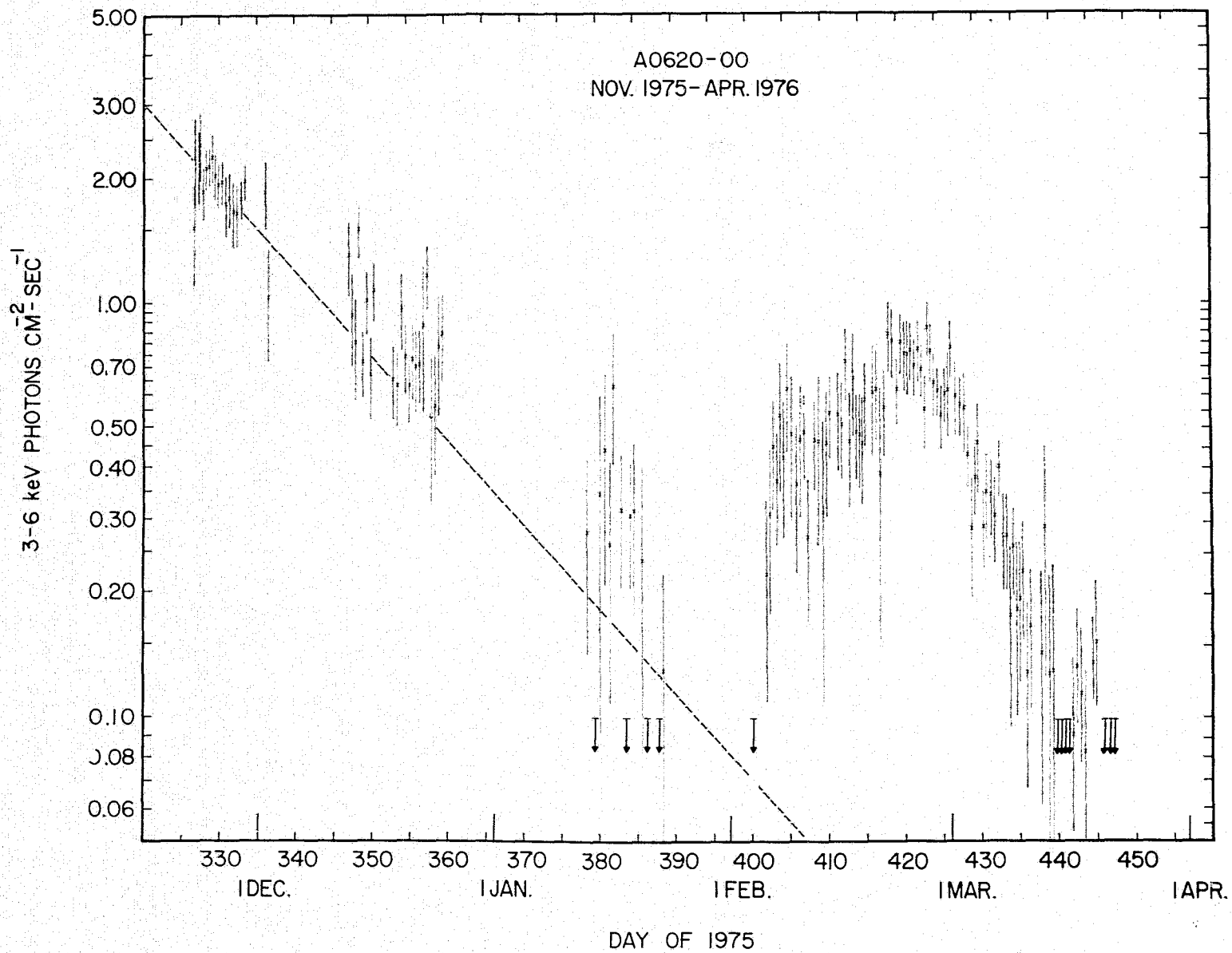


Figure 4.5

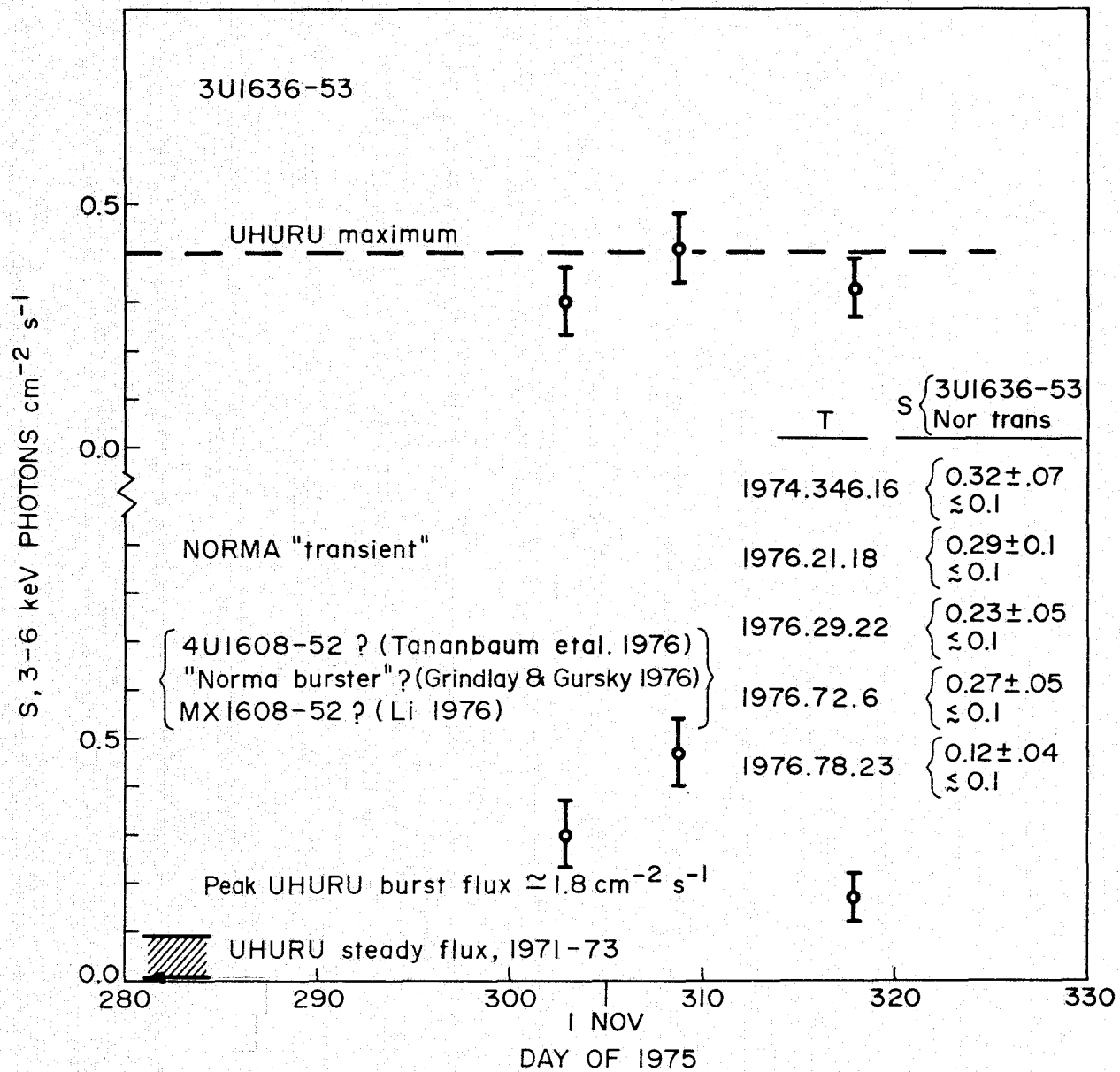


Figure 4.6

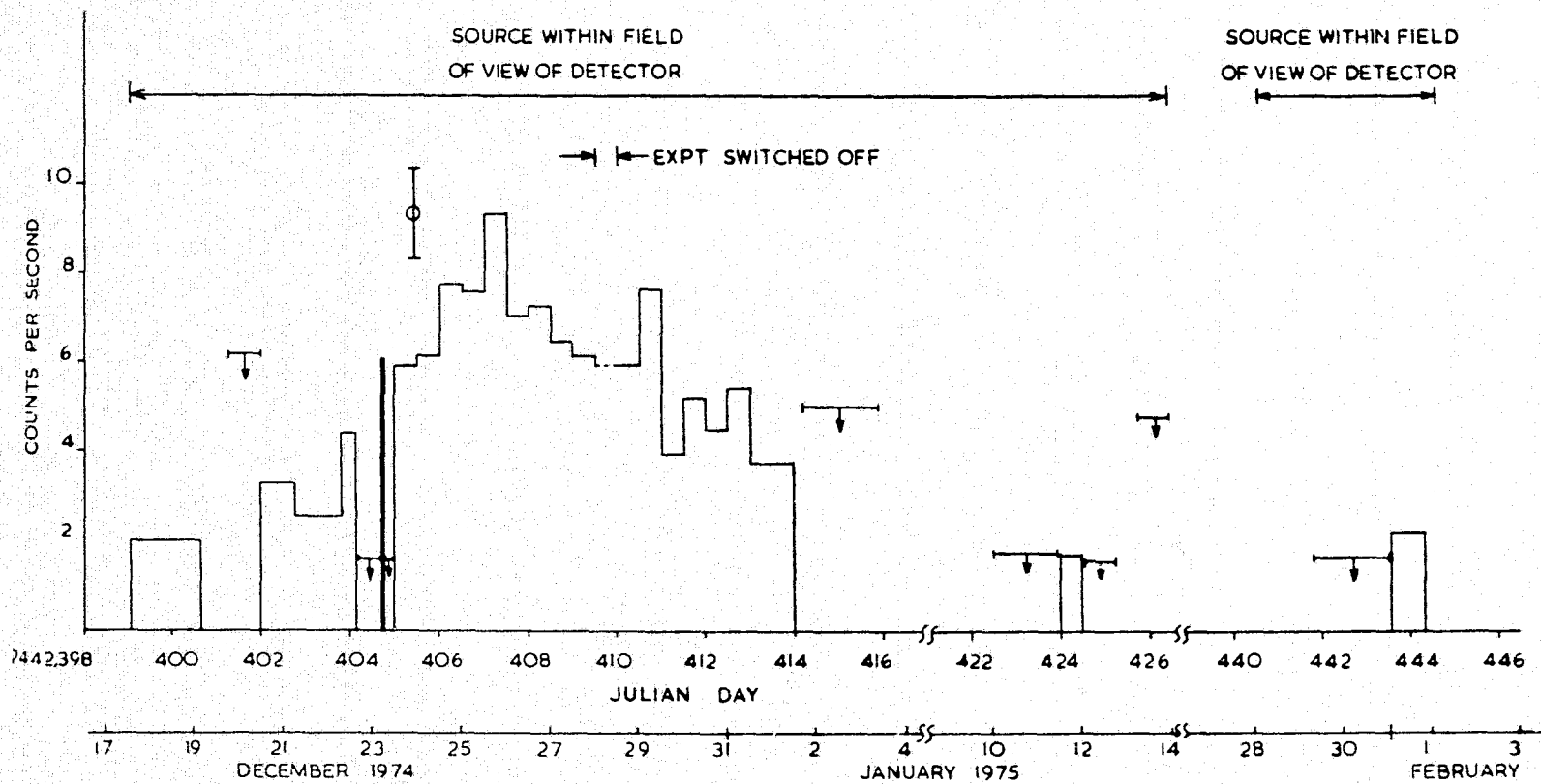


Figure 4.7

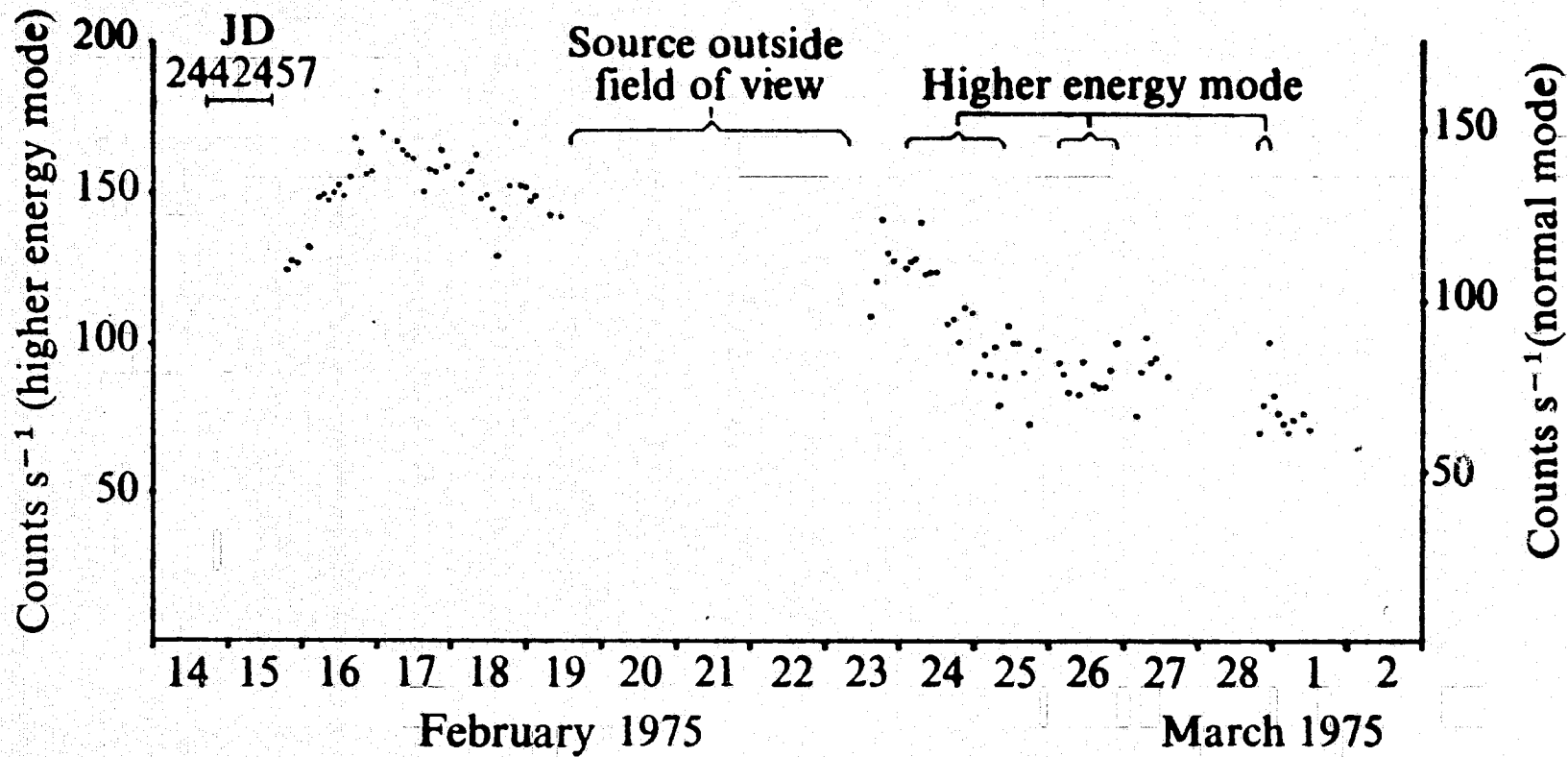


Figure 4.8

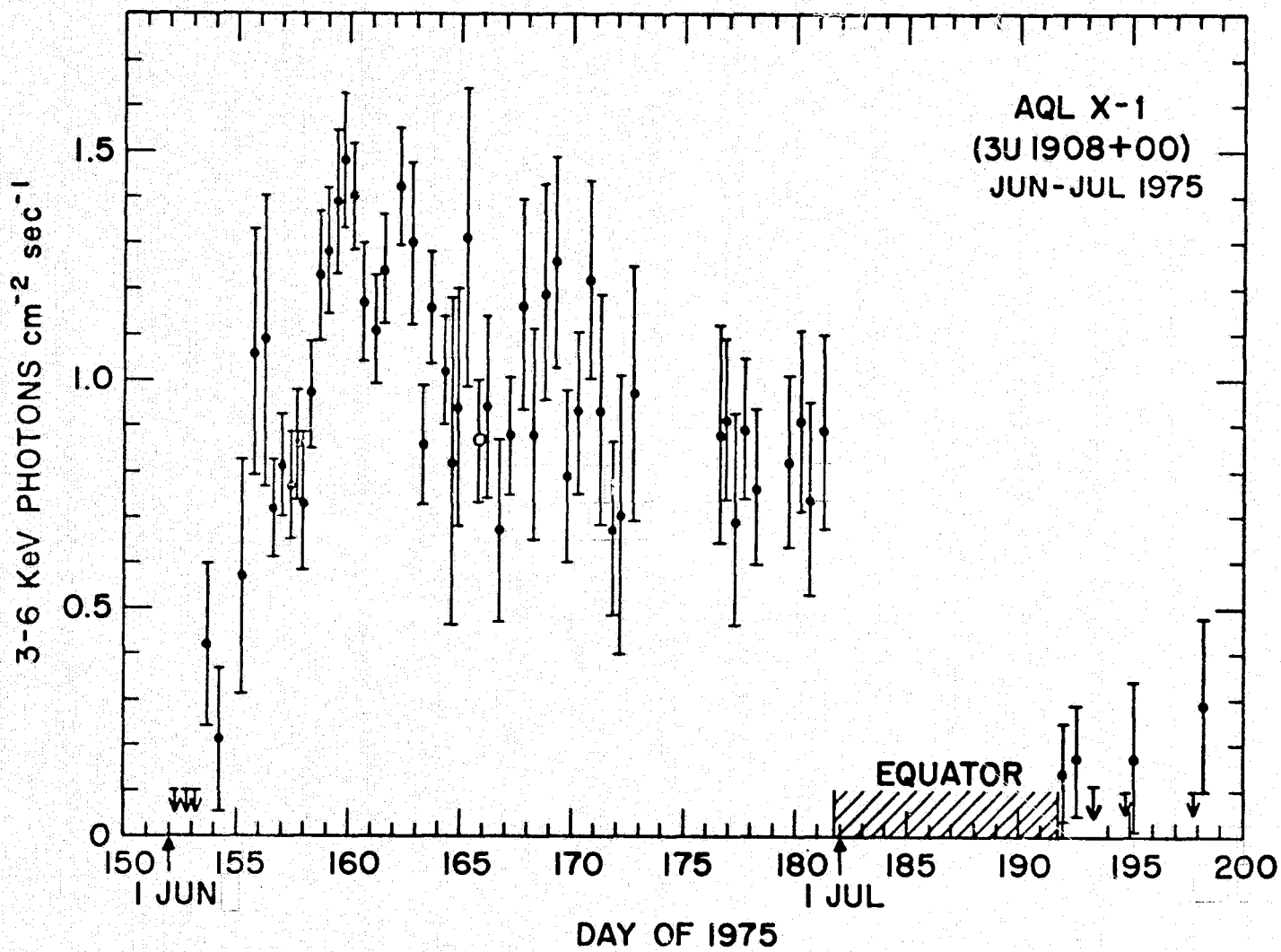


Figure 4.9

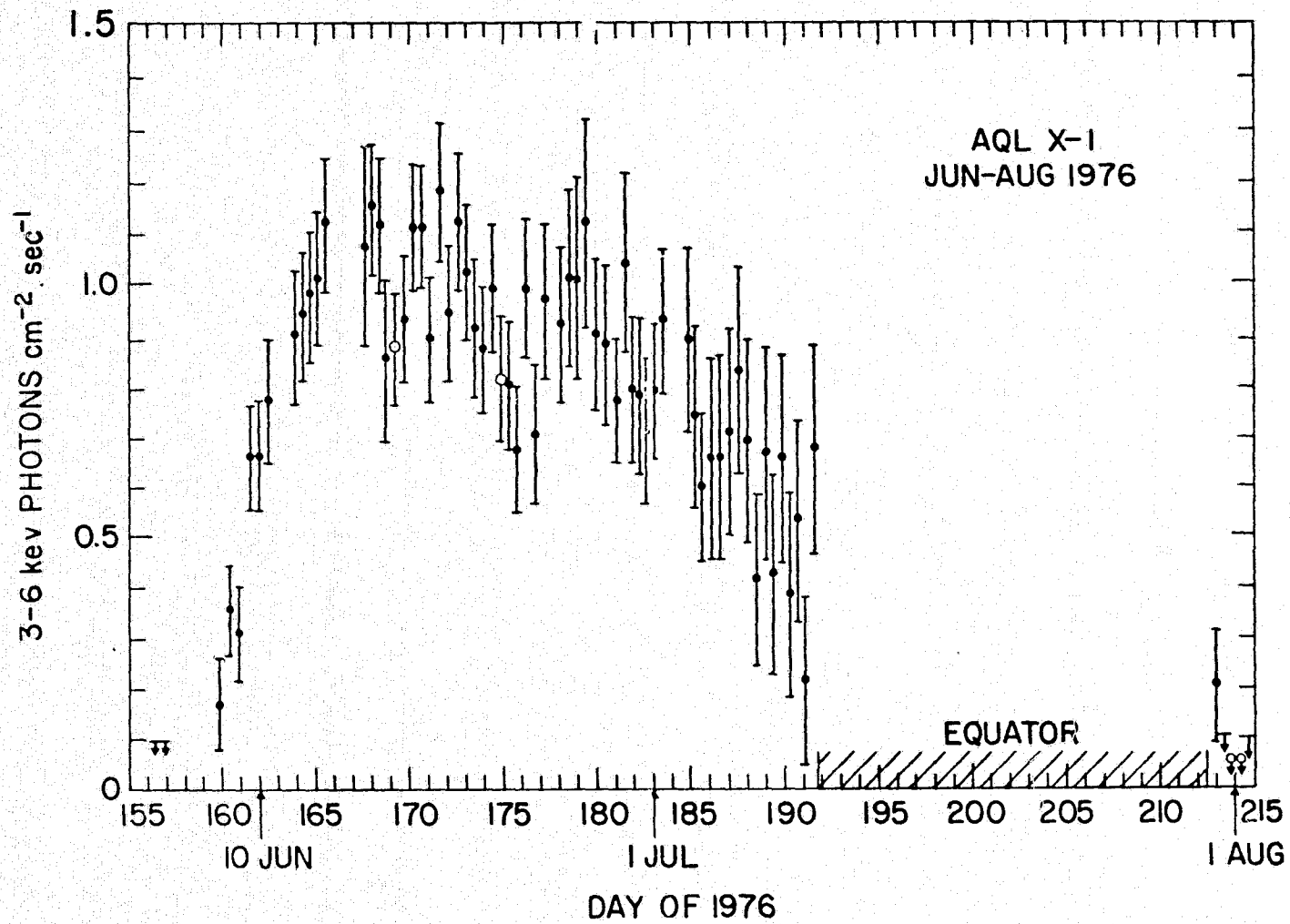


Figure 4.10

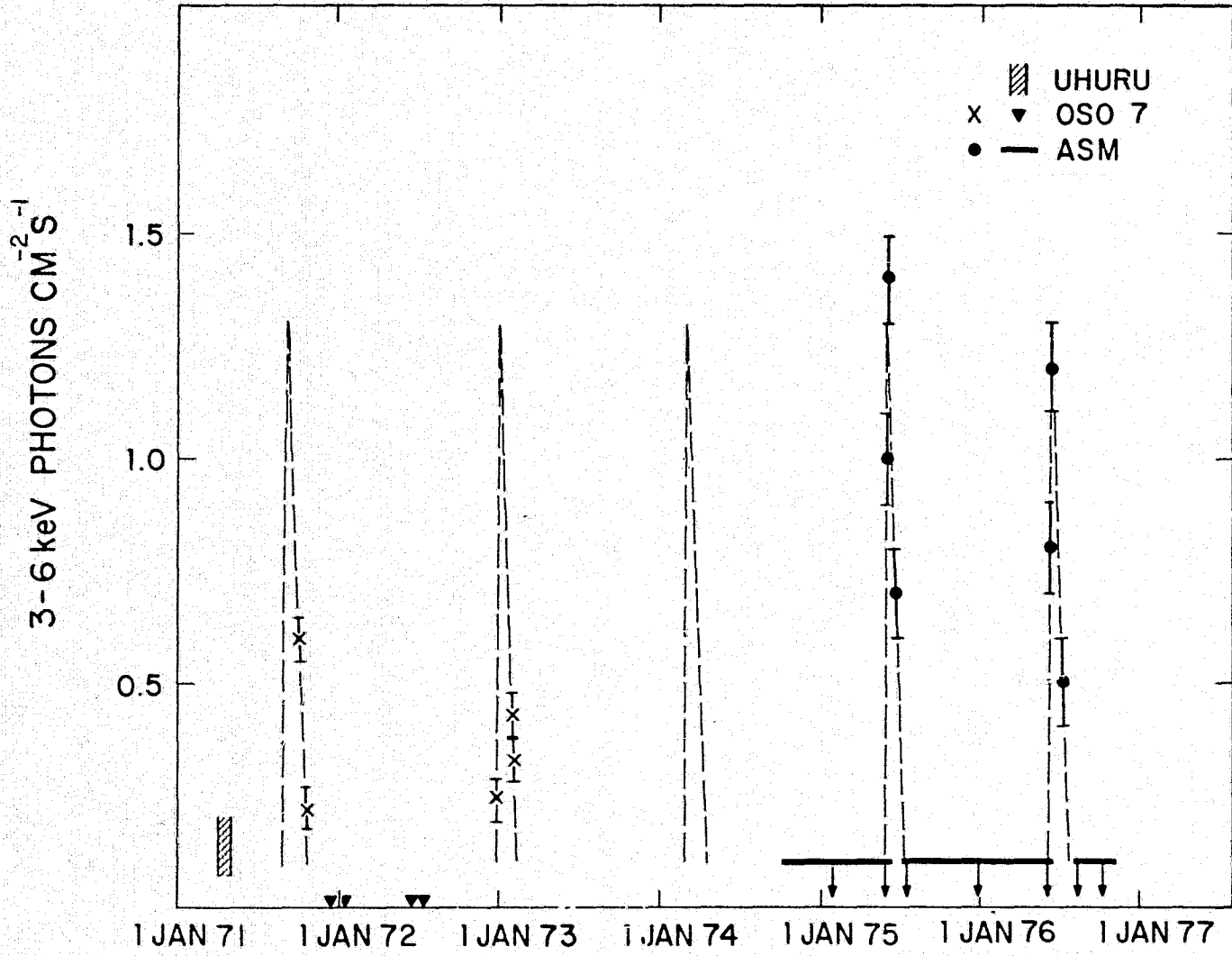


Figure 4.11



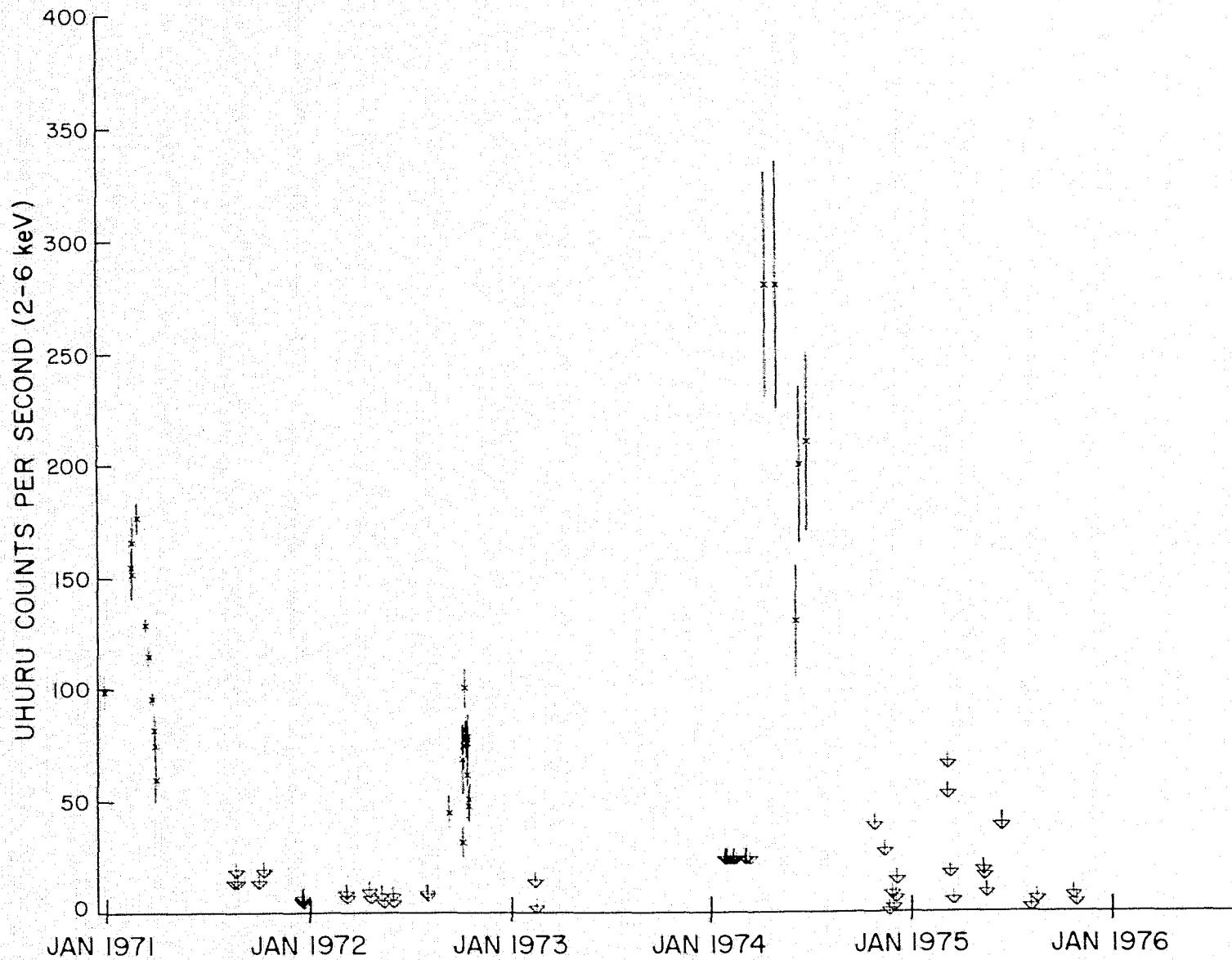


Figure 4.12

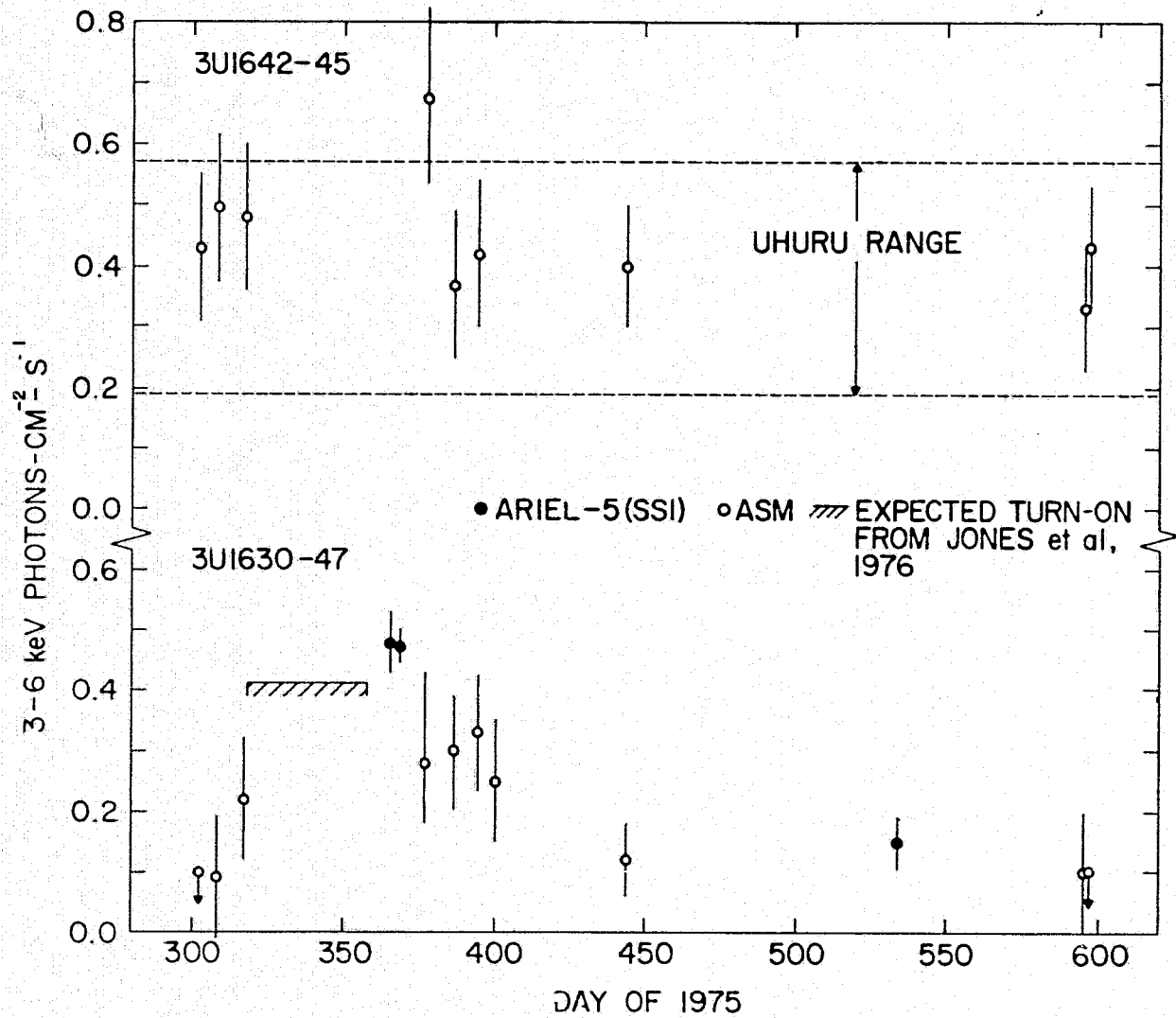


Figure 4.13

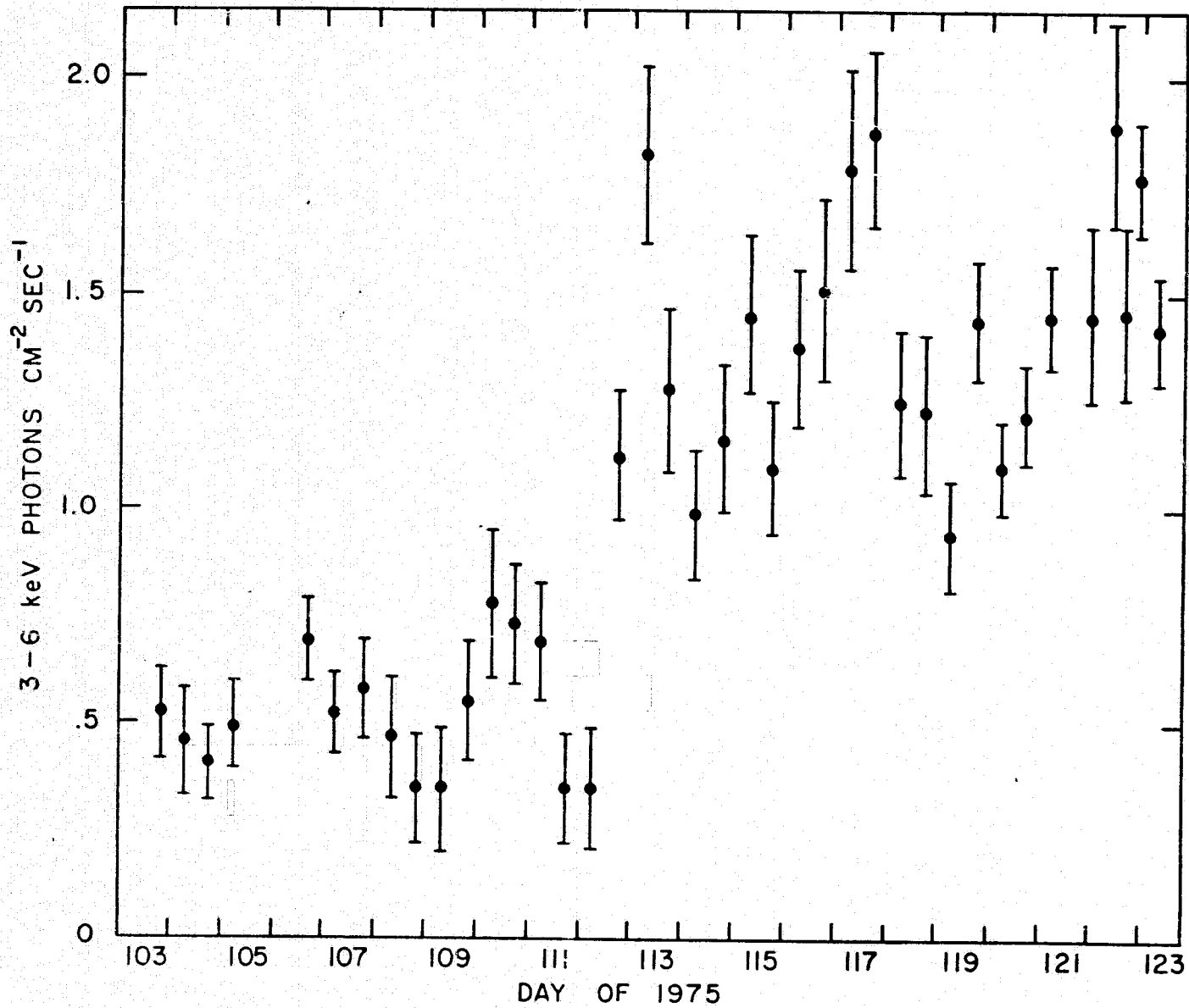


Figure 4.14

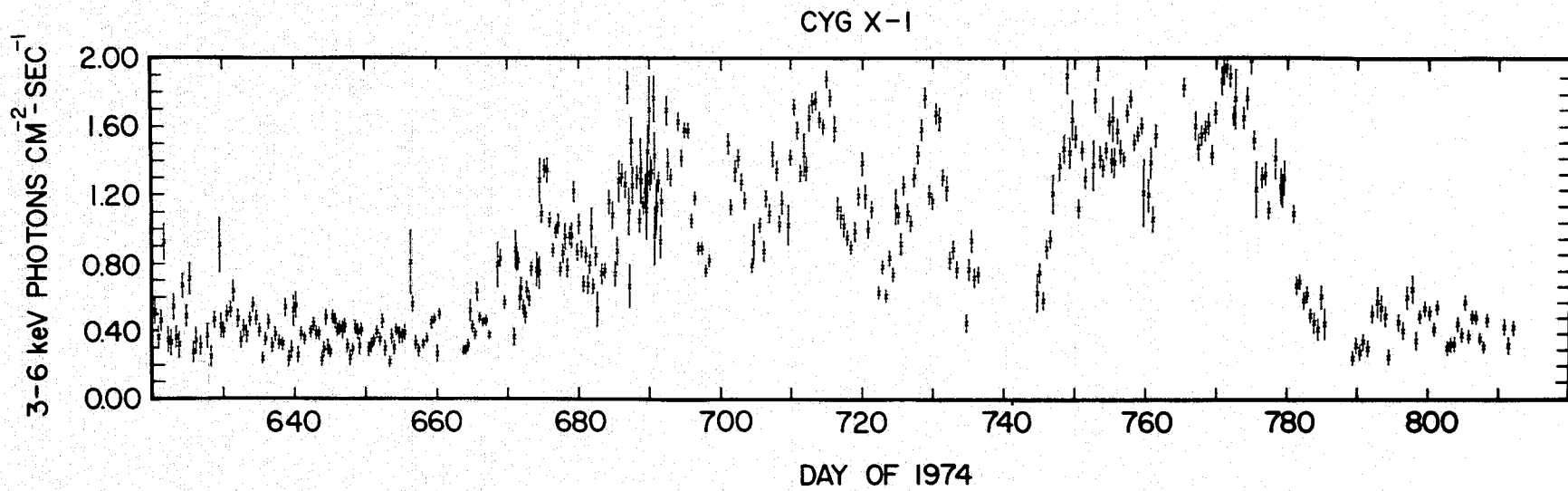


Figure 4.15

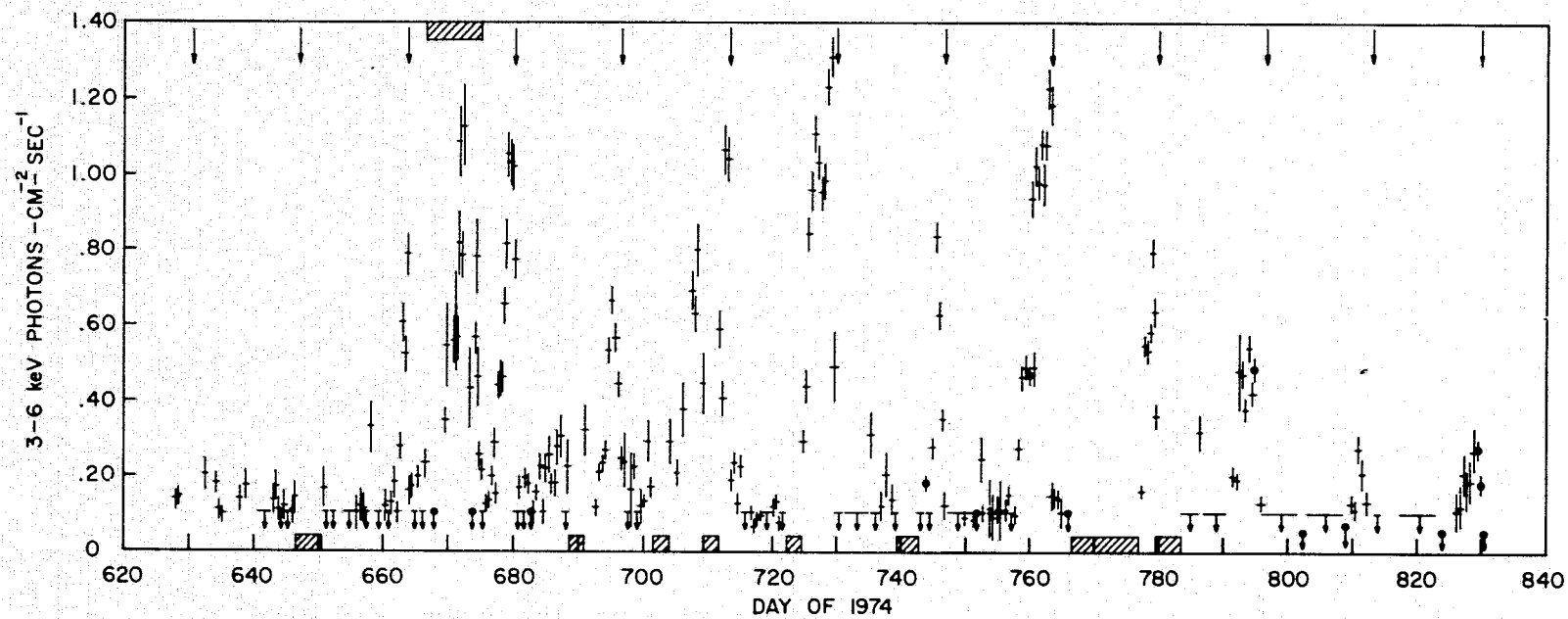


Figure 4.16

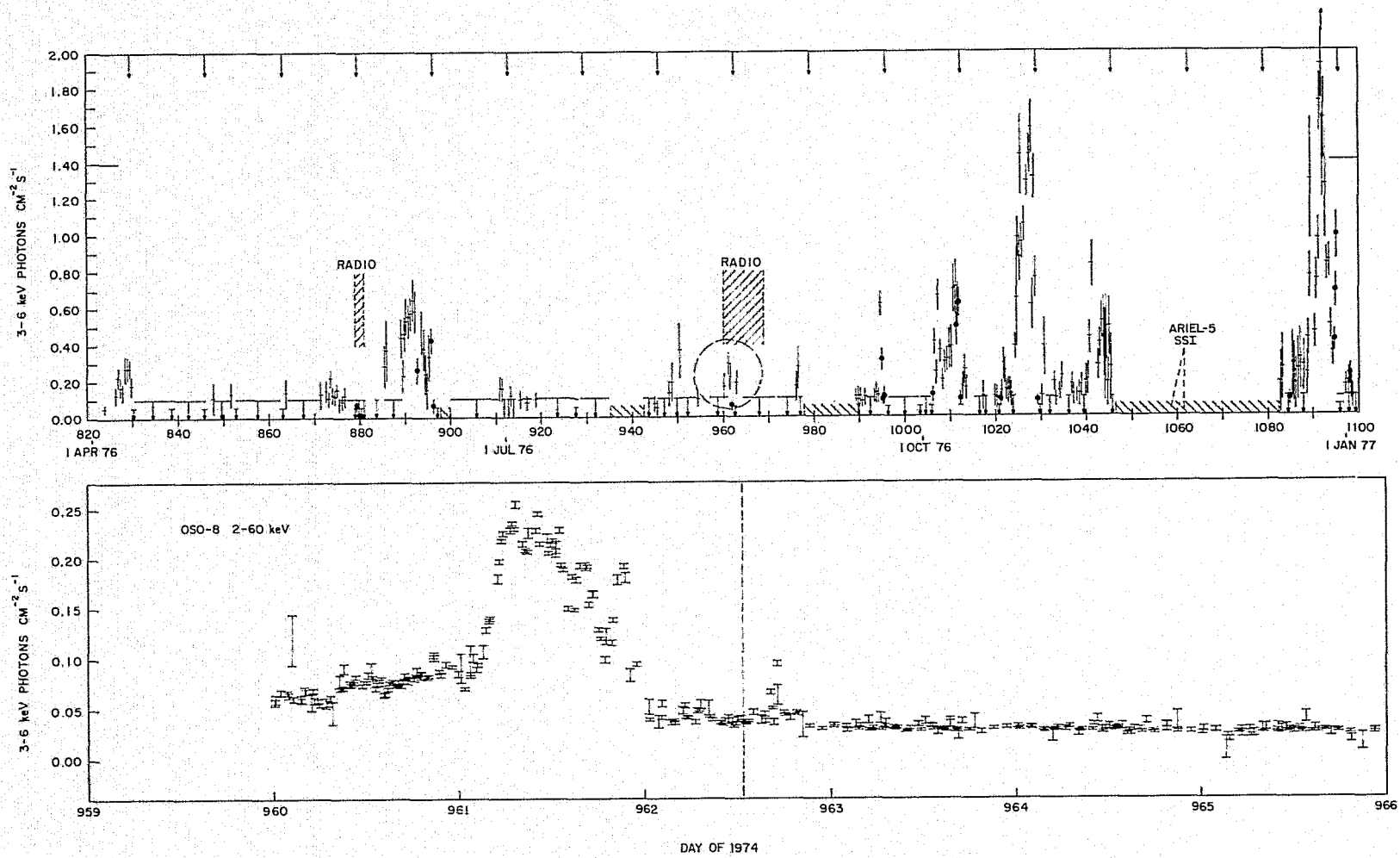


Figure 4.17

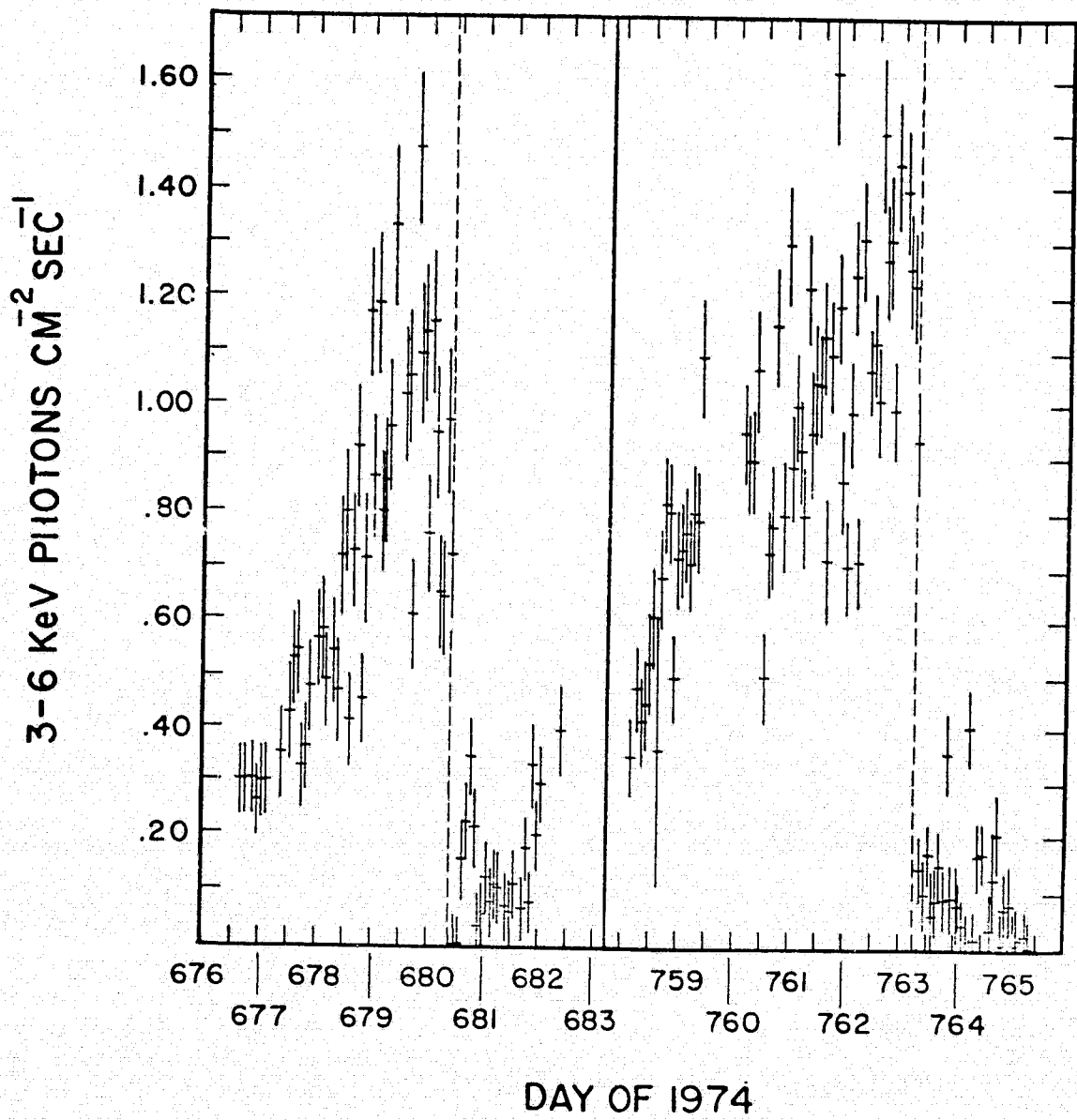


Figure 4.18

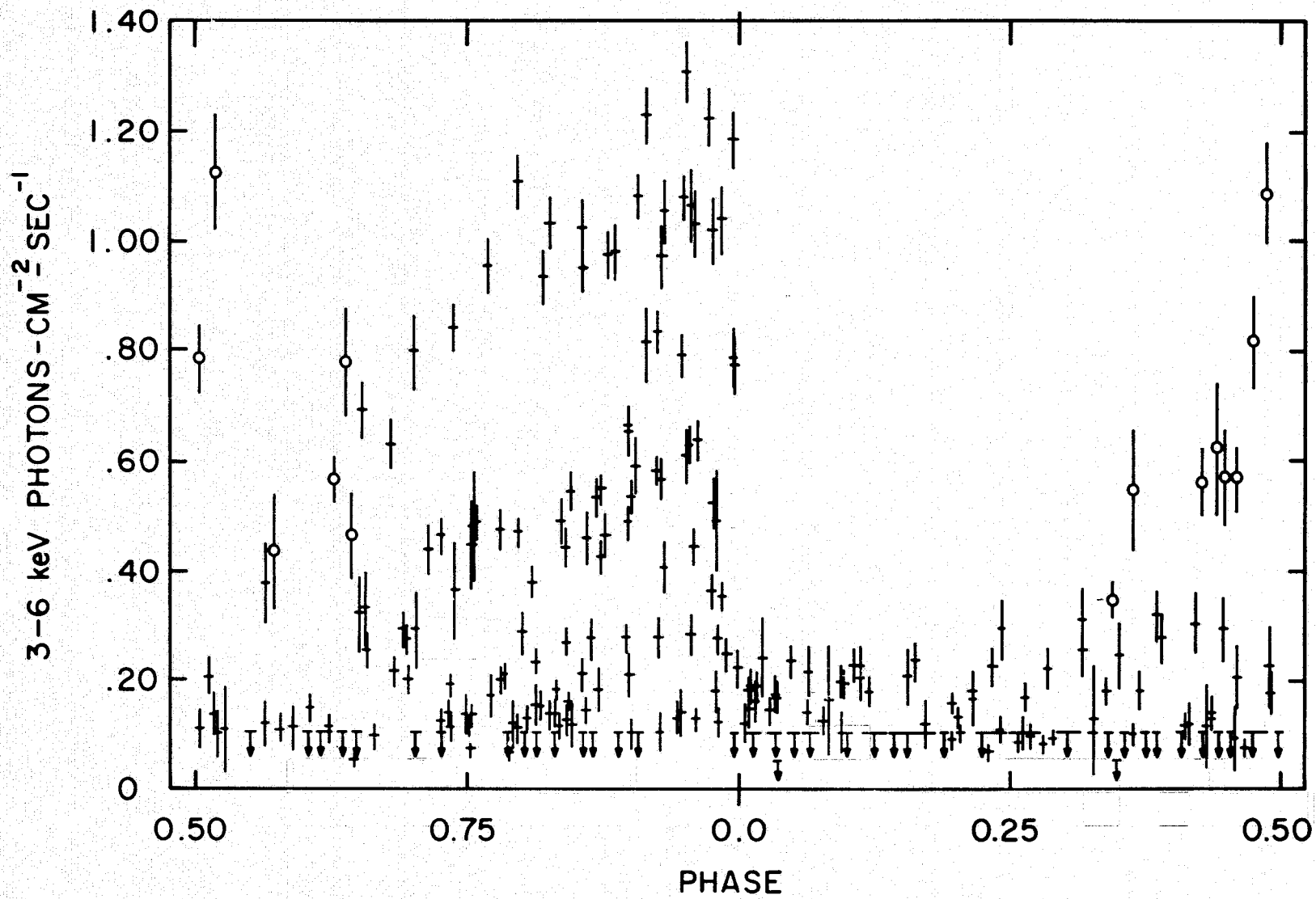


Figure 4.19



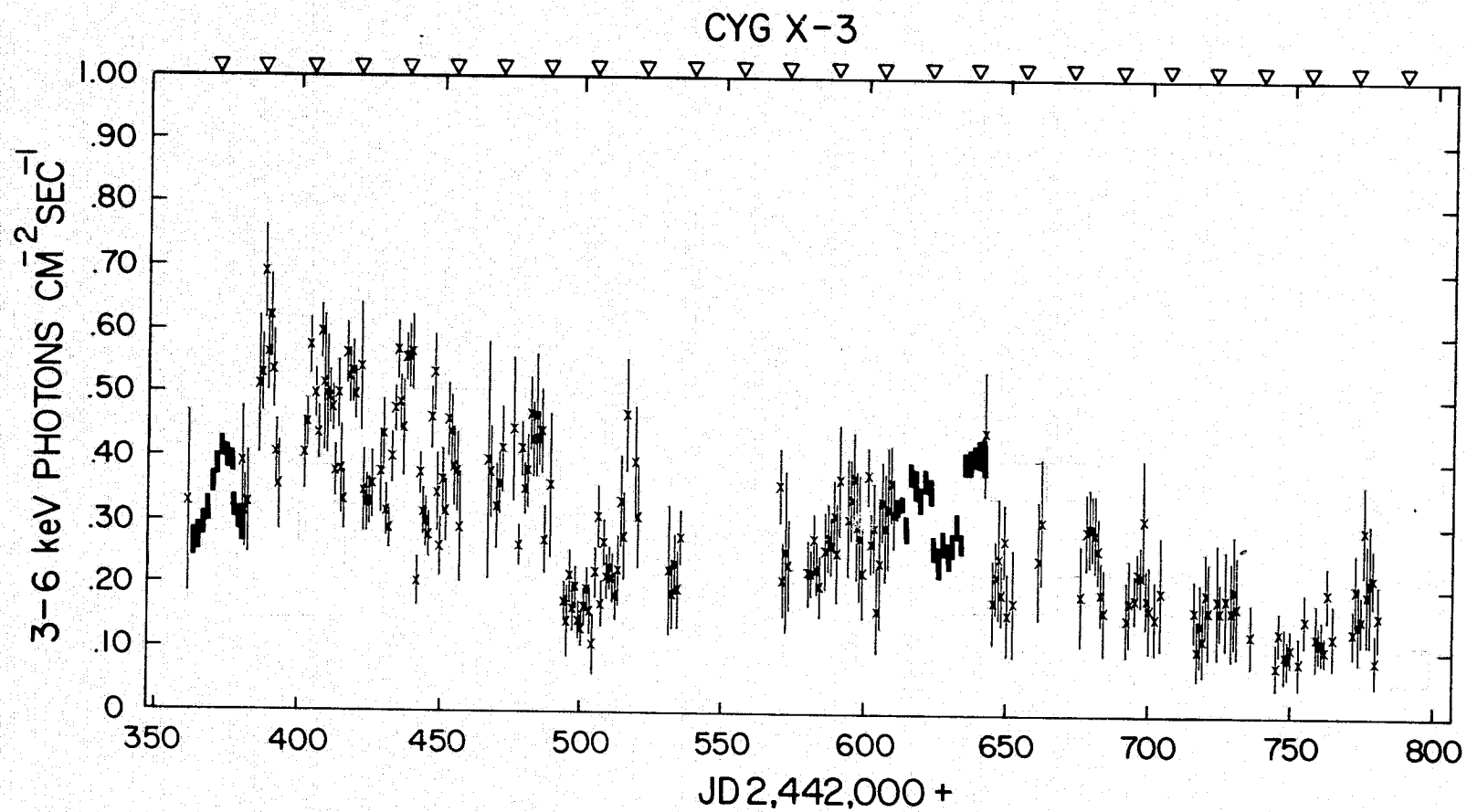


Figure 4.20

GALACTIC MAP OF TRANSIENTS, CANDIDATES AND TRANSIENT-LIKE VARIABLES

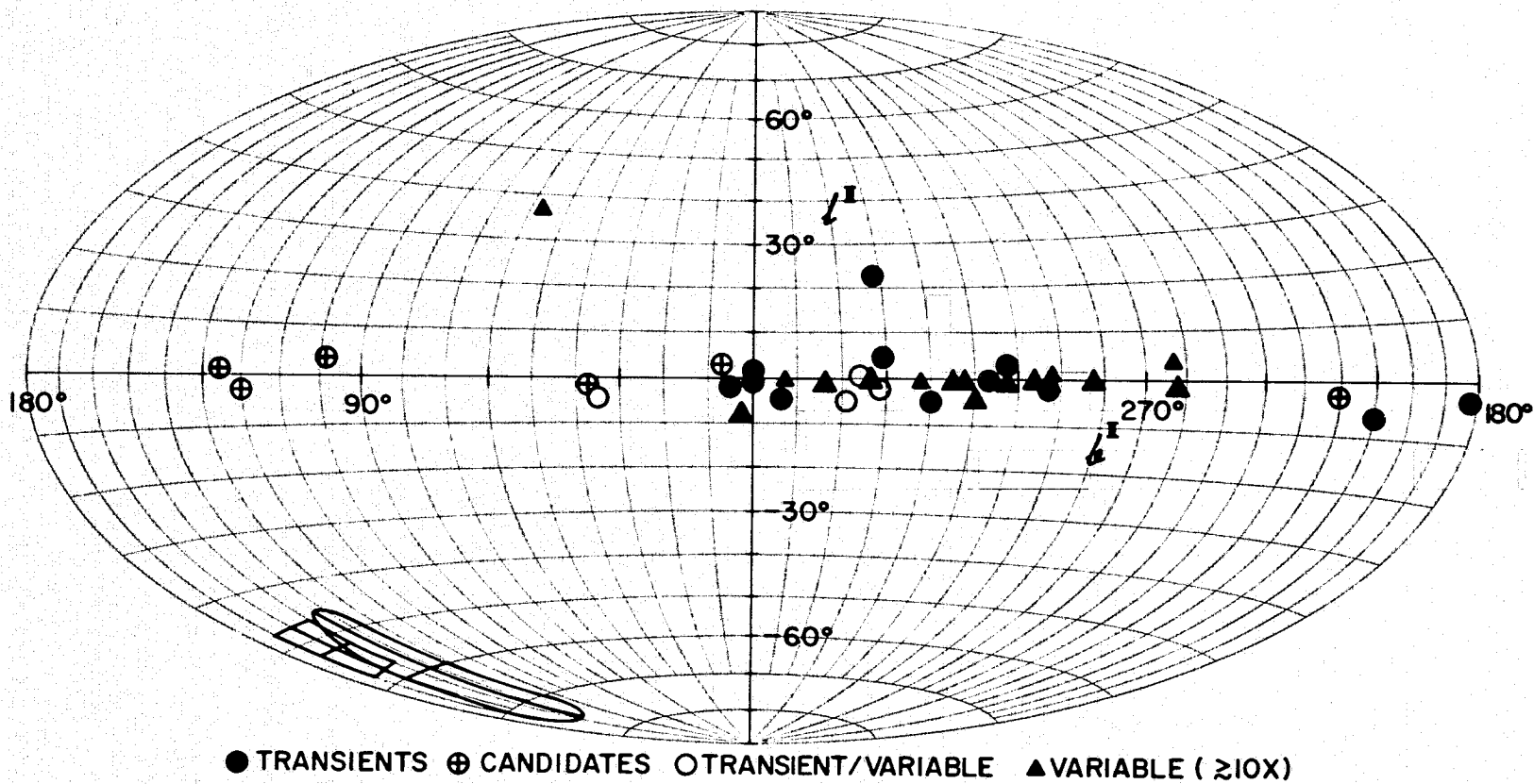


Figure 5.1

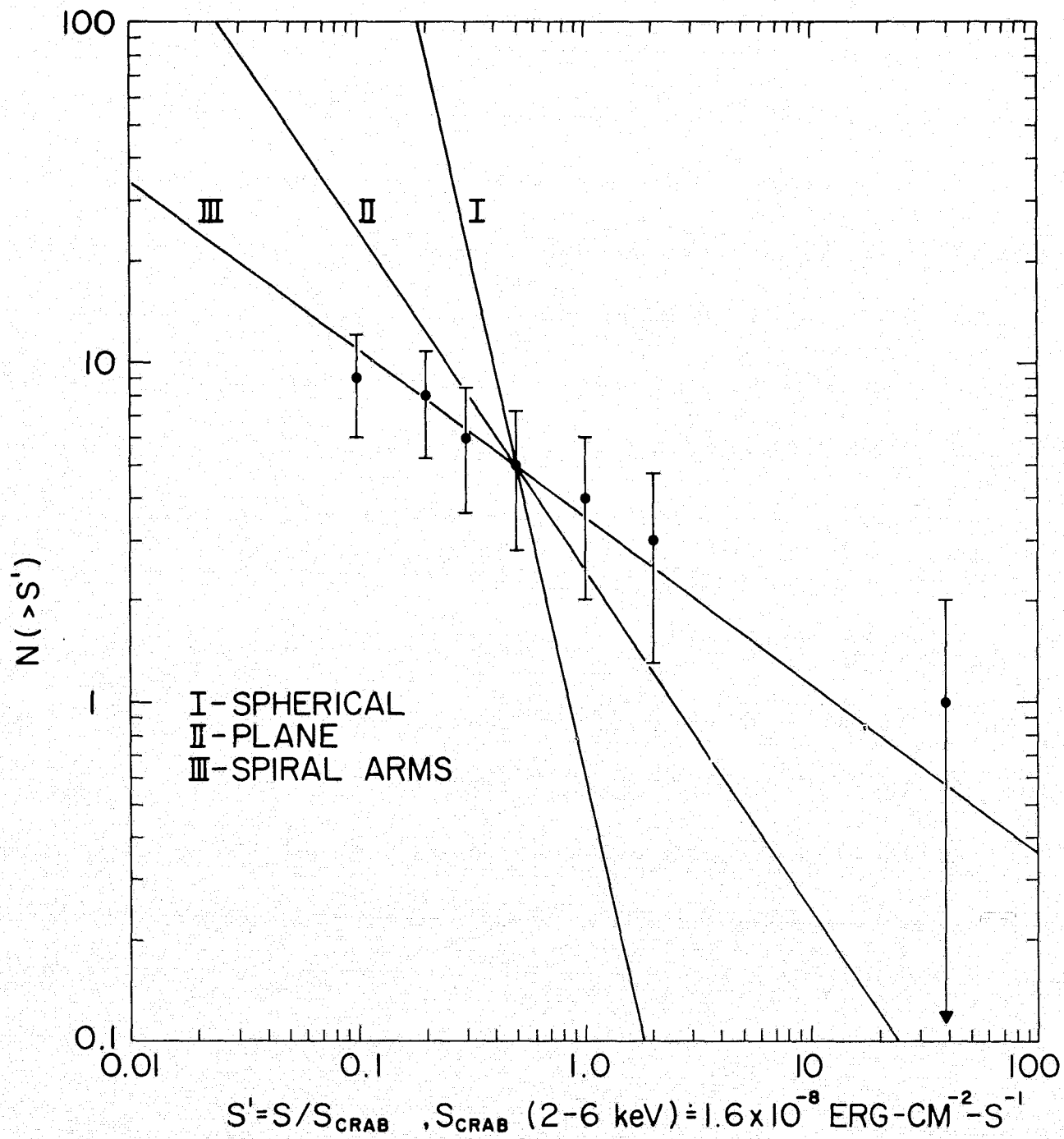


Figure 5.2

GALACTIC PLANE PROJECTION OF TRANSIENT SOURCE POSITIONS

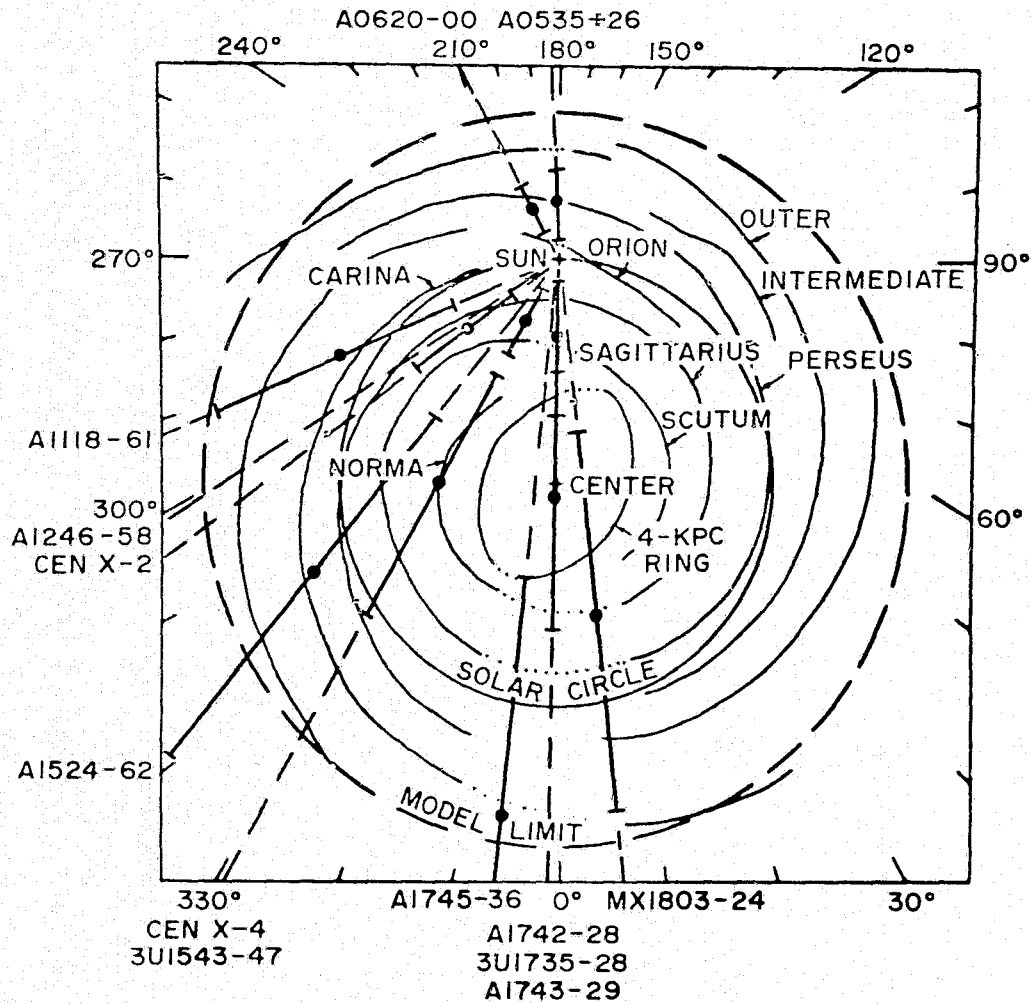


Figure 5.3

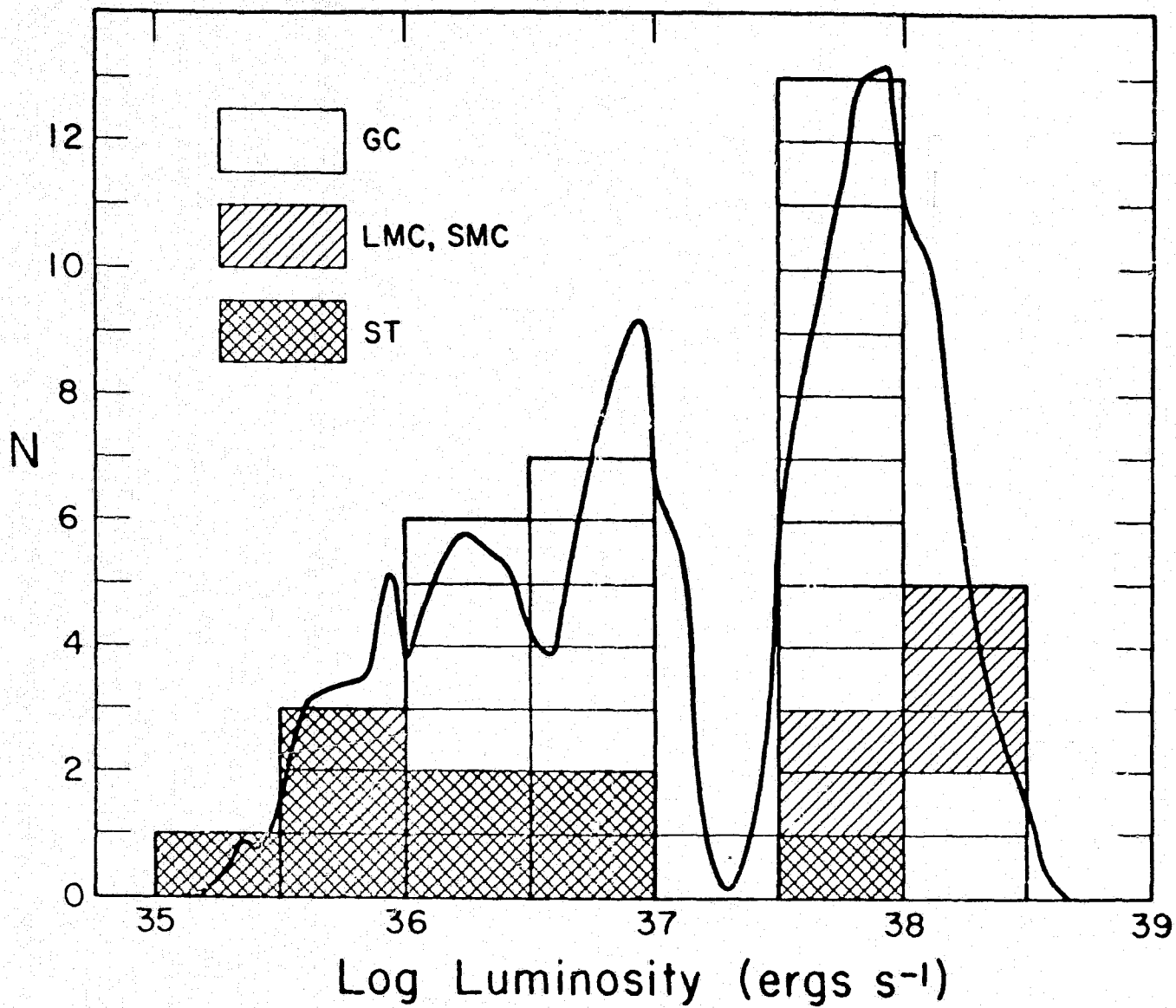


Figure 5.4

$$M_1/M_2 = 0.9$$

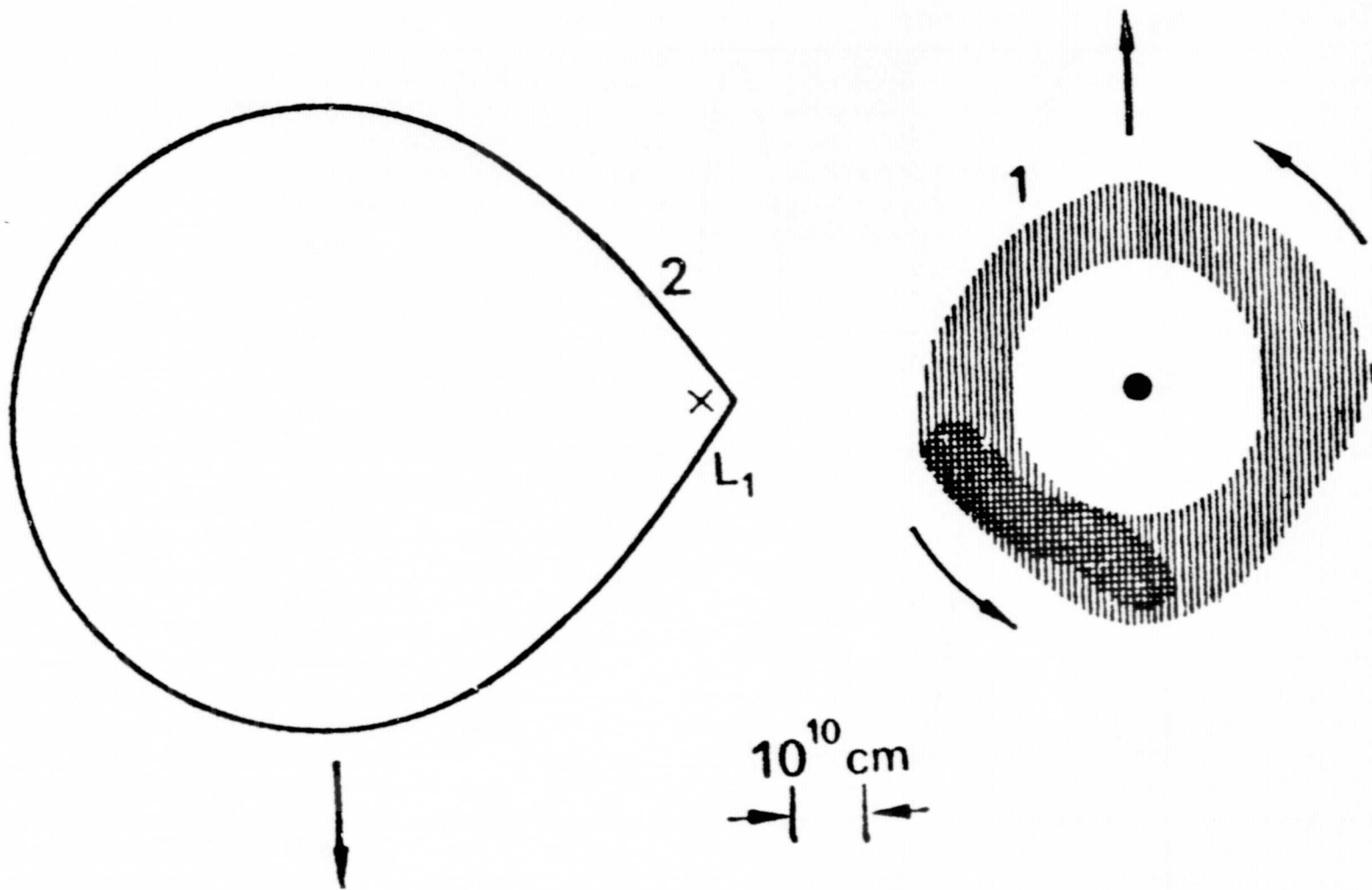
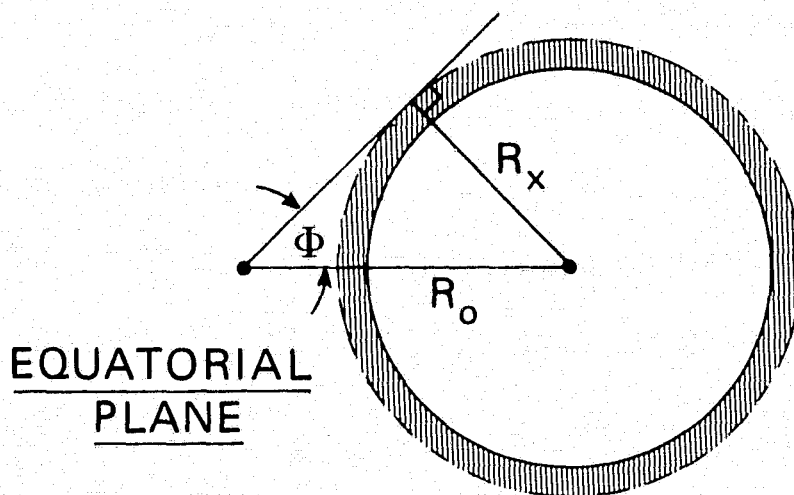
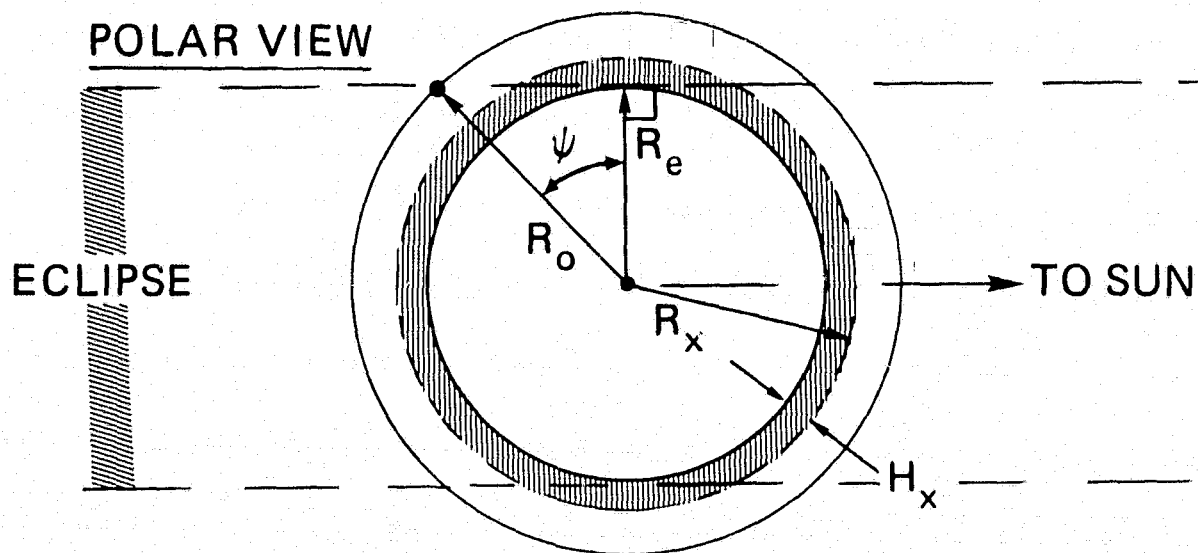


Figure 5.5



$$R_E = \text{Earth Radius} = 6.37817 \times 10^3 \text{ km}$$

$$H_x = \text{Atmospheric X-ray Scale Height} = 1.2 \times 10^2 \text{ km}$$

$$R_x = R_E + H_x = 6.49817 \times 10^3 \text{ km}$$

$$R_o = \text{Orbit Radius} = 6.87817 \times 10^3 \text{ km}$$

$$\psi = \cos^{-1} (R_E/R_o) = 21.98^\circ$$

$$\Phi = \sin^{-1} (R_x/R_o) = 70.87^\circ$$

Figure B.1





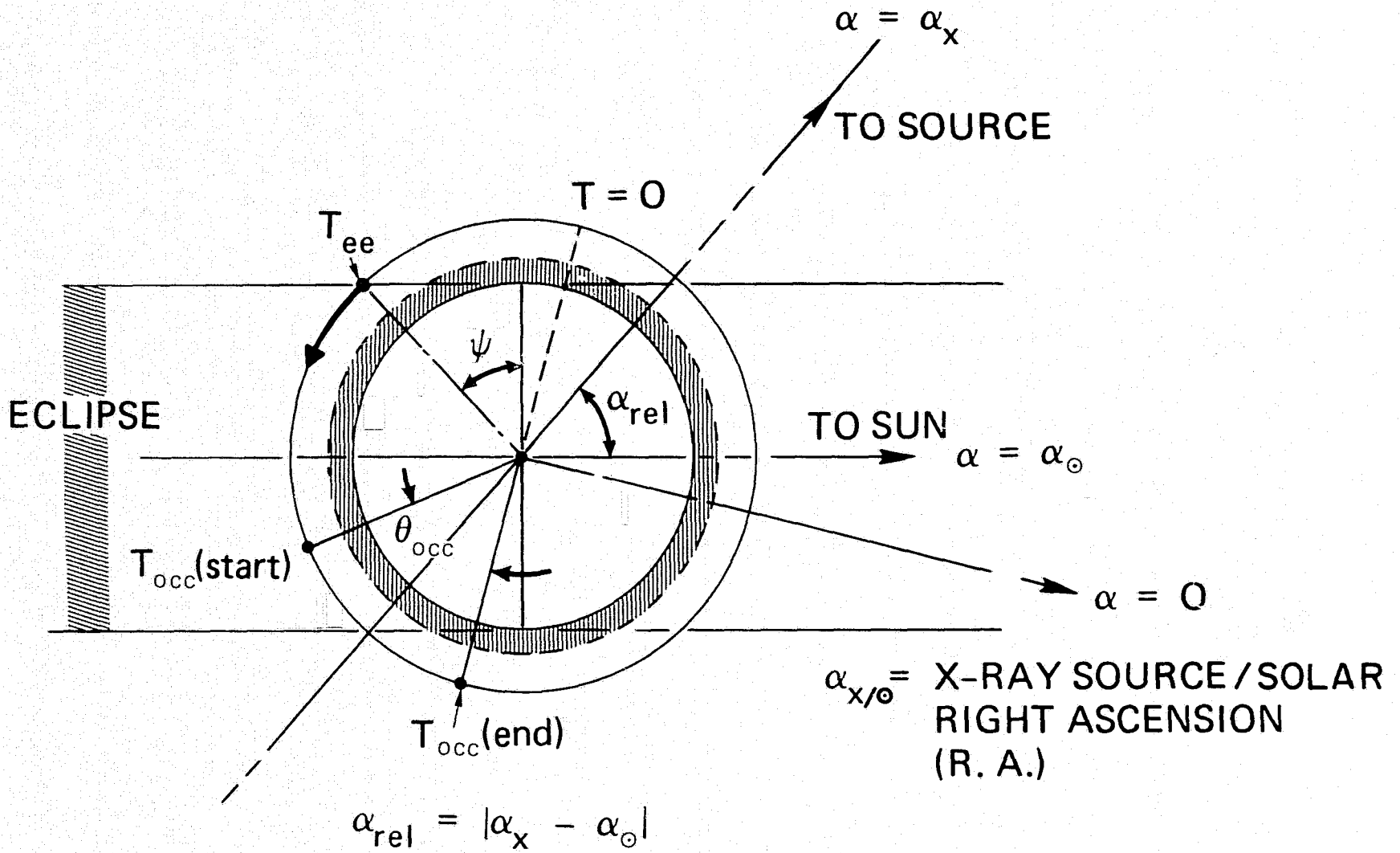
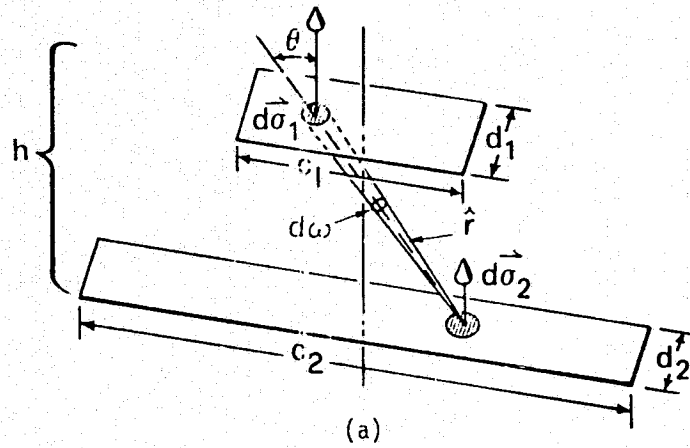


Figure B.3





GEOMETRICAL FACTORS

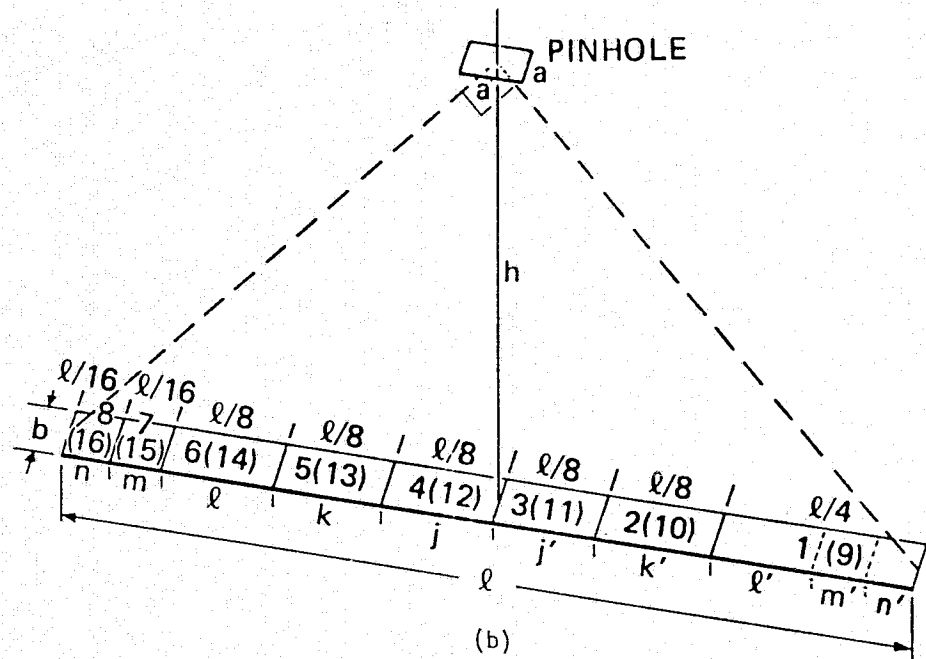


Figure D.1

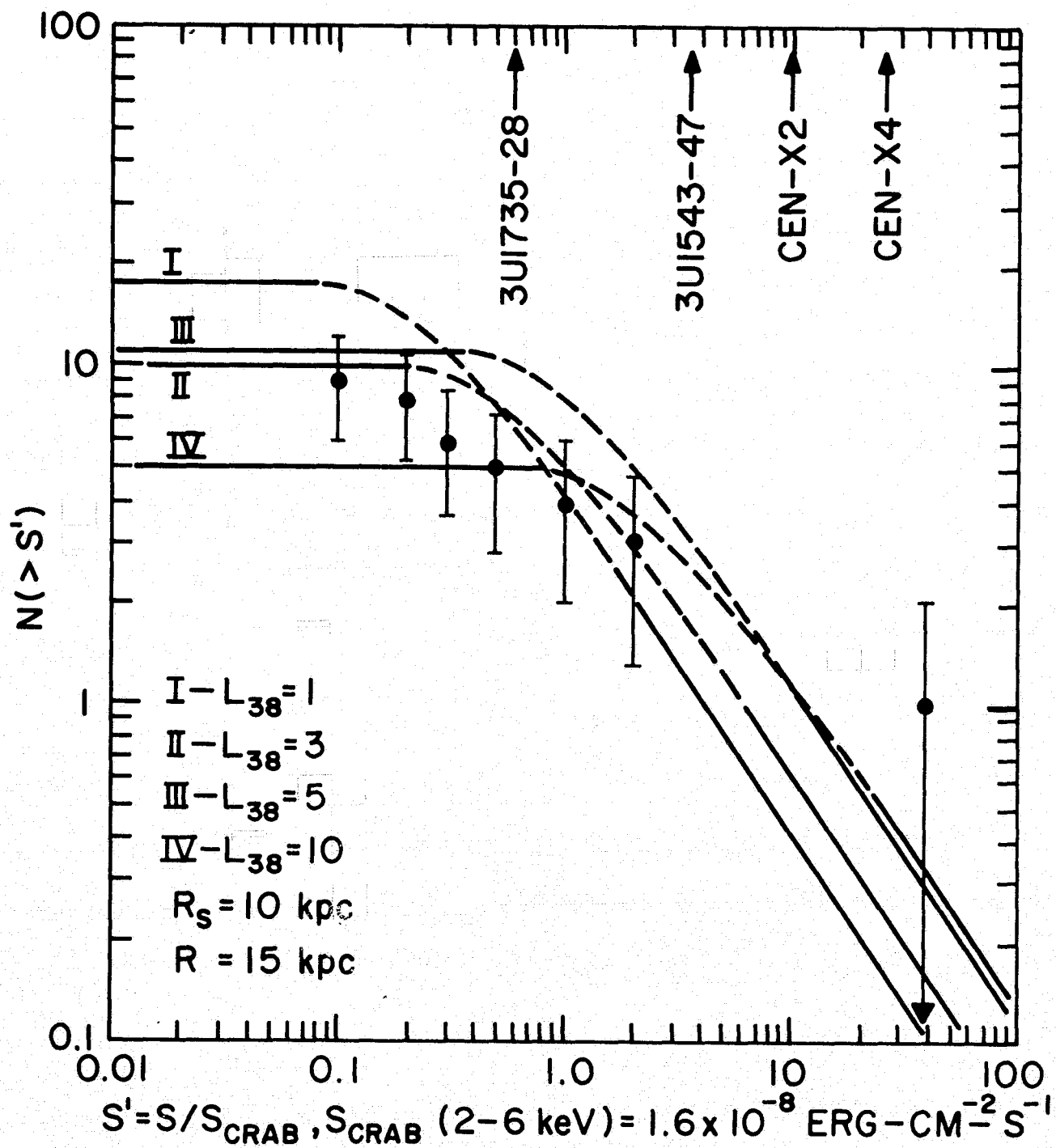


Figure E.1